University of Southampton

PARAMETRIC ADAPTIVE FEEDBACK CANCELLATION IN HEARING AIDS

Joanna Louise Hayes, BSc

Thesis submitted for the award of Doctor of Philosophy

Signal Processing and Control Group
Institute of Sound and Vibration Research
Faculty of Engineering and Applied Science
University of Southampton

July 2003

UNIVERSITY OF SOUTHAMPTON

ABSTRACT

FACULTY OF ENGINEERING AND APPLIED SCIENCE

INSTITUTE OF SOUND AND VIBRATION RESEARCH

Doctor of Philosophy

PARAMETRIC ADAPTIVE FEEDBACK CANCELLATION IN HEARING AIDS

by Joanna Louise Hayes

Adaptive filtering is commonly used to cancel feedback signals in hearing aids. Currently, the most popular approach uses direct closed-loop identification with FIR filtering, using variants of the LMS algorithm. The use of an FIR filter to model the feedback path allows flexibility, but this approach has no prior knowledge of the hearing aid system. This means that the model can often be inaccurate, with the unwanted effects of reduced feedback cancellation and distortion of the desired audio input signal. The aim of this work is to develop a novel adaptive feedback cancellation algorithm that updates the values of physical parameters in a model of the hearing aid system rather than updating filter coefficients. This has the probable advantages of having low order due to the limited number of parameters and of operating within a well-defined range of parameter values corresponding to realistic physical dimensions. Potential benefits include fast convergence, robustness and reduced distortion of the audio input signal. In the first part of this thesis, a two-port network computer model of an *in situ* in-the-ear hearing aid system was developed, from which simplified analytic expressions for the feedback path response and error surface gradients were derived. The model was fitted to a range of measured feedback path responses using numerical optimisation techniques and the convexity of the error surface was explored, since this would affect the use of steepest descent-based algorithms. A new algorithm was then developed that adapted the estimated values of physical parameters in the model to track and cancel changes in the feedback path. Simulation studies with modelled and measured feedback path data were used to investigate the performance of the parametric adaptive algorithm compared to the NLMS algorithm, showing the potential benefits of this new approach.

Contents

List of figures and tables

Acknowledgements

The author would like to thank Dr Boaz Rafaely for his supervision, support and limitless patience. Thanks also go to Professor Steve Elliott and the Signal Processing and Control Group at the Institute of Sound and Vibration Research for their help and support, to Professor Mark Lutman and Emma Payne of the Hearing and Balance Centre, ISVR, for audiological advice and assistance and to Ngwa Shusina for providing the speech-shaped IIR filter used in this work.

Thanks to Karen David and Steve Bright of Knowles Electronics, Inc. for the samples of hearing aid transducers and for the transducer electrical analogues respectively. The Student Version of PSpice 9.1 can be downloaded free of charge from www.orcadpcb.com/pspice.

Figure 1.3 is reproduced by kind permission of Miracle Ear.

The line drawings throughout this thesis were drawn by the author.

List of symbols and abbreviations

Symbols:

a	piston radius
c	expectation value of d^2 (constant)
c	speed of sound
c_1	phase speed
c_p	specific heat at constant pressure
c_v	specific heat at constant volume
d	desired signal
e	error signal
e_{est}	PAA error signal
e_{NLMS}	NLMS error signal
f	frequency
f_s	sampling frequency
$\mathbf{f}(n)$	impulse response of feedback path
$\mathbf{h}$	coefficients of the FIR filter generated by the modelled response, $M(f)$
$\mathbf{h}_{fb}$	coefficients of the FIR filter representing the feedback path, $F(f)$
j	$\sqrt{-1}$
k	wavenumber
l	boundary layer thickness
l_{ent}	entropy mode boundary layer thickness
l_{vor}	vorticity mode boundary layer thickness
p	general parameter
p_i	i^{th} parameter
p_{I-i}	set of all parameters except p_i
Δp	small constant fraction of p
$\mathbf{p}$	cross-correlation vector
$\mathbf{p}$	set of parameters
$\mathbf{p}_{con}$	set of constant parameter values
$\mathbf{p}_{fb1}$	initial set of varying parameter values
$\mathbf{p}_{fb2}$	final set of varying parameter values
r	tube radius
r_{xd}	cross-spectral density of signals x and d
r_{xx}	autocorrelation function of signal x
$\mathbf{u}$	particle velocity
u_F	particle velocity at microphone due to external acoustic feedback path
u_{in}	input particle velocity
v	white noise signal
y	estimated signal
y_{est}	PAA estimated signal
y_{NLMS}	NLMS estimated signal
A	amplifier transfer function
A_{power}	power amplifier transfer function
A_{pre}	preamplifier transfer function
A,B,C,D	two-port network parameters
C_{cavity}	capacitance representing compliance of middle ear cavities
D	desired signal in frequency domain
E	error signal in frequency domain
F	external acoustic feedback path transfer function
$F(f)$	actual feedback path response
$F_{fb1}(f)$	initial actual feedback path response
$F_{fb2}(f)$	final actual feedback path response
FFT^{-1}	Inverse Fast Fourier Transform
G	open-loop transfer function
I	incident path transfer function
$\mathbf{I}$	identity matrix
I_i	input current
I_o	output current
J	cost function, mean square error
J_{excess}	excess mean square error
J_{min}	minimum mean square error
J_n	Bessel function of order n
J_{norm}	normalised mean square error
K	hearing aid internal processing transfer function
L	tube length
L_{mi}	inductance representing mass of part of eardrum attached to malleus, the malleus itself and the incus
M	microphone transfer function
$M(f)$	modelled feedback path response
N	filter length
P	sound pressure at distant point in space
P_{ear}	sound pressure in ear canal near eardrum
P_F	sound pressure at microphone input due to external acoustic feedback path
P_{in}	sound pressure at microphone input following summation of pressures
P_m	sound pressure at microphone input
P_r	receiver transfer function
Pr	Prandtl number
P_V	sound pressure at vent output
R	receiver transfer function
R	external acoustic path length
$\mathbf{R}$	autocorrelation matrix
R_{char}	characteristic impedance of obstruction tube
R_{high}	high load impedance
R_{low}	low load impedance
R_{ob}	obstruction tube termination impedance
R_r	radiation resistance
R_1	piston resistance function
S	cross-sectional area of a tube
S_{vv}	power spectral density of signal v
S_{xd}	cross-spectral density of signals x and d
S_{xx}	power spectral density of signal x
T	shaping filter transfer function
T_1	receiver tube transfer function

T_2	ear canal transfer function	α	convergence coefficient
T_3	vent transfer function	α_0	NLMS convergence coefficient
U_V	volume velocity of layer of air at vent exit	α_i	convergence coefficient for i^{th} parameter
U_0	speed amplitude of piston	α_p	convergence coefficient for parameter p
V_{in}	input voltage	ε	small constant
V_{out}	output voltage	γ	ratio of specific heats
W	adaptive filter transfer function	μ	viscosity of fluid in a large volume
X	input signal in frequency domain	ν	thermal conductivity of fluid
X_r	radiation reactance	ρ_0	density of fluid in tube
X_1	piston reactance function	σ_v^2	power of signal v
Y	estimated signal in frequency domain	σ_x^2	power of signal x
Z	acoustic impedance of a tube	θ	angle from vent centreline to microphone input
$\mathbf{Z}_L$	acoustic impedance of leak exit	ω	angular frequency, $2\pi f$
Z_{obst}	load impedance due to obstruction tube	ζ	misadjustment
$\mathbf{Z}_r$	radiation impedance	Γ	propagation constant
Z_T	acoustic impedance of middle ear	Φ	coefficient of friction for fluid in tube
$\mathbf{Z}_V$	acoustic impedance of vent exit	∇_i	error surface gradient with respect to i^{th} parameter
$\mathbf{Z}_V'$	acoustic impedance of vent exit including pinna effects	∇_p	error surface gradient with respect to p
Z_∞	infinite load impedance	^{T}	transpose

Subscripts:

1	receiver tube parameters	m	microphone parameters
2	ear canal parameters	r	receiver parameters
3	vent parameters	F	external acoustic feedback path parameters
4	leak parameters	Fl	parameters for acoustic feedback path via leak
a	amplifier parameters	Fv	parameters for acoustic feedback path via vent

Abbreviations:

BTE	behind-the-ear	LMS_{sd}	steepest descent Least Mean Square
FIR	finite impulse response	m.s.e.	mean square error
FFT	Fast Fourier Transform	NLMS	Normalised Least Mean Square
IIR	infinite impulse response	OLTF	open-loop transfer function
IFFT	Inverse Fast Fourier Transform	PAA	parametric adaptive algorithm
ITC	in-the-canal	PAA_{sd}	steepest descent parametric adaptive algorithm
ITE	in-the-ear	RMS	root mean square
ITEC	in-the-ear-canal	SPL	sound pressure level
LMS	Least Mean Square	TMJ	temporomandibular joint

Introduction

Introduction to the project

There are several problems associated with hearing aids. One of the most important is that of feedback. This occurs when an amplified sound signal emitted by the receiver (hearing aid loudspeaker) leaks back to the microphone. Instability usually occurs when a frequency component of the feedback signal has an amplitude equal to or greater than that of the input signal and is in phase with the input signal. This causes oscillation, driving the hearing aid to its maximum level in the form of a high-pitched whistling or howling. In this condition, the aid is useless unless gain is reduced (Lybarger, 1982; Maxwell and Zurek, 1995; Rafaely *et al.*, 1999). Feedback tends to occur at high gains. For users with moderate hearing loss, reducing the gain of the aid may be sufficient to avoid the problem. However, severely hearing-impaired users require high gains, and reducing the gain to avoid acoustic feedback will prevent them obtaining full benefit from the device. Some users find feedback so annoying that they stop using their aids altogether (Oliveira, 1997). Feedback has three main effects: oscillation, significant alteration in the frequency response of the hearing aid even if oscillation does not occur, and the creation of sharp peaks in the response as oscillation is approached, causing "ringing" in the sound processed by the aid (Cox, 1982; Lybarger, 1982).

The main cause of feedback in hearing aids is amplified sound leaking back to the microphone around the earmould (due to an imperfect fit, for example), or through the earmould vent. The probability of feedback occurring can be reduced by increasing the separation between the vent exit and the microphone input. However, the physical configuration of a hearing aid is limited by its size and the size of its components.

Feedback cancellation using adaptive filters has proved the most popular approach to the problem. Continuous (closed-loop) adaptation with no probe noise is the preferred method of feedback cancellation at the present time (Kates, 1999; Greenberg *et al.*, 2000; Hellgren, 2002), since, compared to other methods that suspend normal operation of the hearing aid while updating the filter coefficients, it provides a good acoustic signal to noise ratio without disrupting the input signal and reducing its intelligibility. Most feedback cancellation methods use finite impulse response (FIR) filtering with variants of the Least Mean Square (LMS) algorithm since these are efficient and suitable for use with the limited processing power available due to the small size of a hearing aid (Maxwell and Zurek, 1995; Kates, 1999; Greenberg *et al.*, 2000). The LMS algorithm has no prior knowledge of likely changes in the feedback path. Such an approach may perform poorly in the presence of music or

sinusoidal input signals, with a tendency to cancel the input signal, treating it as "howling" (Kates, 1999; Greenberg *at al.*, 2000; Hellgren, 2002). The estimate of the feedback path may also be biased, leading to insufficient cancellation of the feedback signal and the introduction of unwanted artefacts (Kates, 1999). Also, the convergence speed of the algorithm may not be sufficient to track and cancel fast changes in the feedback path.

This thesis presents a feasibility study for a novel method of adaptive feedback cancellation that adapts values of physical parameters in a model of the hearing aid system instead of adapting filter coefficients. The limited number of parameters gives a low order algorithm, which could potentially result in fast convergence. Additionally, such an algorithm has the potential to be more robust to changes in the feedback path (Rafaely and Roccasalva-Firenze, 2000), since the parameter values are well-defined, conforming to possible physical situations such as movement of the jaw or the presence of an obstruction near the ear. Furthermore, the parameters are typically independent of the input signal and of each other, so the algorithm is less likely to suffer from bias or to cancel the input signal.

A computer model of an *in situ* in-the-ear hearing aid system is used in the parametric adaptive algorithm, based on previous models used in the design and study of hearing aid systems (Bade *et al.*, 1984; Kates, 1988a, 1988b, 1990, 1991; Egolf *et al.*, 1989). The ability of the model to fit measured feedback path data for human subjects is investigated before the derivation and testing of the adaptive algorithm.

Aims

This project aims to develop and study a novel adaptive algorithm for feedback cancellation in hearing aids, adapting physical parameters within a computer model of the hearing aid system. It is intended that this will potentially improve performance over current FIR filter-based systems. The thesis presents the development of the parametric adaptive algorithm and an initial feasibility study using computer simulations.

Contributions

1. Development and experimental verification of a computer model of an* in situ *in-the-ear hearing aid system integrating the MATLAB and PSpice software packages

Computer models have been used extensively in the design and study of hearing aid systems. The model developed here used a novel combination of electrical transducer analogues implemented in the PSpice software package with analytic expressions for the parts of the system represented by cylindrical tubes and mean measured data for the human middle ear

impedance implemented in MATLAB. The computer model was used to demonstrate the effects on the feedback path response of changing the physical parameters in the hearing aid system, and was verified experimentally with measured feedback path data.

The feedback path may undergo many variations in any given timeframe due to changes in the physical parameters, such as jaw movements or the presence of an obstruction near the ear. The model was extended to include such variations, aiding understanding of the relationship between physical changes in the hearing aid system and changes in the feedback path response.

2. Derivation, verification and analysis of a simplified analytic expression for the feedback path in hearing aids

The model described above was in two-port network form. An analytic expression for the feedback path response was obtained by multiplication of the two-port matrices. This expression was then simplified without significant loss of accuracy. The simplified expression was more computationally efficient, reducing the running time of simulations. This is important when the analytic expression is used in feedback cancellation studies as the algorithm must eventually operate in real time. This new result facilitates analysis of the feedback path and its variability and control.

The analytic model was verified experimentally and shown to give results comparable with the two-port matrix model. The simplified expression was shown to be valid and could be used as the basis for a novel adaptive feedback cancellation system as presented in this thesis.

The derivation was performed of a set of analytic expressions for the gradient of the error surface obtained when the model is used for the identification of the feedback path. These expressions were intended for use in a frequency domain parametric adaptive feedback cancellation algorithm suggested in this thesis as a topic for future work.

3. Development and study of a new parametric adaptive algorithm for feedback cancellation in hearing aids

The analytic expression was used in a novel approach to feedback cancellation. An adaptive algorithm was developed, based on the method of steepest descent and updating estimated values of the physical parameters within the model rather than updating filter weights. This approach is new and presents an interesting alternative to conventional methods of feedback cancellation such as the Least Mean Square algorithm.

The performance of the parametric adaptive algorithm has been evaluated with both modelled and measured feedback path data with white noise and speech-shaped noise input signals. The effect on performance of changing the number of parameters varied by the algorithm has also been investigated. The performance of the parametric adaptive algorithm has been compared with that of the Normalised Least Mean Square algorithm to allow reference to an accepted method of feedback cancellation.

Publications

The following papers relating to the project were published:

1. Rafaely, B., Hayes, J.L., "On the modeling of the vent path in hearing aid systems", J. Acoust. Soc. Am., Vol. 109, No. 4, April 2001, pp. 1747-1749.

This paper compared two configurations for integrating the forward and feedback paths through the vent of a hearing aid and proposed the preferred configuration. The contribution related to this thesis was an understanding of the construction of the hearing aid system.

2. Hayes, J.L., Rafaely, B., "Parametric Adaptation Algorithm for Feedback Cancellation", ISVR Technical Memorandum No. 871, Institute of Sound and Vibration Research, University of Southampton, October 2001.

This technical memorandum presented the parametric adaptive algorithm for the first time in a basic form with a single varying parameter, using examples similar to those presented in this thesis.

3. Rafaely, B., Shusina, N.A., Hayes, J.L., "Robust compensation with adaptive feedback cancellation in hearing aids", Speech Comm., Vol. 39, January 2003, pp. 163-170.

This paper presented the formulation of a robust hearing aid system with guaranteed closed-loop stability that was free from howling. The paper used the model of the hearing aid system presented in this thesis.

Conference presentations

1. Hayes, J.L., Rafaely, B., "Modelling the feedback path in hearing aids", British Society of Audiology Annual Conference 2001, 6th September 2001, Winchester, U.K.

This presentation suggested adapting physical parameters in the hearing aid system to give faster, more robust cancellation of the feedback path, and presented a single parameter example.

2. Hayes, J.L. and Rafaely, B., "Physical modeling of the feedback path in hearing aids with application to adaptive feedback cancellation," J. Acoust. Soc. Am., Vol. 111, No.5, Part 2, 2002, p. 2380 (a), presented at the 143rd Meeting of the Acoustical Society of America, Pittsburgh, PA, USA.

This presentation suggested that use of a physical model in feedback cancellation might improve the accuracy of the feedback estimate. The parametric adaptive algorithm was presented and the result of a simulation with two varying parameters was compared with that of the NLMS algorithm with a 256-tap FIR filter.

Overview of thesis

Chapter 1 is a review of the literature in relevant fields. After this, the thesis can be considered as consisting of three main sections. The first section (Chapters 2 – 3) covers the development of a computer model of the measurable feedback path from the receiver input to the microphone output. Chapter 2 describes the components of the two-port network model, providing details of the derivation of the two-port network parameters. Chapter 3 presents the verification of the model through computer simulations of simple transducer-tube systems and the entire feedback path with slit leakage around the earmould and an obstruction in the external acoustic feedback path.

The second section (Chapters 4 – 6) covers the development of a simplified analytic model of the feedback path. The derivation and verification of an analytic expression for the feedback path are given in Chapter 4. Numerical optimisation techniques are used to fit the model to measured feedback path responses in Chapter 5 and the analytic expression is used in the investigation of the error surface of the feedback path in Chapter 6.

The third section of the thesis (Chapters 7 – 9) covers the development of the novel parametric adaptive algorithm for feedback cancellation. The theory of the parametric adaptive algorithm is presented in Chapter 7. Chapters 8 and 9 present simulation studies evaluating the performance of the parametric adaptive algorithm compared to that of the NLMS algorithm with modelled and measured feedback path data, respectively.

Chapter 10 presents the conclusions drawn from this project and discusses future development of the PAA for use in real life hearing aid systems. Chapter 11 lists the cited references.

1 Review

1.1 Introduction

This chapter presents a brief examination of the anatomy and physiology of the human ear to provide a basic knowledge of its workings and to familiarise the reader with the anatomical terms referred to in the thesis. This is followed by a discussion of hearing aids and two of the main problems which afflict hearing aid users: the occlusion effect and feedback. This project is concerned with the cancellation of feedback to provide greater usable hearing aid gain before instability occurs. Methods of feedback cancellation are therefore discussed, as are commonly used adaptive algorithms.

1.2 Anatomy and physiology of the human ear

The parametric method of adaptive feedback cancellation developed in this thesis is based on a computer model of an *in situ* in-the-ear hearing aid system, comprising the electrical hearing aid transducers, the external acoustic feedback path through which amplified sound travels from the ear canal to the hearing aid microphone, and the human ear itself. The ear consists of three main sections: the outer, middle and inner ear. This section describes the parts of the human ear included in the model presented in Chapter 2.

A cross-section of the human ear is shown in Figure 1.1 (Gelfand, 1998). This report is concerned mainly with the outer ear, i.e. from the pinna and ear canal to the eardrum, which separates the outer and middle ear. The middle ear contains the small bones known as the ossicles (stapes, incus and malleus), with the associated tendons, ligaments and muscles, and the Eustachian tube, which equalises the pressure in the middle ear with external atmospheric pressure. The inner ear, beginning at the oval window, includes the cochlea and semicircular canals. The latter are organs of balance rather than of hearing. The auditory nerve connects the ear to the brainstem.

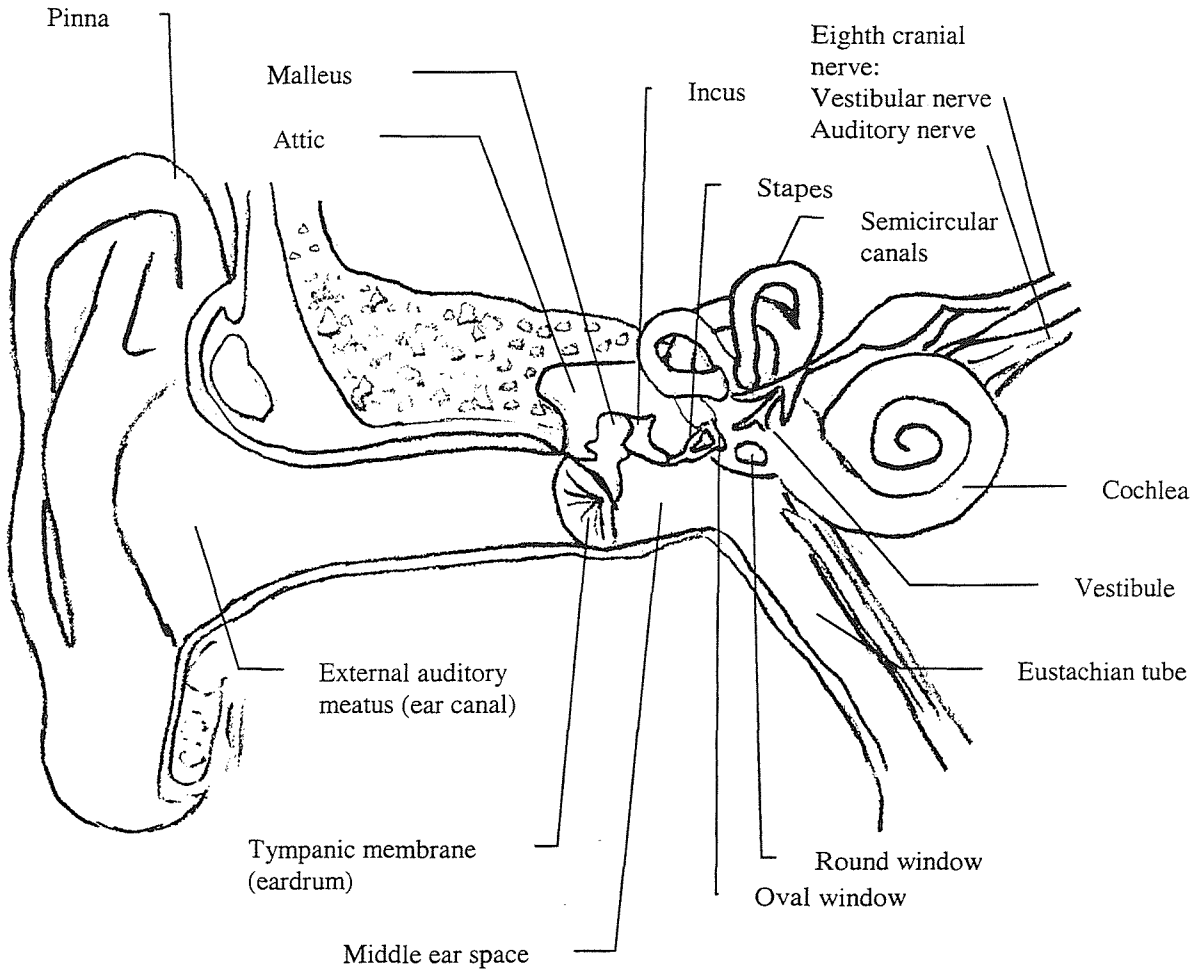

Figure 1.1: Cross-section of the human ear (based on Gelfand, 1998)

The pinna is the external part of the ear, composed of flexible skin-covered cartilage. Sound sources at different positions interact with the ridges and hollows of the pinna to produce different resonances and reflections which are important for the localisation of sound. Also, filtering by the pinna contributes greatly to externalising sound, i.e. perceiving the location of sound outside the head (Agnew, 1994).

The outer third of the external auditory meatus or ear canal is cartilaginous, while the inner two-thirds are osseous (bony) (Alvord and Farmer, 1997; Gelfand, 1998). The cartilaginous part is an extension of the pinna. The osseous part is formed by portions of the temporal bone of the skull (Alvord and Farmer, 1997). The ear canal is not a straight, regular cylinder; rather it is somewhat "S-shaped" with a varying diameter and a non-circular cross-section (Gelfand, 1988). The "twisting" of the ear canal becomes more marked with age (Alvord and Farmer, 1997). In most subjects, the cross-sectional area is greater at the first bend in the ear canal than at the second (Alvord and Farmer, 1997). The skin lining the ear canal contains

ceruminous (wax) glands and sebaceous (oil) glands. This is to lubricate the ear canal and remove debris and foreign objects (Gelfand, 1998). However, a large build-up of wax may cause acoustic feedback for hearing aid users (Madell and Gendel, 1984).

The tympanic membrane (eardrum) is an concave elliptical translucent membrane, approximately 10 mm high and 8 mm wide, set at an angle of about 40° to the ear canal, with the upper part closer to the outer ear than the lower part (Alvord and Farmer, 1997; Gelfand, 1998).

The impedance of the middle ear, also referred to as the eardrum impedance in some papers (Egolf *et al.*, 1989), is an important part of the hearing aid system, and can be represented by an electrical analogue, as shown in Chapter 2. An increase in the middle ear impedance reduces the effective volume of the ear canal, increasing the sound pressure level (SPL) at the eardrum. A schematic diagram of the middle ear is shown in Figure 1.2.

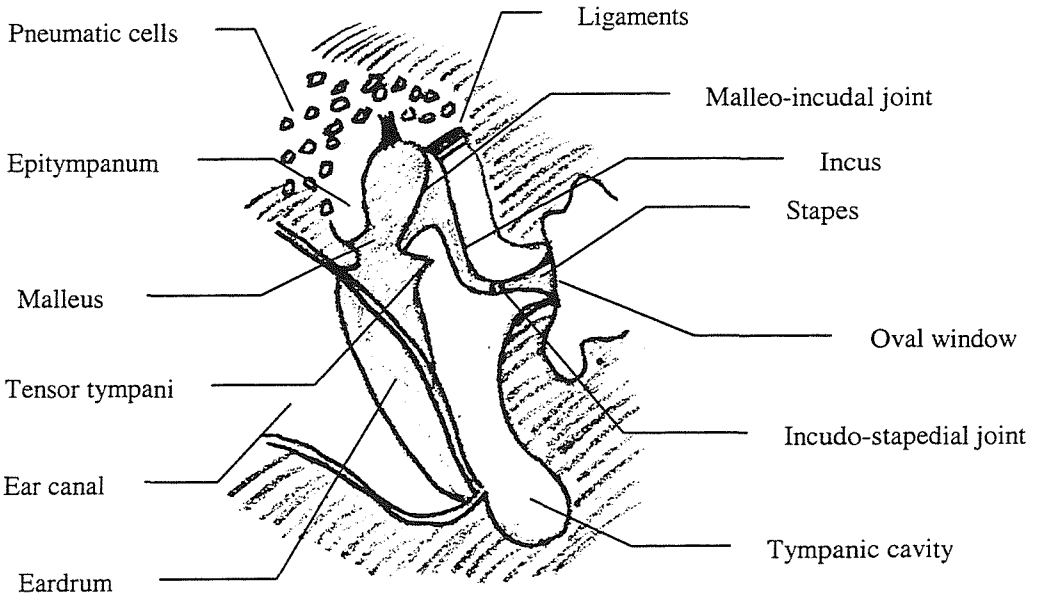

Figure 1.2: Schematic diagram of the human middle ear (based on Zwislocki, 1962)

The eardrum forms the outer part of the middle ear (Zwislocki, 1962). It is connected to the chain of ossicles: the malleus (hammer), incus (anvil) and stapes (stirrup), the small bones which act to transform the impedance at the eardrum to the impedance at the inner ear. Although the coupling between the eardrum and malleus is close, not all of the acoustic energy received by the eardrum is transmitted to the ossicles. Further losses occur in the ossicular joints. Some frictional resistance is introduced by the eardrum, the ligaments and muscles of the middle ear, and the elastic properties of the round window membrane. The

input impedance of the cochlea is the main resistive component. The motion of the eardrum is transmitted to the air-filled cavities of the middle ear as well as to the ossicles, and consequently these cavities contribute to the acoustic characteristics of the middle ear (Zwislocki, 1962).

There are middle ear pathologies which may have a significant impact on the middle ear impedance. The effect of otosclerosis is to immobilise the stapes in the oval window, causing the cochlea to become disconnected from the rest of the middle ear. This increases the middle ear impedance. A discontinuity between the malleus and stapes as a result of a surgical procedure to remove the incus results in lower than normal middle ear impedance (Zwislocki, 1962).

1.3 Hearing aids, the occlusion effect and feedback

A hearing aid is a device used to compensate for impaired hearing by amplifying sound. Much research has been conducted to improve the performance of hearing aids to increase the benefit to the user; this is the ultimate aim of this work. Earmoulds are used to connect the hearing aid to the ear. Blocking the ear canal in this way causes the user to hear their own voice through bone conduction more than through transmission by air, causing it to sound muffled; this is known as the occlusion effect (Killion *et al.*, 1988). A build-up of pressure may also result. These problems may be alleviated by the use of a tube through the earmould, known as the vent. However, amplified sound may leak back to the hearing aid microphone and be amplified further, driving the system into instability and leading to oscillation (a high pitched whistling). This is acoustic feedback, a major problem for hearing aid users. The main aim of this work is to develop a novel method of feedback cancellation, thus allowing higher gain to be used before the onset of oscillation. This section discusses the production of acoustic feedback as a result of venting to reduce the occlusion effect.

A hearing aid should provide the desired gain throughout the entire frequency range of interest and compensate for the loss of the combined resonance due to the ear canal, pinna and head which is obtained when the ear canal is unblocked (Staab and Lybarger, 1994). A typical aid will consist of a microphone, an amplifier, a certain amount of electronic processing (e.g. to shape the desired frequency response to the subject's requirements), and a receiver (hearing aid loudspeaker).

There are several types of hearing aid available at the time of writing: behind-the-ear (BTE) aids, in-the-ear (ITE) aids, in-the-ear-canal or in-the-canal (ITEC or ITC) aids and

completely-in-the-canal (CIC) aids. Body-worn and eyeglass hearing aids (in which the aid is incorporated into spectacles) are less common nowadays. An ITE aid is considered throughout this thesis.

There are several types of ITE aid, classified according to their size and position within the concha (the hollow in the pinna around the entrance to the ear canal). Full concha aids are the most common (Figure 1.3). They offer greater space in which to house components, and filling the concha reduces the probability of acoustic feedback since the aid fits snugly into the contours of the outer ear, reducing sound leakage. Smaller aids are more discreet, but have less space for electroacoustic components. Reduced component space limits the complexity of the circuitry and the power of the aid, which is related to battery size (Agnew, 1994). As technology advances, smaller high power aids will be possible as batteries decrease in size. In 1997, ITE aids made up approximately 85% of the market (Stuart *et al.*, 1999).

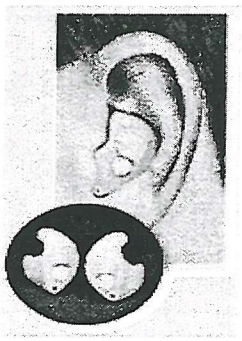

Figure 1.3: In situ *full concha ITE hearing aid*

ITE devices are either "custom" aids, with the electroacoustic components built into a plastic shell made from an impression of the user's ear (as in Figure 1.3), or "modular" aids, in which a standard casing slots into an custom-made earmould (Staab and Lybarger, 1994). Henceforth, the term "earmould" will also include the shell of a custom aid. The acoustics of the earmould are an important part of the hearing aid system (Valente *et al.*, 1996).

The purpose of an earmould (Staab and Lybarger, 1994; Valente *et al.*, 1996) is to:

1. direct sound from the receiver to the ear canal efficiently
2. provide an adequate acoustic seal between the hearing aid and the ear
3. make the hearing aid comfortable to wear for prolonged periods
4. prevent feedback
5. minimise any sensation of blockage (the occlusion effect).

Earmoulds should be comfortable, non-allergenic and cosmetically acceptable to the user (Staab and Lybarger, 1994). The patient should be able to insert and remove the earmould by themselves (Roesel, 1994; Valente *et al.*, 1996). The earmould should not injure the ear, and should be hygienic and accurately-fitting.

In general, there are three types of earmould: closed, vented and open, which is essentially an earmould with a large vent, held in place only by the outer rim (Leavitt, 1986; Valente *et al.*, 1996). Open earmoulds are not used with ITE aids, for obvious reasons. The more powerful the aid, the more difficult it is to make an earmould that is entirely free of feedback (Madell and Gendel, 1984). The fit of the earmould should be tight enough to retain the mould within the ear without causing discomfort (Madell and Gendel, 1984). A good acoustic seal reduces the likelihood of feedback (MacKenzie *et al.*, 1989).

The impression of the ear from which the earmould is cast should be a true representation of the outer ear. Any deviations from the shape of the ear may result in greater sound leakage around the mould, causing acoustic feedback. The probability of feedback occurring may be reduced if the patient is asked to move the jaw while the impression material is setting, e.g. by talking, chewing, smiling, turning the head, etc. (Valente *et al.*, 1996). This may allow the impression to account for the way the shape of the ear canal changes with time. The length of the earmould tip will affect the residual volume of the ear canal and hence the amplitude of the SPL in the ear canal. The smaller the residual volume, the greater the sound pressure level (Lybarger, 1979).

When the earmould is in place, the voice of a hearing aid user reaches their own ear canal through four paths (Schweitzer and Smith 1992; Gelfand, 1998):

1. vibration of the cartilaginous portion of the ear canal and the pinna (which is also cartilaginous)
2. vibration of the skull, radiating sound energy into the ear canal through the ear canal walls and stimulating the eardrum and inner ear in the same way as airborne sound (this is known as osseotympanic bone conduction)
3. acoustic transmission through the earmould vent
4. acoustic transmission through the hearing aid itself, i.e. the amplified path.

In addition, the vent transmits sound in opposite directions simultaneously (Dillon, 1991; Valente *et al.*, 1996). It is not easy to separate these components of the sound by analysis. The interaction in the ear canal between the aid-transmitted sound and the vent-transmitted

sound depends on the amplitude and phase of the signals, and on the frequency responses of the hearing aid, the vent and the subject's ear (Tecca, 1992).

The jawbone is hinged exactly at the ear canal, and forms part of the canal walls (the bony, or osseous, inner part of the ear canal) (Westermann, 1987). When the cartilaginous part of the ear canal is blocked (occluded) so that sound cannot escape from the canal, the subject's own voice is amplified at low frequencies as the vibration caused by vocalisation is transmitted to the ear canal either through bone or cartilage. This causes the subject to perceive an "unnatural" quality to their voice, which is termed the occlusion effect (Killion *et al.*, 1988), since it results from occluding the ear canal (Agnew, 1994). Many hearing aid users describe their voice sounding as if it is "in the bottom of a barrel" (Westermann, 1987; Revit, 1992). They perceive their voice to have shifted from the larynx or mouth to the external ear (Schweitzer and Smith, 1992). This is referred to as "lateralisation" (Northern *et al.*, 1991). They may also hear their own pulse, breathing, and other body sounds (Wimmer, 1986). The effect does not occur when the ear canal is unblocked since the open ear canal acts as a high-pass filter, removing the low frequency sound. Sound will always take the path of least resistance; in the unoccluded case, this will be out of the ear canal into the free field. In the occluded case, sound will travel to the eardrum (Staab and Finlay, 1991).

Objective measurements of the occlusion effect found that the SPL in the occluded ear canal could be more than 20 dB greater for low frequencies (i.e. vowel sounds) than that in the unoccluded ear canal (Macrae, 1980; Wimmer, 1986; Westermann, 1987; Revit, 1992). A 10 dB increase is equivalent to an approximate doubling of perceived loudness (Revit, 1992), so the occlusion effect can make sound seem four times as loud with the ear occluded by the hearing aid. The maximum occlusion effect occurs usually in the region of 250 Hz (Killion *et al.*, 1988), although it can be in the range of 500 Hz (Revit, 1992).

As well as suffering from occlusion, hearing aid users may find that the presence of the earmould or shell causes discomfort through a build-up of pressure in the ear canal, perspiration and itching (MacKenzie *et al.*, 1989). These symptoms may be relieved through the use of a pressure vent (Staab and Lybarger, 1994). These vents have a typical diameter of 0.64 - 1 mm. For a medium length earmould tip (about 16.6 mm (Lybarger, 1980)), the use of a pressure vent does not have a significant effect on the acoustic signal of an unvented aid, although it is possible that a slight reduction of usable gain will result (Gatehouse, 1989).

A vent is a tube through the earmould or shell connecting the ear canal with the outside sound field. This has several purposes (Staab and Lybarger, 1994; Valente *et al.*, 1996):

1. static pressure equalisation between pressure in the ear canal and outside the ear
2. reduction or elimination of the occlusion effect
3. modification of the low frequency response using resonance due to the Helmholtz cavity formed by the vent and ear canal, which can be controlled by the dimensions of the vent
4. to allow unamplified signals to reach the ear canal directly
5. ventilation to reduce the build-up of moisture in the ear canal
6. to provide better perceived sound quality and subjective impression of speech intelligibility than that experienced with a closed earmould due to the occlusion effect
7. medical reasons (such as alleviation of chronic middle ear conditions) (MacKenzie *et al.*, 1989).

Vents can be parallel or diagonal, i.e. either parallel to the tube connecting the receiver output to the ear canal (the receiver tube) or intersecting the receiver tube at a point between the two ends of the tube (Figure 1.4) (Valente *et al.*, 1996). Diagonal venting reduces the amount of gain available at high frequencies which is required for many hearing aid users with high-frequency hearing loss (Valente *et al.*, 1996). As a result of this, parallel venting is preferred in general to diagonal venting, which often is used only if the ear canal is too small to use a parallel vent. It should be noted that the computer model described in Chapter 2 uses a parallel vent; this is the simpler case to model.

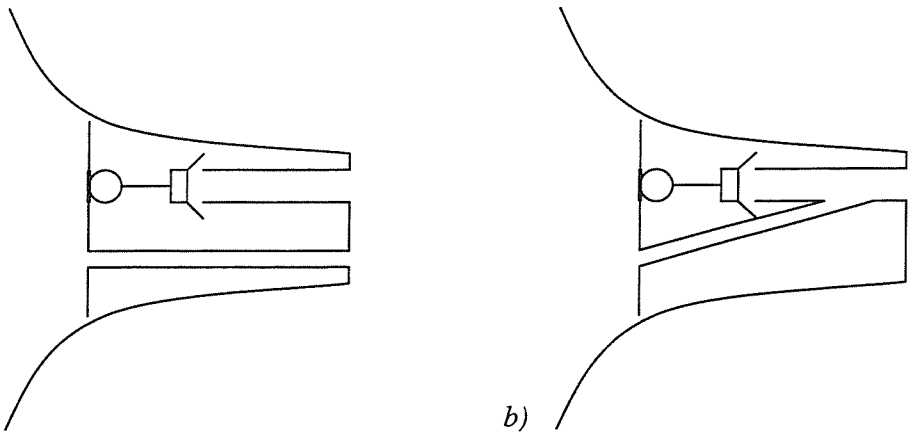

Figure 1.4: Simplified diagram of an ITE hearing aid showing a) parallel venting; b) diagonal venting

The dimensions of the vent affect the frequency response of the hearing aid (Kates, 1988b), causing significant changes from the desired response due to the resonances and antiresonances of the vent and of the Helmholtz resonator formed by the vent and ear canal

(Agnew, 1994; Valente *et al.*, 1996). The amplitude of the high frequency response of the feedback path increases as the tubing diameter increases (Kates, 1991) and venting lowers the gain at which acoustic feedback may occur (Gatehouse, 1989). The vent behaves as an acoustic mass which increases in impedance as its diameter decreases (Leavitt, 1986). This means that low frequency sound can escape through the vent more easily than high frequencies, i.e. the vent acts as a low-pass filter for sound travelling from the ear canal to the external sound field. The size of the vent determines the magnitude of this filtering effect. Vents with short length or large diameter have lower impedance and allow more low frequency sound to pass out into the free field (Leavitt, 1986; Hellgren *et al.*, 1999b). The occlusion effect can be reduced by reducing the input impedance of the earmould vent. This can be done by increasing its diameter or decreasing its length (Hellgren *et al.*, 1999b). The drawback is that this will increase the probability that acoustic feedback will occur. A balance between feedback and occlusion must be reached. In general, feedback is a problem at high frequencies, whereas the occlusion effect is greatest at low frequencies. To improve the hearing aid's performance with respect to both these problems, the vent input impedance would have to be high at high frequencies to reduce the likelihood of feedback and low at low frequencies to reduce the occlusion effect (Hellgren *et al.*, 1999b).

Changes in the physical configuration of the hearing aid can be used to reduce acoustic feedback, though the effects of these changes are limited. Although acoustic damping could be added to hearing aid tubing to smooth peaks in the real ear response of the hearing aid (Kates, 1999), in general this is not possible for ITE aids (Staab and Lybarger, 1994). Reducing the distance between the output of the receiver tube and the eardrum has been found to reduce reflections and produce a smoother response (Staab and Lybarger, 1994; Valente *et al.*, 1996).

Although it is desirable for the earmould to fit the ear as well as possible, unintentional slit leaks around the earmould often occur, typically equivalent to a vent 1.4 mm in diameter and 22 mm in length (Johansen, 1975). The effect of this leakage on the feedback path response is significant for vented aids compared to the response obtained with a tightly sealed earmould (Tecca, 1991). The SPL in the ear canal and the magnitude of the vent-associated Helmholtz resonance are reduced as the size of the leak increases (Leavitt, 1986). The magnitude of the vent-associated resonance for a deliberately vented earmould is not noticeably affected by sealing around the mould to minimise unintentional leakage. However, the presence of the leakage shifts the resonance peaks to higher frequencies. This effect is more noticeable for earmoulds with intentional vents of less than 3 mm diameter (Tecca, 1991). A large leak

caused by the user fitting the aid poorly can result in acoustic feedback (MacKenzie *et al.*, 1989). Some degree of venting is necessary to improve comfort, e.g. by relieving pressure in the ear canal, or to reduce the occlusion effect. The effects of vent size on the feedback path will be investigated with the computer model described in Chapter 2.

Often, it is not possible to easily determine the cause of feedback (Madell and Gendel, 1984). Apart from the effect of deliberate venting, common causes are:

1. an imperfect seal around the earmould
2. radiation of sound through the walls of the earmould tubing
3. internal feedback (electrical and mechanical) within the aid itself
4. the effect of excess cerumen (ear wax) within the ear canal or fluid in the middle ear on the behaviour of the aid response
5. a combination of any of these.

The factors which cause acoustic feedback affect the *in situ* hearing aid response for a gain setting below that which results in audible whistling (Cox, 1982). This suboscillatory feedback often affects the response of the hearing aid in the form of large peaks or undesirable transient distortions in the frequency response (Schweitzer and Smith, 1992). This can cause the user to complain of "ringing" or "echoing" qualities to perceived signals such as speech.

Although there are several other types of feedback present in the hearing aid system, e.g. mechanical and electrical, the best approach is to minimise paths of airborne sound transmission between the ear canal and the external sound field, since acoustic feedback is the most significant and the easiest type of feedback to deal with (Macrae, 1991).

1.4 Methods of feedback cancellation

Feedback is a major problem for hearing aid users. Oscillation occurs when the open-loop gain exceeds 0 dB and the phase is a multiple of 360° (Nyquist, 1932). The feedback signal must be cancelled or reduced in order that higher gains can be used before feedback or suboscillatory feedback occurs. Various methods of feedback cancellation have been developed, with adaptive methods being the most popular. A new method of adaptive feedback cancellation is developed in this thesis which uses a different approach to the conventional methods summarised in this section.

The simplest way to avoid oscillation is to reduce the gain of the hearing aid, thus reducing the open-loop gain so that the aid remains in stable operation. However, this compromises the effectiveness of the device and the user does not get the full benefit (Egolf, 1982). If the gain used in normal operation brings the system close to instability, it can be inferred that the user requires a higher gain than the aid can provide (Maxwell and Zurek, 1995). A variation of this approach is to reduce the gain only in the frequency sub-band at which instability occurs, but this degrades the effectiveness of the aid at that frequency and may lose information from the desired signal in that sub-band.

A more sophisticated alternative to gain reduction is the use of an adaptive notch filter to track and remove the high amplitude peak characteristic of feedback (Egolf, 1982; Bustamante *et al.*, 1989; Agnew, 1993; Maxwell and Zurek, 1995). However, the notch filter will remove desired information at the notch frequency as well as the feedback signal, causing distortion of the desired signal. It cannot strictly be classed as a method of feedback cancellation since it is merely a modification of the forward path through the hearing aid so that it is stable in conjunction with the feedback path (Maxwell and Zurek, 1995). In general, it is preferable to cancel the entire feedback signal rather than attempt to remove the tonal components of acoustic feedback; it is possible that some desired signals, such as alarm signals, will be tonal and should not be cancelled (Kates, 1991).

Other approaches to feedback control modify the output signal by such methods as frequency shifting, phase shifting and modulation of the frequency of the output signal about the frequency of the input signal (Egolf, 1982; Joson *et al.*, 1993). These methods were intended to maintain stability according to Nyquist's stability criterion (Nyquist, 1932), but were found to degrade the desired signal by introducing beating or ringing effects and to reduce the intelligibility of speech signals, all of which would be annoying to the hearing aid user.

Most current methods of feedback cancellation use adaptive filtering. Adaptive algorithms are used to maintain good performance when changes occur in a system. In the context of feedback control, adaptive filters are used to track changes in the feedback path and cancel the feedback signal. At high gains, the stability of the hearing aid system requires close agreement between the response of the actual feedback path and the adaptive filter, as oscillation is more likely to occur at such gain levels. At lower gains, the agreement can be poorer without oscillation occurring (Kates, 1999). However, feedback is a problem for many hearing aid users with severe hearing loss who require high gains, so it is important for the adaptive filter to be designed to be in good agreement with the actual feedback path. An

adaptive feedback cancellation system should increase the usable gain of the hearing aid while preserving speech intelligibility and the subject's awareness of the acoustic environment (Kates, 1991). The algorithm must improve stability while not corrupting the desired signal, i.e. the quality of the output signal reaching the ear must be considered as well as increasing the stable gain of the hearing aid. A practical system for general use should work with any type of hearing aid for any real ear and should be computationally efficient so that it can be implemented on a DSP chip within the aid and work in real time.

Adaptive feedback cancellation systems estimate the feedback signal by filtering the output of the hearing aid with a model of the transfer function of the acoustic feedback path. The estimated signal is then subtracted from the hearing aid input signal (Maxwell and Zurek, 1995) (Figure 1.5). The aim of the feedback cancellation algorithm is usually the minimisation of the error signal, defined as the difference between the desired signal, i.e. the actual feedback signal, and the estimated feedback signal. A good estimate will cancel the effects of the feedback signal, leaving the amplified desired input signal only.

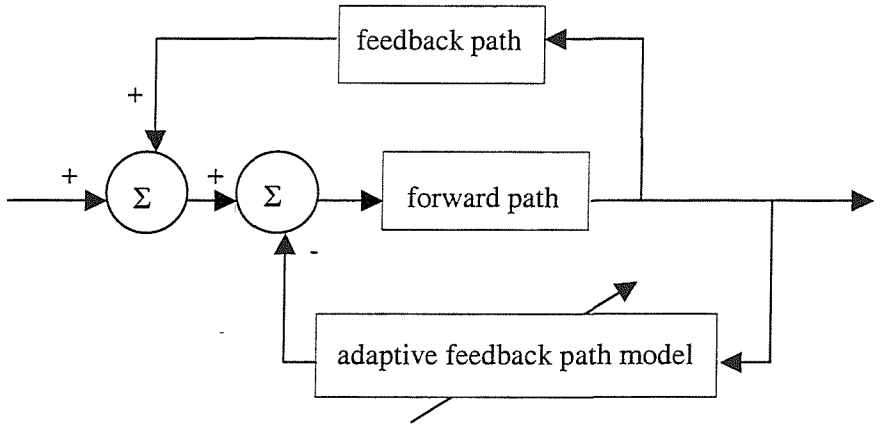

Figure 1.5: Schematic diagram of a hearing aid with adaptive feedback cancellation

Adaptation must be able to take place in the presence of ambient signals since the user will rarely be in a completely quiet acoustic environment (Maxwell and Zurek, 1995). The presence of ambient stimuli at the hearing aid microphone as well as the feedback signal can degrade the performance of adaptive feedback cancellation systems. This can be considered as the interference of uncorrelated signals with the adaptation process, resulting in fluctuations in the filter weights around the optimal values, i.e. misadjustment (Maxwell and Zurek, 1995). The performance of adaptive feedback cancellation may be degraded if the desired input signal is sinusoidal, as the adaptive system may track and cancel the input signal rather than the feedback path (Kates, 1991). Also, some changes in the feedback path

can be very fast and the adaptive feedback cancellation algorithm may not converge quickly enough to cancel these changes.

There are two main types of adaptive cancellation methods: continuous and non-continuous adaptation. Non-continuous adaptive feedback cancellation systems break the signal path (i.e. suspend the normal operation of the hearing aid) when a certain condition is met, usually the detection of strong oscillation or, additionally, a period of quiet in which interruption of the feedback path would not affect the intelligibility of the desired input signal (Kates, 1991; Maxwell and Zurek, 1995; Greenberg *et al.*, 2000). A broadband noise probe is passed through the system and the filter coefficients are adapted to give an estimate of the feedback path. On completion of the adaptation, the hearing aid resumes its normal processing. The probe noise may need to have a high level to allow accurate estimation of the feedback path, so it must be of short duration if degradation of the ratio of the desired acoustic signal to the probe noise signal (acoustic signal to noise ratio (SNR)) is to be avoided. Shaping the probe noise to parallel the absolute threshold of each ear, using psychoacoustic effects such as masking, may be beneficial in maintaining a good acoustic SNR (Greenberg *et al.*, 2000; Hellgren, 2002). Non-continuous adaptation has the advantage of interrupting the feedback loop at the onset of oscillation (Maxwell and Zurek, 1995), eliminating oscillation at maximum gain and improving the acoustic SNR during estimation (Kates, 1991). However, changes may occur in the feedback path which degrade the output signal without being detected by the adaptive feedback cancellation system, e.g. suboscillatory feedback (Cox, 1982).

Since many hearing impaired people have difficulty understanding speech in the presence of background noise, quiet-period adaptation would be of little use in the acoustic environments in which the user requires most assistance. Higher amplitude probe noise would be required in the presence of background noise and this would degrade the acoustic SNR. Informal studies indicated that subjects found probe noise annoying and the interruptions of the input signal had an adverse effect on speech intelligibility (Greenberg *et al.*, 2000). Feedback detection could be suspended for a short period of time after updating the filter coefficients so that the input signal would not be repeatedly interrupted, for example if the input signal were a sinusoid (Kates, 1991). However, this could result in instability occurring while the adaptation was suspended.

Continuous adaptation systems adjust the adaptive filter weights continually, simultaneously processing the input signal (Bustamante *et al.*, 1989; Engebretson *et al.*, 1990; Dyrlund and

Bisgaard, 1991; Bisgaard, 1993; French-St. George *et al.*, 1993; Maxwell and Zurek, 1995). This method has the advantage of accounting for small changes in the feedback path that affect the desired signal adversely without causing instability, i.e. suboscillatory feedback (Kates, 1991), and does not interrupt the desired input signal. Probe noise may or may not be used to determine the response of the feedback path (Bustamante *et al.*, 1989; Engebretson *et al.*, 1990; Dyrlund and Bisgaard, 1991). A reference path delay is used frequently to compensate for the delay associated with the feedback path (Maxwell and Zurek, 1995).

Continuous adaptation may be unable to reduce the correlation between the error signal and the input signal (Greenberg *et al.*, 2000), leading to bias in the filter estimate (Kates, 1999). With a short filter length, correlation inherent in a sinusoidal ambient signal (e.g. an alarm signal or tonal signals in music) cannot be reduced. Increasing the filter length causes the algorithm to reduce the error signal by cancelling the sinusoid. A delay can be inserted into the system to decorrelate the component of the desired signal in the error signal from the input signal to the adaptive filter (Bustamante *et al.*, 1989; Kates, 1999; Greenberg *et al.*, 2000). Care must be taken to ensure that the delay is not so long that it has an adverse effect on perception of the desired signal. If the delays are not chosen carefully, the adaptive filter is unable to model the feedback path sufficiently to reduce the correlation and the hearing aid system becomes unstable. The choice of delays is also important in non-continuous adaptation, but instability does not occur as a result of a poor choice of delays with that method (Greenberg *et al.*, 2000). Bias can also be due to an error in the estimate of the input signal used in the calculation of the estimated feedback path (Hellgren and Forsell, 2001). Continuous adaptation with a sinusoidal input signal can lead to unwanted artefacts as well as undesired cancellation of the input signal. One method to prevent this is the constraint of the adaptive filter weights so that they do not deviate excessively from a reference set of weights obtained by measuring the feedback path with a broadband noise probe in optimum conditions (i.e. in the absence of ambient noise) (Kates, 1999).

A closed-loop feedback path could be modelled by an infinite impulse response (IIR) filter, including the poles of the transfer functions of the receiver, the acoustic feedback path through the vent and the microphone. However, even with a small step size, the adaptive system could be unstable. Lattice structures could be used to ensure stability, but this would require a great computational load (Kates, 1991), hence it is more efficient for a feedback cancellation system to use a non-recursive filter. Again, the large computational loads associated with adaptive lattice and delay line structures must be avoided (Kates, 1991), so the Least Mean Square (LMS) algorithm (Widrow and Stearns, 1985), or one of its variants,

is often preferred over more sophisticated algorithms to estimate the optimum set of filter weights, based on the correlation between the error signal and the output of the hearing aid system. It is computationally efficient and suitable for use in a hearing aid with limited processing power (Kates, 1999).

Currently, the most popular method of adaptive feedback cancellation is the direct method, i.e. continuous adaptation in closed loop, with no probe noise (Kates, 1999; Hellgren and Forsell, 2001; Hellgren, 2002). The estimate of the feedback path is usually obtained with an FIR filter using a variant of the LMS algorithm.

To summarise, the aim of feedback control in hearing aids is to remove the effects of acoustic feedback while preserving the desired input signal (usually speech) without interference effects, reduced intelligibility or loss of information (Kates, 1991, 1999). Several studies have shown that it is preferable to do this without introducing excessive noise (e.g. probe noise for determining the feedback path response) which the hearing aid users would find irritating or an impairment of intelligibility (Kates, 1999; Greenberg *et al.*, 2000). A practical system must operate in real time and be small enough to be implemented within the signal processing of the device itself (Kates, 1991). Successful feedback reduction allows the use of higher gains with an open vent, thus increasing audibility and intelligibility with a more comfortable hearing aid fitting (Greenberg *et al.*, 2000). Note that not all subjects will receive the same amount of benefit from a particular cancellation method, depending on the severity of their hearing loss and other factors such as the transducers within the hearing aid (Greenberg *et al.*, 2000).

The method of adaptive feedback cancellation presented in this thesis differs from conventional methods by using knowledge of the physical parameters in the hearing aid system to produce a modelled feedback path from which the cancellation filter is formed. Conventional methods have no prior knowledge of the factors affecting the feedback path and simply act on the feedback signal. The work presented here is a feasibility study of the new parametric adaptive algorithm

1.5 Adaptive filters

Adaptive filters are widely used in feedback cancellation, with many methods using variants of the Least Mean Square (LMS) algorithm (Kates, 1999). The optimal filtering problem and the LMS algorithm are summarised in this section. These topics are not discussed in detail here since they are widely known. The reader is referred to Widrow and Stearns (1985) for

further information throughout this section. The parametric adaptive algorithm developed in this thesis is based on the method of steepest descent and its performance is compared with that of the LMS algorithm in the feasibility study presented in Chapters 8 and 9.

Consider the system in Figure 1.6:

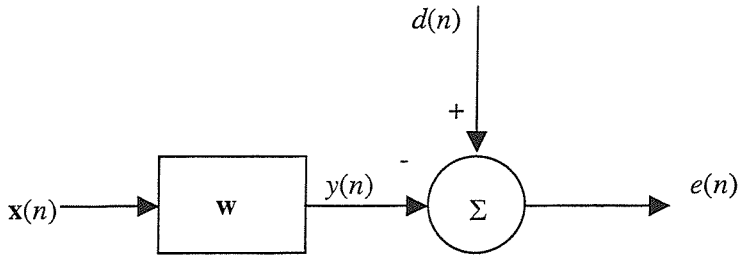

Figure 1.6: Optimal filtering configuration for an adaptive system

$\mathbf{x}(n)$ is the N x 1 vector of input signal. $\mathbf{w}$ is the N x 1 vector of filter coefficients, $y(n)$ is the filtered output signal, $d(n)$ is the desired signal and $e(n)$ is the error signal, where

$$e(n) = d(n) - y(n) \qquad (1.1)$$

The algorithm used to adjust the system parameters needs a clear objective, which is usually the minimisation of some cost function or error function, or the maximisation of some fitness function. Plotting the cost function against the adapting parameters produces an error surface or performance surface. This may have local minima as well as a global minimum.

A simple, widely used method of adapting parameters to reduce the cost function and travel down the error surface towards the global minimum is the method of steepest descent or gradient descent:

new parameter = old parameter - α (local gradient)

α is the convergence coefficient. The local gradient is defined as ∂(cost function) / ∂(parameter) evaluated at the current parameter value.

For reliable convergence, α must be positive but not too large, and the error surface must be unimodal or convex, i.e. must not have any local minima.

For the system in Figure 1.6 above, a suitable cost function to minimise would be the mean square error:

$$J = E\left[e^2(n)\right] \tag{1.2}$$

$e(n)$ is given by Equation (1.1).

The desired signal, $d(n)$, may be used to train the filter, as in an identification application, or may represent an unwanted signal to be cancelled, such as in a noise cancellation application.

For an FIR (finite impulse response) filter with all signals steady,

$$y(n) = \mathbf{w}^T \mathbf{x}(n) = \mathbf{x}^T(n)\mathbf{w} \tag{1.3}$$

So the error signal can be written as:

$$e(n) = d(n) - \mathbf{w}^T \mathbf{x}(n) = d(n) - \mathbf{x}^T(n)\mathbf{w} \tag{1.4}$$

and

$$e^2(n) = \left(d(n) - \mathbf{w}^T \mathbf{x}(n)\right)\left(d(n) - \mathbf{x}^T(n)\mathbf{w}\right) = \mathbf{w}^T \mathbf{x}(n)\mathbf{x}^T(n)\mathbf{w} - 2\mathbf{w}^T \mathbf{x}(n)d(n) + d^2(n) \tag{1.5}$$

Taking the mean across all samples (the expectation value):

$$J = E\left[e^2(n)\right] = \mathbf{w}^T \mathbf{R}\mathbf{w} - 2\mathbf{w}^T \mathbf{p} + c \tag{1.6}$$

$\mathbf{R}$ is the N x N matrix of autocorrelation functions of the input (reference) signals:

$$\mathbf{R} = E\left[\mathbf{x}(n)\mathbf{x}^T(n)\right] \tag{1.7}$$

$\mathbf{p}$ is the vector of cross-correlations between the reference and desired signals:

$$\mathbf{p} = E\left[\mathbf{x}(n)d(n)\right] \tag{1.8}$$

The constant $c = E[d^2(n)]$ is the value of J when $\mathbf{w} = \mathbf{0}$.

The cost function J has quadratic dependence on the gain $\mathbf{w}$. The variation of the cost function with a single filter coefficient is a quadratic curve. With two coefficients, it is a quadratic surface. Generalising further, with N coefficients, it is an N-dimensional surface in $(N+1)$-dimensional space. The optimum value of $\mathbf{w}$ is found by calculating the gradient of J with respect to $\mathbf{w}$ and setting it to zero, i.e. finding the minimum.

The filter minimising the mean square error (m.s.e.) must have

$$\frac{\partial J}{\partial w_i} = 0 \text{ for } i = 0, 1, \ldots, I - 1 \qquad (1.9)$$

This optimum least squares solution is known as the Wiener filter.

The gradient vector, **g**, is defined as:

$$\mathbf{g} = \left[\frac{\partial J}{\partial w_0} \frac{\partial J}{\partial w_1} \cdots \frac{\partial J}{\partial w_{I-1}} \right]^T = 2\mathbf{R}\mathbf{w} - 2\mathbf{p} \qquad (1.10)$$

The Wiener filter is found by setting each element of **g** to zero, so that

$$2\mathbf{R}\mathbf{w}_{opt} - 2\mathbf{p} = 0 \qquad (1.11)$$

Therefore

$$\mathbf{w}_{opt} = \mathbf{R}^{-1}\mathbf{p} \qquad (1.12)$$

The Wiener filter is the set of filter coefficients, $\mathbf{w}_{opt}$, giving the lowest m.s.e. at the minimum of the error surface. This is the optimum least squares solution to the FIR filtering problem. Many auto- and cross-correlation coefficients need to be calculated and an I x I matrix must be inverted, so the Wiener filter is generally unsuitable for online calculation.

The Least Mean Square (LMS) algorithm (Widrow and Stearns, 1985) is a widely used practical alternative to the Wiener filter. It is based on the method of steepest descent and updates the estimated filter coefficients so that they converge towards the optimal solution. The aim is that the m.s.e. should decrease after every iteration on average so that $J \rightarrow 0$. The filter coefficients are updated according to:

$$\mathbf{w}(n+1) = \mathbf{w}(n) + \alpha e(n)\mathbf{x}(n) \qquad (1.13)$$

where α is the convergence coefficient. A practical condition for convergence and stability for a filter of length N is:

$$0 < \alpha < \frac{2}{N\sigma_x^2} \qquad (1.14)$$

The average convergence behaviour of the LMS algorithm is the same as that of the method of steepest descent, i.e. its average gradient is the true gradient $E[e(n)\mathbf{x}(n)]$. However, its instantaneous value is noisy. The amount of noise can be reduced by using smaller α, but this means the algorithm will not converge as quickly. If the input signal power, σ_x^2, fluctuates, the speed of convergence will fluctuate. If σ_x^2 is unknown, we cannot choose α to ensure stability.

The normalised LMS (NLMS) algorithm is used to circumvent these problems:

$$\mathbf{w}(n+1)=\mathbf{w}(n)+\frac{\alpha_0}{\hat{\sigma}_x^2}e(n)\mathbf{x}(n) \qquad (1.15)$$

α_0 is a new convergence coefficient. $\hat{\sigma}_x^2$ is an estimate of the power of the signal at the n^{th} iteration. The rectangular windowed estimate is widely used:

$$\hat{\sigma}_x^2=\frac{1}{L}\sum_{i=0}^{L-1}x(n-i)^2=\frac{\mathbf{x}^T(n)\mathbf{x}(n)}{L} \qquad (1.16)$$

Therefore the normalised LMS algorithm can be written as:

$$\mathbf{w}(n+1)=\mathbf{w}(n)+\frac{\alpha_0}{\mathbf{x}^T(n)\mathbf{x}(n)+\varepsilon}e(n)\mathbf{x}(n) \qquad (1.17)$$

where L is incorporated into α_0, or it can be written as Equation (1.13) with

$$\alpha=\frac{\alpha_0}{\mathbf{x}^T(n)\mathbf{x}(n)+\varepsilon} \qquad (1.18)$$

ε is a small constant used to ensure that division by zero does not occur.

When $\hat{\sigma}_x^2$ is large, α is reduced; when $\hat{\sigma}_x^2$ is small, α is increased. Therefore the rate of convergence is constant even when the input signal power is fluctuating.

1.6 Conclusions

The anatomy and physiology of the human ear have been discussed to provide an understanding of terms used throughout this thesis. The problems associated with the use of hearing aids have been examined. Acoustic feedback is one of the greatest problems; past and current methods for feedback control in hearing aids have been presented, followed by a summary of adaptive filtering methods used in common feedback cancellation algorithms.

2 Computer model of an in situ in-the-ear hearing aid system

2.1 Introduction

This chapter explores a typical in-the-ear hearing aid system. This system is used throughout the thesis, so an understanding of it is essential. Mathematical models of each component of the system are revised, followed by the development of a two-port network model of the feedback path. This model forms the basis of the new parametric adaptive feedback cancellation algorithm presented in this thesis.

Computer models have been used previously to investigate the behaviour of hearing aid systems (Egolf, 1976; Bade *et al.*, 1984; Kates, 1988a, 1988b, 1990; Egolf *et al.*, 1989). Some of this work examined the feedback behaviour of hearing aids (Egolf *et al.*, 1989; Kates, 1991). The main advantage of a comprehensive, validated model of the complete *in situ* hearing aid system is that, unlike experimental work, it allows investigation of the effects of specific aspects of the system on the feedback path while keeping all other parts constant.

The model can be used to determine which components of the hearing aid system are likely to cause the greatest changes in the feedback path, and which of these changes are likely to result in the system becoming unstable. In this thesis, the model is used to develop a method of feedback cancellation which adapts physical parameters instead of filter coefficients to model changes in the actual feedback path (see Chapters 7 – 9). Ultimately, it is intended that this should result in faster adaptation and cancellation while remaining robust to changes in the feedback path, i.e. remaining stable even if there are some small differences between the model and the actual feedback path while the model is in the process of adapting to the changes.

The model developed here combines the MATLAB and PSpice software packages. MATLAB is a flexible mathematical and analytical tool, and PSpice is a powerful circuit simulator used by the manufacturers of hearing aid transducers to model the components. The program gives the user control over the transducers, tubing dimensions and impedances within the model. The derivation of the model itself is not new, but this combination of software packages is a novel approach.

2.2 The *in situ* in-the-ear hearing aid system

A typical full concha in-the-ear (ITE) hearing aid system on which the model is based is shown in Figure 2.1. This is a simplified representation, excluding any digital processing that may be included in commercial devices at the amplification stage.

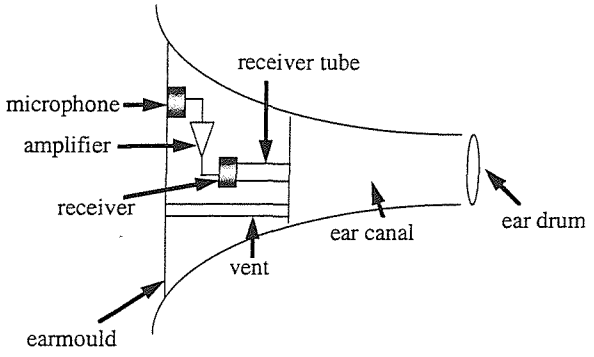

Figure 2.1: Schematic diagram of a typical in-the-ear hearing aid system

A block diagram of the system is shown in Figure 2.2, based on that presented by Egolf *et al.* (1989). Each block can be represented mathematically, except the incident path, which is not examined here.

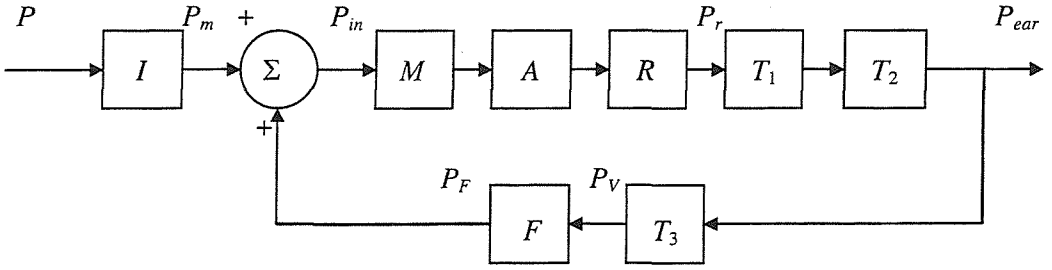

Figure 2.2: Block diagram of ITE hearing aid system shown in Figure 2.1

P is the sound pressure at a distant point in space. I is the incident path transfer function which transforms sound pressure at a distant point in space to sound pressure P_m at the microphone input. P_{in} is the sound pressure at the microphone input following summation of pressures. M is the microphone transfer function. A is the amplifier transfer function. R is the receiver (hearing aid loudspeaker) transfer function. P_r is the sound pressure at the receiver output. T_1 is the transfer function of the receiver tube. T_2 is the transfer function of the ear canal. P_{ear} is the sound pressure in the ear canal near the eardrum. T_3 is the transfer function of the earmould vent. P_V is the sound pressure at the vent output. F is the transfer function of the external acoustic feedback path from the vent exit to the microphone input. P_F is the sound pressure at the microphone input due to the acoustic feedback path. All sound pressures and impedances are complex.

2.3 Two-port network theory

Each block in Figure 2.2 (apart from the incident path, *I*) is modelled in this thesis using two-port network transfer functions. This section revises two-port network theory. A two-port network, or fourpole, is a set of expressions linking the amplitudes of a wave process at the input to a system to those at the output (Rschevkin, 1963). Two-port networks are used in electrical and acoustic applications, and allow impedance loading between system components to be accounted for (Egolf *et al.*, 1989). Each part of the hearing aid can be considered as a "black box", a component for which only the input and output parameters are known. Consider the electrical example (Attia, 1999), with input voltage and current V_i, I_i and output voltage and current V_o, I_o. Note that current flowing *out of* the box is described as positive, so I_o is positive.

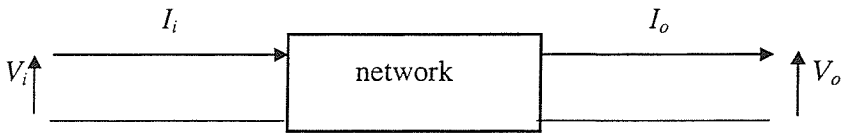

Figure 2.3: Simple two-port network

The two-port network describing the "black box" is:

$$\begin{bmatrix} V_i \\ I_i \end{bmatrix} = \begin{bmatrix} A & B \\ C & D \end{bmatrix} \begin{bmatrix} V_o \\ I_o \end{bmatrix} \qquad (2.1)$$

This gives the equations:

$$V_i = AV_o + BI_o \qquad (2.2)$$

$$I_i = CV_o + DI_o \qquad (2.3)$$

For a high load impedance, i.e. an open circuit at the output, I_o is zero, which gives:

$$V_i = AV_o \qquad (2.4)$$

$$I_i = CV_o \qquad (2.5)$$

For a low load impedance, i.e. a short circuit at the output, V_o is zero, giving:

$$V_i = BI_o \qquad (2.6)$$

$$I_i = DI_o \tag{2.7}$$

Rearranging Equations (2.4) - (2.7), the two-port parameters for the "black box" are:

$$A = \left.\frac{V_i}{V_o}\right|_{I_o=0} \tag{2.8}$$

$$B = \left.\frac{V_i}{I_o}\right|_{V_o=0} \tag{2.9}$$

$$C = \left.\frac{I_i}{V_o}\right|_{I_o=0} \tag{2.10}$$

$$D = \left.\frac{I_i}{I_o}\right|_{V_0=0} \tag{2.11}$$

These equations can be applied to the microphone and receiver, and to the acoustic components of the feedback path, such as the tubes, allowing derivation of their two-port parameters. Sound pressure and volume velocity are analogous to voltage and current respectively.

Two-port blocks of this form can be cascaded, i.e. connected in series. The two-port matrix describing the entire system can be obtained by matrix multiplication of the component blocks.

2.4 The open-loop transfer function and Nyquist's stability theory

The likelihood of the hearing aid system becoming unstable is given by Nyquist's stability theory (Nyquist, 1932), which uses the open-loop transfer function (OLTF) of the feedback path to determine the frequencies at which instability is most likely to occur. This section presents this theory and describes the OLTF.

The *in situ* ITE hearing aid system can be represented as a two-port network, excluding the incident path, *I*, and the summation of pressures from Figure 2.2. Figure 2.4 shows the position of the cut in the feedback path used to obtain the OLTF. Figure 2.5 describes the OLTF of the feedback path system. Note that the termination by an infinite impedance Z_∞ indicates that the path has been cut, i.e. an open circuit. u_{in} is the input particle velocity and u_F is the output particle velocity; both are complex. P_F is the sound pressure at the output of

the two-port network. Z_T is the acoustic impedance of the middle ear, and Z_V is the acoustic impedance of the vent exit, i.e. the vent radiation impedance converted to an acoustic load (see Section 2.6).

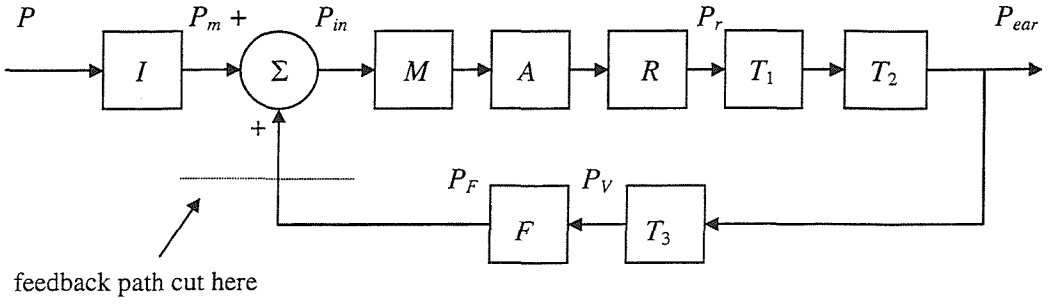

Figure 2.4: Feedback path cut in the external acoustic feedback path to obtain the open-loop transfer function

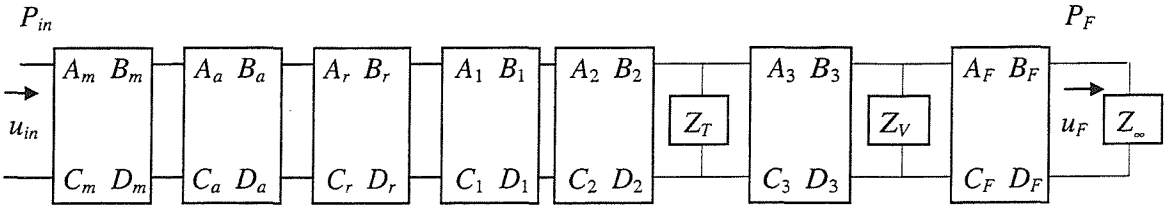

Figure 2.5: Two-port diagram of the open-loop transfer function of the hearing aid system

The load impedances Z_T and Z_V can be converted to two-port blocks (Figure 2.6). Each block can be represented as a 2 x 2 matrix. The OLTF is found by multiplication of the matrices.

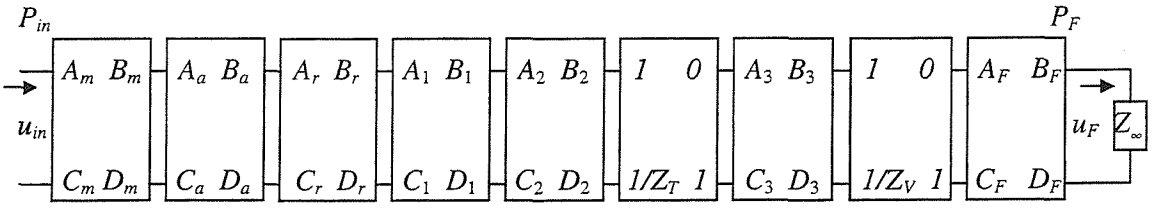

Figure 2.6: Two-port diagram of the OLTF with converted load impedances

The OLTF is a complex quantity with magnitude $|G|$ and phase $\angle G$ (Egolf *et al.*, 1989), such that:

$$G = |G| e^{j\angle G} \qquad (2.12)$$

Nyquist's stability theory (Nyquist, 1932) states that the open-loop system will be unstable if the (-1, 0) point on the Nyquist plot is encircled. For most systems, instability will occur when

$$20 \log_{10} |G| \geq 0 \text{ dB} \qquad (2.13)$$

and

$$\angle G = m\,360°,\ m = 0, 1, 2, 3, \ldots \qquad (2.14)$$

An unstable system is one for which a small input disturbance produces a non-decaying response of infinite duration or level. This response may increase until it reaches the limit of the amplifier (Nyquist, 1932).

The feedback path can be cut and opened out to give the OLTF in this way since the output particle velocity u_F is approximately zero before the path is cut. If we consider Figure 2.5, it can be seen that both the input particle velocity u_{in} and the output particle velocity u_F are present at the microphone input. Miniature hearing aid microphones, such as the one described below, draw little particle velocity from the surrounding sound field due to the small diameter of the input port, so $u_{in} = u_F \approx 0$ (Egolf *et al.*, 1988a).

2.5 The measurable feedback path

The OLTF described in Section 2.4 is given by the response of the ratio of the pressure at the microphone input due to the feedback path to the pressure at the microphone input due to the incident path. It is not easy to measure this, since both these pressures would occur simultaneously at the same point in space and it would not be possible to separate them (Egolf *et al.*, 1989). Also, the small size of the microphone input port would mean that the sound field would be disturbed by the introduction of a probe microphone. Therefore, another method must be used. The feedback path can be cut electrically between the transducers and measured directly with a spectrum analyser. Although this is not the true OLTF, if the model predicts the measured feedback path response accurately, it can be used to simulate the actual OLTF (Egolf *et al.*, 1989). The parametric adaptive feedback cancellation method presented later in this thesis uses this measurable feedback path. Figure 2.7 shows the electrically-cut feedback path.

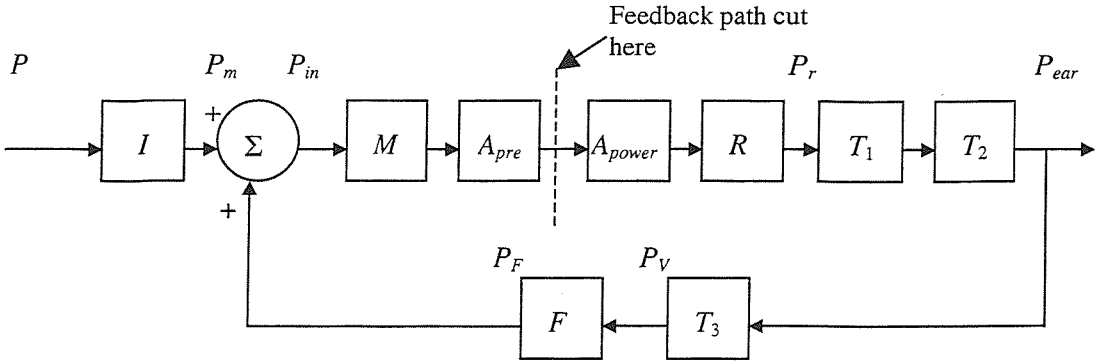

Figure 2.7: Block diagram of the electrically-cut feedback path

The amplifier block, A, can be considered as a pre-amplifier, A_{pre}, in series with a power amplifier, A_{power}. The loop is cut between these, as shown in Figure 2.7. The pre-amplifier has a low output impedance and the power amplifier has a high input impedance. Cutting the loop in this way is equivalent to preceding the power amplifier with a voltage source and terminating the path after the pre-amplifier with an infinite impedance load. The measurable feedback path considered here omitted the hearing aid amplifier and any internal signal processing for simplicity. Experimentally, the output of the spectrum analyser was connected to the receiver input and the microphone output was connected to the input of the analyser. The amplification within the analyser was therefore omitted from the model of the hearing aid feedback path. The two-port network representation of the measurable feedback path is shown in Figure 2.8.

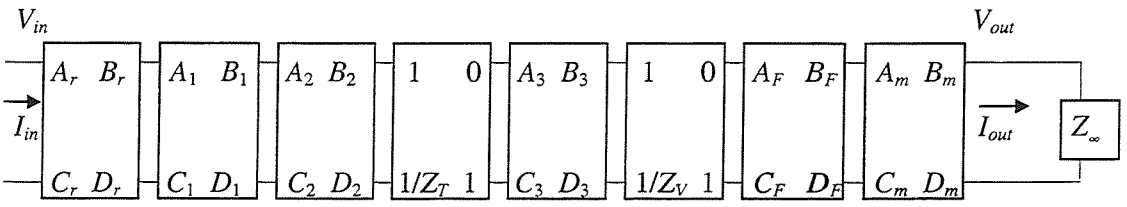

Figure 2.8: Two-port diagram of the measurable feedback path with converted load impedances

The matrix describing the entire measurable feedback path is calculated by the multiplication of all the component matrices at each frequency:

$$\begin{bmatrix} A_{total} & B_{total} \\ C_{total} & D_{total} \end{bmatrix} = \begin{bmatrix} A_r & B_r \\ C_r & D_r \end{bmatrix} \begin{bmatrix} A_1 & B_1 \\ C_1 & D_1 \end{bmatrix} \begin{bmatrix} A_2 & B_2 \\ C_2 & D_2 \end{bmatrix} \begin{bmatrix} 1 & 0 \\ 1/Z_T & 1 \end{bmatrix} \begin{bmatrix} A_3 & B_3 \\ C_3 & D_3 \end{bmatrix} \begin{bmatrix} 1 & 0 \\ 1/Z_V & 1 \end{bmatrix} \begin{bmatrix} A_F & B_F \\ C_F & D_F \end{bmatrix} \begin{bmatrix} A_m & B_m \\ C_m & D_m \end{bmatrix} \quad (2.15)$$

The voltage and current at the microphone output are related to those at the receiver input by:

$$\begin{bmatrix} V_{in} \\ I_{in} \end{bmatrix} = \begin{bmatrix} A_{total} & B_{total} \\ C_{total} & D_{total} \end{bmatrix} \begin{bmatrix} V_{out} \\ I_{out} \end{bmatrix} \tag{2.16}$$

The feedback path response is given at each frequency, f, by:

$$\frac{V_{out}(f)}{V_{in}(f)} = \frac{1}{A_{total}(f)} \tag{2.17}$$

We shall consider the methods used to model each block before calculating the feedback path response.

2.6 Components of the *in situ* in-the-ear hearing aid system

In this section, the two-port network parameters are derived for each of the components of the hearing aid system: the receiver, the receiver tube, the ear canal, the middle ear impedance, the vent, the vent acoustic impedance, the external acoustic feedback path and the microphone. The theoretical aspect of the derivations is presented in this section; the MATLAB implementation and experimental verification of the two-port network models of the components are presented in Chapter 3.

Derivation of the transducer parameters using the two-load method

Egolf and Leonard (1977) developed a computer-aided experimental procedure for obtaining the two-port network parameters of electroacoustic transducers, such as hearing aid receivers. Two widely differing acoustic loads were applied to the transducer and the response to each load was measured and transferred to the computer. The two-port network parameters were calculated from the measured responses and described the behaviour of the transducer completely. This approach was valid as long as the transducer was in linear operation. The method was verified by comparison with experimental measurements over the frequency range 10 Hz to 10 kHz. The method was replicated successfully by Bade *et al.* (1984) in a similar experiment, using a personal computer and the BASIC programming language.

The two-load method was also applied to a receiver connected to a hearing aid amplifier to yield the parameters for the combination of the two devices (Egolf *et al.*, 1988b), loading the receiver with acoustic impedances. It was also applied to a hearing aid microphone, loading the device with electrical resistors (Egolf *et al.*, 1988a).

In this work, the two-load method was applied to electrical analogues representing the transducers in simulations using a combination of the PSpice and MATLAB software packages. This is presented in Chapter 3.

Derivation of two-port equations for narrow cylindrical tubes

The tube connecting the output of the receiver to the ear canal, the ear canal itself and the vent through the earmould can be modelled as cylindrical tubes (Egolf *et al.*, 1989). Vents can be parallel or diagonal to the receiver tube; the former is easier to model and is used here. Although the shape of the human ear canal is complicated, it can be approximated as a cylinder. Assuming that an *in situ* ITE aid occludes the ear up to the second bend in the ear canal, the remaining portion of the ear canal can be modelled as a tube with length 12 mm and diameter 3.3 mm (Kates, 1988b).

The cascade parameters given by Rschevkin (1963) for the two-port model of a cylindrical tube of length L have the general form:

$$\begin{aligned} A &= \cosh(\Gamma L) \\ B &= Z\sinh(\Gamma L) \\ C &= \sinh(\Gamma L)/Z \\ D &= \cosh(\Gamma L) \end{aligned} \qquad (2.18)$$

Γ is the propagation constant, and Z is the acoustic impedance of the tube. Z is defined as $\rho_0 c/S$ (Kinsler and Frey, 1982), where $S = \pi r_0^2$ is the cross-sectional area of a tube of radius r_0, and Γ, the propagation constant, is defined as (Rscehvkin, 1963):

$$\Gamma = j\frac{\omega}{c_1} = j\frac{\omega}{c}\sqrt{1-2j\frac{\Phi}{2\omega\rho_0}} \qquad (2.19)$$

c_1 is the phase speed of the wave. Φ is the coefficient of friction for the fluid in the tube, ω is the angular frequency, $2\pi f$, and ρ_0 is the density of the fluid in the tube. Since Γ is less than the wavenumber $k = \omega / c$, the speed of sound in the pipe is less than that in free space, c = 347 ms^{-1} (Pierce, 1981).

However, these results apply only to large diameter tubes at high audio frequencies (Egolf, 1977). All tubing in the hearing aid system can be considered as narrow and more accurate results are obtained using expressions for transient fluid flow in narrow pipes (Iberall, 1950; Egolf, 1977):

$$\Gamma = j\frac{\omega}{c}\left(\frac{1+2(\gamma-1)[J_1(\alpha r_0)/\alpha r_0 J_0(\alpha r_0)]}{1-2J_1(\beta r_0)/\beta r_0 J_0(\beta r_0)}\right)^{1/2} \quad (2.20)$$

$$Z = \frac{\rho_0 c}{\pi r_0^{\,2}}\left(\left(1-\frac{2J_1(\beta r_0)}{\beta r_0 J_0(\beta r_0)}\right)\left(1+2(\gamma-1)\frac{J_1(\alpha r_0)}{\alpha r_0 J_0(\alpha r_0)}\right)\right)^{-1/2} \quad (2.21)$$

$J_n(\,)$ is a Bessel function of order n.

$$\alpha = \left(\frac{-j\omega\rho_0 \,\mathrm{Pr}}{\mu}\right)^{1/2} \quad (2.22)$$

$$\beta = \left(\frac{-j\omega\rho_0}{\mu}\right)^{1/2} \quad (2.23)$$

Pr is the Prandtl number, μ is the viscosity of the fluid in a large volume, γ is the ratio of specific heats c_p/c_v, c_p is the specific heat of the fluid at constant pressure and c_v is the specific heat of the fluid at constant volume. For air at 300 K (27 °C, i.e. approximately room temperature), ρ_0 = 1.21 kg m^{-3}, Pr = 0.707 (dimensionless), μ = 1.846 x 10^{-5} kg m^{-1}s^{-1}, γ = 1.402, c_p = 1004.5 J kg^{-1}K^{-1}.

This model has been verified experimentally and shown to have less than 2 dB error in predicting the behaviour of small diameter tubes over a frequency range of 10 to 10 000 Hz (Egolf, 1977). The assumptions made for this model were (Iberall, 1950; Egolf, 1977):

1. Damping is due to viscous friction and heat loss at the tube walls.
2. The tube walls are rigid and at constant temperature.
3. The fluid medium in the tube is continuous.
4. The perturbation of the fluid medium is small.
5. The length of the tube is such that radial end effects are negligible, i.e. tube length is much greater than the radius of the tube.
6. Plane wave propagation occurs.

Absorption in pipes is often greater than that which occurs in a large volume of fluid (Kinsler and Frey, 1982). This is due to losses occurring at the walls of the tube through viscous resistance to fluid motion and exchange of heat between the fluid and the walls.

If it is assumed that the layer of fluid in contact with the tube wall is isothermal, i.e. at a constant temperature, and can have no velocity, then the effective viscosity, μ', of the fluid in the tube is given by (Kinsler and Frey, 1982):

$$\mu' = \mu\left(1+(\gamma-1)\sqrt{\frac{\nu}{c_p\mu}}\right)^2 = 2.19\mu \qquad (2.24)$$

ν is the thermal conductivity of the fluid, i.e. a measure of the ability of the fluid to conduct heat, $\nu = 2.624 \times 10^{-2}$ W m^{-1}K^{-1} for air at 300 K.

It can be assumed that the acoustic fluid velocity is composed of a superposition of the velocities of the vorticity-mode[†], acoustic-mode and entropy-mode[‡] fields (Pierce, 1981). For a given frequency, it can be shown that the vorticity-mode and entropy-mode fields die out rapidly with increasing distance from the walls of the tube, so that a disturbance in an extended space, i.e. in a tube which is wide compared to the boundary layer, is expected to consist mainly of the acoustic-mode field, except near the walls or other perturbations.

The boundary layers, l_{vor} and l_{ent}, are a measure of how far the vorticity-mode and entropy-mode fields extend from a boundary (Pierce, 1981).

$$l_{vor} = \left(\frac{2\mu}{\omega\rho_0}\right)^{\frac{1}{2}} \qquad (2.25)$$

$$l_{ent} = \left(\frac{2\nu}{\omega\rho_0 c_p}\right)^{\frac{1}{2}} = \frac{l_{vor}}{(\mathrm{Pr})^{1/2}} \qquad (2.26)$$

These lengths are not necessarily small; they tend to infinity as ω tends to zero. However, they are much less than the corresponding acoustic wavelength divided by 2π.

[†] Vorticity is the rotational flow of the fluid (Kinsler and Frey, 1982), defined as the curl of the acoustic fluid velocity, $\nabla\times\mathbf{v}$. The vorticity-mode field is the only one of the three classes of disturbance field for which the vorticity is non-zero (Pierce, 1981), the other classes being the acoustic-mode field and the entropy-mode field.

[‡] Entropy is a measure of the unavailability of the energy of a system to do work (Isaacs, 1990). For a reversible thermodynamic process, the change in entropy is given by the energy transferred to the system by heat, divided by the temperature at which this process occurs. No real system is truly reversible, leading to an increase in entropy (the second law of thermodynamics). The entropy-mode field is the disturbance field in which entropy fluctuations are a major feature (Pierce, 1981). There are no entropy fluctuations in the vorticity-mode field, and they are negligible in the acoustic-mode field.

If we define the boundary layer thickness $l = \max(l_{vor}, l_{ent})$, then taking frequencies representing the range used in the model of the hearing aid feedback path response, we obtain the thicknesses given in Table 2.1:

	Thickness at:		
Layer	*100 Hz*	*1000 Hz*	*10000 Hz*
Velocity-mode l_{vor}	2.20×10^{-4} m	6.97×10^{-5} m	2.20×10^{-5} m
Entropy mode l_{ent}	2.62×10^{-4} m	8.29×10^{-5} m	2.62×10^{-5} m
Boundary layer $l = \max(l_{vor}, l_{ent})$	2.62×10^{-4}m	8.29×10^{-5} m	2.62×10^{-5} m

Table 2.1: Boundary layer thicknesses at different frequencies

		Radius / Thickness at:		
Tube	*Radius*	*100 Hz*	*1000 Hz*	*10000 Hz*
receiver tube	0.7×10^{-3} m	2.67	8.44	26.72
ear canal	3.3×10^{-3} m	12.60	39.81	125.95
vent	0.8×10^{-3} m	3.05	9.65	30.53

Table 2.2: Ratio of tube radius to boundary layer thickness for different frequencies

Comparing the ratios of the radii of the tubes in the model and the total boundary layer thicknesses at these frequencies (Table 2.2), we find that the smaller the ratio, the greater the proportion of the tube cross-section filled by the boundary layer. The boundary layer would fill the tube if the ratio equalled unity. Hence boundary layer effects dominate at low frequencies for narrow tubes. The walls of the tube are assumed to be rigid and always at ambient temperature.

The boundary layer at the wall of the tube results from viscous resistance to the fluid motion and exchange of heat between the fluid and the wall. This effect is more pronounced in narrow tubes where the boundary layer takes up a greater proportion of the cross-sectional area of the tube. In the context of the hearing aid feedback path model, this effect is more pronounced in the vent and receiver tubes than in the ear canal, due to the relative sizes of their radii. The tubes in the model are of short length (about 2 cm or less), so the effect of damping due to viscous resistance and heat loss is small. Consequently, the viscosity μ is used in the model rather than the effective viscosity μ' in the simulations throughout this thesis.

Middle ear impedance

The middle ear impedance (also referred to as eardrum impedance) has been represented in several ways by other researchers. Egolf *et al.* (1989) approximated it using the impedance of the diaphragm of a measuring microphone representing the eardrum in their experiment. Kates (1988a, 1988b, 1990, 1991) modelled the middle ear as a four-branch Zwislocki coupler, which was used in measurements on a KEMAR mannequin (Burkhard and Sachs, 1975).

In this work, the middle ear impedance was modelled using both mean measured data for human subjects and an electrical analogue.

The mean of measurements of acoustic impedance of the human middle ear for subjects with normal hearing (i.e. no middle ear pathologies) was published by Shaw (1974). This data was used to model the middle ear impedance in MATLAB using interpolation between data points (See Figure 2.12).

Zwislocki developed an electrical analogue of the human ear, based on the ear's functional anatomy (Zwislocki, 1962). This has been developed further by Lutman and Martin (1979) and de Jonge (1996). Each component of the analogue approximates the behaviour of part of the middle ear. The numerical values of each element were derived from anatomical data obtained from live subjects and post mortem preparations and from impedance measurements on normal and pathologic ears (Zwislocki, 1962). A schematic diagram of the middle ear mechanism is shown in Figure 1.2.

It was found that de Jonge's normal ear analogue produced impedance curves with some similarity to Shaw's mean data (Figure 2.12). de Jonge's analogue for a normal middle ear is shown below in Figure 2.9.

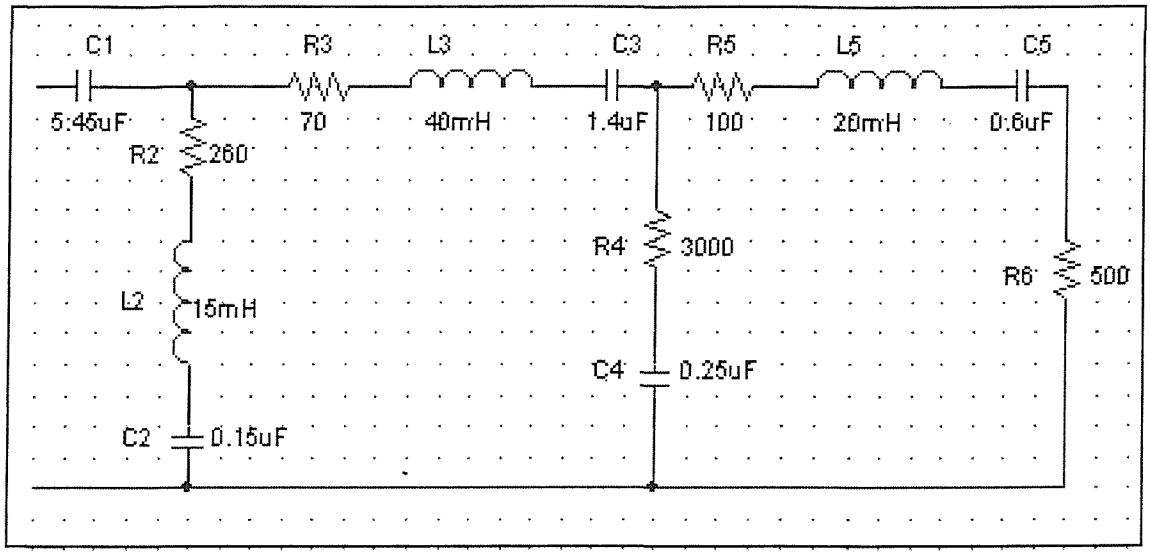

Figure 2.9: Electrical analogue of the normal middle ear (de Jonge, 1996)

Each branch of the analogue represents part of the middle ear. The numeral 1 denotes the middle ear cavities, 2 the uncoupled part of the eardrum, 3 the part of the eardrum attached to the malleus, the malleus itself and the incus, 4 the incudo-stapedial joint, 5 the stapes and 6 the cochlea.

It is possible to adapt the electrical analogue to approximate the impedance of pathologic ears, such as ears with otosclerosis (higher impedance than normal) and ossicular discontinuity (lower impedance than normal).

The effect of otosclerosis is to immobilise the stapes in the oval window, causing the cochlea to become disconnected from the rest of the middle ear (Zwislocki, 1962). This is modelled by removing the components representing the stapes, cochlea and round window (Figure 2.10). A discontinuity between the malleus and stapes as a result of a surgical procedure to remove the incus results in lower than normal middle ear impedance. The effects of the incudo-stapedial joint, stapes, cochlea and round window membrane are eliminated (Zwislocki, 1962). This is modelled by the electrical analogue shown in Figure 2.11.

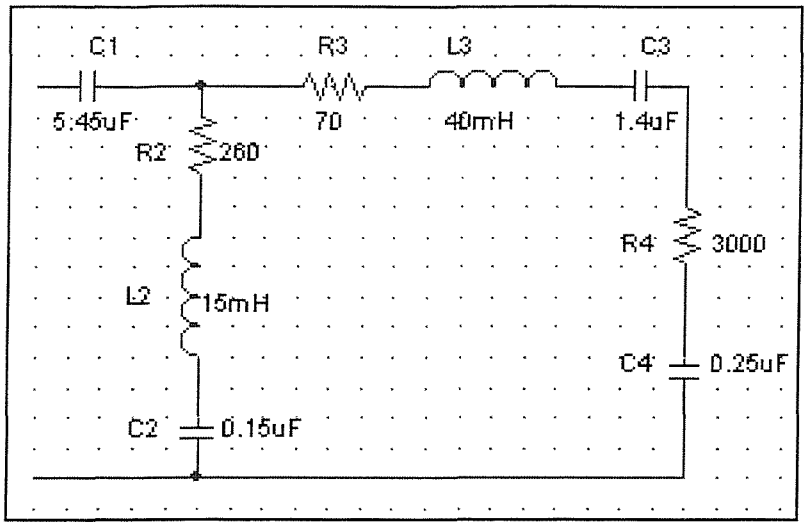

Figure 2.10: Electrical analogue of an otosclerotic ear

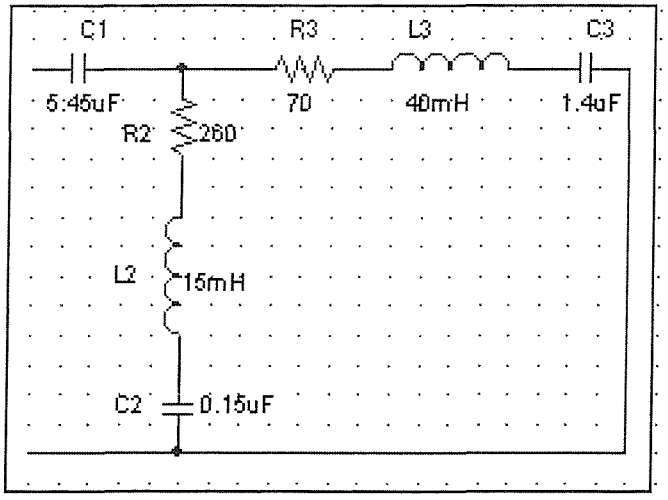

Figure 2.11: Electrical analogue of an ear with an ossicular discontinuity

Figure 2.12 compares the mean measured middle ear impedance with the impedance of the normal middle ear, otosclerotic and ossicular discontinuity electrical analogues.

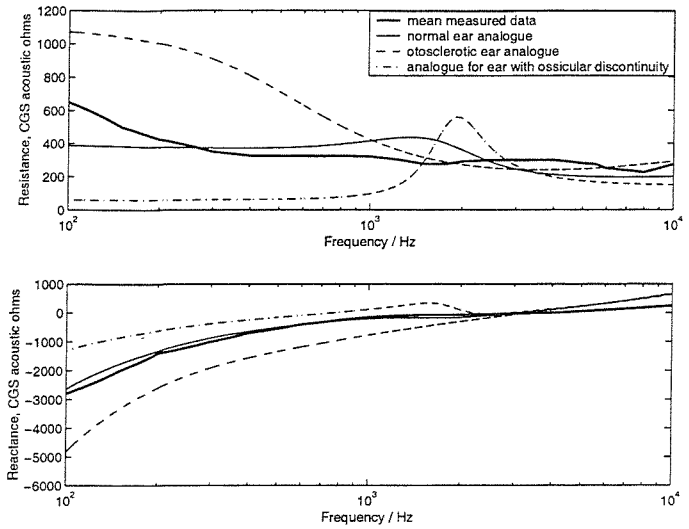

Figure 2.12: Comparison of impedance of middle ear analogues

Vent acoustic impedance

The acoustic impedance due to the vent exit, $\mathbf{Z}_V$, was obtained by modelling the vent exit as a cylindrical piston in an infinite plane baffle, which represented the side of the head (Egolf *et al.*, 1985; Kates, 1988b; Hellgren *et al.*, 1999a; Hellgren *et al.*, 1999b). The layer of air at the exit of an open-ended cylinder can be treated as a piston, assuming that all parts of the layer vibrate in phase with the same amplitude. The situation can also be modelled as a piston in a spherical baffle (Egolf *et al.*, 1985); this is more complicated and will not be considered here. Also, it has been shown that results obtained compared better with actual measurements for a plane baffle than for a spherical baffle (Egolf *et al.*, 1985).

It should be noted here that there are three main kinds of impedance, and these should not be confused (Kinsler & Frey, 1982). Specific acoustic impedance **z** is the ratio of sound pressure **P** to particle velocity **u**.

$$\mathbf{z} = \frac{\mathbf{P}}{\mathbf{u}} \qquad (2.27)$$

Acoustic impedance **Z** is the ratio of sound pressure **P** to volume velocity **U**.

$$\mathbf{Z} = \frac{\mathbf{P}}{\mathbf{U}} \qquad (2.28)$$

Radiation impedance $\mathbf{Z}_r$ is given by the ratio of force to speed, and is part of the mechanical impedance of a vibrating system radiating sound (Kinsler and Frey, 1982).

Acoustic impedance is related to specific acoustic impedance by

$$\mathbf{Z} = \frac{\mathbf{z}}{S} \tag{2.29}$$

where S is the cross-sectional area of the piston, πa^2, and a is the radius of the piston.

Radiation impedance is related to specific acoustic impedance by

$$\mathbf{Z}_r = S\mathbf{z} \tag{2.30}$$

and is related to acoustic impedance by

$$\mathbf{Z}_r = S^2\mathbf{Z} \tag{2.31}$$

The radiation impedance, $\mathbf{Z}_r$, of the vent exit was found using the following equations (Kinsler and Frey, 1982):

$$\mathbf{Z}_r = R_r + jX_r \tag{2.32}$$

where

$$R_r = \pi r_V^{\,2} \rho_0 c R_1(2kr_V) \tag{2.33}$$

and

$$X_r = \pi r_V^{\,2} \rho_0 c X_1(2kr_V) \tag{2.34}$$

r_V is the vent radius in metres. $R_1(2kr_V)$ is the piston resistance function,

$$R_1(2kr_V) = 1 - \frac{2J_1(2kr_V)}{2kr_V} = \frac{(2kr_V)^2}{2^2 1!2!} - \frac{(2kr_V)^4}{2^4 2!3!} + \ldots \tag{2.35}$$

and $X_1(2kr_V)$ is the piston reactance function,

$$X_1(2kr_V) = \frac{4}{\pi}\left[\frac{2kr_V}{3} - \frac{(2kr_V)^3}{3^2 5} + \frac{(2kr_V)^5}{3^2 5^2 7} - \ldots\right] \tag{2.36}$$

$R_1(2kr_V)$ can be implemented directly in MATLAB using the command `besselj`. It can be shown that the first three terms of $X_1(2kr_V)$ are sufficient to describe the function; higher order terms are virtually negligible. The model used the first eight terms to increase accuracy. Following the model developed by Egolf *et al.* (1989), this radiation impedance was converted to acoustic impedance so that the whole model was in terms of pressure and volume velocity:

$$\mathbf{Z}_V = \frac{\mathbf{Z}_r}{\left(\pi r_V^2\right)^2} \tag{2.37}$$

The vent acoustic impedance, $\mathbf{Z}_V$, was converted into two-port form, as shown in Figure 2.6.

Modifying the response to account for the effects of the pinna

Kates (1988b) presented an expression for the modification of the vent acoustic impedance due to the effects of the pinna. The expression is given by Equation 2.38:

$$\mathbf{Z}_V' = \left\{1+\frac{1}{2}\left(\frac{(\omega/\omega_1)^2}{1+(\omega/\omega_1)^2}\right)^{\frac{1}{2}}\left[1-\cos\left(\pi\frac{\omega}{\omega_0}\right)\right]\right\}\mathbf{Z}_V \tag{2.38}$$

Kates used $\omega_0 = 2\pi \cdot 5000$ Hz and $\omega_1 = 2\pi \cdot 2500$ Hz, although other values or other expressions may be found to represent the pinna effects more accurately. This modification did not affect the phase of the feedback path response.

The feedback path model did not use the pinna modification unless stated explicitly.

Modelling the external acoustic feedback path

The external acoustic feedback path is described by the ratio of pressure at the vent exit to pressure at the microphone input due to the feedback path, rather than that due to the incident path.

If we assume that nearly all of the volume velocity from the vent, $\mathbf{U}_V$, is absorbed by the vent radiation impedance, virtually no volume velocity reaches the input of the block representing the external acoustic feedback path. The sound pressure leaving the vent, $\mathbf{P}_V$, is then unaffected by this and forms the input pressure to the external acoustic feedback path block (Egolf *et al.*, 1989) (see Figure 2.7).

Following the two-port model given by Egolf *et al.* (1989), the external acoustic feedback path was defined by the A_F parameter only, with $B_F = C_F = D_F = 0$. B_F and D_F can be set to zero because the microphone draws very little current from the surrounding sound field, and C_F can be set to zero since almost no volume velocity reaches the input of the block (Egolf *et al.*, 1989). A_F is given at each frequency by:

$$A_F = \frac{\mathbf{P}_V}{\mathbf{P}_F} \tag{2.39}$$

The complex pressure in the farfield for a circular piston in an infinite plane baffle is given by (Kinsler and Frey, 1982):

$$\mathbf{P}_F = j\frac{\rho_0 c}{2}U_0\frac{a}{R}kae^{j(\omega t-kR)}\left[\frac{2J_1(ka\sin\theta)}{(ka\sin\theta)}\right] \qquad (2.40)$$

a is the piston radius in metres, R is the distance in metres from the piston to the point of interest (i.e. the distance from the vent exit to the microphone input), t is time in seconds and θ is the angle in degrees from the vent centreline to the point of interest.

U_0 is the speed amplitude of the piston, not its volume velocity, so that a piston of radius a, vibrating radially with speed amplitude U_0 and frequency ω has particle velocity:

$$\mathbf{u}_V = U_0 e^{j\omega t} \qquad (2.41)$$

Substituting Equation (2.41) into Equation (2.40) and setting $a = r_V$, we obtain

$$\mathbf{P}_F = j\frac{\rho_0 c}{2}u_V\frac{r_V}{R}kr_V e^{-jkR}\left[\frac{2J_1(kr_V\sin\theta)}{(kr_V\sin\theta)}\right] \qquad (2.42)$$

The pressure at the vent exit, $\mathbf{P}_V$, is given by

$$\mathbf{P}_V = \mathbf{u}_V\mathbf{z}_V \qquad (2.43)$$

where

$$\mathbf{z}_V = \frac{\mathbf{Z}_r}{S} \qquad (2.44)$$

Therefore, the external acoustic feedback path is given at each frequency by

$$\frac{1}{A_F} = \frac{\mathbf{P}_F}{\mathbf{P}_V} = \frac{\rho_0 c r_V^2 k e^{j\left(\frac{\pi}{2}-kR\right)}}{2R\mathbf{z}_V}\left[\frac{2J_1(kr_V\sin\theta)}{(kr_V\sin\theta)}\right] \qquad (2.45)$$

The term in square parentheses is the directivity of the piston. On axis, i.e. when θ is zero, this term goes to unity and the piston behaves as a point source. However, in an ITE aid, the microphone and vent are more or less in the same plane, i.e. $\theta \approx 90°$, and the directivity must be considered, even though it is close to unity over the frequency range considered here (100 Hz to 10 kHz). Equation (2.45) has the same form as that derived by Egolf *et al.* (1989).

To summarise, modelling techniques have been applied to all parts of the hearing aid system. Most are derived from acoustic theory, although some are based on experimental measurements. The resulting two-port network parameters will be used in the computer model of an *in situ* in-the-ear hearing aid system.

2.7 Variations in the feedback path due to sound leakage

Adaptive feedback cancellation aims to track and cancel changes in the feedback path rapidly to prevent the hearing aid system becoming unstable. Broadly speaking, changes in the feedback path fall into two categories: increased leakage of amplified sound from the receiver back to the microphone, or the presence of an obstruction in the external acoustic feedback path. The changes can take place over varying time frames (Oliveira, 1997); this work is concerned with changes that occur over a span of seconds or minutes.

Examples of such changes have been investigated in previous studies (Hellgren *et al.*, 1999b; Rafaely *et al.*, 2000). Leakage of sound around the edges of the earmould can be caused by jaw movements, such as when the subject smiles, chews or yawns. These movements can cause the earmould to shift position, breaking the acoustic seal and allowing leaks to occur. Also, jaw movements may alter the shape of the ear canal (Oliveira, 1997); for example, movement of the lower jaw relative to the skull compresses the cartilaginous part of the ear canal (Zwislocki, 1953). Again, these movements can cause an increase in sound leakage, as well as altering the shape of the frequency response of the feedback path. Increased leakage of sound makes it more likely that oscillation will occur as the amplified signal reinforces the input signal, driving the hearing aid into instability.

Incorrectly fitting the earmould to the pinna is another cause of increased sound leakage. This can occur when a patient is new to wearing a hearing aid and is not used to positioning the earmould correctly.

This section will examine the effect of adding a slit leak to the model of the hearing aid system. The effects of the presence of an obstruction in the external acoustic feedback path are discussed in the next section.

Oliveira (1997) described changes in the shape of the ear canal. Those most likely to affect the OLTF are short-term changes due to jaw movements such as chewing, yawning or vowel sounds (Hellgren *et al.*, 1999b). In simple terms, the outer third of the ear canal consists of cartilage (an extension of the tissue forming the pinna (Austin, 1991), and the inner two-

thirds consist of bone (Alvord and Farmer, 1997; Gelfand, 1998). This bony or osseous part is formed in part by the jawbone, which is hinged exactly at the ear canal (Westermann, 1987). In more detail, the osseous region begins above and behind the ear canal at the second turn, limiting the portion of the ear canal that can be changed by jaw movement. Bone surrounds the ear canal completely by the halfway point, and from hereon in jaw movement has no effect on ear canal shape (Oliveira, 1997). Note that the ear canal has a complicated shape and a generally downward slant; the cylindrical approximation of its shape is a mathematical convenience. The ear canal is relatively straight in children, becoming more "S" shaped in adulthood, and increasingly twisted and narrow with old age (Alvord and Farmer, 1997).

As the jaw opens, the condyle of the mandible (jawbone) moves forward (see Figure 2.13) and pulls on the cartilaginous part of the ear canal, causing widening of the canal in the anterior-posterior direction (front of head to back of head) (Oliveira, 1997). There is no significant change in the inferior-superior direction (bottom to top). With the jaw open fully, the increase in ear canal width can be as much as 10 % (Oliveira, 1997), so it is not surprising that slit leakage can occur around the edges of the earmould when the jaw moves.

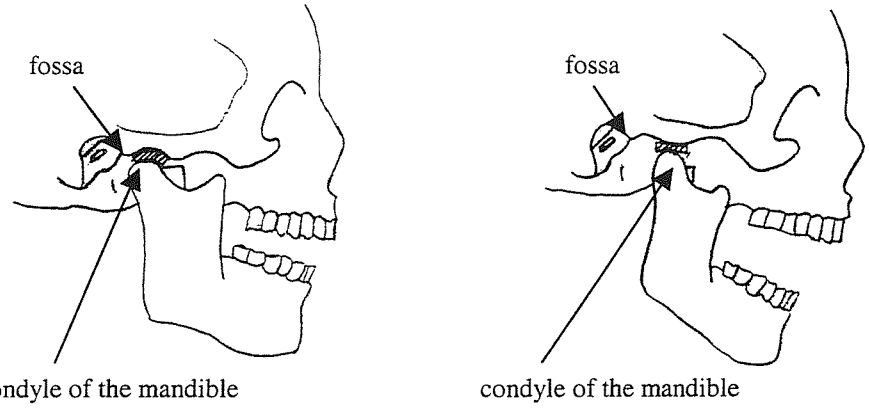

a) Jaw closed *b) Jaw open*

Figure 2.13: Effect of opening the jaw (based on Oliveira, 1997)

In some subjects, it has been found that the temporomandibular joint (TMJ), i.e. the "hinge" of the jaw, wears on one side, leading to asymmetry in the changes of the ear canal dimensions in either ear. This results in larger slit leakage on the side with the larger change, and hence a greater probability of feedback occurring in that ear. Clinical experience has shown that feedback often occurs in one ear rather than the other. Also, the hearing aid may be displaced by jaw movements, resulting in feedback or loss of gain (Oliveira, 1997).

It is almost impossible to achieve a perfect seal around the edges of the earmould. A typical slit leak could be represented by a tube of length 22 mm and diameter 1.4 mm (Johansen, 1975). The slit leak behaves in the same way as a deliberate vent and can be modelled accordingly as a tube in parallel with the vent.

Hellgren *et al.* (1999b) calculated the transfer function from the beginning of the vent at the ear canal to the microphone input and likewise for the leak. These two transfer functions were added to obtain an estimate of the acoustic feedback path for an *in situ* hearing aid with vent and leak. This ignored the effect of pressure at the ear canal due to feedback of the signal radiating from the vent via the leak and vice versa, and the effect of the leak on the vent radiation impedance and vice versa. It was judged that this had little effect on the results.

The additional acoustic load impedance due to the leak must be taken into account by converting the leak tube and its exit acoustic impedance to a single load impedance block in parallel with the converted ear impedance. In this way, the leak loads the vent (see Figure 2.14). The path from the microphone input to the output of the vent external acoustic feedback path with the leak acting as a load will be referred to as the vent path from now on. The subscripts used in the diagram were the same as those used in Section 2.2. In addition, the subscript 4 denotes the tube representing the effective leak, and $\mathbf{Z}_L$ denotes the leak acoustic impedance. The subscript *Fv* denotes the external acoustic feedback path via the vent and *Fl* denotes the external acoustic feedback path via the leak. The leak and its exit impedance can be treated in the same way to produce the leak path (Figure 2.15).

If it is assumed that the pressure at the output of the vent path combines linearly with the pressure at the output of the leak path to produce the pressure at the output of the total hearing aid system, the total OLTF is given by:

$$\frac{P_F(f)}{P_{in}(f)} = \frac{P_{Fv}(f)}{P_{in}(f)} + \frac{P_{Fl}(f)}{P_{in}(f)} = \frac{P_{Fv}(f) + P_{Fl}(f)}{P_{in}(f)} \qquad (2.46)$$

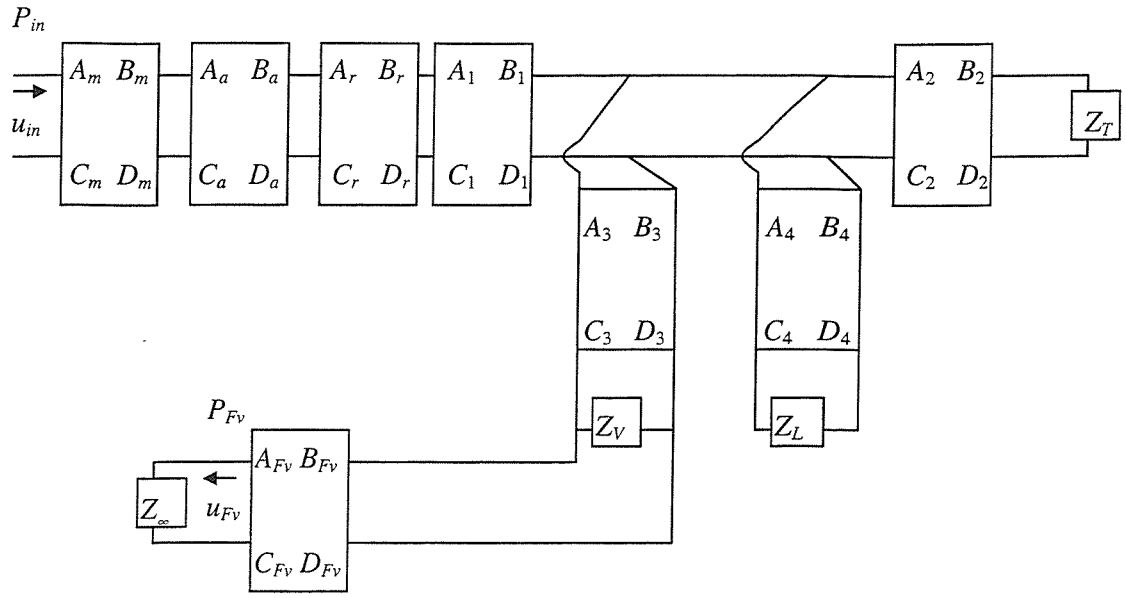

Figure 2.14: Two-port network diagram of vent path with leak impedance load in parallel with converted ear impedance

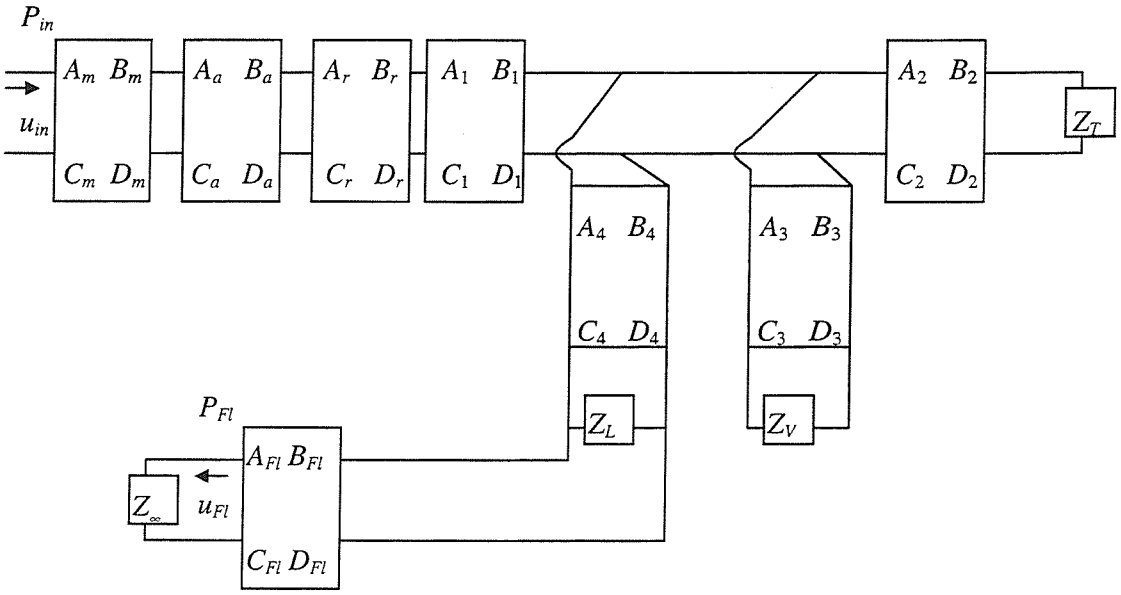

Figure 2.15: Two-port network diagram of leak path with vent impedance load in parallel with converted ear impedance

The measurable feedback path is cut electrically between the microphone and receiver, omitting the amplifier and any other internal processing (see Section 2.5). Figure 2.16 shows the block diagram of the measurable vent path. Compare this to Figure 2.14. The external acoustic feedback path is now loaded by the microphone. The leak path can be modelled in the same way. The total feedback path response is calculated in the same way as before:

$$\frac{V_F(f)}{V_{in}(f)} = \frac{V_{Fv}(f) + V_{Fl}(f)}{V_{in}(f)} \tag{2.47}$$

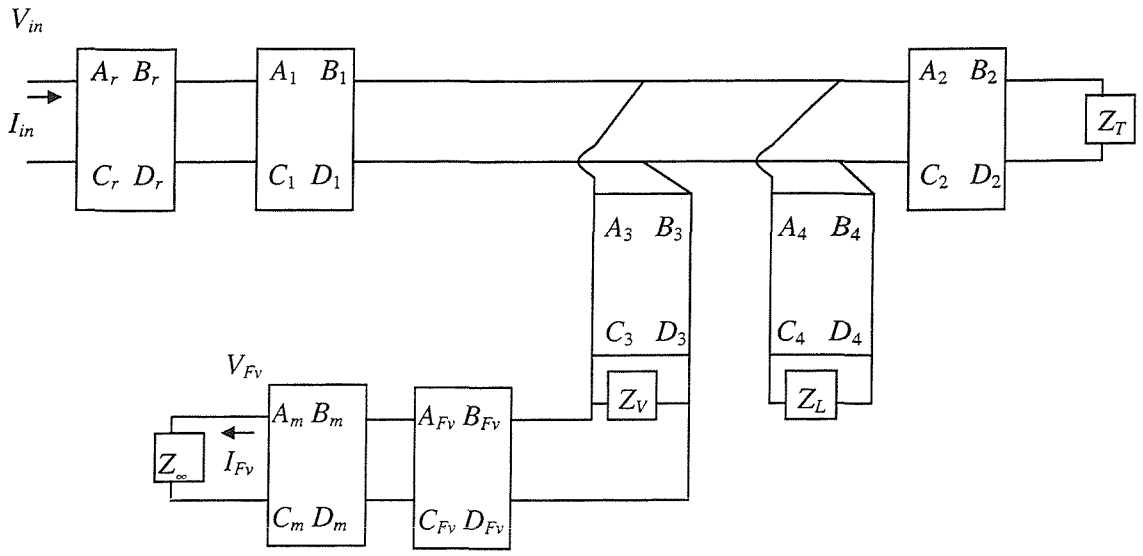

Figure 2.16: Two-port network diagram of the measurable vent path with leak impedance load in parallel with converted ear impedance

If we assume that the leak tube has the same length and distance from the microphone as the vent, we can model these as a single tube, increasing the tube radius r_3 to represent increasing leak size. It is assumed that the cross-sectional area of the combined tube is the sum of the cross-sectional areas of the vent and leak:

$$\pi r_3^2 = \pi r_V^2 + \pi r_l^2 \tag{2.48}$$

Hence the radius of the combined tube, referred to as the vent in general, is given by:

$$r_3 = \sqrt{\left(r_V^2 + r_l^2\right)} \tag{2.49}$$

This assumption is made throughout the rest of the thesis, although it is an oversimplification of the actual physical situation.

2.8 Obstructions in the external acoustic feedback path

The other main cause of feedback in hearing aids is the presence of an obstruction in the external acoustic feedback path, such as a hand or telephone handset near the ear. The presence of the obstruction alters the external acoustic feedback path and the radiation impedance of the vent or leak, which in turn alters the load impedance on the receiver. It also

gives rise to reflections off the obstruction itself, which may have a considerable effect on the shape and amplitude of the feedback path response. In extreme cases, an obstruction very close to the ear may form a cavity with the vent or with the residual concha volume, i.e. the part of the concha not filled by the earmould or faceplate of an in-the-canal device. This will lead to resonance effects, affecting the feedback path response and often resulting in oscillation. The presence of an obstruction in the external acoustic feedback path results in significant changes in the feedback path with an increased likelihood that instability will occur. Studies of the effects of obstructions in the external acoustic feedback path have been conducted previously (Hellgren *et al.*, 1999b; Rafaely *et al.*, 1999; Rafaely *et al.*, 2000), but to date no reliable model of the effects has been proposed.

There are several approaches to modelling an obstruction in the feedback path. The cavity formed by the presence of the obstruction over the ear could be modelled as a volume compliance, but this would not model high frequency effects, i.e. above 1 kHz, such as changes in the system resonances due to interaction with the obstruction. An obstruction near the ear could be modelled as an infinite plane baffle parallel to the side of the head, but this would not model the low frequency effects caused by cavity resonance. A good approach may be to model an enclosure over the ear using the modal model (Kinsler and Frey, 1982). It is likely that many modes will be required at high frequencies. It should be possible to develop a model of an enclosure with the sound source (i.e. the vent exit) at a point on one wall and the point of interest (i.e. the microphone input) at another point on the same wall, near the vent exit. This would represent the microphone and vent exit positioned on the faceplate of the hearing aid, with sound radiating into an enclosure formed by a hand or telephone handset over or near the ear. Although this method is likely to be the most successful, it is not attempted here (as the main aim of the project is to develop a new parametric adaptive algorithm rather than to develop a fully comprehensive model of all possible feedback paths) and is suggested as a topic for future work.

A possible simple alternative method would be to model the enclosure formed by the obstruction near the ear as a large tube, using the two-port equations derived previously. However, this may not model transverse reflections accurately. The large tube approach is investigated in this section.

If we assume that placing a microphone in the sound field does not affect the piston modelling the layer of air at the vent exit, then we can use the same external acoustic feedback path model as described in Section 2.6, and assume that the presence of the

microphone does not affect the load on the vent. It was found that for tubes with radius greater than 1 cm, the two-port network equations for narrow cylindrical tubes (Equations (2.20) – (2.23)) returned values of 1/∞. Therefore alternative equations for Γ and L must be derived for large diameter tubes and used to model the tube representing the cavity formed by the presence of the obstruction ("the obstruction tube"). The other tubes will be modelled using the narrow tube expressions as before.

The propagation constant for sound waves in a tube of radius r with absorption is defined as (Kinsler and Frey. 1982):

$$\mathbf{k} = k - j\alpha \tag{2.50}$$

where k is the wavenumber and

$$\alpha = \frac{1}{rc}\sqrt{\frac{\mu\omega}{2\rho_0}} \tag{2.51}$$

The frequency response of a standing wave in a tube driven at $x = 0$ and closed at $x = L$ is given by (Kinsler and Frey, 1982):

$$\frac{1}{\cos(\mathbf{k}L)} \tag{2.52}$$

It can be shown that

$$\cos(\mathbf{k}L) = \cosh(\Gamma L) \tag{2.53}$$

where

$$j\mathbf{k} = \Gamma \tag{2.54}$$

Recall that the two-port network parameters for a cylindrical tube of length L have the form (Rschevkin, 1963):

$$\begin{aligned} A &= \cosh(\Gamma L) \\ B &= Z\sinh(\Gamma L) \\ C &= \sinh(\Gamma L)/Z \\ D &= \cosh(\Gamma L) \end{aligned} \tag{2.55}$$

This can be written as:

$$A = \cosh(j\mathbf{k}L)$$
$$B = Z\sinh(j\mathbf{k}L) \qquad (2.56)$$
$$C = \sinh(j\mathbf{k}L)/Z$$
$$D = \cosh(j\mathbf{k}L)$$

Z is the acoustic impedance of the tube, defined as

$$Z = \frac{\rho_0 c}{S} \qquad (2.57)$$

where $S = \pi r^2$ is the cross-sectional area of a tube of radius r (Kinsler and Frey, 1982).

Comparing the response of the large tube model with that of the narrow tube model presented in Section 2.6, for a tube of length 0.1 m and radius 1 cm, i.e. the upper limit of the narrow tube model, it can be seen that the large tube model behaves as the narrow tube model (Figure 2.17).

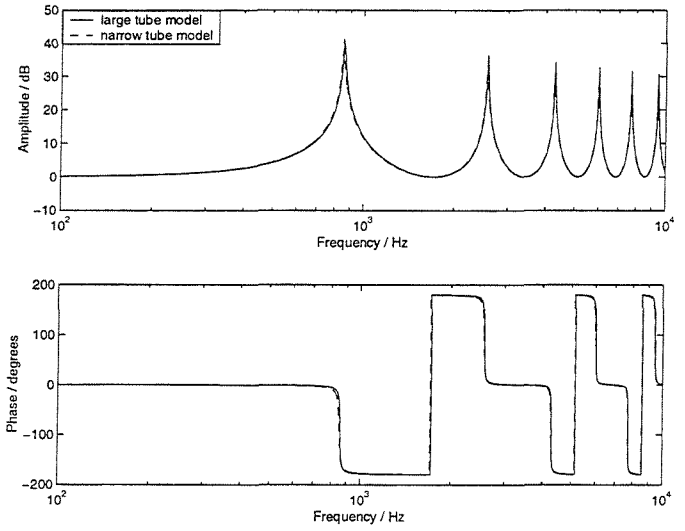

Figure 2.17: Comparison of narrow and large tube models for a tube of length 0.1 m and radius 1 cm

For a tube of length 0.1 m and radius 2.5 mm, i.e. a narrower tube, the large tube model is less accurate (Figure 2.18). Recall that the narrow tube model was verified experimentally over the frequency range 10 Hz – 10 kHz (Egolf, 1977) and so can be considered correct.

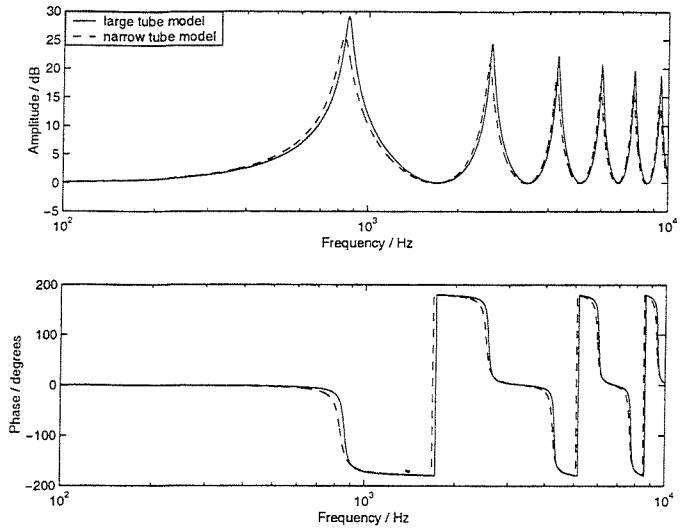

Figure 2.18: Comparison of narrow and large tube models for a tube of length 0.1 m and radius 2.5 mm

For a tube of length 0.1 m and radius 1 mm, i.e. a very narrow tube, the large tube model is even less accurate (Figure 2.19). Clearly the accuracy of the model decreases as the tube radius decreases.

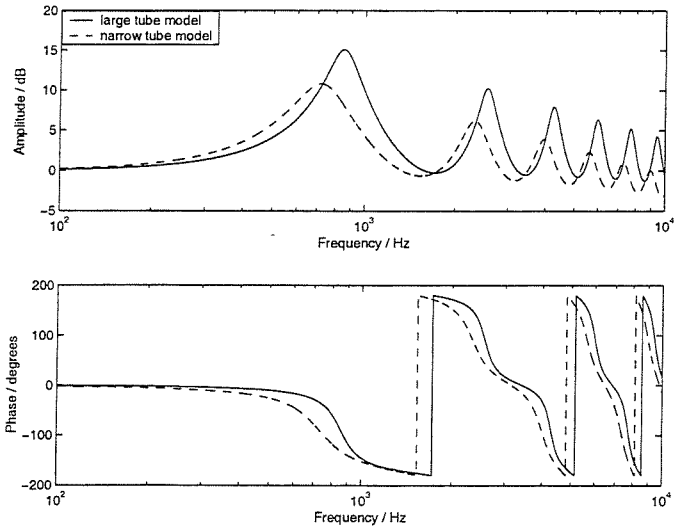

Figure 2.19: Comparison of narrow and large tube models for a tube of length 0.1 m and radius 1 mm

Therefore the two-port network equations presented in this section are applicable to wide tubes, i.e. tubes with radius greater than or equal to 1 cm, but for narrow tubes (radius less than 1 cm) the equations presented in Section 2.6 should be used.

We would expect that for a very large obstruction tube, the model would act like no obstruction was present, i.e. the vent is radiating into free space.

Figure 2.20 shows how the obstruction tube and its terminating impedance, R_{ob}, are added to the original model. The subscripts are as defined in Section 2.2, with the subscript *ob* referring to the obstruction tube.

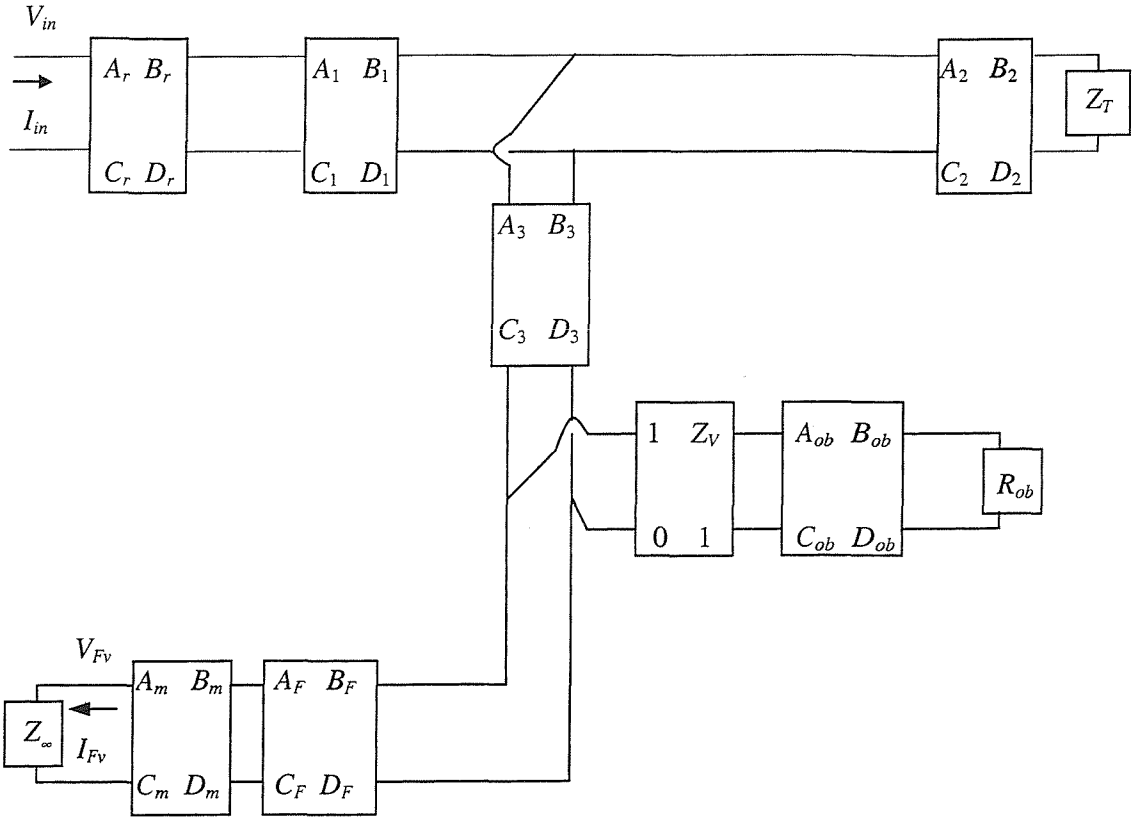

Figure 2.20: Two-port network diagram of the measurable feedback path with obstruction tube loading the vent in series with the vent exit impedance

Consider the section of the model from the vent input to the termination of the obstruction tube (Figure 2.21).

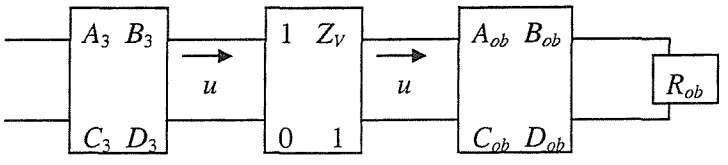

Figure 2.21: Section of model from vent input to obstruction tube termination

The radiation impedance is connected in series between the vent and the obstruction tube. If the obstruction tube is not present (a short circuit), this will reduce to the original model, with Z_V loading the vent in parallel (Figure 2.22).

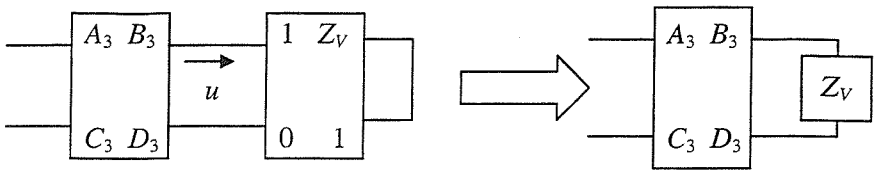

Figure 2.22: Reduction to original model on removal of obstruction tube

The obstruction tube is terminated with some resistance R_{ob}. If $R_{ob} = \rho_0 c/\pi r_{ob}^2$, i.e. is equal to the characteristic impedance of the tube, there will be no impedance mismatch and no reflection. If $R_{ob} \neq \rho_0 c/\pi r_{ob}^2$, reflections will occur. If necessary, damping can be added to the model to reduce the amount of reflection. Setting the tube termination to infinite impedance is like blocking the vent so that nothing reaches the microphone and $u = 0$. Otherwise, we can consider u to be the velocity of a piston in an infinite plane baffle as before.

Therefore the two-port model of the hearing aid system with an obstruction in the external acoustic feedback path can be written as:

$$\begin{bmatrix} A_{total(ob)} & B_{total(ob)} \\ C_{total(ob)} & D_{total(ob)} \end{bmatrix} = \begin{bmatrix} A_r & B_r \\ C_r & D_r \end{bmatrix} \begin{bmatrix} A_1 & B_1 \\ C_1 & D_1 \end{bmatrix} \begin{bmatrix} 1 & 0 \\ 1/Z_E & 1 \end{bmatrix} \begin{bmatrix} A_3 & B_3 \\ C_3 & D_3 \end{bmatrix} \begin{bmatrix} 1 & Z_V \\ 0 & 1 \end{bmatrix} \begin{bmatrix} 1 & 0 \\ 1/Z_{obst} & 1 \end{bmatrix} \begin{bmatrix} A_F & 0 \\ 0 & 0 \end{bmatrix} \begin{bmatrix} A_m & 0 \\ 0 & 0 \end{bmatrix} \quad (2.58)$$

where

$$Z_{obst} = \frac{A_{ob} R_{ob} + B_{ob}}{C_{ob} R_{ob} + D_{ob}} \quad (2.59)$$

Note that pinna effects have not been included in the model here.

Equation (2.58) can be rewritten as:

$$\begin{bmatrix} A_{total(ob)} & B_{total(ob)} \\ C_{total(ob)} & D_{total(ob)} \end{bmatrix} = \begin{bmatrix} A_r & B_r \\ C_r & D_r \end{bmatrix} \begin{bmatrix} A_1 & B_1 \\ C_1 & D_1 \end{bmatrix} \begin{bmatrix} 1 & 0 \\ 1/Z_E & 1 \end{bmatrix} \begin{bmatrix} A_3 & B_3 \\ C_3 & D_3 \end{bmatrix} \begin{bmatrix} 1 & 0 \\ 1/(Z_V + Z_{obst}) & 1 \end{bmatrix} \begin{bmatrix} A_F & 0 \\ 0 & 0 \end{bmatrix} \begin{bmatrix} A_m & 0 \\ 0 & 0 \end{bmatrix} \quad (2.60)$$

This approach assumes that the presence of the obstruction changes the pressure outside the vent, but also assumes that the external acoustic feedback path is unchanged from the model presented in Section 2.6. This is unlikely to be the case, as the effect of the obstruction close to the ear is to enclose both the source of sound, i.e. the vent, and the hearing aid

microphone, resulting in reflections as well as a change in pressure. The obstruction will affect the external acoustic feedback path block as well as the side branch in Figure 2.20.

Therefore the model developed in this section is unlikely to be accurate, although its usefulness is evaluated in Chapter 3. Unless otherwise stated, the model used throughout this thesis is that given by Equation 2.15.

2.9 Conclusions

A two-port network model of an *in situ* in-the-ear hearing aid system has been developed. The model has been extended to include variations in the system due to changes in jaw movements, causing increased acoustic slit leakage around the earmould, or due to obstructions in the external acoustic feedback path such as a hand or telephone handset near the ear. The model is verified experimentally in Chapter 3. The model should be able to describe a range of variations in the feedback path, although a more comprehensive validation study should be performed in future, investigating a specific hearing aid system in greater detail. This is proposed for future work. For most of this thesis, the leak and vent are modelled as a single tube for simplicity, assuming that the length and distance from the microphone of both the vent and leak are the same.

3 Implementation and verification of the computer model

3.1 Introduction

This chapter describes the development of a computer model combining the PSpice circuit simulator and the MATLAB mathematical software package. This approach allows each component of the hearing aid system to be modelled individually, with full control of the physical parameters within the model. Hence a wide range of hearing aid configurations can be simulated by varying the transducer electrical analogues or the dimensions of the hearing aid tubing, for example. The model is verified by comparison with measured data. The model must be valid to be used in a method of feedback cancellation.

The modelling techniques described in the previous chapter were used to develop a program designed to simulate the frequency response of the feedback path for an *in situ* in-the-ear hearing aid system. The main program was implemented in MATLAB, with transducer data derived from electrical analogues implemented in the PSpice circuit simulation software package. Note that the model used CGS units throughout since these were the units used by the manufacturer's electrical analogues.

3.2 Computational model of the microphone and receiver

The manufacturers of the transducers used in this research, Knowles Electronics, Inc., use electrical analogues to model the microphones and receivers with the PSpice software package. PSpice is a powerful circuit simulator used by companies such as Knowles to design and test devices. Electrical analogues for a wide range of Knowles hearing aid microphones and receivers were supplied by Knowles Electronics, Inc. The simulations in this chapter were performed with the Student Version of PSpice 9.1.

The Knowles EA-1843 hearing aid microphone was used in this study. The schematic used to derive the microphone parameters is shown in Figure 3.1.

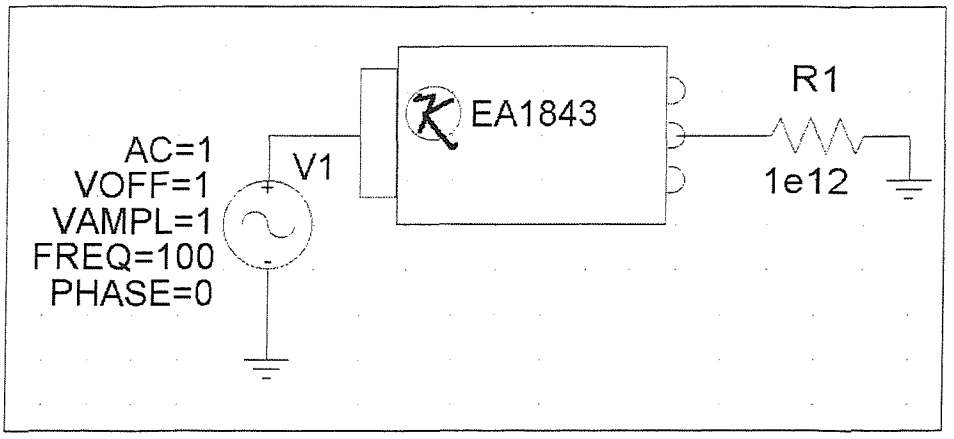

Figure 3.1: PSpice schematic used to derive two-port network parameters for the Knowles EA-1843 hearing aid microphone

The "two-load" method uses two widely differing impedance loads to calculate the two-port network parameters (Egolf and Leonard, 1977). A high load impedance approximates an open circuit at the output, and a low load impedance approximates a short circuit. In this case, R_{high} = 1 x 10^{12} Ω and R_{low} = 1 x 10^{-12} Ω, and a 1 V sinusoidal voltage source was used to drive the microphone. The microphone ABCD parameters were derived from Equations (2.8) - (2.11). A -70 dB amplification block could be used in PSpice as a correction factor to convert the microphone output to SI units (LoPresti and Carlson, 1999), although this was not used here.

Writing the two-port model of the microphone in matrix form, at each frequency:

$$\begin{bmatrix} P_i \\ u_i \end{bmatrix} = \begin{bmatrix} A_m & B_m \\ C_m & D_m \end{bmatrix} \begin{bmatrix} V_o \\ I_o \end{bmatrix} \tag{3.1}$$

P_i and u_i are the input complex sound pressure and complex particle velocity, respectively. A_m, B_m, C_m and D_m are the microphone two-port network parameters. V_o is the complex output voltage and I_o is the complex output current, related by:

$$V_o = R_{high} I_o \tag{3.2}$$

Similarly, with the low load impedance,

$$\begin{bmatrix} P_i' \\ u_i' \end{bmatrix} = \begin{bmatrix} A_m & B_m \\ C_m & D_m \end{bmatrix} \begin{bmatrix} V_o' \\ I_o' \end{bmatrix} \tag{3.3}$$

where the primes indicate changes in the variables dependent on the load impedance, and:

$$V_o' = R_{low} I_o' \tag{3.4}$$

For a free sound field, the small diameter of the hearing aid microphone input port (typically about 1 mm) results in an input impedance that is much greater than the impedance of the surrounding sound field (Egolf *et al.*, 1988a). In consequence, the microphone draws very little particle velocity from this sound field, so we can assume that:

$$u_i = u_i' \approx 0 \qquad (3.5)$$

This allows us to set C_m and D_m to zero in the model if the input impedance of the microphone is much greater than that of the preceding block. If this block had high impedance, e.g. if it represented a narrow tube, Equation (3.5) would not be valid and C_m and D_m would be non-zero.

The microphone two-port network parameters at each frequency are given by Equations (3.6) - (3.9).

$$A_m = \left.\frac{P_i}{V_o}\right|_{I_o=0} \qquad (3.6)$$

$$B_m = \left.\frac{P_i}{I_o}\right|_{V_o=0} \qquad (3.7)$$

$$C_m = \left.\frac{u_i}{V_o}\right|_{I_o=0} \qquad (3.8)$$

$$D_m = \left.\frac{u_i}{I_o}\right|_{I_o=0} \qquad (3.9)$$

It was necessary to multiply C_m and D_m by -1 if the parameters were derived from the electrical analogues since the source current is negative in PSpice. This was also the case for the derived receiver C and D parameters.

Figure 3.2 shows the magnitude and phase of the frequency response generated with the derived two-port network parameters compared with the response simulated with PSpice to reproduce the manufacturer's published sensitivity curve (magnitude in dB relative to 1.0 V / 0.1 Pa). It can be seen that the curves are identical. The manufacturer did not supply phase data, though the phase generated by the MATLAB model agrees with that extracted from the PSpice simulation.

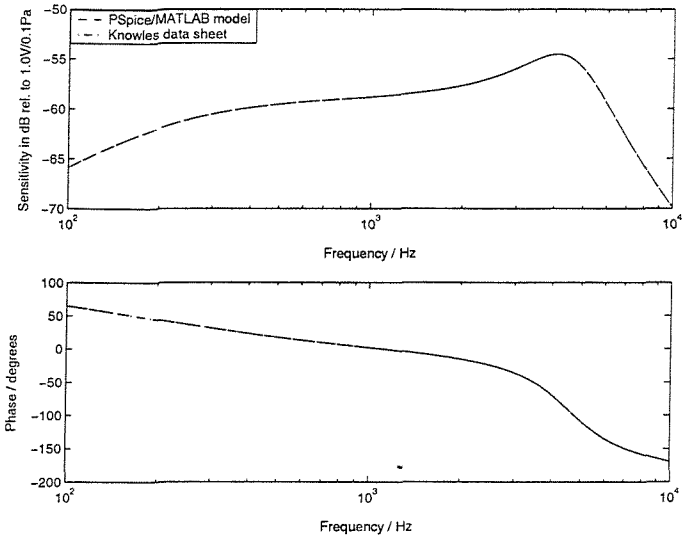

Figure 3.2: Comparison of magnitude and phase of the frequency response generated with the derived two-port network parameters with the reproduced manufacturer's response curve for the Knowles EA-1843 hearing aid microphone

The parameters of the ED-1912 receiver were derived in the same way (although C_r and D_r were not zero), with R_{low} = 1 x 10^{-9} Ω and R_{high} = 1 x 10^{12} Ω. (A different value of R_{low} was used for the receiver since the derived response was noisy when 1 x 10^{-12} Ω was used.) The PSpice schematic is shown in Figure 3.3.

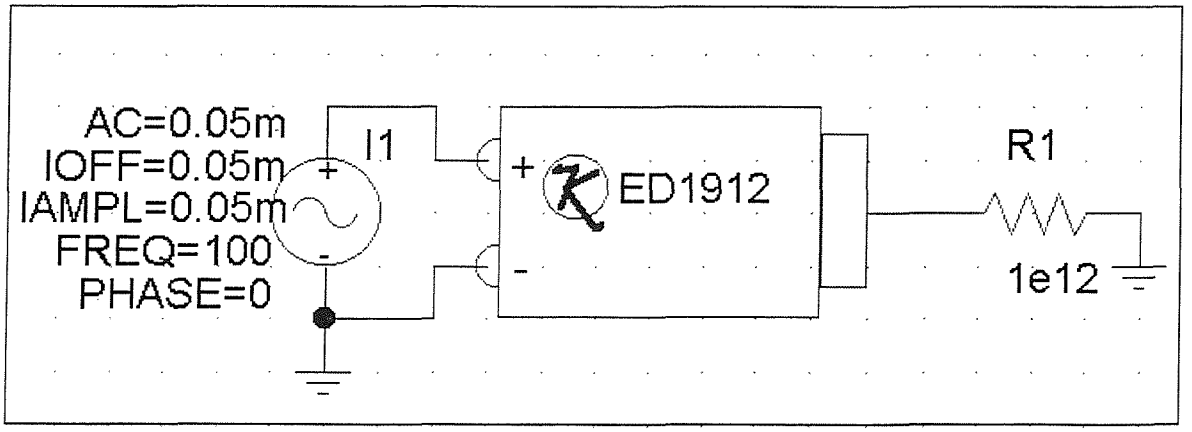

Figure 3.3: PSpice schematic used to derive two-port network parameters for the Knowles ED-1912 hearing aid receiver

A +144 dB correction factor was required to convert the output of the PSpice receiver analogue to SI units (LoPresti and Carlson, 1999), although, again, this was not used here. The receiver ABCD parameters are given by Equations (3.10) - (3.13).

$$A_r = \left.\frac{V_i}{P_o}\right|_{u_o=0} \qquad (3.10)$$

$$B_r = \left.\frac{V_i}{u_o}\right|_{P_o=0} \qquad (3.11)$$

$$C_r = \left.\frac{I_i}{P_o}\right|_{u_o=0} \qquad (3.12)$$

$$D_r = \left.\frac{I_i}{u_o}\right|_{P_0=0} \qquad (3.13)$$

Figure 3.4 compares the modelled input-output response for the ED-1912 receiver connected in series to a 10 mm long, 1 mm diameter tube and a 2 cm^3 coupler with that produced in PSpice, i.e. the sensitivity curve supplied by the manufacturer.

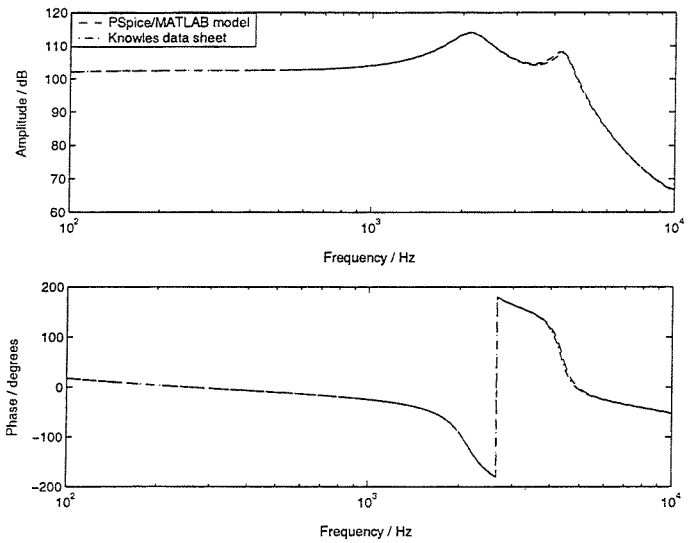

Figure 3.4: Comparison of magnitude and phase of the frequency response generated with the derived two-port network parameters in MATLAB with the PSpice response curve for the Knowles ED-1912 hearing aid receiver connected in series to a 10 mm long, 1 mm diameter tube and a 2 cm^3 coupler

Good agreement is seen between the responses. The slight differences around the second resonance peak near 4 kHz are due to the limitations of the PSpice tubing model (LoPresti and Carlson, 1999); the MATLAB model used the validated accurate tube model described in Section 2.6. The PSpice schematic used to produce the data sheet response did not use a grounded source, so it was necessary to derive the receiver parameters with a source that was not grounded. The spectrum analyser used to generate the source voltage for the experiments

described in Sections 3.4 – 3.7 was grounded, hence the schematic in Figure 3.3 was the correct form for modelling experimental procedures.

3.3 Computational model of the tubing and middle ear impedance

The two-port network equations for transient fluid flow in narrow pipes and the calculation of the vent radiation impedance and the external acoustic feedback path were implemented directly in MATLAB. It should be noted that the walls of the ear canal are not rigid, so the tubing model can only approximate the behaviour of the ear canal.

The model of the hearing aid system used both mean measured data for human subjects (Shaw, 1974) and an electrical analogue (de Jonge, 1996) to represent the middle ear impedance. The measured data was used to model the middle ear impedance in MATLAB using interpolation between data points. The electrical analogue was implemented in MATLAB directly.

The various parts of the hearing aid system were modelled using the methods described above. The matrix multiplication was performed (Equation 2.15), and from this, the response of the feedback path could be calculated.

3.4 Experimental verification of transducer and tubing models

The computer model of the *in situ* hearing aid system is intended to be used to develop a novel method of feedback cancellation. It was necessary that the model should be verified by comparison with experimental data before being used in any subsequent simulation investigations. The model of the feedback path was constructed gradually, verifying the component models in stages. This allowed examination of each part of the model and confirmed that the methods used were valid.

The simplest case modelled a receiver in series with a tube. Since it had already been demonstrated that the two-port equations for cylindrical tubes were valid (Egolf, 1977), it was concluded that the tubing would be simulated correctly and the experiment would aim to verify the receiver model.

The Knowles ED-1912 receiver was connected to a standard 2 cm^3 coupler, which was terminated by a Brüel and Kjaer type 4144 one inch pressure microphone connected to a Brüel and Kjaer type 2619 preamplifier. The receiver was encased in a mould of the coupler so that only the 2 cm^3 cavity occurred between the receiver and the reference microphone. The mould was made with Starsil 'C' silicone ear-impression material. The reference

microphone was calibrated with a Brüel and Kjaer type 4230 sound level calibrator before any measurements were made. The calibrator produced a 94 dB SPL 1 kHz tone when connected to the one inch microphone, from which the microphone's sensitivity could be determined. The frequency response of the receiver and coupler was measured over the frequency range 100 Hz to 10 kHz with an Advantest R9211C two-channel spectrum analyser. A mechanical block diagram of the experiment is shown in Figure 3.5.

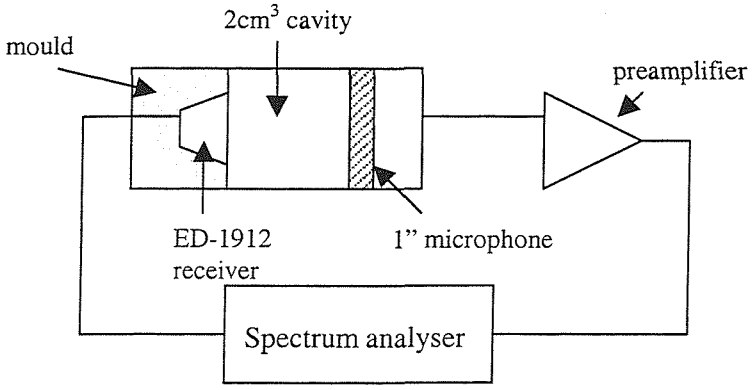

Figure 3.5: Mechanical block diagram of the experiment to verify the receiver model

The PSpice analogue for a 2 cm^3 coupler provided by Knowles modelled the coupler as a 1 Ω resistor in parallel with a 0.141 x 10^{-5} F capacitor. In MATLAB, it could be modelled in the same way, or as a cylindrical tube of length 7.44 mm and radius 9.25 mm (Kates, 1988b). In Figure 3.6, the modelled response is compared with measured responses for two different receivers, labelled ED-1912_1 and ED-1912_2, connected to the cavity. Good agreement is seen between the magnitudes of the responses, although there is a 180° phase difference between the ED-1912_2 response and the ED-1912_1 and modelled responses, indicating that connections to the terminals of the ED-1912_2 receiver were reversed. The slight differences between modelled and measured responses are due to the variations of individual transducers from the ideal model provided by the electrical analogue. The differences between the two measured responses of the actual receivers are due to variations between the devices.

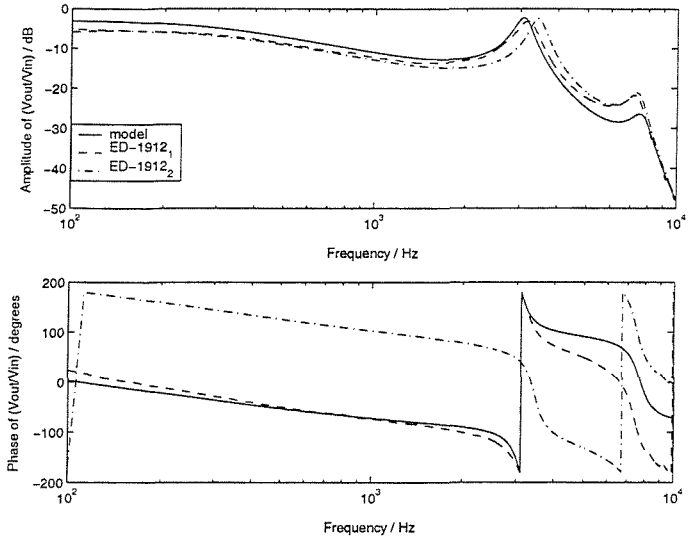

Figure 3.6: Comparison of measured and modelled responses for two ED-1912 receivers connected to a 2 cm^3 cavity

Having verified the receiver model, the microphone model was verified by an experiment connecting the receiver and 2 cm^3 cavity to an EA-1843 microphone encased in a mould of the reference microphone end of the coupler. The microphone was connected to the LM111 microphone amplifier, which was built around two Analog Device OP27 operational amplifiers (Rafaely *et al.*, 2000). The amplifier was set to supply 20 dB gain. The response was measured over the frequency range 100 Hz to 10 kHz as before. The mechanical block diagram is shown in Figure 3.7.

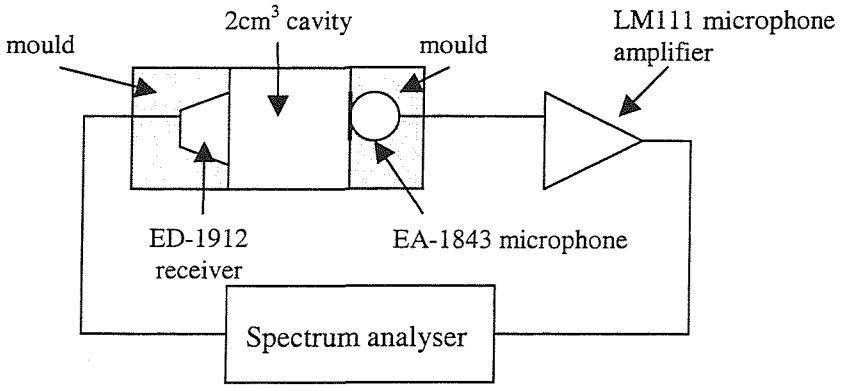

Figure 3.7: Mechanical block diagram of the experiment to verify the microphone model

Again, good agreement was observed between the measured and modelled responses (Figure 3.8). The slight discrepancies in amplitude may be attributed to transducer variability from the ideal response. Note that the gain of the measured response was adjusted to compensate for the gain and inverting effects of the amplifier, using the measured amplifier response to make this correction. This was done because the amplifier was not included in the model.

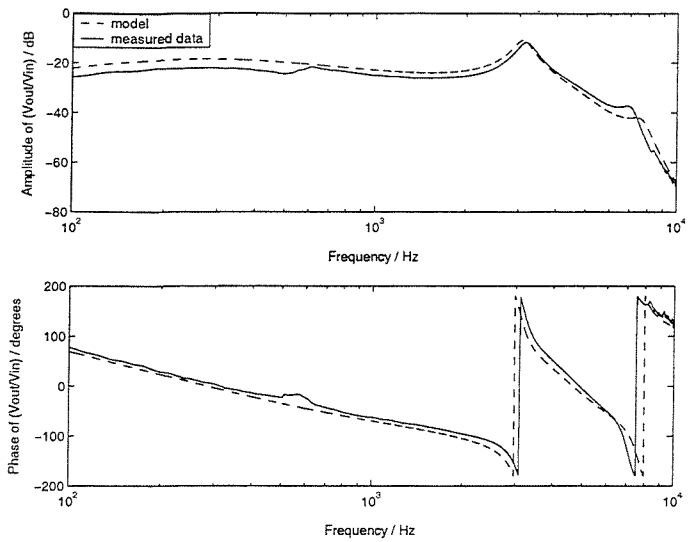

Figure 3.8: Comparison of measured and modelled responses for an ED-1912 receiver connected to a 2 cm^3 cavity and an EA-1843 microphone

It was concluded that both the receiver and microphone models were valid, and that this approach could be applied to any transducer if its electrical analogue was known. Some variability was observed between devices, and between the responses of the modelled and actual devices. This places a limit on the ability of any model to cancel the feedback path exactly. This stresses the importance of developing an adaptive feedback cancellation system which is robust to changes in the feedback path, even when there are slight differences between the actual feedback path and the model.

3.5 Experimental verification of the complete feedback path model

Having shown that the modelling techniques applied to the transducers and tubing were valid, the model was used to simulate the feedback path of an *in situ* in-the-ear hearing aid. The simulated response was compared with experimental data measured on an adult male with normal hearing. There were several sources of uncertainty in the model. Although the radii of the receiver tube and vent were known, their exact lengths had not been recorded and estimates were made. The accuracy of these was limited by the difficulty in measuring the tubes, which were not straight. Also, the dimensions of the subject's ear canal and the middle ear impedance were not known. These were approximated by average ear canal dimensions (Kates, 1988a, 1988b) and the mean impedance data for a set of normal ears (Shaw, 1974). Note that the presence of the earmould reduces the volume of the ear canal, and the model is concerned only with the unoccluded (unblocked) part of the canal.

As stated in Section 2.5, it is difficult to measure the sound pressure at the output of the external acoustic feedback path and the sound pressure at the microphone input as these

occupy the same area of space simultaneously and introducing a probe microphone to make the measurements would disturb the sound field. The feedback path may be cut between the microphone output and the receiver input and electrical measurements made. The form of the model used throughout the thesis is given at each frequency by Equation 2.15, reproduced below as Equation 3.14:

$$\begin{bmatrix} A_{total} & B_{total} \\ C_{total} & D_{total} \end{bmatrix} = \begin{bmatrix} A_r & B_r \end{bmatrix} \begin{bmatrix} A_1 & B_1 \\ C_1 & D_1 \end{bmatrix} \begin{bmatrix} A_2 & B_2 \\ C_2 & D_2 \end{bmatrix} \begin{bmatrix} 1 & 0 \\ 1/Z_T & 1 \end{bmatrix} \begin{bmatrix} A_3 & B_3 \\ C_3 & D_3 \end{bmatrix} \begin{bmatrix} 1 & 0 \\ 1/Z_V & 1 \end{bmatrix} \begin{bmatrix} A_F & 0 \\ 0 & 0 \end{bmatrix} \begin{bmatrix} A_m & 0 \\ 0 & 0 \end{bmatrix} \quad (3.14)$$

C_m and D_m can be set to zero because the input impedance of the microphone is much greater than that of the preceding block (see Equation 3.5). B_m can be set to zero because cutting the feedback path after the microphone is equivalent to setting the microphone output current to zero (Egolf *et al.*, 1989). The amplifier has been omitted here, so the gain was unity (0 dB).

The electrically-measured feedback path response is defined in Section 2.5 by Equation 2.17, reproduced as Equation 3.15 below:

$$\frac{V_{out}(f)}{V_{in}(f)} = \frac{1}{A_{total}(f)} \quad (3.15)$$

The MATLAB model was used to simulate the measured feedback path for an *in situ* ITE hearing aid worn by a subject with normal hearing. The data was taken from a previous study (Rafaely *et al.*, 2000). The hearing aid was a Starkey 11M ITE device with a Knowles ED-1975 receiver and a Knowles EM-3046 microphone. The analogue for the ED-1975 receiver was the same as that for the ED-1913 receiver, and differed slightly from that of the ED-1912 receiver (Knowles, 1997). The amplifier was disconnected. Details of each component in the model are given in Table 3.1.

Component	*Details*
Microphone	Knowles EM-3046 hearing aid microphone
Amplifier	Constant 0 dB gain, i.e. no amplification
Receiver	Knowles ED-1975 hearing aid receiver
Receiver tube	12 mm long, 0.7 mm radius
Ear canal	12 mm long, 3.3 mm radius (unoccluded portion with aid in place)
Middle ear impedance	Mean normal human eardrum impedance given by Shaw (1974)
Vent	18 mm long, 0.8 mm radius
External acoustic feedback path	15 mm vent-microphone distance, $\theta = 90$ °

Table 3.1: Details of the in situ *vented hearing aid model*

The radii of the receiver tube and vent were supplied by the earmould manufacturer; the lengths were measured approximately and may not be accurate. The length of the external acoustic feedback path was estimated also. The dimensions of the unoccluded part of the ear canal were not known, so average dimensions were used (Kates, 1988b) and the middle ear impedance was approximated by data for mean normal ear impedance (Shaw, 1974). The modelled feedback path is compared with the measured response for the subject's right ear in Figure 3.9.

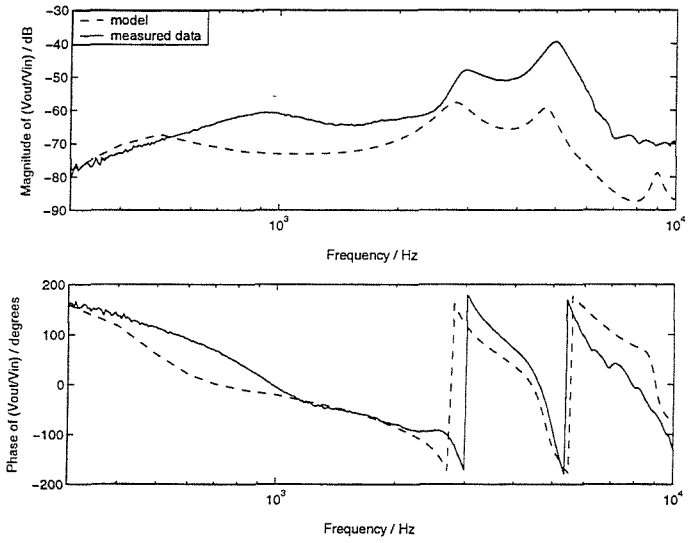

Figure 3.9: Measured and modelled feedback path responses for an in situ *ITE hearing aid fitted to a human subject*

It can be seen that there is general agreement between the shape of the measured and modelled responses and there is good agreement for the phase. The differences in amplitude

and resonance frequencies are due to the approximations made in the model and the variation of the transducers from the ideal devices described by the electrical analogues. It is possible to get better agreement between the shape of the responses by adjusting the parameters in the model. For example, the response in Figure 3.10 was obtained by altering the external acoustic feedback path length to 10 mm and the vent radius to 1.2 mm, simulating the addition of slit leakage around the earmould. However, this is only an example to show the effect of altering the model parameters. The vent radius is known and should not be altered without good reason.

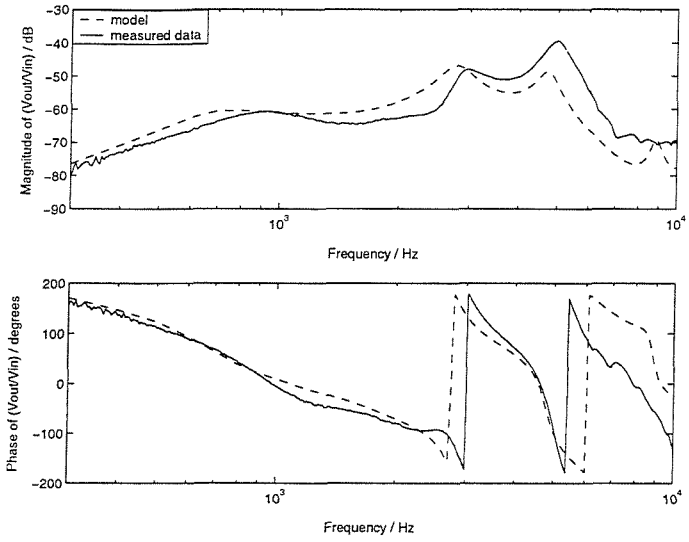

Figure 3.10: The effect of altering parameters in the model on the simulated feedback path response

Apart from the differences between the response of the modelled and actual transducers, the main source of error between the model and the measured data is the lack of knowledge about the actual ear canal dimensions and middle ear impedance of the subject. These have been approximated by average values, but it is unlikely that these are in exact agreement with the real physical parameters. The effects of the pinna, neck, shoulders and torso were not accounted for in the model.

The simulation of the *in situ* feedback path was repeated using the pinna modification given by Equation (2.38) (Kates, 1988b). The components of the model were as before (see Table 3.1). It can be seen in Figure 3.11 that the pinna modification has most effect in the region of the receiver resonances, increasing the amplitude of the peak near 5 kHz relative to that near 3 kHz, and increasing the amplitude in general above about 1.5 kHz. This improves the agreement between the modelled and measured responses. This is a better approach than altering the tubing dimensions without physical evidence of such changes.

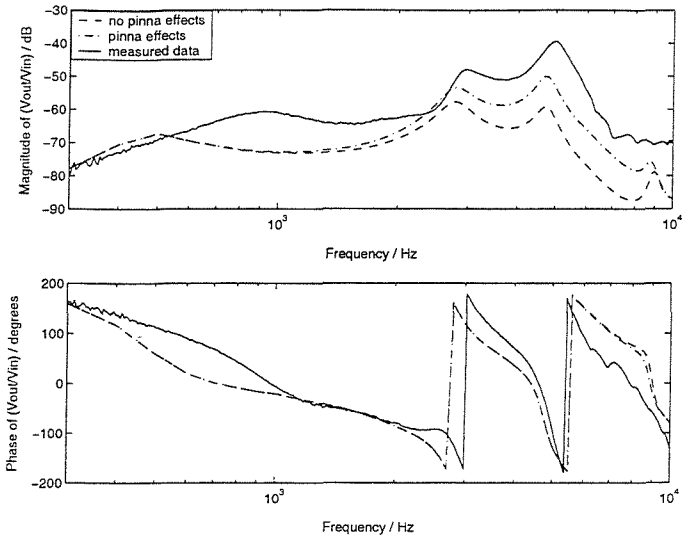

Figure 3.11: Measured and modelled feedback path responses for an in situ *ITE hearing aid fitted to a human subject with modifications to account for the effects of the pinna*

It has been shown that variation between transducers and the corresponding analogues and lack of knowledge of the dimensions and impedance of the human ear are the main sources of error in the model. Altering the parameters within the model can have a significant effect on the shape of the response. The difference between simulated and actual feedback path responses will limit the accuracy of any method of feedback cancellation based on the model, therefore it is important that the feedback cancellation must be robust to the effects of these differences when compensating for changes in the feedback path. Despite these approximations and uncertainties, the general good agreement between the simulated and actual feedback path responses implies that the model is valid and can be used to investigate the effects of individual parameters on the feedback path, and to develop a method of parametric adaptation for feedback control.

3.6 Experimental verification of the *in situ* in-the-ear hearing aid model with slit leakage

For the model to be used in a new method of feedback cancellation, it must be able to fit a range of feedback paths that might occur in real life, such as with varying amounts of slit leakage or with an obstruction near the ear. In a previous study (Rafaely *et al.*, 2000), measurements were made of the feedback path under different conditions: normally-fitted earmould, hand close to the ear, hand 10 cm from the ear, hand 20 cm from the ear, subject with mouth open fully, subject smiling, and earmould fitted incorrectly, with the top prong of the earmould removed from its position in the helix of the outer ear, such that the earmould was no longer fitted tightly to the ear. This section examines the ability of the model to represent the slit leak conditions; the obstruction conditions are examined in Section 3.7.

Adjustments were made to the parameters in the model of the hearing aid system with slit leakage to obtain good agreement with the latter three measured responses while maintaining a realistic size for the parameters. It should be noted that measurements were made by cutting the feedback path electrically between the microphone and receiver, omitting the amplifier and any other internal processing. Figure 2.16 shows the block diagram of the measured feedback path via the vent, with the external acoustic feedback path loaded by the microphone. The leak path can be modelled in the same way. The total feedback path response is calculated in the same way as before (Equation (2.47)).

Figure 3.12 shows the modelled and measured responses for the feedback path of a subject with the mouth open fully. Reasonably good agreement was obtained, allowing for the differences between specific transducers and the electrical analogues and errors in estimation of the dimensions of the tubes and external acoustic feedback path length. Opening the mouth to its fullest extent increases the width of the ear canal by up to 10 % (Oliveira, 1997); see Section 2.7. This was implemented in the model. The leak dimensions were determined empirically to obtain the best fit to the measured data, although typical slit leak dimensions (Johansen, 1974) were used as an initial estimate. The dimensions used to obtain the modelled response shown in Figure 3.12 are given in Table 3.2. The modification for pinna effects was used in the model for all the simulations in this chapter unless stated otherwise.

Component	*Details*
Microphone	Knowles EM-3046 hearing aid microphone
Amplifier	Constant 0 dB gain, i.e. no amplification
Receiver	Knowles ED-1975 hearing aid receiver
Receiver tube	12 mm long, 0.7 mm radius
Ear canal	12 mm long, 3.6 mm radius (10 % greater radius than normal fit)
Middle ear impedance	Mean normal human eardrum impedance given by Shaw (1974)
Vent	17 mm long, 0.8 mm radius
Vent external path	20 mm vent-microphone distance, $\theta = 90$ °
Leak	20 mm long, 0.6 mm radius
Leak external path	10 mm leak-microphone distance, $\theta = 90$ °

Table 3.2: Details of the in situ *vented hearing aid model with leak, subject's mouth open fully*

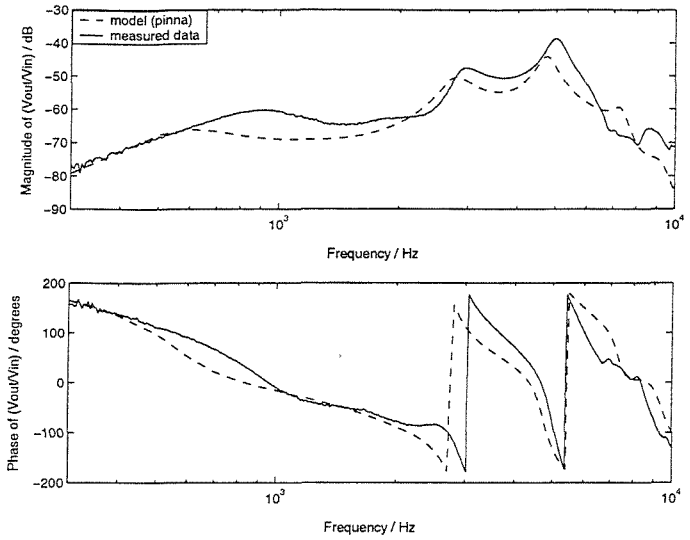

Figure 3.12: Modelled and measured responses for the feedback path with the subject's mouth open fully

The modelled and measured responses for the feedback path measured for a smiling subject are shown in Figure 3.13. It was assumed that the jaw was not open to its fullest extent, so the increase in ear canal diameter was less than for the previous example. Again, the leak dimensions were estimated. The dimensions used to obtain the modelled response shown in Figure 3.13 are given in Table 3.3.

Component	*Details*
Microphone	Knowles EM-3046 hearing aid microphone
Amplifier	Constant 0 dB gain, i.e. no amplification
Receiver	Knowles ED-1975 hearing aid receiver
Receiver tube	12 mm long, 0.7 mm radius
Ear canal	12 mm long, 3.4 mm radius (radius increased, but less than for open mouth)
Middle ear impedance	Mean normal human eardrum impedance given by Shaw (1974)
Vent	17 mm long, 0.8 mm radius
Vent external path	20 mm vent-microphone distance, $\theta = 90$ °
Leak	20 mm long, 0.6 mm radius
Leak external path	10 mm leak-microphone distance, $\theta = 90$ °

Table 3.3: Details of the in situ *vented hearing aid model with slit leak, subject smiling*

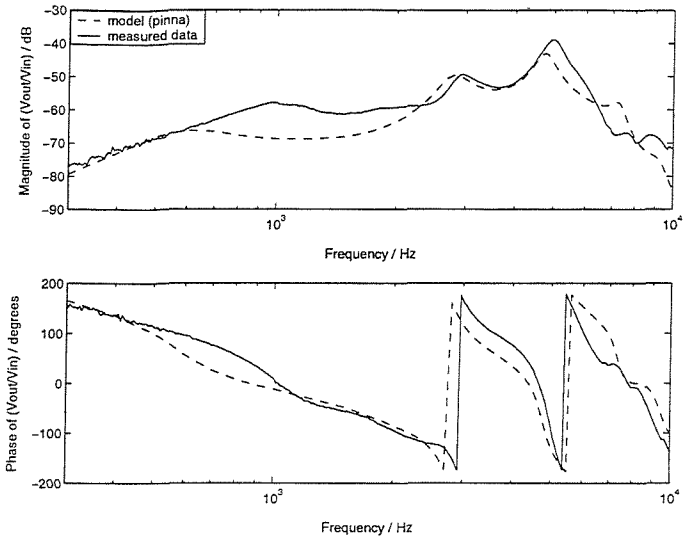

Figure 3.13: Modelled and measured responses for the feedback path with the subject smiling

When the earmould was fitted incorrectly to the pinna, the leak dimensions and the length of the leak external path were the only parameters varied. It was assumed that all other parts of the model would be the same as for the normal fitting since the subject's jaw had not moved. The modelled and measured responses are shown in Figure 3.14. The dimensions used to obtain the modelled response shown in Figure 3.14 are given in Table 3.4.

Component	*Details*
Microphone	Knowles EM-3046 hearing aid microphone
Amplifier	Constant 0 dB gain, i.e. no amplification
Receiver	Knowles ED-1975 hearing aid receiver
Receiver tube	12 mm long, 0.7 mm radius
Ear canal	12 mm long, 3.3 mm radius (unoccluded portion with aid in place)
Middle ear impedance	Mean normal human eardrum impedance given by Shaw (1974)
Vent	17 mm long, 0.8 mm radius
Vent external path	20 mm vent-microphone distance, $\theta = 90$ °
Leak	28 mm long, 0.7 mm radius
Leak external path	10 mm leak-microphone distance, $\theta = 90$ °

Table 3.4: Details of the in situ *vented hearing aid model with slit leak, earmould fitted incorrectly*

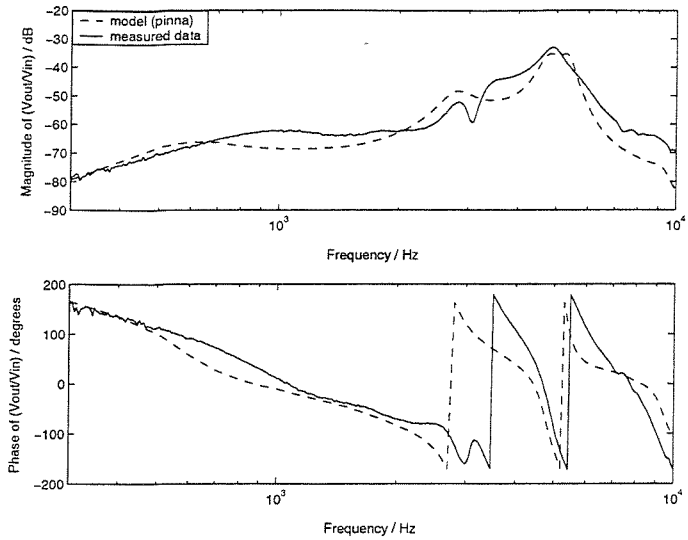

Figure 3.14: Modelled and measured responses for the feedback path with the earmould fitted incorrectly to the subject's ear

In all four examples (normal fit, open mouth, smiling face and incorrectly fitted earmould), the modelled response has been in good general agreement with the measured responses. Therefore it has been shown that the model is applicable to feedback path response data from a previous study (Rafaely *et al.*, 2000). It should be noted that all these modelled responses are approximations since accurate measurements of the leak were not possible and the actual ear canal dimensions and middle ear impedance were not known. In general, increasing the leak size raises the amplitude of the response over the entire frequency range.

3.7 Experimental verification of the *in situ* in-the-ear hearing aid model with an obstruction in the external acoustic feedback path

Feedback often occurs in practice due to the presence of an obstruction near the ear, such as a hand or a telephone handset. The model of the feedback path has been extended to simulate the effects of an obstruction (see Section 2.8). In this section, the validity of this model is tested.

Before verifying the model of the feedback path with an obstruction in the external acoustic feedback path with measured data, it was necessary to confirm that the model proposed in Section 2.8 was reasonable. If the model is behaving as expected, the response of the obstructed model should go to that of the normal model when the obstruction tube is large, i.e. the model should behave as if the vent is radiating into unobstructed space. The effects of altering the properties of the obstruction tube were investigated in turn, starting with the radius. Figure 3.15 compares the normal fit model with that of the model with an obstruction tube of length 10 cm and radius 1 cm, and with that of the model with an obstruction tube of

length 10 cm and radius 20 cm. The termination impedance R_{ob} = 10*R_{char}, where the characteristic impedance $R_{char} = \rho_0 c/\pi r_{ob}^2$. It can be seen that the very wide tube results in a response matching that of the normal fit model.

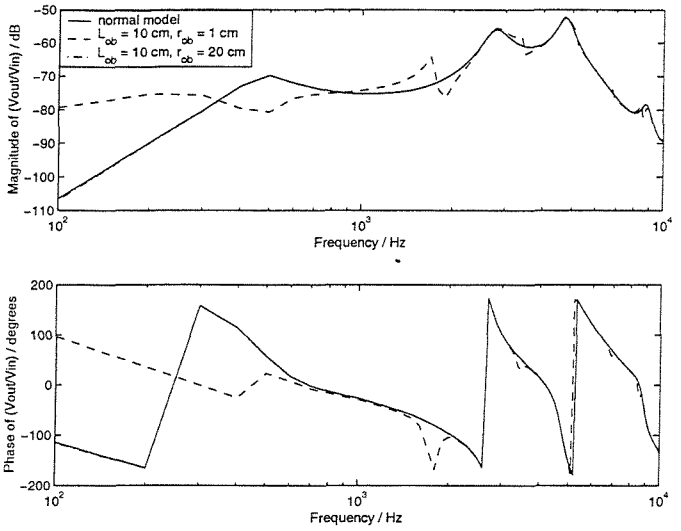

Figure 3.15: Comparison of modelled responses for the normal fit and obstructed feedback paths

As the length of the obstruction tube increases, keeping the radius and termination impedance constant (r_{ob} = 1 cm and R_{ob} = 10*R_{char}), the resonance frequency of the tube becomes lower so that less peaks occur in the response. The response above 1 kHz is largely unchanged as L_{ob} becomes large compared to the dimensions within the original hearing aid system itself, and as L_{ob} becomes very long, the model approaches the normal fit response. See Figure 3.16 below.

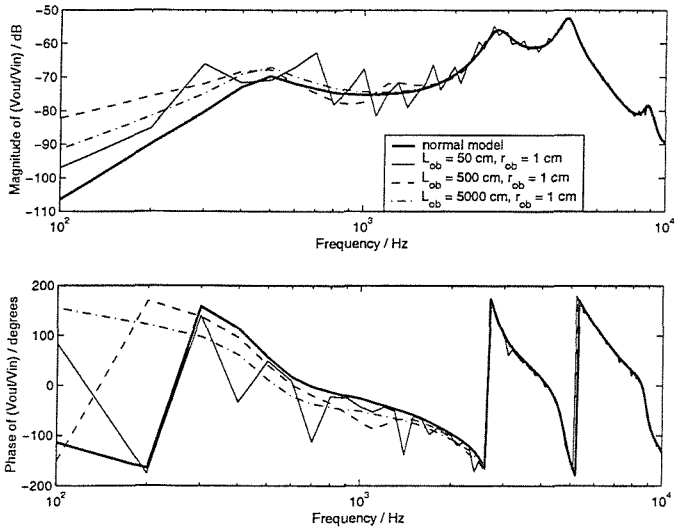

Figure 3.16: Effect of changing the length of the obstruction tube

There is a limit to the amount of reflection caused by changing the termination impedance R_{ob}. This limit occurs when all the energy is reflected and none is absorbed. This is illustrated by Figure 3.17, which compares the responses obtained with a 10 cm long, 1 cm radius obstruction tube with termination impedance $R_{ob} = R_{char}$, $R_{ob} = 10*R_{char}$, $R_{ob} = 50*R_{char}$ and $R_{ob} = 500*R_{char}$. It can be seen that the responses with $R_{ob} = 50*R_{char}$ and $500*R_{char}$ are almost equivalent. No reflections occur when the characteristic impedance is used to terminate the tube, as expected.

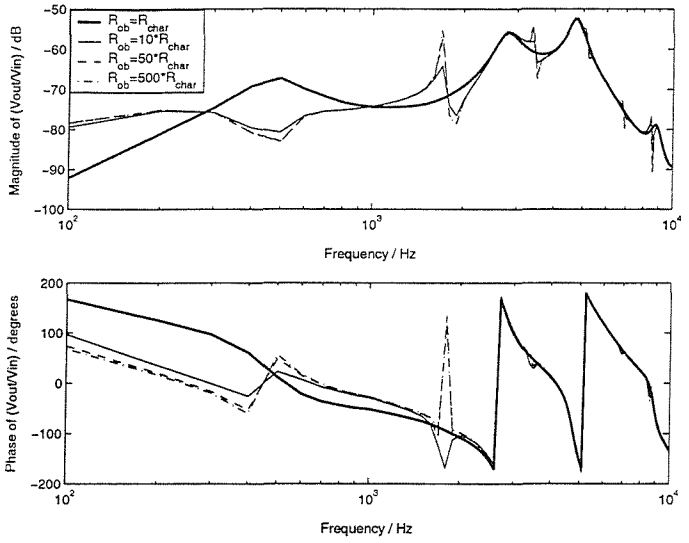

Figure 3.17: Limiting effect on the amount of possible reflection caused by increasing the termination impedance of the obstruction tube

Therefore it has been shown that the model behaves as expected: low frequency amplitude increases when L_{ob} and r_{ob} are decreased, and reflections and resonances at high frequencies are increased as R_{ob} is increased.

In the previous study (Rafaely *et al.*, 2000), the obstructed feedback path was measured under three conditions: hand over the ear, hand 10 cm from the ear and hand 20 cm from the ear. As for the slit leak and normal fit responses, the measurements were made by cutting the feedback path electrically between the microphone and receiver, omitting the amplifier and any internal processing. The block diagram of the model is shown in Figure 2.20.

The obstruction model is compared with measured data for a hand 10 cm from the ear in Figure 3.18. It is also compared with the normal fit model without pinna effects. It can be seen that the obstruction model gives almost the same response as the normal fit model. The use of a large tube to model the presence of an obstruction only has a significant effect at low frequencies. Modelling the enclosure formed by the obstruction and the pinna as a large tube

affects the radiation impedance of the vent, but does not account for changes in the external acoustic feedback path caused by the presence of the obstruction. Therefore the large tube model is insufficient to represent the presence of an obstruction near the ear and the modal model suggested in Section 2.8 would be a better approach as this would account for reflections between the obstruction and the ear, which have a greater effect at high frequencies.

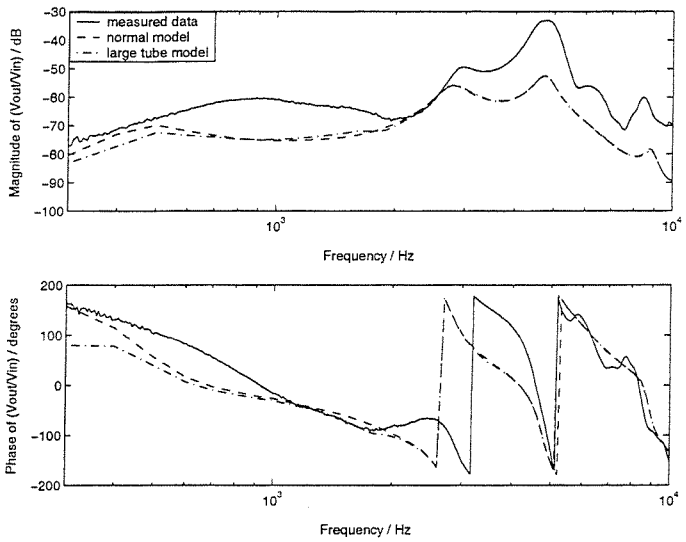

Figure 3.18: Measured and modelled feedback path responses for an in situ *ITE hearing aid with a hand 10 cm from the ear using both the normal fit and obstruction models*

The model needs to be developed further to give an accurate representation of high frequency reflection and resonance effects. This is outside the scope of this project and is a subject for future work.

3.8 Application of the model: The time-varying feedback path

A real feedback path changes continuously over time. A simple approximation of the time-varying feedback path was implemented as a series of feedback path OLTF responses produced with increasing effective leak radius. This represented a leak increasing in size over a short time frame, simulating a "continuous" change in the feedback path. Modelling changes in the feedback path in this way is used in Chapters 8 and 9 to simulate changes in the feedback path to be tracked by adaptive feedback cancellation methods.

If we assume that the hearing aid fills the ear canal up to the second bend (Kates, 1988b), and consider the simple situation where movement of the jaw changes the diameter of the slit leak while keeping all other parameters constant, it can be seen that the amplitude of the resonance peaks near 2.5 kHz and 5 kHz increases with increasing leak size (Figure 3.19). The 2.5 kHz

peak exceeds 0 dB for leak radii of 4 mm, 6 mm and 8 mm with 50 dB constant amplifier gain. The phase of the OLTF is near 0° at this point, so it is likely that the hearing aid would become unstable under these conditions (Nyquist, 1932).

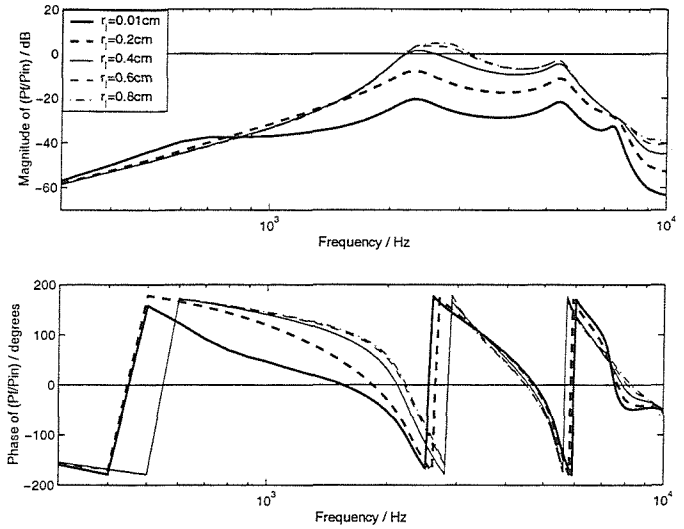

Figure 3.19: OLTF of an in situ *vented ITE hearing aid showing the effect of increasing slit leak size*

This simulation serves as an illustration of the effects of increasing leak size and was not verified experimentally.

3.9 Conclusions

Methods have been presented for modelling an *in situ* in-the-ear hearing aid system using a combination of electrical analogues in PSpice and acoustic theory in MATLAB. The models of the components and the entire system response were verified experimentally. There was some uncertainty in the feedback path model due to variation between the analogues and the actual transducers and middle ear impedance and uncertainty in the tube dimensions, but the modelled responses were in good agreement with the measured data for a range of feedback path conditions with slit leakage. The proposed model of the effects of an obstruction in the external acoustic feedback path was found to be inadequate; developing an accurate model of this condition is a subject for future work.

The model verified in this chapter will be used to develop a new parametric method of adaptive feedback cancellation in subsequent chapters.

4 Simplified analytic model of an in situ in-the-ear hearing aid system

4.1 Introduction

The matrix model described in the previous two chapters has a large computational load. It would be beneficial to reduce this load by simplifying the computation of any adaptive feedback cancellation algorithm based on the model. This chapter presents the derivation and subsequent simplification of an analytic expression for the feedback path response and compares its response with that obtained with the full matrix model. The model derived in this chapter is expected to cover a range of variations in the feedback path such as slit leakage or changes in the shape of the ear canal due to jaw movements. The analytic model is verified experimentally, indicating that it will be valid in later work on the development of a parametric adaptive algorithm for feedback cancellation. A set of analytic expressions is also derived for the gradient of the feedback path error surface for use in a steepest-descent based adaptive algorithm (see Chapter 7).

4.2 Deriving a full analytic expression for the measurable feedback path with slit leakage

In Chapter 2, a two-port network model of the *in situ* ITE hearing aid feedback path was developed. The response of the measurable feedback path was given by:

$$\frac{V_{out}(f)}{V_{in}(f)} = \frac{1}{A_{total}(f)} \tag{4.1}$$

where, at each frequency,

$$\begin{bmatrix} A_{total} & B_{total} \\ C_{total} & D_{total} \end{bmatrix} = \begin{bmatrix} A_r & B_r \end{bmatrix} \begin{bmatrix} A_1 & B_1 \\ C_1 & D_1 \end{bmatrix} \begin{bmatrix} A_2 & B_2 \\ C_2 & D_2 \end{bmatrix} \begin{bmatrix} 1 & 0 \\ 1/Z_T & 1 \end{bmatrix} \begin{bmatrix} A_3 & B_3 \\ C_3 & D_3 \end{bmatrix} \begin{bmatrix} 1 & 0 \\ 1/Z_V & 1 \end{bmatrix} \begin{bmatrix} A_F & 0 \\ 0 & 0 \end{bmatrix} \begin{bmatrix} A_m & 0 \\ 0 & 0 \end{bmatrix} \tag{4.2}$$

The subscripts are defined as in Chapter 2: r denotes the receiver, 1 the receiver tube, 2 the ear canal, 3 the vent, F the external acoustic feedback path and m the microphone. Z_T is the middle ear impedance and Z_V is the vent acoustic impedance. In this section, the vent and leak are treated as a single tube, referred to as the vent (denoted by the subscript 3). B_F, C_F and D_F are set to zero (see Section 2.6), as are B_m (Section 3.3), C_m and D_m (Section 3.2).

Since the feedback path response depends on A_{total} only, it should be possible to calculate the feedback path response directly from an expression for A_{total}. As long as the feedback path has the same form given by Equation (4.2), the expression for A_{total} should be valid. Calculating the feedback path response directly from an expression for A_{total} should require less computation than conducting matrix multiplication. Simplifying the expression for A_{total}

will also reduce the running time, which will benefit any method of feedback cancellation based on the model.

The measurable feedback path is described by Equation (4.2). Multiplying out the matrices, A_{total} is given by:

$$A_{total} = \left[\begin{array}{l} \left\{ \left(A_r \cosh(\Gamma_1 L_1) + B_r \dfrac{\sinh(\Gamma_1 L_1)}{Z_1} \right) + \dfrac{(A_r Z_1 \sinh(\Gamma_1 L_1) + B_r \cosh(\Gamma_1 L_1))}{\dfrac{Z_T \cosh(\Gamma_2 L_2) + Z_2 \sinh(\Gamma_2 L_2)}{(Z_T \sinh(\Gamma_2 L_2)/Z_2) + \cosh(\Gamma_2 L_2)}} \right\} \cosh(\Gamma_3 L_3) \\ + (A_r Z_1 \sinh(\Gamma_1 L_1) + B_r \cosh(\Gamma_1 L_1)) \dfrac{\sinh(\Gamma_3 L_3)}{Z_3} \\ + \dfrac{\left\{ \left(\left(A_r \cosh(\Gamma_1 L_1) + B_r \dfrac{\sinh(\Gamma_1 L_1)}{Z_1} \right) + \dfrac{(A_r Z_1 \sinh(\Gamma_1 L_1) + B_r \cosh(\Gamma_1 L_1))}{\dfrac{Z_T \cosh(\Gamma_2 L_2) + Z_2 \sinh(\Gamma_2 L_2)}{(Z_T \sinh(\Gamma_2 L_2)/Z_2) + \cosh(\Gamma_2 L_2)}} \right) Z_3 \sinh(\Gamma_3 L_3) \right\}}{\dfrac{\rho_0 c}{\pi r_3^2} (R_1(2kr_3) + jX_1(2kr_3))} \end{array} \right] \times \left[\frac{\rho_0 c r_3^2 k e^{j\left(\frac{\pi}{2} - kR\right)}}{2R\rho_0 c (R_1(2kr_3) + jX_1(2kr_3))} \left(\frac{2J_1(kr_3 \sin\theta)}{kr_3 \sin\theta} \right) \right]^{-1} \times A_m \qquad (4.3)$$

Some parts of this expression change over a very long time scale after fitting the hearing aid, e.g. the transducer parameters and receiver tube dimensions, and these can be considered constant for the purposes of the model. Other parts will change over a much shorter time scale, e.g. ear canal dimensions, the external acoustic feedback path and the vent/leak dimensions (slit leak size varying with time), and are considered variable in the model.

Figure 4.1 compares the response of $1/A_{total}$ with the response calculated by matrix multiplication. It can be seen that the responses are identical, thus the analytic expression can be used to model the measurable feedback path.

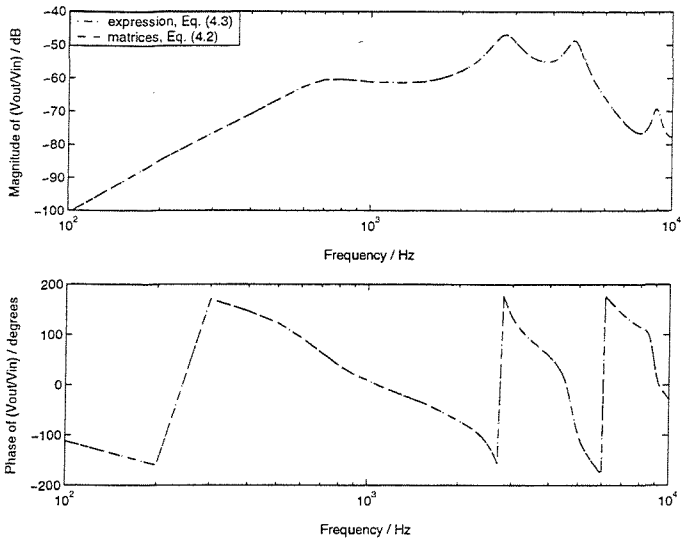

Figure 4.1: Comparison of feedback path responses obtained with matrix multiplication (Equation (4.2)) and the analytic expression (Equation (4.3))

4.3 Deriving a simplified expression for the measurable feedback path

The expression for A_{total} is the product of three main terms: (receiver to vent exit) x (external acoustic feedback path) x (microphone). First, let us examine the (receiver to vent exit) term:

$$\left[\begin{array}{l} \left\{\left(A_r\cosh(\Gamma_1 L_1)+B_r\frac{\sinh(\Gamma_1 L_1)}{Z_1}\right)+\frac{(A_r Z_1\sinh(\Gamma_1 L_1)+B_r\cosh(\Gamma_1 L_1))}{\frac{Z_T\cosh(\Gamma_2 L_2)+Z_2\sinh(\Gamma_2 L_2)}{(Z_T\sinh(\Gamma_2 L_2)/Z_2)+\cosh(\Gamma_2 L_2)}}\right\}\cosh(\Gamma_3 L_3) \\ +(A_r Z_1\sinh(\Gamma_1 L_1)+B_r\cosh(\Gamma_1 L_1))\frac{\sinh(\Gamma_3 L_3)}{Z_3} \\ +\frac{\left\{\left[\left(A_r\cosh(\Gamma_1 L_1)+B_r\frac{\sinh(\Gamma_1 L_1)}{Z_1}\right)+\frac{(A_r Z_1\sinh(\Gamma_1 L_1)+B_r\cosh(\Gamma_1 L_1))}{\frac{Z_T\cosh(\Gamma_2 L_2)+Z_2\sinh(\Gamma_2 L_2)}{(Z_T\sinh(\Gamma_2 L_2)/Z_2)+\cosh(\Gamma_2 L_2)}}\right]Z_3\sinh(\Gamma_3 L_3)\right\}}{+(A_r Z_1\sinh(\Gamma_1 L_1)+B_r\cosh(\Gamma_1 L_1))\cosh(\Gamma_3 L_3)} \\ \frac{\rho_0 c}{\pi r_3^2}(R_1(2kr_3)+jX_1(2kr_3)) \end{array}\right] \quad (4.4)$$

It was found empirically that

$$\left\{\left(A_r\cosh(\Gamma_1 L_1)+B_r\frac{\sinh(\Gamma_1 L_1)}{Z_1}\right)+\frac{(A_r Z_1\sinh(\Gamma_1 L_1)+B_r\cosh(\Gamma_1 L_1))}{\frac{Z_T\cosh(\Gamma_2 L_2)+Z_2\sinh(\Gamma_2 L_2)}{(Z_T\sinh(\Gamma_2 L_2)/Z_2)+\cosh(\Gamma_2 L_2)}}\right\}\cosh(\Gamma_3 L_3) \tag{4.5}$$

could be simplified to

$$\left\{\frac{(A_r Z_1\sinh(\Gamma_1 L_1)+B_r\cosh(\Gamma_1 L_1))}{\frac{Z_T\cosh(\Gamma_2 L_2)+Z_2\sinh(\Gamma_2 L_2)}{(Z_T\sinh(\Gamma_2 L_2)/Z_2)+\cosh(\Gamma_2 L_2)}}\right\}\cosh(\Gamma_3 L_3) \tag{4.6}$$

since

$$\frac{(A_r Z_1\sinh(\Gamma_1 L_1)+B_r\cosh(\Gamma_1 L_1))}{\frac{Z_T\cosh(\Gamma_2 L_2)+Z_2\sinh(\Gamma_2 L_2)}{(Z_T\sinh(\Gamma_2 L_2)/Z_2)+\cosh(\Gamma_2 L_2)}} \tag{4.7}$$

was about 30 times greater in amplitude than

$$\left(A_r\cosh(\Gamma_1 L_1)+B_r\frac{\sinh(\Gamma_1 L_1)}{Z_1}\right) \tag{4.8}$$

This is shown in Figures 4.2 and 4.3.

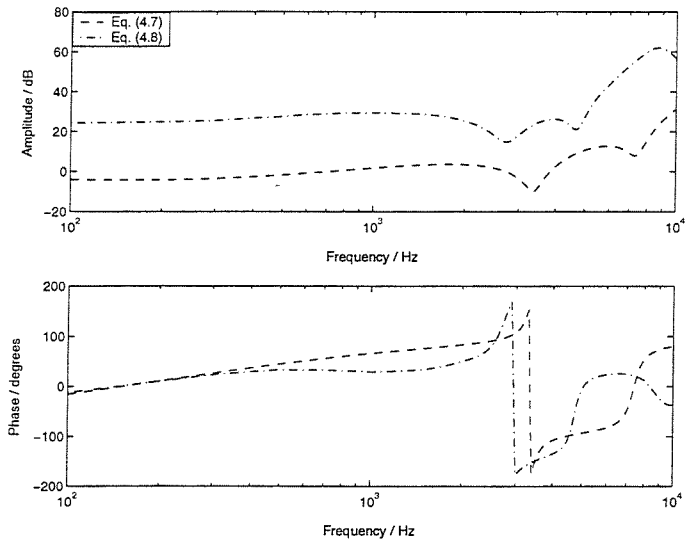

Figure 4.2: Comparing responses of Equations (4.7) and (4.8)

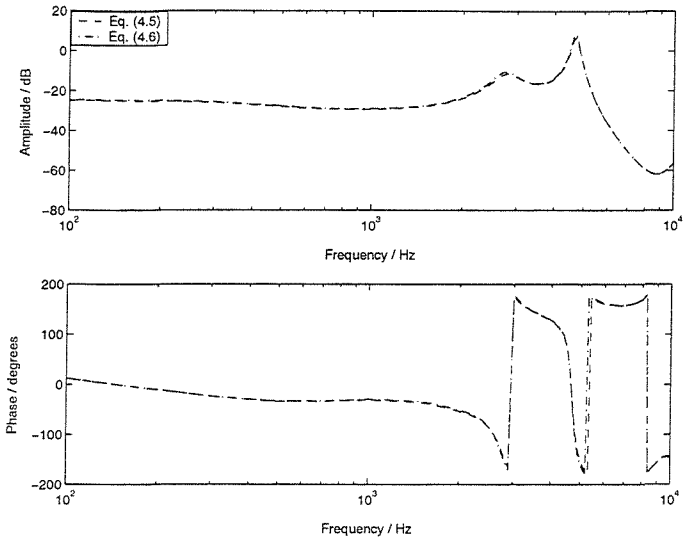

Figure 4.3: The effect of simplifying Equation (4.5) to Equation (4.6)

Using Equation (4.6) in the expression for A_{total}, very good agreement with the full expression was obtained (Figure 4.4).

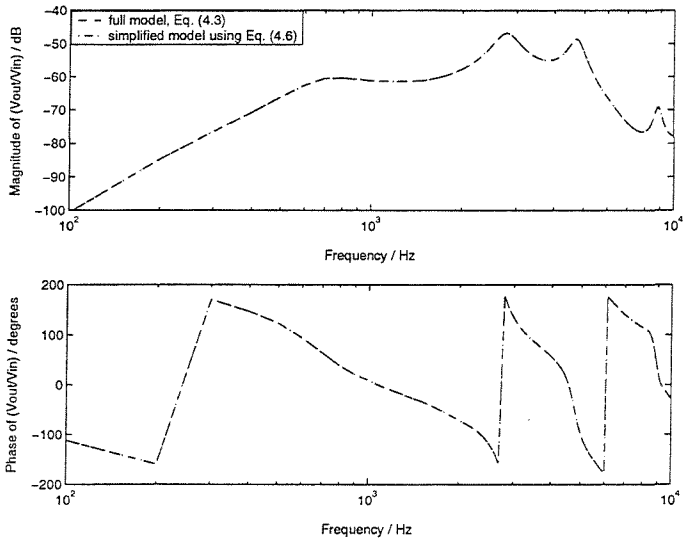

Figure 4.4: Comparing responses of full and simplified expressions for A_{total}

Examining the third part of this term, the same form occurs:

$$\frac{\left\{\left(\left(A_r\cosh(\Gamma_1 L_1)+B_r\frac{\sinh(\Gamma_1 L_1)}{Z_1}\right)+\frac{(A_r Z_1\sinh(\Gamma_1 L_1)+B_r\cosh(\Gamma_1 L_1))}{(Z_T\cosh(\Gamma_2 L_2)+Z_2\sinh(\Gamma_2 L_2))/(Z_T\sinh(\Gamma_2 L_2)/Z_2)+\cosh(\Gamma_2 L_2)}\right)Z_3\sinh(\Gamma_3 L_3)\right\}}{+(A_r Z_1\sinh(\Gamma_1 L_1)+B_r\cosh(\Gamma_1 L_1))\cosh(\Gamma_3 L_3)} \qquad (4.9)$$

$$\frac{\rho_0 c}{\pi r_3^2}(R_1(2kr_3)+jX_1(2kr_3))$$

Making the same simplification, this becomes:

$$\frac{\left\{\left(\frac{(A_r Z_1 \sinh(\Gamma_1 L_1)+B_r \cosh(\Gamma_1 L_1))}{Z_T \cosh(\Gamma_2 L_2)+Z_2 \sinh(\Gamma_2 L_2)}{(Z_T \sinh(\Gamma_2 L_2)/Z_2)+\cosh(\Gamma_2 L_2)}\right) Z_3 \sinh(\Gamma_3 L_3)+(A_r Z_1 \sinh(\Gamma_1 L_1)+B_r \cosh(\Gamma_1 L_1))\cosh(\Gamma_3 L_3)\right\}}{\frac{\rho_0 c}{\pi r_3^2}(R_1(2kr_3)+jX_1(2kr_3))} \quad (4.10)$$

Using this in the feedback path expression, good agreement with the response of the full expression is observed (Figure 4.5).

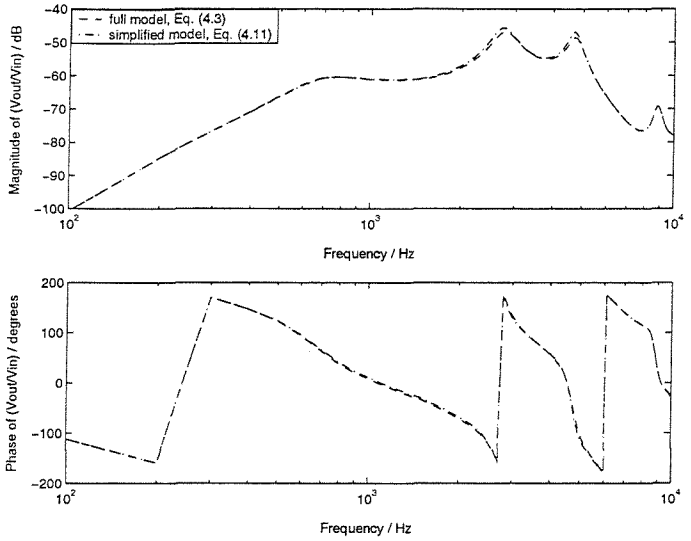

Figure 4.5: Comparing responses of full and simplified expressions for A_{total}

The simplified expression now has the form:

$$A_{total} = \left[\frac{\left\{\left(\frac{(A_r Z_1 \sinh(\Gamma_1 L_1)+B_r \cosh(\Gamma_1 L_1))}{Z_T \cosh(\Gamma_2 L_2)+Z_2 \sinh(\Gamma_2 L_2)}{(Z_T \sinh(\Gamma_2 L_2)/Z_2)+\cosh(\Gamma_2 L_2)}\right) \cosh(\Gamma_3 L_3)+(A_r Z_1 \sinh(\Gamma_1 L_1)+B_r \cosh(\Gamma_1 L_1))\frac{\sinh(\Gamma_3 L_3)}{Z_3}\right\}}{+\frac{\left\{\left(\frac{A_r Z_1 \sinh(\Gamma_1 L_1)+B_r \cosh(\Gamma_1 L_1)}{Z_T \cosh(\Gamma_2 L_2)+Z_2 \sinh(\Gamma_2 L_2)}{(Z_T \sinh(\Gamma_2 L_2)/Z_2)+\cosh(\Gamma_2 L_2)}\right) Z_3 \sinh(\Gamma_3 L_3)+(A_r Z_1 \sinh(\Gamma_1 L_1)+B_r \cosh(\Gamma_1 L_1))\cosh(\Gamma_3 L_3)\right\}}{\frac{\rho_0 c}{\pi r_3^2}(R_1(2kr_3)+jX_1(2kr_3))}}\right] \quad (4.11)$$

$$\times\left[\frac{\rho_0 c r_3^2 k e^{j\left(\frac{\pi}{2}-kR\right)}}{2R\rho_0 c(R_1(2kr_3)+jX_1(2kr_3))}\left(\frac{2J_1(kr_3\sin\theta)}{kr_3\sin\theta}\right)\right]^{-1}\times A_m$$

There is a common factor, $(A_r Z_1 \sinh(\Gamma_1 L_1) + B_r \cosh(\Gamma_1 L_1))$, in all parts of the first term, so we can rewrite the expression as:

$$A_{total} = (A_r Z_1 \sinh(\Gamma_1 L_1) + B_r \cosh(\Gamma_1 L_1)) \tag{4.12}$$
$$\times \left[\frac{\cosh(\Gamma_3 L_3)}{\dfrac{Z_T \cosh(\Gamma_2 L_2) + Z_2 \sinh(\Gamma_2 L_2)}{(Z_T \sinh(\Gamma_2 L_2)/Z_2) + \cosh(\Gamma_2 L_2)}} + \frac{\sinh(\Gamma_3 L_3)}{Z_3} + \frac{\left\{ \left(\dfrac{Z_3 \sinh(\Gamma_3 L_3)}{\dfrac{Z_T \cosh(\Gamma_2 L_2) + Z_2 \sinh(\Gamma_2 L_2)}{(Z_T \sinh(\Gamma_2 L_2)/Z_2) + \cosh(\Gamma_2 L_2)}} \right) + \cosh(\Gamma_3 L_3) \right\}}{\dfrac{\rho_0 c}{\pi r_3^2} (R_1(2kr_3) + jX_1(2kr_3))} \right]$$
$$\times \left[\frac{\rho_0 c r_3^2 k e^{j\left(\frac{\pi}{2} - kR\right)}}{2R\rho_0 c (R_1(2kr_3) + jX_1(2kr_3))} \left(\frac{2J_1(kr_3 \sin\theta)}{kr_3 \sin\theta} \right) \right]^{-1} \times A_m$$

Since the expression is not dependent on the order of the components, unlike matrix multiplication, the expression can be rearranged:

$$A_{total} = A_m \times (A_r Z_1 \sinh(\Gamma_1 L_1) + B_r \cosh(\Gamma_1 L_1)) \tag{4.13}$$
$$\times \left[\frac{\cosh(\Gamma_3 L_3)}{\dfrac{Z_T \cosh(\Gamma_2 L_2) + Z_2 \sinh(\Gamma_2 L_2)}{(Z_T \sinh(\Gamma_2 L_2)/Z_2) + \cosh(\Gamma_2 L_2)}} + \frac{\sinh(\Gamma_3 L_3)}{Z_3} + \frac{\left\{ \left(\dfrac{Z_3 \sinh(\Gamma_3 L_3)}{\dfrac{Z_T \cosh(\Gamma_2 L_2) + Z_2 \sinh(\Gamma_2 L_2)}{(Z_T \sinh(\Gamma_2 L_2)/Z_2) + \cosh(\Gamma_2 L_2)}} \right) + \cosh(\Gamma_3 L_3) \right\}}{\dfrac{\rho_0 c}{\pi r_3^2} (R_1(2kr_3) + jX_1(2kr_3))} \right]$$
$$\times \left[\frac{\rho_0 c r_3^2 k e^{j\left(\frac{\pi}{2} - kR\right)}}{2R\rho_0 c (R_1(2kr_3) + jX_1(2kr_3))} \left(\frac{2J_1(kr_3 \sin\theta)}{kr_3 \sin\theta} \right) \right]^{-1}$$

Consider the three terms dependent on Γ_3 and L_3:

$$\frac{\cosh(\Gamma_3 L_3)}{\dfrac{Z_T \cosh(\Gamma_2 L_2) + Z_2 \sinh(\Gamma_2 L_2)}{(Z_T \sinh(\Gamma_2 L_2)/Z_2) + \cosh(\Gamma_2 L_2)}} \tag{4.14}$$

$$\frac{\sinh(\Gamma_3 L_3)}{Z_3} \tag{4.15}$$

$$\frac{\left\{\left(\frac{Z_3\sinh(\Gamma_3 L_3)}{\frac{Z_T\cosh(\Gamma_2 L_2)+Z_2\sinh(\Gamma_2 L_2)}{(Z_T\sinh(\Gamma_2 L_2)/Z_2)+\cosh(\Gamma_2 L_2)}}\right)+\cosh(\Gamma_3 L_3)\right\}}{\frac{\rho_0 c}{\pi r_3^2}(R_1(2kr_3)+jX_1(2kr_3))} \qquad (4.16)$$

Examining the responses of these terms (Figure 4.6), it can be seen that the magnitude of Equation (4.16) is much greater than the magnitude of the other two terms, so these smaller terms can be neglected.

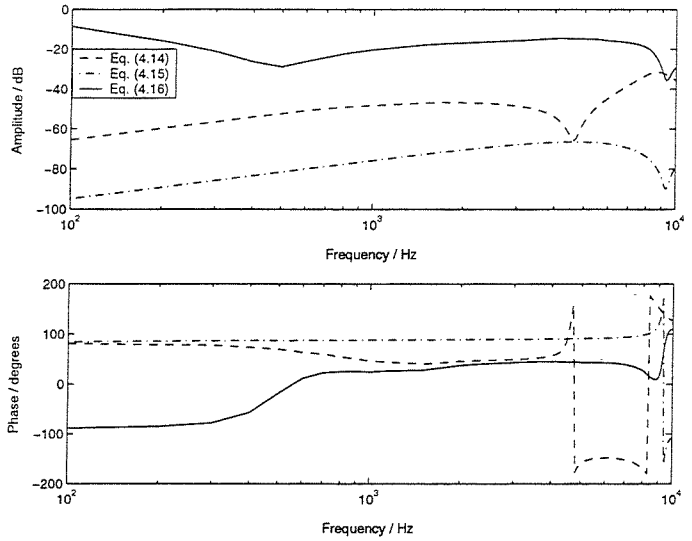

Figure 4.6: Comparing responses of Equations (4.14), (4.15) and (4.16)

The simplified feedback path expression now becomes:

$$A_{total}=A_m\times(A_r Z_1\sinh(\Gamma_1 L_1)+B_r\cosh(\Gamma_1 L_1)) \qquad (4.17)$$
$$\times\left[\frac{\left\{\left(\frac{Z_3\sinh(\Gamma_3 L_3)}{\frac{Z_T\cosh(\Gamma_2 L_2)+Z_2\sinh(\Gamma_2 L_2)}{(Z_T\sinh(\Gamma_2 L_2)/Z_2)+\cosh(\Gamma_2 L_2)}}\right)+\cosh(\Gamma_3 L_3)\right\}}{\frac{\rho_0 c}{\pi r_3^2}(R_1(2kr_3)+jX_1(2kr_3))}\right]\times\left[\frac{\rho_0 c r_3^2 k e^{j\left(\frac{\pi}{2}-kR\right)}}{2R\rho_0 c(R_1(2kr_3)+jX_1(2kr_3))}\left(\frac{2J_1(kr_3\sin\theta)}{kr_3\sin\theta}\right)\right]^{-1}$$

The simplified response was within 2 - 3 dB of that of the full expression (Figure 4.7), apart from above about 7.5 kHz, i.e. in the region of the high frequency resonance peak. However,

the amplitude of the responses at this frequency was about 20 dB below that of the receiver resonance peaks, where instability is more likely to occur. Therefore, this simplification could be deemed valid.

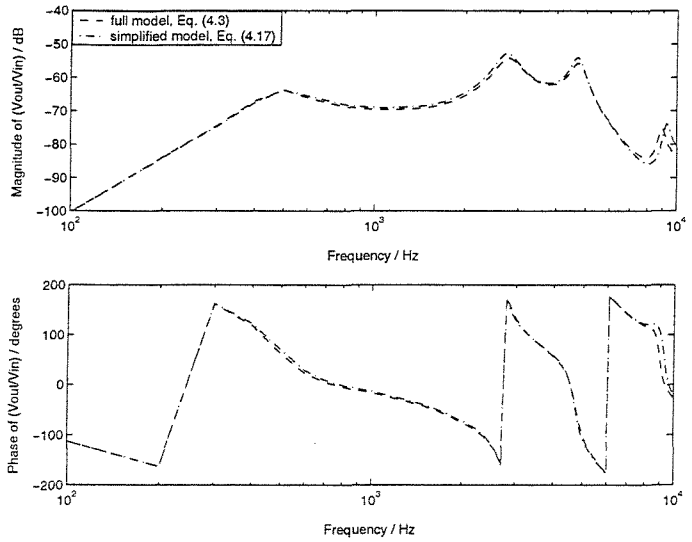

Figure 4.7: Comparing responses of full and simplified expressions for A_{total}

The term representing the external acoustic feedback path, A_F, can be simplified by neglecting the directivity term, since

$$\frac{2J_1(kr_3 \sin 90°)}{kr_3 \sin 90°} \approx 1 \text{ over the range 100 Hz to 10 kHz} \qquad (4.18)$$

This is shown in Figure 4.8.

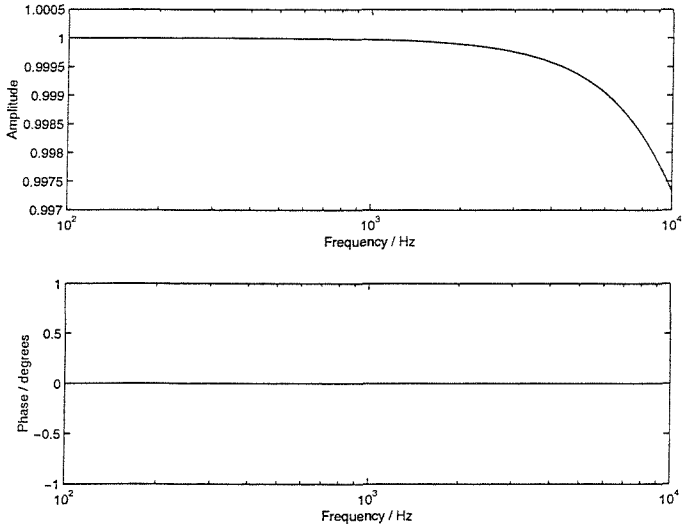

Figure 4.8: Frequency response of the directivity factor

Omitting the directivity term may cause a slight increase (about 1 dB) in the peak near 9 kHz, but otherwise does not seem to have a noticeable effect on the response (Figure 4.9).

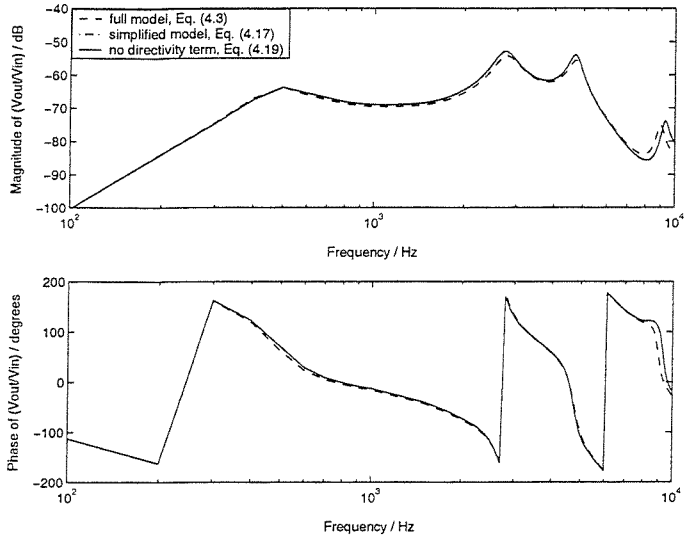

Figure 4.9: Effect on the response of omitting the directivity factor

Consider the current form of the simplified expression:

$$A_{total} = A_m \times \left(A_r Z_1 \sinh\left(\Gamma_1 L_1\right) + B_r \cosh\left(\Gamma_1 L_1\right)\right) \times \left[\frac{\left\{\left(\frac{Z_3 \sinh\left(\Gamma_3 L_3\right)}{Z_T \cosh\left(\Gamma_2 L_2\right) + Z_2 \sinh\left(\Gamma_2 L_2\right)}{\left(Z_T \sinh\left(\Gamma_2 L_2\right)/Z_2\right) + \cosh\left(\Gamma_2 L_2\right)}\right) + \cosh\left(\Gamma_3 L_3\right)\right\}}{\frac{\rho_0 c}{\pi r_3^2}\left(R_1\left(2kr_3\right) + jX_1\left(2kr_3\right)\right)}\right] \times \left[\frac{\rho_0 c r_3^2 k e^{j\left(\frac{\pi}{2} - kR\right)}}{2R\rho_0 c\left(R_1\left(2kr_3\right) + jX_1\left(2kr_3\right)\right)}\right]^{-1} \quad (4.19)$$

Rewriting:

$$A_{total} = A_m \times \left(A_r Z_1 \sinh\left(\Gamma_1 L_1\right) + B_r \cosh\left(\Gamma_1 L_1\right)\right) \times \left[\frac{\left\{\left(\frac{Z_3 \sinh\left(\Gamma_3 L_3\right)}{Z_T \cosh\left(\Gamma_2 L_2\right) + Z_2 \sinh\left(\Gamma_2 L_2\right)}{\left(Z_T \sinh\left(\Gamma_2 L_2\right)/Z_2\right) + \cosh\left(\Gamma_2 L_2\right)}\right) + \cosh\left(\Gamma_3 L_3\right)\right\}}{\frac{\rho_0 c}{\pi r_3^2}\left(R_1\left(2kr_3\right) + jX_1\left(2kr_3\right)\right)}\right] \times \left[\frac{2R\rho_0 c\left(R_1\left(2kr_3\right) + jX_1\left(2kr_3\right)\right)}{\rho_0 c r_3^2 k e^{j\left(\frac{\pi}{2} - kR\right)}}\right] \quad (4.20)$$

Cancelling $\rho_0 c(R_1(2kr_3) + jX_1(2kr_3))$:

$$A_{total} = A_m \times (A_r Z_1 \sinh(\Gamma_1 L_1) + B_r \cosh(\Gamma_1 L_1)) \times \left\{ \left(\frac{Z_3 \sinh(\Gamma_3 L_3)}{\frac{Z_T \cosh(\Gamma_2 L_2) + Z_2 \sinh(\Gamma_2 L_2)}{(Z_T \sinh(\Gamma_2 L_2)/Z_2) + \cosh(\Gamma_2 L_2)}} \right) + \cosh(\Gamma_3 L_3) \right\} \times \left[\frac{2R\pi r_3^2}{\rho_0 c r_3^2 k e^{j\left(\frac{\pi}{2} - kR\right)}} \right] \quad (4.21)$$

and cancelling r_3^2 in the last multiplying term, we obtain:

$$A_{total} = A_m \times (A_r Z_1 \sinh(\Gamma_1 L_1) + B_r \cosh(\Gamma_1 L_1)) \times \left\{ \left(\frac{Z_3 \sinh(\Gamma_3 L_3)}{\frac{Z_T \cosh(\Gamma_2 L_2) + Z_2 \sinh(\Gamma_2 L_2)}{(Z_T \sinh(\Gamma_2 L_2)/Z_2) + \cosh(\Gamma_2 L_2)}} \right) + \cosh(\Gamma_3 L_3) \right\} \times \left[\frac{2R\pi}{\rho_0 c k e^{j\left(\frac{\pi}{2} - kR\right)}} \right] \quad (4.22)$$

Further simplification cannot be made. Good agreement is observed between the responses of the full and simplified expressions (Figure 4.10).

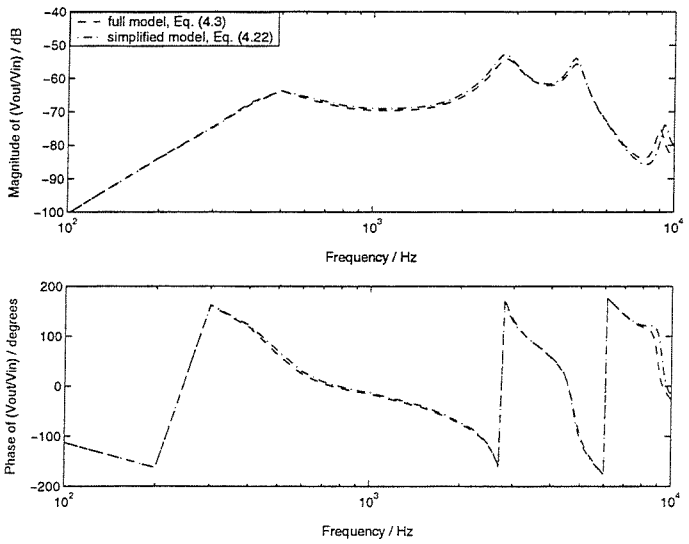

Figure 4.10: Comparing responses of full and simplified expressions for A_{total}

This implies that only the terms in curly parentheses are dependent on the vent/leak dimensions. The simplified expression now has the form:

A_{total} = (microphone)(receiver & receiver tube)(ear & vent)(external acoustic feedback path).

In this form, it is quite clear which parts of the expression will vary over a short time frame and which will not. It is likely that the parameters in the simplified expression describe the dominant characteristics of each component of the feedback path, i.e. these parameters make

the greatest contribution to the modelled response. Further work is necessary to determine the exact physical meaning of the simplified model.

Recall the expression given in Section 2.6 for the modification of the vent acoustic impedance due to the effects of the pinna (Kates, 1988b):

$$\mathbf{Z}_V' = \left\{1+\frac{1}{2}\left(\frac{(\omega/\omega_1)^2}{1+(\omega/\omega_1)^2}\right)^{\frac{1}{2}}\left[1-\cos\left(\pi\frac{\omega}{\omega_0}\right)\right]\right\}\mathbf{Z}_V \qquad (4.23)$$

The simplified expression for the measurable feedback path can be written to include the pinna effects by substituting Equation (4.25) for $\mathbf{Z}_V$ in Equation (4.2) and following the same process of simplification until no further simplification can be made. This yields:

$$A_{total} = A_m \times \left(A_r Z_1 \sinh(\Gamma_1 L_1) + B_r \cosh(\Gamma_1 L_1)\right) \qquad (4.24)$$
$$\times\left[\frac{\left\{\left(\frac{Z_3\sinh(\Gamma_3 L_3)}{\frac{Z_T\cosh(\Gamma_2 L_2)+Z_2\sinh(\Gamma_2 L_2)}{(Z_T\sinh(\Gamma_2 L_2)/Z_2)+\cosh(\Gamma_2 L_2)}}\right)+\cosh(\Gamma_3 L_3)\right\}}{\left\{1+\frac{1}{2}\left(\frac{(\omega/\omega_1)^2}{1+(\omega/\omega_1)^2}\right)^{\frac{1}{2}}\left[1-\cos\left(\pi\frac{\omega}{\omega_0}\right)\right]\right\}\frac{\rho_0 c}{\pi r_3^2}\left(R_1(2kr_3)+jX_1(2kr_3)\right)}\right]\times\left[\frac{2R\rho_0 c\left(R_1(2kr_3)+jX_1(2kr_3)\right)}{\rho_0 c r_3^2 k e^{j\left(\frac{\pi}{2}-kR\right)}}\right]$$

Cancelling $\rho_0 c(R_1(2kr_3) + jX_1(2kr_3)) / r_3^2$:

$$A_{total} = A_m \times \left(A_r Z_1 \sinh(\Gamma_1 L_1) + B_r \cosh(\Gamma_1 L_1)\right) \qquad (4.25)$$
$$\times\left[\frac{\left\{\left(\frac{Z_3\sinh(\Gamma_3 L_3)}{\frac{Z_T\cosh(\Gamma_2 L_2)+Z_2\sinh(\Gamma_2 L_2)}{(Z_T\sinh(\Gamma_2 L_2)/Z_2)+\cosh(\Gamma_2 L_2)}}\right)+\cosh(\Gamma_3 L_3)\right\}}{\left\{1+\frac{1}{2}\left(\frac{(\omega/\omega_1)^2}{1+(\omega/\omega_1)^2}\right)^{\frac{1}{2}}\left[1-\cos\left(\pi\frac{\omega}{\omega_0}\right)\right]\right\}}\right]\times\left[\frac{2R\pi}{\rho_0 c k e^{j\left(\frac{\pi}{2}-kR\right)}}\right]$$

Good agreement is obtained between the full and simplified expressions with pinna modifications (Figure 4.11). There are some slight differences above about 6.5 kHz due to the omission of the first added $\cosh(\Gamma_3 L_3)$ term, as observed for the model without pinna effects (see Figure 4.7).

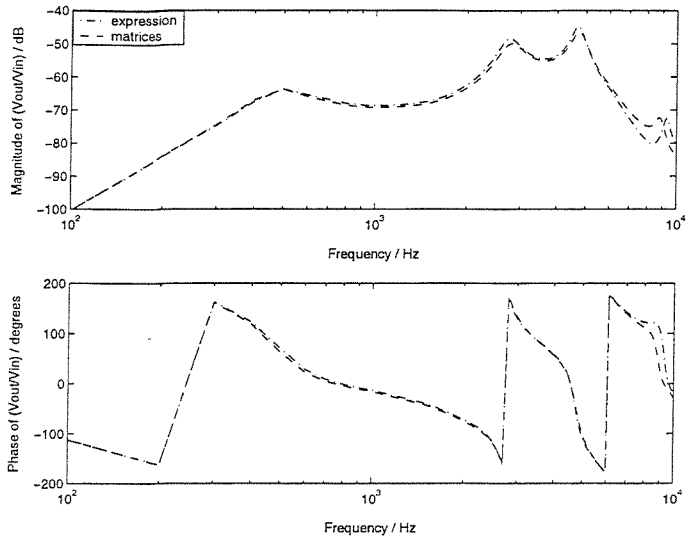

Figure 4.11: Comparing responses of full and simplified expressions for A_{total} with modifications for pinna effects

Therefore it is possible to derive an analytic expression for the measurable feedback path from the two-port model developed in Chapter 2. The expression can be simplified without great loss of accuracy. It is possible to include in the expression the effects of the pinna on the feedback path response.

4.4 Deriving the analytic gradient with respect to all varying parameters in the hearing aid system

The parametric adaptive feedback cancellation algorithm presented in Chapters 7, 8 and 9 estimates the gradient of the error surface with respect to the varying parameters. A more accurate method would use analytic expressions for these gradients. This method is not used in this work and is proposed as an area for future investigation. However, the analytic gradient expressions are presented here.

The simplified expression for A_{total} with no pinna effects is:

$$A_{total} = A_m \times \left(A_r Z_1 \sinh\left(\Gamma_1 L_1\right) + B_r \cosh\left(\Gamma_1 L_1\right)\right) \qquad (4.26)$$
$$\times \left\{ \left(\frac{Z_3 \sinh\left(\Gamma_3 L_3\right)}{\left(Z_T \cosh\left(\Gamma_2 L_2\right) + Z_2 \sinh\left(\Gamma_2 L_2\right)\right)} \Big/ \left(Z_T \sinh\left(\Gamma_2 L_2\right)/Z_2\right) + \cosh\left(\Gamma_2 L_2\right) \right) + \cosh\left(\Gamma_3 L_3\right) \right\} \times \left[\frac{2R\pi}{\rho_0 c k e^{j\left(\frac{\pi}{2} - kR\right)}} \right]$$

Recall the expressions for Γ_n and Z_n (Egolf, 1977):

$$\Gamma_n = j\frac{\omega}{c}\left(\frac{1+2(\gamma-1)[J_1(\alpha r_n)/\alpha r_n J_0(\alpha r_n)]}{1-2J_1(\beta r_n)/\beta r_n J_0(\beta r_n)}\right)^{1/2} \tag{4.27}$$

$$Z_n = \frac{\rho_0 c}{\pi r_0^{\,2}}\left(\left(1-\frac{2J_1(\beta r_n)}{\beta r_n J_0(\beta r_n)}\right)\left(1+2(\gamma-1)\frac{J_1(\alpha r_n)}{\alpha r_n J_0(\alpha r_n)}\right)\right)^{-1/2} \tag{2.28}$$

Both these expressions contain Bessel functions. For a Bessel function of order m (Pipes, 1958),

$$J_{-m}(x) = (-1)^m J_m(x) \tag{4.29}$$

and

$$J_m'(x) = \frac{d(J_m(x))}{dx} = \frac{J_{m-1}(x) - J_{m+1}(x)}{2} \tag{4.30}$$

Recall the chain rule for differentiation (James, 1996). If $z = g(x)$ and $y = f(z)$ then

$$\frac{dy}{dx} = \frac{dy}{dz}\frac{dz}{dx} = f'(z)g'(x) \tag{4.31}$$

If $y = f(ax + b)$ and a and b are constants, then

$$\frac{dy}{dx} = af'(ax+b) \tag{4.32}$$

Applying the chain rule to the hyperbolic functions, we have:

$$\frac{\partial \sinh(\Gamma_n L_n)}{\partial r_n} = \frac{\partial \sinh(\Gamma_n L_n)}{\partial \Gamma_n}\frac{\partial \Gamma_n}{\partial r_n} \tag{4.33}$$

Let $x = \Gamma_n L_n$, so

$$\frac{\partial \sinh(\Gamma_n L_n)}{\partial \Gamma_n} = \frac{\partial \sinh(x)}{\partial x}\frac{\partial x}{\partial \Gamma_n} = \cosh(x)L_n = L_n \cosh(\Gamma_n L_n) \tag{4.34}$$

and

$$\frac{\partial \sinh(\Gamma_n L_n)}{\partial r_n} = L_n \cosh(\Gamma_n L_n)\frac{\partial \Gamma_n}{\partial r_n} \tag{4.35}$$

$$\frac{\partial \Gamma_n}{\partial r_n} = j\frac{\omega}{c}\frac{1}{2}\left(\frac{1+2(\gamma-1)\dfrac{J_1(\alpha r_n)}{\alpha r_n J_0(\alpha r_n)}}{1-2\dfrac{J_1(\beta r_n)}{\beta r_n J_0(\beta r_n)}}\right)^{-\frac{1}{2}} \frac{\partial}{\partial r_n}\left(\frac{1+2(\gamma-1)\dfrac{J_1(\alpha r_n)}{\alpha r_n J_0(\alpha r_n)}}{1-2\dfrac{J_1(\beta r_n)}{\beta r_n J_0(\beta r_n)}}\right) \tag{4.36}$$

$$= j\frac{\omega}{c}\frac{1}{2}\left(\frac{1+2(\gamma-1)\dfrac{J_1(\alpha r_n)}{\alpha r_n J_0(\alpha r_n)}}{1-2\dfrac{J_1(\beta r_n)}{\beta r_n J_0(\beta r_n)}}\right)^{-\frac{1}{2}}$$

$$\times \frac{\left\{\left(1-2\dfrac{J_1(\beta r_n)}{\beta r_n J_0(\beta r_n)}\right)\left(2(\gamma-1)\dfrac{\partial}{\partial r_n}\left(\dfrac{J_1(\alpha r_n)}{\alpha r_n J_0(\alpha r_n)}\right)\right)\right.}{\left.-\left(1+2(\gamma-1)\dfrac{J_1(\alpha r_n)}{\alpha r_n J_0(\alpha r_n)}\right)\left(-2\dfrac{\partial}{\partial r_n}\left(\dfrac{J_1(\beta r_n)}{\beta r_n J_0(\beta r_n)}\right)\right)\right\}}{\left(1-2\dfrac{J_1(\beta r_n)}{\beta r_n (\beta r_n)}\right)^2}$$

where

$$\frac{\partial}{\partial r_n}\left(\frac{J_1(\alpha r_n)}{\alpha r_n J_0(\alpha r_n)}\right) = \frac{\alpha r_n J_0(\alpha r_n)\dfrac{\partial J_1(\alpha r_n)}{\partial r_n} - J_1(\alpha r_n)\left(\alpha r_n \dfrac{\partial J_0(\alpha r_n)}{\partial r_n} + \alpha J_0(\alpha r_n)\right)}{(\alpha r_n J_0(\alpha r_n))^2} \tag{4.37}$$

$$= \frac{r_n J_0(\alpha r_n)\dfrac{\alpha}{2}(J_0(\alpha r_n) - J_2(\alpha r_n)) - J_1(\alpha r_n)\left(r_n \dfrac{\alpha}{2}(J_{-1}(\alpha r_n) - J_1(\alpha r_n)) + J_0(\alpha r_n)\right)}{\alpha(r_n J_0(\alpha r_n))^2}$$

and

$$\frac{\partial}{\partial r_n}\left(\frac{J_1(\beta r_n)}{\beta r_n J_0(\beta r_n)}\right) = \frac{\beta r_n J_0(\beta r_n)\dfrac{\partial J_1(\beta r_n)}{\partial r_n} - J_1(\beta r_n)\left(\beta r_n \dfrac{\partial J_0(\beta r_n)}{\partial r_n} + \beta J_0(\beta r_n)\right)}{(\beta r_n J_0(\beta r_n))^2} \tag{4.38}$$

$$= \frac{r_n J_0(\beta r_n)\dfrac{\beta}{2}(J_0(\beta r_n) - J_2(\beta r_n)) - J_1(\beta r_n)\left(r_n \dfrac{\beta}{2}(J_{-1}(\beta r_n) - J_1(\beta r_n)) + J_0(\beta r_n)\right)}{\beta(r_n J_0(\beta r_n))^2}$$

Similarly,

$$\frac{\partial \cosh(\Gamma_n L_n)}{\partial r_n} = L_n \sinh(\Gamma_n L_n)\frac{\partial \Gamma_n}{\partial r_n} \tag{4.39}$$

Differentiating Z_n with respect to r_n,

$$\frac{\partial Z_n}{\partial r_n} = -2\frac{\rho_0 c}{\pi r_n^3}\left[\left(1-2\frac{J_1(\beta r_n)}{\beta r_n J_0(\beta r_n)}\right)\left(1+2(\gamma-1)\frac{J_1(\alpha r_n)}{\alpha r_n J_0(\alpha r_n)}\right)\right]^{-\frac{1}{2}} \tag{4.40}$$

$$+\left(\begin{array}{l}\dfrac{\rho_0 c}{\pi r_n^2}\left(-\dfrac{1}{2}\right)\left[\left(1-2\dfrac{J_1(\beta r_n)}{\beta r_n J_0(\beta r_n)}\right)\left(1+2(\gamma-1)\dfrac{J_1(\alpha r_n)}{\alpha r_n J_0(\alpha r_n)}\right)\right]^{-\frac{3}{2}} \\ \times\left\{\begin{array}{l}\left(1-2\dfrac{J_1(\beta r_n)}{\beta r_n J_0(\beta r_n)}\right)\left(2(\gamma-1)\dfrac{\partial}{\partial r_n}\left(\dfrac{J_1(\alpha r_n)}{\alpha r_n J_0(\alpha r_n)}\right)\right) \\ +\left(1+2(\gamma-1)\dfrac{J_1(\alpha r_n)}{\alpha r_n J_0(\alpha r_n)}\right)\left(-2\dfrac{\partial}{\partial r_n}\left(\dfrac{J_1(\beta r_n)}{\beta r_n J_0(\beta r_n)}\right)\right)\end{array}\right.\end{array}\right)$$

Using these expressions, we can derive the gradients of A_{total} with respect to r_1, r_2, and r_3.

$$\frac{\partial A_{total}}{\partial r_1} = A_m\left(A_r\left(Z_1\frac{\partial \sinh(\Gamma_1 L_1)}{\partial r_1}+\sinh(\Gamma_1 L_1)\frac{\partial Z_1}{\partial r_1}\right)+B_r\frac{\partial \cosh(\Gamma_1 L_1)}{\partial r_1}\right) \tag{4.41}$$

$$\times\left\{\frac{Z_3\sinh(\Gamma_3 L_3)}{\dfrac{Z_T\cosh(\Gamma_2 L_2)+Z_2\sinh(\Gamma_2 L_2)}{(Z_T\sinh(\Gamma_2 L_2)/Z_2)+\cosh(\Gamma_2 L_2)}}+\cosh(\Gamma_3 L_3)\right\}\left[\frac{2R\pi}{\rho_0 cke^{j\left(\frac{\pi}{2}-kR\right)}}\right]$$

$$\frac{\partial A_{total}}{\partial r_2} = A_m\times(A_r Z_1\sinh(\Gamma_1 L_1)+B_r\cosh(\Gamma_1 L_1)) \tag{4.42}$$

$$\times\left\{Z_3\sinh(\Gamma_3 L_3)\frac{\partial}{\partial r_2}\left(\frac{(Z_T\sinh(\Gamma_2 L_2)/Z_2)+\cosh(\Gamma_2 L_2)}{Z_T\cosh(\Gamma_2 L_2)+Z_2\sinh(\Gamma_2 L_2)}\right)\right\}\times\left[\frac{2R\pi}{\rho_0 cke^{j\left(\frac{\pi}{2}-kR\right)}}\right]$$

where

$$\frac{\partial}{\partial r_2}\left(\frac{(Z_T\sinh(\Gamma_2 L_2)/Z_2)+\cosh(\Gamma_2 L_2)}{Z_T\cosh(\Gamma_2 L_2)+Z_2\sinh(\Gamma_2 L_2)}\right)=\frac{\partial}{\partial r_2}\left(\frac{\sigma}{\varphi}\right)=\frac{\varphi\dfrac{\partial\sigma}{\partial r_2}-\sigma\dfrac{\partial\varphi}{\partial r_2}}{\varphi^2} \tag{4.43}$$

in which

$$\frac{\partial\sigma}{\partial r_2}=\frac{\partial}{\partial r_2}((Z_T\sinh(\Gamma_2 L_2)/Z_2)+\cosh(\Gamma_2 L_2)) \tag{4.44}$$

$$=Z_T\frac{\left(Z_2\dfrac{\partial\sinh(\Gamma_2 L_2)}{\partial r_2}-\sinh(\Gamma_2 L_2)\dfrac{\partial Z_2}{\partial r_2}\right)}{Z_2^2}+\frac{\partial\cosh(\Gamma_2 L_2)}{\partial r_2}$$

and

$$\frac{\partial \varphi}{\partial r_2} = \frac{\partial}{\partial r_2}\left(Z_T \cosh\left(\Gamma_2 L_2\right) + Z_2 \sinh\left(\Gamma_2 L_2\right)\right) \tag{4.45}$$
$$= Z_T \frac{\partial \cosh\left(\Gamma_2 L_2\right)}{\partial r_2} + Z_2 \frac{\partial \sinh\left(\Gamma_2 L_2\right)}{\partial r_2} + \sinh\left(\Gamma_2 L_2\right)\frac{\partial Z_2}{\partial r_2}$$

$$\frac{\partial A_{total}}{\partial r_3} = A_m \times \left(A_r Z_1 \sinh\left(\Gamma_1 L_1\right) + B_r \cosh\left(\Gamma_1 L_1\right)\right) \tag{4.46}$$
$$\times \left\{ \left(\frac{Z_3 \dfrac{\partial \sinh\left(\Gamma_3 L_3\right)}{\partial r_3} + \sinh\left(\Gamma_3 L_3\right)\dfrac{\partial Z_3}{\partial r_3}}{\dfrac{Z_T \cosh\left(\Gamma_2 L_2\right) + Z_2 \sinh\left(\Gamma_2 L_2\right)}{\left(Z_T \sinh\left(\Gamma_2 L_2\right)/Z_2\right) + \cosh\left(\Gamma_2 L_2\right)}} \right) + \frac{\partial \cosh\left(\Gamma_3 L_3\right)}{\partial r_3} \right\} \times \left[\frac{2R\pi}{\rho_0 c k e^{j\left(\frac{\pi}{2} - kR\right)}} \right]$$

Similarly, we can obtain expressions for the gradients with respect to the tube lengths:

$$\frac{\partial A_{total}}{\partial L_1} = A_m \times \left(A_r Z_1 \Gamma_1 \cosh\left(\Gamma_1 L_1\right) + B_r \Gamma_1 \sinh\left(\Gamma_1 L_1\right)\right) \tag{4.47}$$
$$\times \left\{ \left(\frac{Z_3 \sinh\left(\Gamma_3 L_3\right)}{\dfrac{Z_T \cosh\left(\Gamma_2 L_2\right) + Z_2 \sinh\left(\Gamma_2 L_2\right)}{\left(Z_T \sinh\left(\Gamma_2 L_2\right)/Z_2\right) + \cosh\left(\Gamma_2 L_2\right)}} \right) + \cosh\left(\Gamma_3 L_3\right) \right\} \times \left[\frac{2R\pi}{\rho_0 c k e^{j\left(\frac{\pi}{2} - kR\right)}} \right]$$

$$\frac{\partial A_{total}}{\partial L_2} = A_m \times \left(A_r Z_1 \sinh\left(\Gamma_1 L_1\right) + B_r \cosh\left(\Gamma_1 L_1\right)\right) \tag{4.48}$$
$$\times \left\{ Z_3 \sinh\left(\Gamma_3 L_3\right) \frac{\partial}{\partial L_2} \left(\frac{\left(Z_T \sinh\left(\Gamma_2 L_2\right)/Z_2\right) + \cosh\left(\Gamma_2 L_2\right)}{Z_T \cosh\left(\Gamma_2 L_2\right) + Z_2 \sinh\left(\Gamma_2 L_2\right)} \right) \right\} \times \left[\frac{2R\pi}{\rho_0 c k e^{j\left(\frac{\pi}{2} - kR\right)}} \right]$$

where

$$\frac{\partial}{\partial L_2} \left(\frac{\left(Z_T \sinh\left(\Gamma_2 L_2\right)/Z_T\right) + \cosh\left(\Gamma_2 L_2\right)}{Z_T \cosh\left(\Gamma_2 L_2\right) + Z_2 \sinh\left(\Gamma_2 L_2\right)} \right) \tag{4.49}$$
$$= \frac{\left\{ \begin{array}{l} \left(Z_T \cosh\left(\Gamma_2 L_2\right) + Z_2 \sinh\left(\Gamma_2 L_2\right)\right)\left(\left(Z_T \Gamma_2 \cosh\left(\Gamma_2 L_2\right)/Z_2\right) + \Gamma_2 \sinh\left(\Gamma_2 L_2\right)\right) \\ -\left(\left(Z_T \sinh\left(\Gamma_2 L_2\right)/Z_2\right) + \cosh\left(\Gamma_2 L_2\right)\right)\left(Z_T \Gamma_2 \sinh\left(\Gamma_2 L_2\right) + Z_2 \Gamma_2 \cosh\left(\Gamma_2 L_2\right)\right) \end{array} \right\}}{\left(Z_T \cosh\left(\Gamma_2 L_2\right) + Z_2 \sinh\left(\Gamma_2 L_2\right)\right)^2}$$

$$\frac{\partial A_{total}}{\partial L_3} = A_m \times \left(A_r Z_1 \sinh\left(\Gamma_1 L_1\right) + B_r \cosh\left(\Gamma_1 L_1\right)\right) \tag{4.50}$$

$$\times \left\{ \left(\frac{Z_3 \Gamma_3 \cosh\left(\Gamma_3 L_3\right)}{\frac{Z_T \cosh\left(\Gamma_2 L_2\right) + Z_2 \sinh\left(\Gamma_2 L_2\right)}{\left(Z_T \sinh\left(\Gamma_2 L_2\right)/Z_2\right) + \cosh\left(\Gamma_2 L_2\right)}} \right) + \Gamma_3 \sinh\left(\Gamma_3 L_3\right) \right\} \times \left[\frac{2R\pi}{\rho_0 cke^{j\left(\frac{\pi}{2} - kR\right)}} \right]$$

Differentiating with respect to the transducer parameters, external acoustic feedback path length and middle ear impedance:

$$\frac{\partial A_{total}}{\partial A_m} = \left(A_r Z_1 \sinh\left(\Gamma_1 L_1\right) + B_r \cosh\left(\Gamma_1 L_1\right)\right) \tag{4.51}$$

$$\times \left\{ \left(\frac{Z_3 \sinh\left(\Gamma_3 L_3\right)}{\frac{Z_T \cosh\left(\Gamma_2 L_2\right) + Z_2 \sinh\left(\Gamma_2 L_2\right)}{\left(Z_T \sinh\left(\Gamma_2 L_2\right)/Z_2\right) + \cosh\left(\Gamma_2 L_2\right)}} \right) + \cosh\left(\Gamma_3 L_3\right) \right\} \times \left[\frac{2R\pi}{\rho_0 cke^{j\left(\frac{\pi}{2} - kR\right)}} \right]$$

$$\frac{\partial A_{total}}{\partial A_r} = A_m \times \left(Z_1 \sinh\left(\Gamma_1 L_1\right)\right) \tag{4.52}$$

$$\times \left\{ \left(\frac{Z_3 \sinh\left(\Gamma_3 L_3\right)}{\frac{Z_T \cosh\left(\Gamma_2 L_2\right) + Z_2 \sinh\left(\Gamma_2 L_2\right)}{\left(Z_T \sinh\left(\Gamma_2 L_2\right)/Z_2\right) + \cosh\left(\Gamma_2 L_2\right)}} \right) + \cosh\left(\Gamma_3 L_3\right) \right\} \times \left[\frac{2R\pi}{\rho_0 cke^{j\left(\frac{\pi}{2} - kR\right)}} \right]$$

$$\frac{\partial A_{total}}{\partial B_r} = A_m \times \left(\cosh\left(\Gamma_1 L_1\right)\right) \tag{4.53}$$

$$\times \left\{ \left(\frac{Z_3 \sinh\left(\Gamma_3 L_3\right)}{\frac{Z_T \cosh\left(\Gamma_2 L_2\right) + Z_2 \sinh\left(\Gamma_2 L_2\right)}{\left(Z_T \sinh\left(\Gamma_2 L_2\right)/Z_2\right) + \cosh\left(\Gamma_2 L_2\right)}} \right) + \cosh\left(\Gamma_3 L_3\right) \right\} \times \left[\frac{2R\pi}{\rho_0 cke^{j\left(\frac{\pi}{2} - kR\right)}} \right]$$

$$\frac{\partial A_{total}}{\partial R} = A_m \times \left(A_r Z_1 \sinh\left(\Gamma_1 L_1\right) + B_r \cosh\left(\Gamma_1 L_1\right)\right) \tag{4.54}$$

$$\times \left\{ \left(\frac{Z_3 \sinh\left(\Gamma_3 L_3\right)}{\frac{Z_T \cosh\left(\Gamma_2 L_2\right) + Z_2 \sinh\left(\Gamma_2 L_2\right)}{\left(Z_T \sinh\left(\Gamma_2 L_2\right)/Z_2\right) + \cosh\left(\Gamma_2 L_2\right)}} \right) + \cosh\left(\Gamma_3 L_3\right) \right\} \times \left[\frac{2\pi\left(1 + jkR\right)}{\rho_0 cke^{j\left(\frac{\pi}{2} - kR\right)}} \right]$$

$$\frac{\partial A_{total}}{\partial Z_T} = A_m \times \left(A_r Z_1 \sinh\left(\Gamma_1 L_1\right) + B_r \cosh\left(\Gamma_1 L_1\right)\right) \tag{4.55}$$

$$\times \left\{ Z_3 \sinh\left(\Gamma_3 L_3\right) \frac{\partial}{\partial Z_T} \left(\frac{\left(Z_T \sinh\left(\Gamma_2 L_2\right)/ Z_2\right) + \cosh\left(\Gamma_2 L_2\right)}{Z_T \cosh\left(\Gamma_2 L_2\right) + Z_2 \sinh\left(\Gamma_2 L_2\right)} \right) \right\} \times \left[\frac{2R\pi}{\rho_0 cke^{j\left(\frac{\pi}{2} - kR\right)}} \right]$$

where

$$\frac{\partial}{\partial Z_T} \left(\frac{\left(Z_T \sinh\left(\Gamma_2 L_2\right)/ Z_2\right) + \cosh\left(\Gamma_2 L_2\right)}{Z_T \cosh\left(\Gamma_2 L_2\right) + Z_2 \sinh\left(\Gamma_2 L_2\right)} \right) \tag{4.56}$$

$$= \frac{\left(Z_T \cosh\left(\Gamma_2 L_2\right) + Z_2 \sinh\left(\Gamma_2 L_2\right)\right)\left(\sinh\left(\Gamma_2 L_2\right)/ Z_2\right) - \left(\left(Z_T \sinh\left(\Gamma_2 L_2\right)/ Z_2\right) + \cosh\left(\Gamma_2 L_2\right)\right)\cosh\left(\Gamma_2 L_2\right)}{\left(Z_T \cosh\left(\Gamma_2 L_2\right) + Z_2 \sinh\left(\Gamma_2 L_2\right)\right)^2}$$

These expressions can be used in a frequency domain form of the parametric adaptive algorithm described Section 7.8.

4.5 Implementation of the simplified analytic model

The simplified analytic expression was implemented in MATLAB version 6.1.0.450, release 12.1 (May 2001), on a Hi-Grade Ultis PV2 PC with a Pentium II 400 MHz processor and 131072K total memory, running Windows 2000. The program called the data files containing the transducer two-port network parameters and middle ear impedance data. Since the expression contained fewer terms than the matrix multiplication used previously, the computational efficiency of the model was improved. It was found that simulating the measurable feedback path with the simplified analytic expression took about 87% of the running time of the two-port network matrix multiplication calculation. Further to this, the MATLAB code could be made more efficient through the use of vector calculations that were not possible in the matrix form, so that the analytic expression calculated the feedback path response in 14% of the running time of the matrix multiplication calculation. The average running time of the analytic expression function was 0.311s. (MATLAB version 6 no longer has the facility to count floating point operations, so the running time is given in seconds.)

A practical feedback cancellation algorithm would need to be implemented on a DSP (digital signal processing) chip within the hearing aid. Hyperbolic functions can be expressed in terms of power series (Stroud, 1995):

$$\sinh x = \frac{e^x - e^{-x}}{2} \tag{4.57}$$

$$\cosh x = \frac{e^{x} + e^{-x}}{2} \tag{4.58}$$

where

$$e^{x} = 1 + x + \frac{x^{2}}{2!} + \frac{x^{3}}{3!} + \ldots \tag{4.59}$$

These functions can be evaluated using look-up tables, as can the Bessel functions (Stremler, 1990). Alternatively, approximated functions can be implemented with optimised C code (Press *et al.*, 1988). This will take up less memory than a look-up table but will be slower to run. There is a trade-off between speed and the required amount of memory.

4.6 Experimental verification of the analytic model for the measurable feedback path with slit leakage

The analytic expression (Equation (4.22)) was used to calculate the measurable feedback path for the normally fitted earmould example from Chapter 3. The dimensions and transducers used in the expression were as before (Table 3.1). In Figure 4.12, the response obtained with the analytic expression is compared with the two-port model response from Chapter 3 and the measured response from a previous study for an *in situ* ITE hearing aid fitted normally to the right ear of an adult male subject (Rafaely *et al.*, 2000).

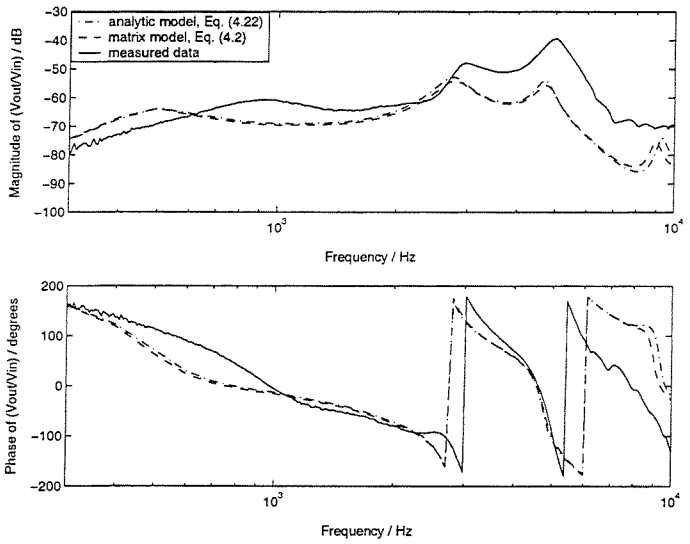

Figure 4.12: Measured and modelled feedback path responses for an in situ ITE hearing aid fitted normally to a human subject

As in Chapter 3, it can be seen that there is general agreement between the shape of the measured and modelled responses and there is good agreement for the phase. The differences

in amplitude and resonance frequencies are due to the approximations made in the model and the variation of the transducers from the ideal devices described by the electrical analogues.

Simulating the feedback path using the simplified expression with modifications for pinna effects (Equation (4.25)), it can be seen that the expression with pinna modifications gives better agreement with the measured feedback path than without the pinna modifications (Figure 4.13), as seen in Chapter 3.

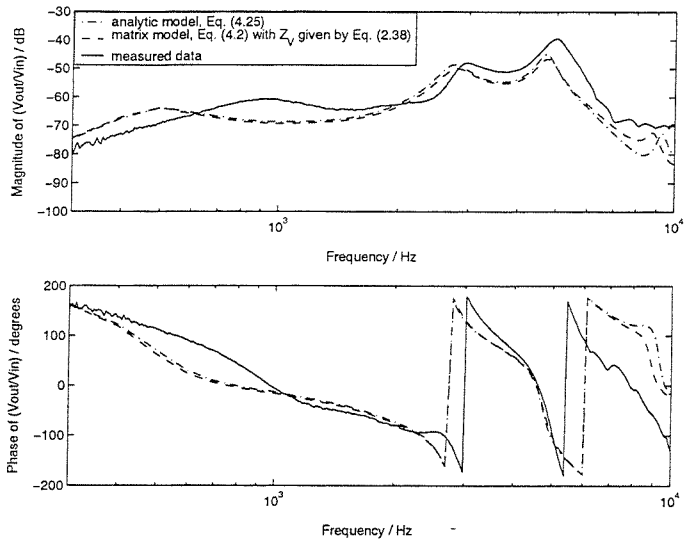

Figure 4.13: Measured and modelled feedback path responses for an in situ ITE hearing aid fitted to a human subject with modifications for pinna effects

These results show that the analytic expression can be used in place of the matrix model to simulate the measurable feedback path for normal fit examples. For the remainder of this thesis, it is assumed that the vent and slit leak are modelled as a single tube, varying the radius of the tube to represent a varying amount of sound leakage (see Section 2.7). Therefore the simplified analytic model can also be used to simulate the measurable feedback path with slit leakage. This will be verified in Chapter 5 using numerical optimisation techniques.

4.7 Conclusions

An analytic expression for the measurable feedback path has been developed, modelling the vent and leak as a single tube, and including the effects of the pinna. It has been shown that the expression can be simplified, as many terms in the original expression were found to be negligible. The simplified analytic model can represent a measured feedback path with a normally fitted hearing aid and with slit leakage, and will be used to develop the new

parametric adaptive feedback cancellation algorithm in Chapter 7. The set of expressions derived for the analytic gradient with respect to each varying parameter is intended to be used in a future form of the parametric adaptive algorithm.

5 Ability of the simplified analytic model to fit measured feedback paths

5.1 Introduction

The aim of this project is to develop a parametric adaptive algorithm (PAA) that uses the feedback path model described in Chapters 2 – 4 to cancel the feedback signal; this is a novel approach to the feedback problem. In order to use the simplified analytic model in this algorithm, it must be shown that the model is able to represent the full range of possible measured feedback paths. It has been shown in Sections 3.4 – 3.6 that reasonably good agreement can be obtained between the modelled feedback path response and the measured data by careful choice of the values of the parameters within the model. However, to demonstrate that the model is valid, it needs to be applied to a wide range of measurements, including data for different types of feedback path (e.g. with large amounts of slit leakage and obstructions in the external acoustic feedback path) and for different human subjects, and show a very close fit to the measured responses. In this chapter, the simplified analytic model is fitted to a range of measured feedback path responses using numerical optimisation techniques. At this stage, the closeness of the fit is more important than the parameter values returned by the optimisation, which may not correspond to realistic physical dimensions. The subjects featured in this chapter were adult males; the data were obtained in a previous study (Rafaely *et al.*, 2000).

5.2 Methods of optimisation

Numerical optimisation techniques often aim to minimise some objective function, J, in order to achieve the best fit between a model and experimental data. In this case, the 2-norm of the difference between the modelled and measured responses was chosen:

$$J = \left\| M(f) - F(f) \right\|_2^2 \qquad (5.1)$$

where $M(f)$ is the modelled feedback path response and $F(f)$ is the measured feedback path response.

There are two main types of optimisation: unconstrained and constrained. The former allows the parameters to take any values, while the second imposes limits and conditions. MATLAB version 6.1, release 12.1 (May 2001), was used for the simulations performed in this thesis (see Section 4.5 for further details). The MATLAB Optimisation toolbox (version 2.1.1, release 12.1, May 2001) has a set of built-in functions which were used throughout this chapter. Several functions from the MATLAB optimisation toolbox were considered. It was found that the best results were obtained using `fminunc`, which found the minimum of a nonlinear unconstrained multivariable function using a quasi-Newton method consisting of

determination of the direction of search followed by a mixed quadratic and cubic polynomial line search (for further details, see the release notes for MATLAB release 12.1).

5.3 Possible limitations on the optimisation

In this chapter, numerical optimisation is used to adjust the parameters in the model to fit the response to measured data. However, limitations in the model may prevent the achievement of a very close fit, and if a close fit cannot be obtained, any method of feedback cancellation based on the model may not be able to cancel feedback signals sufficiently to prevent oscillation. It was shown in Section 3.4 that the responses of the transducer analogues differ from those of the actual devices. Also, we have no knowledge of the subject's middle ear impedance and must represent it by mean data or an electrical analogue. Differences in the middle ear impedance can have a significant effect on the response of the hearing aid system (Gilman *et al.*, 1981). These factors mean that there is some uncertainty in the model. Since we are only varying the physical dimensions in the hearing aid model to begin with, it may not be possible to obtain exact agreement with the measured responses. Altering the tube dimensions may not be sufficient to compensate for the approximations in the transducer and middle ear models.

Inspection of the code for the transducer analogues showed that altering the values of certain resistors, capacitors and inductors was used to model different devices while retaining the overall structure of the analogue (Kates 1988b; LoPresti and Carlson, 1999). From this, we can infer that changing components of the transducer analogues, either manually or through some sort of adaptation, would change the response. Therefore optimising the values of analogue components could improve the fit of the model to the measured data. Similarly, optimising the component values in the middle ear analogue could improve the fit of the model. This is investigated in Section 5.5.

5.4 Optimisation of the model with mean middle ear impedance to fit measured normal fit responses

Optimisation was performed to fit the simplified analytic model described by Equation (4.22) to a range of measured feedback paths. The simplest case to consider is that of the normal fit response, as each part of the hearing aid system can be represented by the model and there are no unknown parameters such as the size of a slit leak around the earmould. The model was fitted to the measured normal fit response for the left ear of subject BO, obtained in a previous study (Rafaely *et al.*, 2000). The receiver tube length L_1, the ear canal length L_2, the ear canal radius r_2, the vent length L_3 and the external acoustic feedback path length R were optimised. The receiver tube radius r_1 and the vent radius r_3 were provided by the earmould

manufacturer and so had known, constant values; these values are given in Table 5.1 for all the examples in this chapter. The initial values of L_2 and r_2 were taken from estimated ear canal dimensions (Kates, 1988b). The other dimensions were taken from approximate measurements on the earmould for subject BO's left ear. The transducer analogues used throughout this chapter were those of the ED-1913 receiver (which was identical to that of the ED-1975 receiver used experimentally; the transducers differed only in their physical configuration and had identical properties (Knowles, 1997)) and the EM-3046 microphone, which was used in the experiment. Throughout this chapter, the maximum optimised radii values were limited to 1.0 cm to prevent $1/\infty$ errors in the simulation due to limitations in the narrow tubing model (see Section 2.8); this is indicated where appropriate.

Subject	*Ear*	*Receiver tube radius*	*Vent radius*
BO	Left	0.07 cm	0.08 cm
BO	Right	0.07 cm	0.08 cm
AL	Left	0.07 cm	0.105 cm
AL	Right	0.07cm	0.105 cm
WK	Left	0.07cm	0.105 cm

Table 5.1: Known constant values of the receiver tube and vent radii for all examples in this chapter

Table 5.2 gives the initial and optimised parameter values:

Parameter	*Symbol*	*Initial value*	*Optimised value*
Receiver tube length	L_1	1.4 cm	1.5691 cm
Ear canal length	L_2	1.2 cm	0.0603 cm
Ear canal radius	r_2	0.33 cm	1.0 cm (value limited)
Vent length	L_3	2.0 cm	1.1336 cm
External acoustic feedback path length	R	1.0 cm	3.7012 cm

Table 5.2: Initial and optimised parameter values for the normal fit response, subject BO, left ear

These values were not all in good agreement with the expected values based on physical observations. This was because the model had to alter the values of the physical dimensions to compensate for the errors introduced by lack of knowledge of the actual transducer responses and the subject's ear canal dimensions and middle ear impedance. Although the

values were not realistic, the modelled response was closer to the actual response after optimisation had been performed. A constant gain of 10 dB had been added to the model before optimisation to improve the ability of the optimisation procedure to fit the model to the measured response by partially compensating for the intrinsic errors in the model. The pinna effect modifications were not included in the model. Compare the agreement between the modelled and measured responses in Figure 5.1 below with that in Figure 4.12 in Section 4.6.

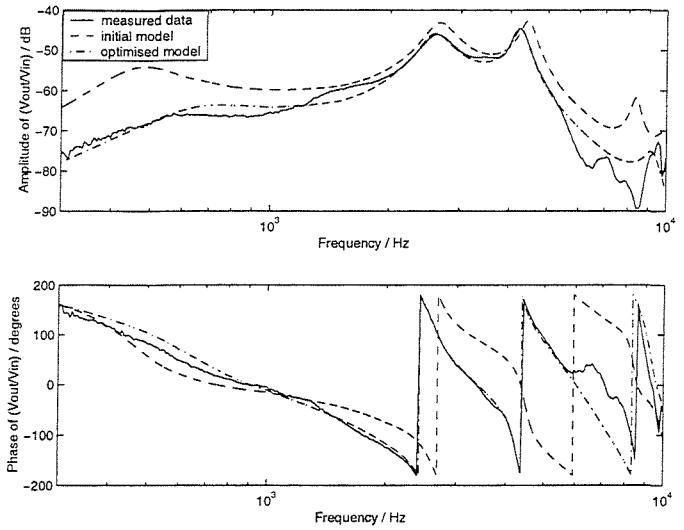

Figure 5.1: Comparison of modelled response with measured data before and after unconstrained optimisation for subject BO's left ear

The same procedure was carried out on the modelled response for subject AL's left ear. The constant receiver tube and vent radii are given in Table 5.1. The initial and optimised values of the variable parameters were (Table 5.3):

Parameter	*Symbol*	*Initial value*	*Optimised value*
Receiver tube length	L_1	1.2 cm	1.4498 cm
Ear canal length	L_2	1.2 cm	0.1428 cm
Ear canal radius	r_2	0.33 cm	1.0 cm (value limited)
Vent length	L_3	1.3 cm	1.6555 cm
External acoustic feedback path length	R	1.0 cm	3.5092 cm

Table 5.3: Initial and optimised parameter values for the normal fit response, subject AL, left ear

As before, after optimisation, the model was in close agreement with the measured data. See Figure 5.2.

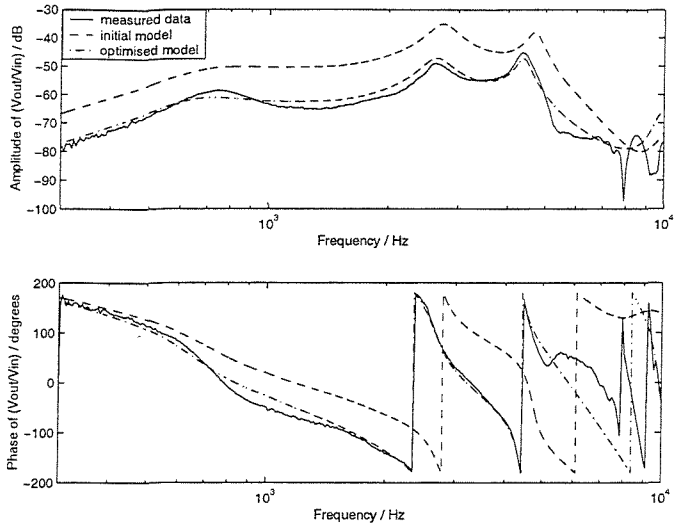

Figure 5.2: Comparison of modelled response with measured data before and after unconstrained optimisation for subject AL's left ear

The same procedure was applied to subject WK's left ear. The constant receiver tube and vent radii are given in Table 5.1. The initial and optimised values of the variable parameters were (Table 5.4):

Parameter	*Symbol*	*Initial value*	*Optimised value*
Receiver tube length	L_1	1.3 cm	1.3552 cm
Ear canal length	L_2	1.2 cm	1.3321 cm
Ear canal radius	r_2	0.33 cm	0.3071 cm
Vent length	L_3	1.6 cm	0.5102 cm
External acoustic feedback path length	R	1.0 cm	4.5912 cm

Table 5.4: Initial and optimised parameter values for the normal fit response, subject WK, left ear

Again, after optimisation, the model was in reasonably close agreement with the measured data. See Figure 5.3.

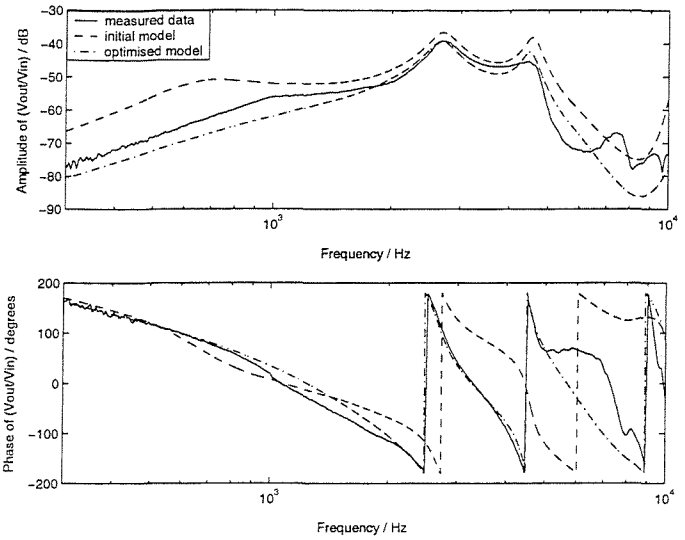

Figure 5.3: Comparison of modelled response with measured data before and after unconstrained optimisation for subject WK's left ear

Therefore numerical optimisation has been shown to improve the fit of the model to measured feedback path responses. The optimal parameter values may not be realistic physical dimensions, but at this stage only a few parameters are varied and the values of these must compensate for the uncertainty in the model

5.5 Optimisation of the model with middle ear electrical analogue to fit measured normal fit responses

Up to this point, the model has been using mean middle ear impedance data (Shaw, 1974) since no information was available for the human subjects. However, an electrical analogue (de Jonge, 1996) could also be used to represent the middle ear impedance (see Section 2.6). It was possible to optimise some of the components within this analogue to further improve the fit of the model to the measured data.

Two components, the capacitance C_{cavity} representing the compliance of the middle ear cavities (termed C1 in Figure 2.9) and the inductance L_{mi} representing the mass of the part of the eardrum attached to the malleus, the malleus itself and the incus (termed L3 in Figure 3.6), were chosen to be optimised, along with L_1, L_2, r_2, L_3 and R as before. The initial values for the electrical analogue elements were those given in Figure 3.6: C_{cavity} = 5.45 μF and L_{mi} = 40 mH. Again, optimisation was performed using the function `fminunc` to fit the model to the measured normal fit data for three human subjects.

The initial and optimised values for the left ear of subject BO are given in Table 5.5. The constant parameter values are given in Table 5.1.

Parameter	*Symbol*	*Initial value*	*Optimised value*
Receiver tube length	L_1	1.4 cm	1.5684 cm
Ear canal length	L_2	1.2 cm	- 0.1450 cm
Ear canal radius	r_2	0.33 cm	0.9869 cm
Vent length	L_3	2.0 cm	0.8255 cm
External acoustic feedback path length	R	1.0 cm	3.2753 cm
Middle ear cavity compliance	C_{cavity}	5.45 μF	- 87.2948 F
Mass of malleus and incus	L_{mi}	40 mH	- 23.7 mH

Table 5.5: Initial and optimised values for the normal fit response, subject BO, left ear

As in the previous section, the optimised values were not all physically realistic, especially that of C_{cavity}, but the optimised model was in good agreement with the measured data (see Figure 5.4). Note that some of the values returned by the optimisation were negative. The absolute values were taken when calculating the modelled feedback path responses throughout this section, unless the negative values gave a better fit. (Since we are only optimising two elements of the electrical analogue, realistic values are not expected to result. Obtaining a greater understanding of which elements give the best fit when varied is a subject for future work.)

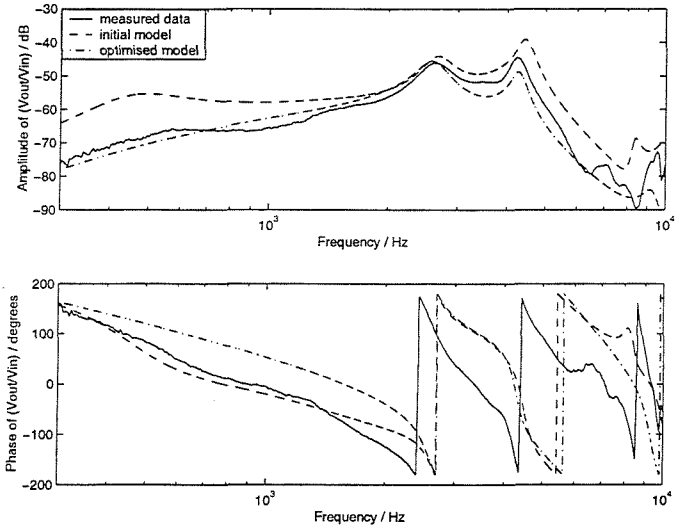

Figure 5.4: Comparison of modelled response with measured data before and after unconstrained optimisation for subject BO's left ear

Performing the optimisation for subject AL, left ear data, the constant parameters are given in Table 5.1 and the initial and optimised parameter values are given in Table 5.6:

Parameter	*Symbol*	*Initial value*	*Optimised value*
Receiver tube length	L_1	1.2 cm	1.4497 cm
Ear canal length	L_2	1.2 cm	0.1488 cm
Ear canal radius	r_2	0.33 cm	1.0000 cm (value limited)
Vent length	L_3	1.3 cm	1.5993 cm
External acoustic feedback path length	R	1.0 cm	3.6856 cm
Middle ear cavity compliance	C_{cavity}	5.45 μF	- 725.7076 F
Mass of malleus and incus	L_{mi}	40 mH	- 83 mH

Table 5.6: Initial and optimised parameter values for the normal fit response, subject AL, left ear

Again, not all the values were physically realistic, but good agreement with the measured data was obtained (Figure 5.5).

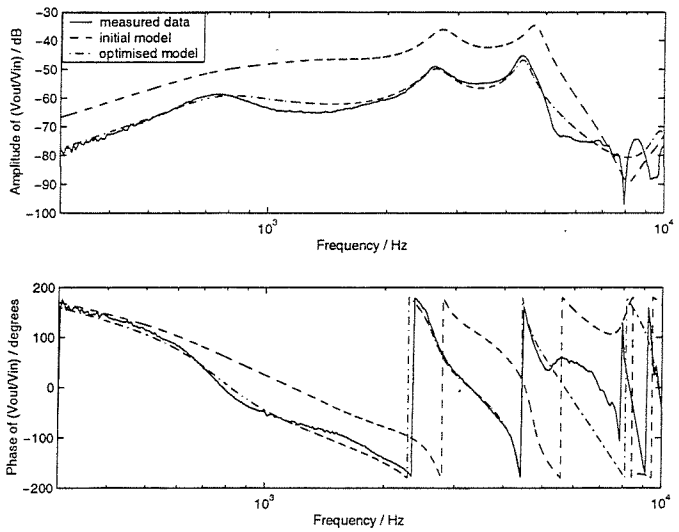

Figure 5.5: Comparison of modelled response with measured data before and after unconstrained optimisation for subject AL's left ear

The initial and optimised parameter values obtained after performing the optimisation for subject WK, left ear data, are given in Table 5.7 and the constant parameter values are given in Table 5.1.

Parameter	*Symbol*	*Initial value*	*Optimised value*
Receiver tube length	L_1	1.3 cm	1.2527 cm
Ear canal length	L_2	1.2 cm	1.9010 cm
Ear canal radius	r_2	0.33 cm	0.3334 cm
Vent length	L_3	1.6 cm	0.2537 cm
External acoustic feedback path length	R	1.0 cm	5.1735 cm
Middle ear cavity compliance	C_{cavity}	5.45 μF	- 88.3409 F
Mass of malleus and incus	L_{mi}	40 mH	15.8 mH

Table 5.7: Initial and optimised parameter values for the normal fit response, subject AL, left ear

As for the previous examples, some of the values were not physically realistic, but reasonably good agreement with the measured data was obtained (Figure 5.6).

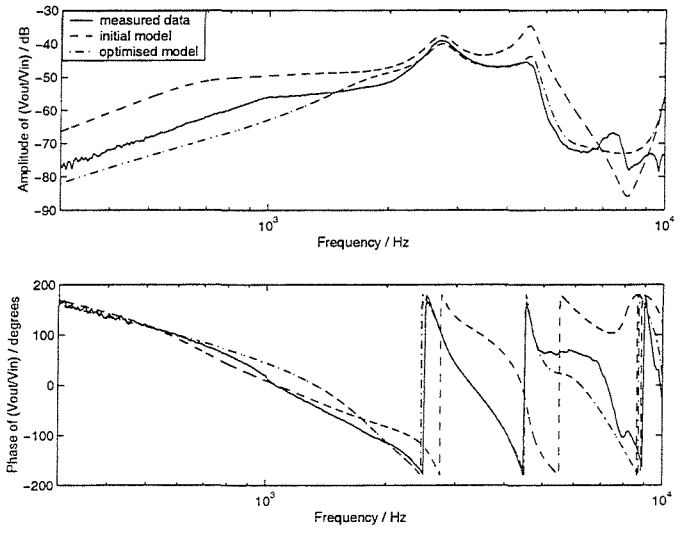

Figure 5.6: Comparison of modelled response with measured data before and after unconstrained optimisation for subject WK's left ear

Performing the optimisation for subject AL, right ear data, the constant receiver tube and vent radii are given in Table 5.1 and the initial and optimised values of the variable parameters are given in Table 5.8:

Parameter	*Symbol*	*Initial value*	*Optimised value*
Receiver tube length	L_1	1.4 cm	1.4110 cm
Ear canal length	L_2	1.2 cm	0.1223 cm
Ear canal radius	r_2	0.33 cm	0.7641 cm
Vent length	L_3	1.6 cm	1.2747 cm
External acoustic feedback path length	R	1.0 cm	3.7677 cm
Middle ear cavity compliance	C_{cavity}	5.45 μF	- 44.0127 F
Mass of malleus and incus	L_{mi}	40 mH	- 60.8 mH

Table 5.8: Initial and optimised parameter values for the normal fit response, subject AL, right ear

Reasonably good agreement with the measured data was obtained (Figure 5.7) although the parameter values were not all physically realistic.

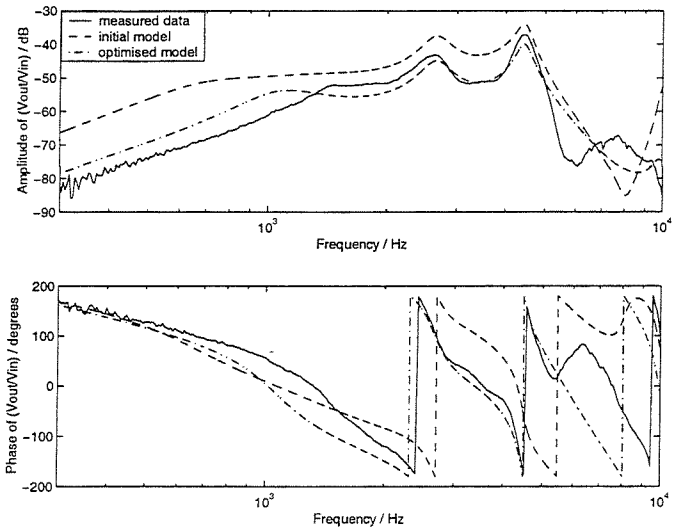

Figure 5.7: Comparison of modelled response with measured data before and after unconstrained optimisation for subject AL's right ear

Therefore in all cases, good agreement with the measured data was achieved by optimising the physical parameters and some elements of the middle ear analogue, although the optimal values did not all correspond to observed measurements.

5.6 Optimisation of the model to fit measured slit leak responses

Examining the measured responses for the three slit leak conditions (open mouth (Figure 3.12), smiling face (Figure 3.13) and wrong fit (Figure 3.14)) and comparing them with the

normal fit response (Figure 3.10)), it can be seen that the open mouth and smiling face conditions are very similar to the normal fit. Therefore the best demonstration of the ability of the model to cover a range of responses is to show that it can represent the wrong fit response adequately. The uncertainty introduced by the large leak means that it is more difficult to get good agreement between the modelled and measured responses.

Optimisation was performed to fit the model to the wrong fit, left ear data for subject BO, using the same initial values and constant receiver tube radius as before, but this time also varying the vent radius, r_3, from an initial value of 0.5 cm. The parameter values before and after optimisation were (Table 5.9):

Parameter	*Symbol*	*Initial value*	*Optimised value*
Receiver tube length	L_1	1.4 cm	1.6150 cm
Ear canal length	L_2	1.2 cm	0.1305 cm
Ear canal radius	r_2	0.33 cm	1.0000 cm (value limited)
Vent length	L_3	2.0 cm	2.0180 cm
Vent radius	r_3	0.5 cm	- 0.0764 cm
External acoustic feedback path length	R	1.0 cm	2.5851 cm
Middle ear cavity compliance	C_{cavity}	5.45 μF	- 295.4110 F
Mass of malleus and incus	L_{mi}	40 mH	51.5 mH

Table 5.9: Initial and optimised parameter values for the normal fit response, subject BO, left ear

A negative radius is physically meaningless, but the response is the same as with a positive radius value since all the functions acting on r_3 in the model are even.

The fit was reasonably good (see Figure 5.8). Fitting the earmould wrongly leads to changes in the feedback path that may be hard to predict.

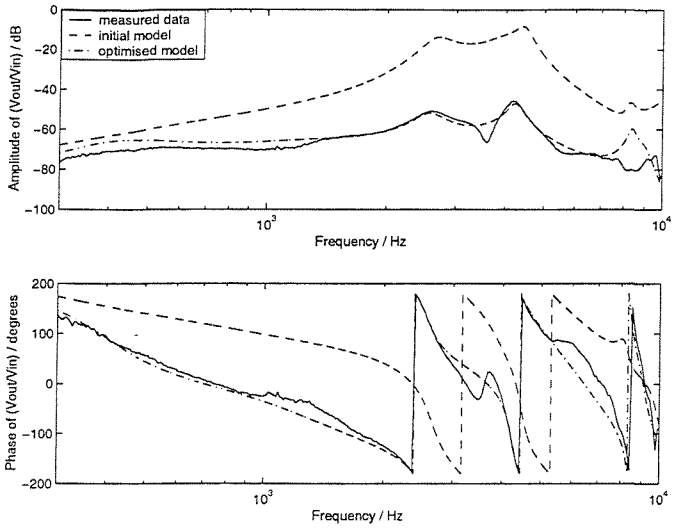

Figure 5.8: Comparison of modelled response with measured wrong fit data before and after unconstrained optimisation for subject BO's left ear

Optimisation was also performed to fit the model to the wrong fit, right ear data for subject BO. The constant receiver tube radius r_1 is given in Table 5.1. The initial and optimised values of the variable parameters are given in Table 5.10 below:

Parameter	*Symbol*	*Initial value*	*Optimised value*
Receiver tube length	L_1	1.2 cm	1.0623 cm
Ear canal length	L_2	1.2 cm	1.6755 cm
Ear canal radius	r_2	0.33 cm	0.1610 cm
Vent length	L_3	1.8 cm	2.6632 cm
Vent radius	r_3	0.106 cm	0.0370 cm
External acoustic feedback path length	R	1.0 cm	0.9716 cm
Middle ear cavity compliance	C_{cavity}	5.45 μF	- 130.3255 F
Mass of malleus and incus	L_{mi}	40 mH	53 mH

Table 5.10: Initial and optimised parameter values for the normal fit response, subject BO, right ear

The fit was reasonable, though again agreement was not as close as for the normal fit condition (Figure 5.9). Despite this, in both cases, the model showed fairly close agreement around the high amplitude receiver resonance peaks at which instability is most likely to occur.

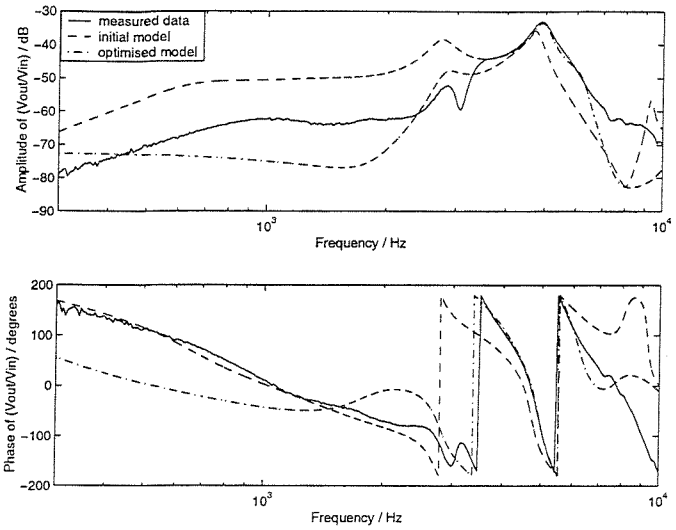

Figure 5.9: Comparison of modelled response with measured wrong fit data before and after unconstrained optimisation for subject BO's right ear

The optimal values in these examples bear little relation to observed physical parameters, but show that a reasonably good fit is achievable by altering components of the middle ear electrical analogue as well as the physical dimensions in the model. Better understanding of the effects of alterations in the transducer and middle ear analogues would lead to optimal values which are closer to the measured dimensions.

Therefore it can be concluded that the model is capable of fitting a wide range of feedback path conditions with varying slit leakage, and that a better fit could be achieved if an investigation was made into which elements of the middle ear electrical analogue gave greatest control over the response.

5.7 Optimisation of the model to fit measured responses with an obstruction in the external acoustic feedback path

It was found in Section 3.7 that the proposed large tube model of an obstruction in the external acoustic feedback path was not valid. However, the existing feedback path model has been shown to fit reasonably closely to a range of measured responses with slit leakage so the model may be able to compensate for the reflection and resonance effects caused by the obstruction.

The normal fit model with the middle ear electrical analogue was fitted to the measured response for a hand 20 cm from the ear for the right ear of subject BO (Figure 5.10). The constant receiver tube and vent radii are given in Table 5.1. The initial and optimised parameter values are given in Table 5.11. The normal fit model was able to give a good

representation of the measured feedback path since the response was similar to that with no obstruction present.

Parameter	*Symbol*	*Initial value*	*Optimised value*
Receiver tube length	L_1	1.2 cm	0.9920 cm
Ear canal length	L_2	1.2 cm	1.4374 cm
Ear canal radius	r_2	0.33 cm	0.2152 cm
Vent length	L_3	1.8 cm	1.9663 cm
External acoustic feedback path length	R	1.0 cm	1.9410 cm
Middle ear cavity compliance	C_{cavity}	5.45 μF	0.8691 μF
Mass of malleus and incus	L_{mi}	40 mH	15.991 nH

Table 5.11: Initial and optimised parameter values for the response with a hand 20 cm from the ear, subject BO, right ear

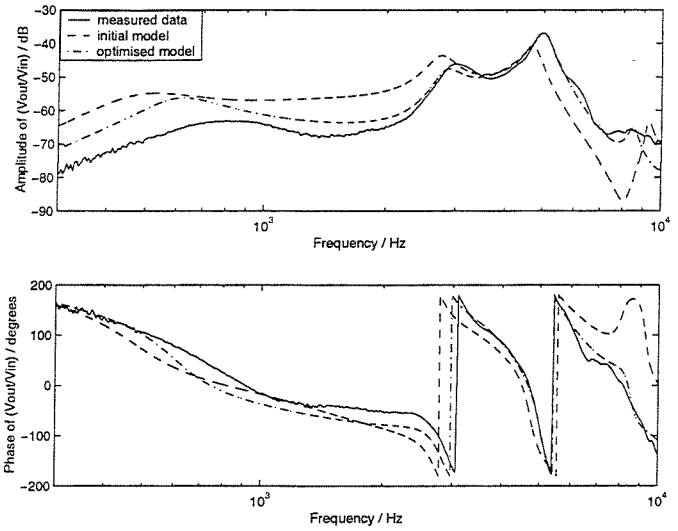

Figure 5.10: Comparison of modelled response using normal fit model with measured data for a hand 20 cm from the ear before and after unconstrained optimisation for subject BO's right ear

The model was fitted to the measured response for a hand close to the ear for the right ear of subject BO (Figure 5.11). Agreement was not good at all frequencies, though the general shape of the modelled response was similar to that of the measured response. Bearing in mind the lack of knowledge of parts of the system, the fit is reasonable as a first approximation. The constant radii values were as before. The initial and optimised parameters are given in Table 5.12:

Parameter	*Symbol*	*Initial value*	*Optimised value*
Receiver tube length	L_1	1.2 cm	1.6034 cm
Ear canal length	L_2	1.2 cm	1.5884 cm
Ear canal radius	r_2	0.33 cm	0.1822 cm
Vent length	L_3	1.8 cm	2.0573 cm
External acoustic feedback path length	R	1.0 cm	1.6902 cm
Middle ear cavity compliance	C_{cavity}	5.45 μF	0.1304 μF
Mass of malleus and incus	L_{mi}	40 mH	21.7 mH

Table 5.12: Initial and optimised parameter values for the response with a hand close to the ear, subject BO, right ear

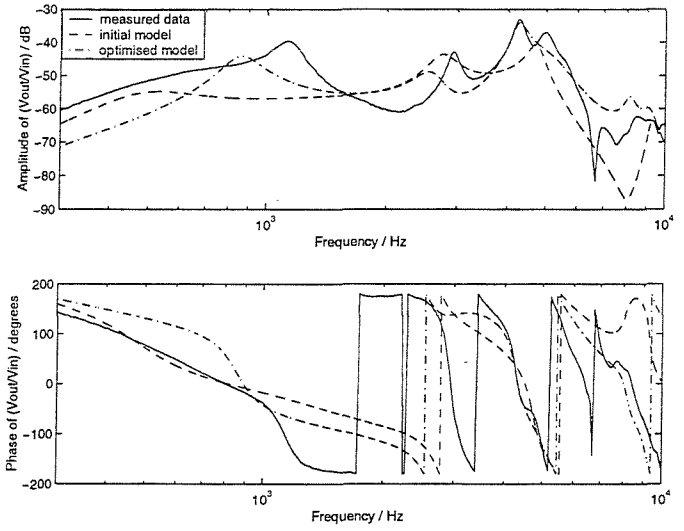

Figure 5.11: Comparison of modelled response using normal fit model with measured data for a hand close to the ear before and after unconstrained optimisation for subject BO's right ear

The hand close to the ear is the hardest case to model as there will be reflections from the hand interfering with the signal as it travels from the vent to the microphone. These effects are hard to predict. The fairly reasonable fit to the data indicates that the model is versatile in its simplest form and may be used if an improved obstruction model is not available.

5.8 Conclusions

It has been shown that unconstrained numerical optimisation can be used to improve the fit of the model of the feedback path to measured data obtained for different human subjects under various conditions, such as in the presence of slit leakage or with an obstruction near the ear.

The choice of the variables to be optimised may affect the fit. Future work could address the optimisation of more elements of the middle ear analogue, and the optimisation of elements of the transducer analogues so that the optimal values of the physical dimensions were in closer agreement with the observed values.

Good agreement between the optimised model and the measured data was observed for responses where the earmould was fitted normally to the subject. It has been shown that the basic, normal fit model can be fitted reasonably well to responses with slit leakage and with an obstruction in the external acoustic feedback path. Therefore the basic model can represent a wide range of measured feedback paths with slit leakage and obstructions, and will be used in the development of a new parametric adaptive feedback cancellation algorithm in Chapters 7 – 9.

6 Suitability of the analytic model for use in adaptive feedback cancellation

6.1 Introduction

In this chapter, the simplified analytic model derived in Chapter 4 is evaluated for use in a new method of adaptive feedback cancellation, presented in Chapter 7, which updates estimated parameter values in a model of the feedback path used to cancel the feedback signal. Adaptive algorithms require a cost function or objective function; the theory of this is explored in the following section. Simulation results are presented for error surfaces calculated using modelled and measured feedback path data. The error surfaces demonstrate the degree of suitability of the analytic model for use in an adaptive algorithm. A smooth, convex error surface results in convergence of a steepest descent-based algorithm to the minimum. An irregular, non-convex surface can make convergence to the global minimum slower, more difficult or even impossible. Local minima may occur and the algorithm may converge to these minima instead of the global minimum, producing an inaccurate model of the feedback path, which results in insufficient cancellation of the feedback signal.

6.2 Cost functions

Adaptive algorithms require a clear objective when adjusting parameters. Frequently, this objective is the minimisation of some cost function, J. The cost function is a function of the set of varying parameters, $\mathbf{p}$: $J = J(\mathbf{p})$. Plotting this cost function against the varying parameters produces an error, or performance, surface. A common cost function is the mean square error, $E[e^2]$, where the error signal is the difference between the estimated and desired signals.

The method of steepest descent is a common way of traversing the error surface (see Section 1.5). To ensure that the algorithm converges to the minimum, the surface must be convex with a global, unique minimum and no local minima. An error surface is convex if all points on the curve lie below a line drawn between two points on the curve. If the surface was concave, i.e. had a global maximum rather than a minimum, the mean square error would be negative. This is impossible with real, physical signals (Widrow and Stearns, 1985).

Recall the method of steepest descent:

$$\text{new parameter} = \text{old parameter} - \alpha\ (\text{local gradient})$$

α is the convergence coefficient.

The local gradient is defined as ∂(cost function)/∂(parameter), evaluated at the current parameter value.

Consider the simple system with a single filter weight in Figure 6.1:

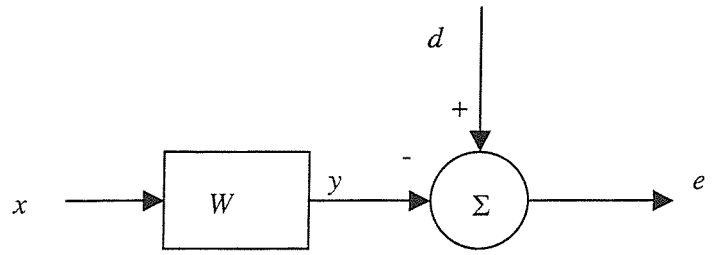

Figure 6.1: Adaptive system with a single filter weight

The estimated signal is:

$$y(n) = Wx(n) \tag{6.1}$$

and the error signal is:

$$e(n) = d(n) - y(n) = d(n) - Wx(n) \tag{6.2}$$

Hence the cost function is:

$$J = E[e^2] = E[(d - Wx)^2] = E[d^2] - 2WE[dx] + W^2 E[x^2] \tag{6.3}$$

so J has quadratic dependence on the parameter W.

The optimum value of W can be found by setting $\partial J/\partial W$ to zero, i.e. by finding the minimum of the error surface. With a single coefficient, the cost function varies as a quadratic curve. With two coefficients, it varies as a quadratic surface. A quadratic surface has a unique minimum and no local minima if $E[x^2] > 0$. With N coefficients, the cost function will vary as an N-dimensional surface in $N + 1$ dimensions. The error surface is a fixed quadratic function of the filter weights when the input and desired responses are both statistically stationary (Widrow and Stearns, 1985), and is rigid in its coordinate system. The adaptive algorithm must move down the slope of the error surface towards the minimum. If the signals are nonstationary, the error surface moves within its coordinate system and the algorithm must track the minimum as it moves (Widrow and Stearns, 1985).

Infinite impulse response (IIR) filters, i.e. those with poles as well as zeroes, can produce non-quadratic error surfaces with local minima and unstable regions (Widrow and Stearns, 1985), so a steepest descent-based algorithm may not be a suitable approach to finding the global minimum in this case. Before using any adaptive algorithms, it is necessary to

determine whether the error surface has a unique global minimum and no local minima. If local minima occur, a steepest descent-based algorithm might not converge to the correct solution and would not give exact agreement with the actual feedback path.

In the simulations presented in this chapter, the cost function was the 2-norm of the difference between the actual feedback path, $F(f)$, and the modelled feedback path, $M(f, \mathbf{p})$. F can be a measured feedback path response or a known model.

The 2-norm is the squared difference between M and F summed over all frequencies:

$$J = \left\| M(f,\mathbf{p}) - F(f) \right\|_2^2 \tag{6.4}$$

Expanding this and using discrete frequencies, we can see that the cost function has quadratic dependence on M:

$$J(\mathbf{p}) = \sum_{k=0}^{K-1} \left| M(k,\mathbf{p}) - F(k) \right|^2 = \sum_{k=0}^{K-1} (M-F)(M-F)^* = \sum_{k=0}^{K-1} |M|^2 - 2\mathrm{Re}\{MF\} + |F|^2 \tag{6.5}$$

There is no prior knowledge of the actual feedback path response F.

6.3 Error surface produced by fitting the analytic model to a modelled feedback path

In this section, the error surface was calculated using a known model to represent the actual feedback path, $F(f)$, so that the modelled feedback path $M(f)$ was capable of exact agreement with the actual path and a global minimum would be expected to occur. The model had the form shown in Figure 2.8 and was described by Equation 4.22. The known model had seven fixed physical parameter dimensions, given in Table 6.1. The other constant parts of the model, the transducers and middle ear impedance, are given in Table 6.2. The modelled feedback path, $M(f)$, varied the physical parameter values to produce the error surface. Each parameter was varied over a range of feasible physical dimensions, given in Table 6.3. As each parameter was varied, the other six parameters remained constant at the default values (Table 6.1) unless stated otherwise. It is not possible to visualise an error surface in eight dimensions (seven varying parameters plus the objective function), so the objective function was plotted against each variable on a separate graph (Figures 6.2 – 6.8). Throughout this chapter, the vent incorporated slit leakage, assuming that both the vent and effective slit leak tube were of the same length and at the same distance from the microphone input (see Section 2.7)

Parameter	*Symbol*	*Default value*
Receiver tube length	L_1	1.2 cm
Receiver tube radius	r_1	0.7 mm
Ear canal length	L_2	1.5 cm
Ear canal radius	r_2	3.5 mm
Vent length	L_3	1.7 cm
Vent radius	r_3	4.176 mm
External acoustic feedback path length	R	2.0 cm

Table 6.1: Default physical parameter values for the modelled feedback path, M(f)

Feedback path component	*Parameter symbols*	*Modelled by:*
Microphone	A_m	Knowles EM-3046 analogue
Receiver	A_r, B_r	Knowles ED-1913 analogue
Middle ear impedance	Z_T	Mean measured data (Shaw, 1974)

Table 6.2: Models used for constant parts of the feedback path

Parameter	*Symbol*	*Range of values*	*Error surface shown in Figure:*
Receiver tube length	L_1	0.5 – 2.0 cm	6.2
Receiver tube radius	r_1	0.5 – 1.5 mm	6.3
Ear canal length	L_2	1.0 – 2.0 cm	6.4
Ear canal radius	r_2	2.0 – 6.0 mm	6.5
Vent length	L_3	1.0 – 2.5 cm	6.6
Vent radius	r_3	0.1 – 8.0 mm	6.7
External acoustic feedback path length	R	0.5 – 3.0 cm	6.8

Table 6.3: Range of physical parameter values used in the model to produce the set of error surfaces shown in Figures 6.2 – 6.8

It can be seen from Figures 6.2 – 6.8 that each error surface obtained using a known model to represent the actual feedback path has a unique minimum at the expected parameter value. This shows that if the constant parameter values in the model allow close agreement with the actual path (i.e. if the fixed parts of the model are the same as those in the actual feedback path), the model can reproduce the actual response and the minimum of the error surface will be defined clearly. However, although a global minimum was observed, this was within a pre-

defined range; local minima may occur outside this range. Note that even though the minimum was well defined, the error surfaces were not convex, indicating that the multidimensional error surface is complicated and may prove difficult for a steepest descent-based algorithm to navigate.

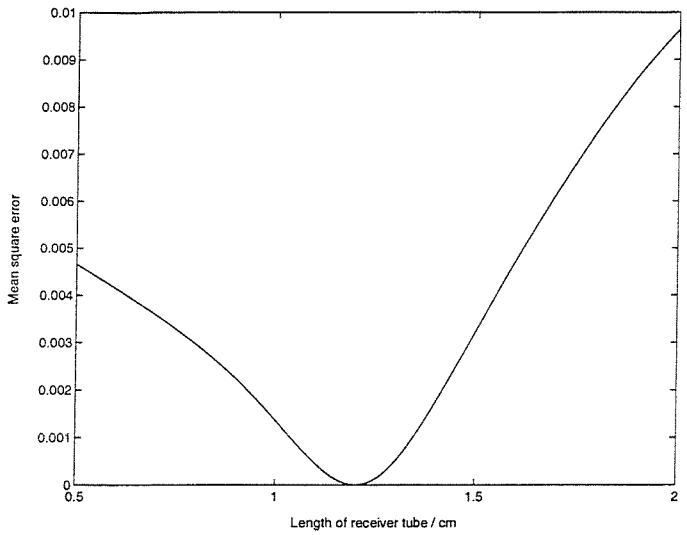

Figure 6.2: Receiver tube length error surface: modelled actual feedback path, F(f)

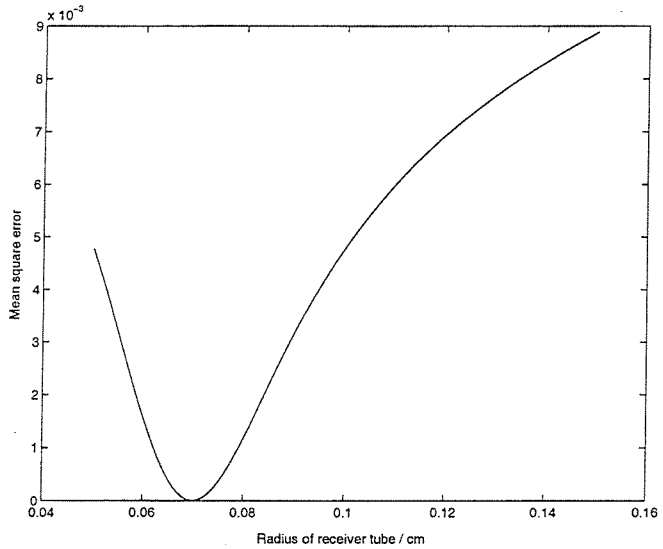

Figure 6.3: Receiver tube radius error surface: modelled actual feedback path, F(f)

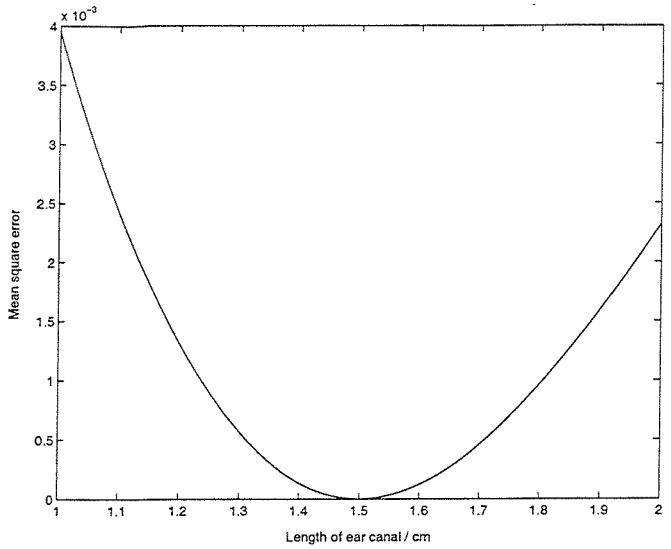

Figure 6.4: Ear canal length error surface: modelled actual feedback path, F(f)

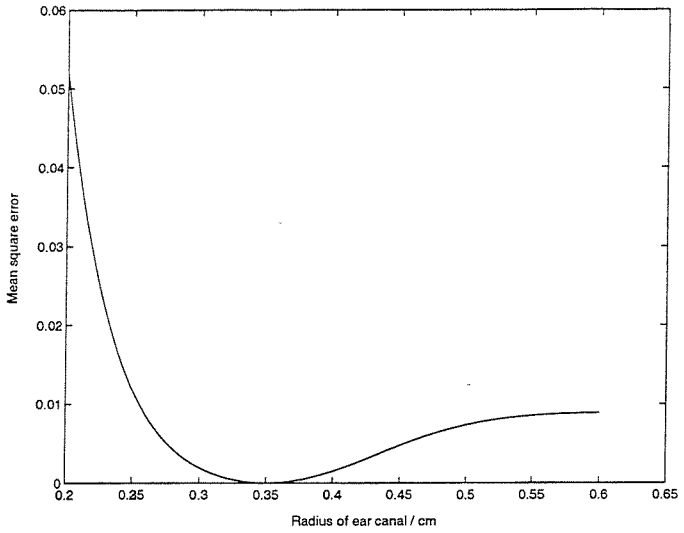

Figure 6.5: Ear canal radius error surface: modelled actual feedback path, F(f)

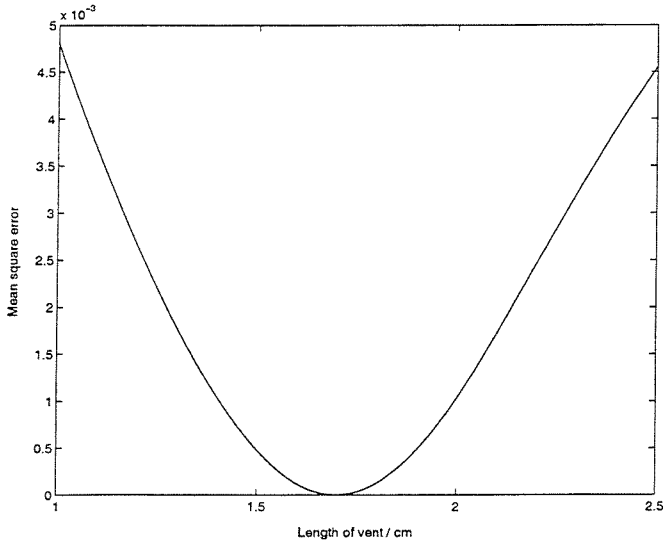

Figure 6.6: Vent length error surface: modelled actual feedback path, F(f)

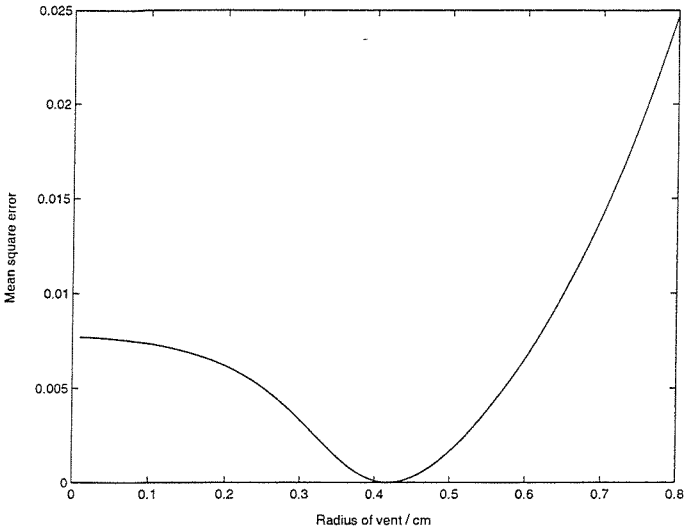

Figure 6.7: Vent radius error surface: modelled actual feedback path, F(f)

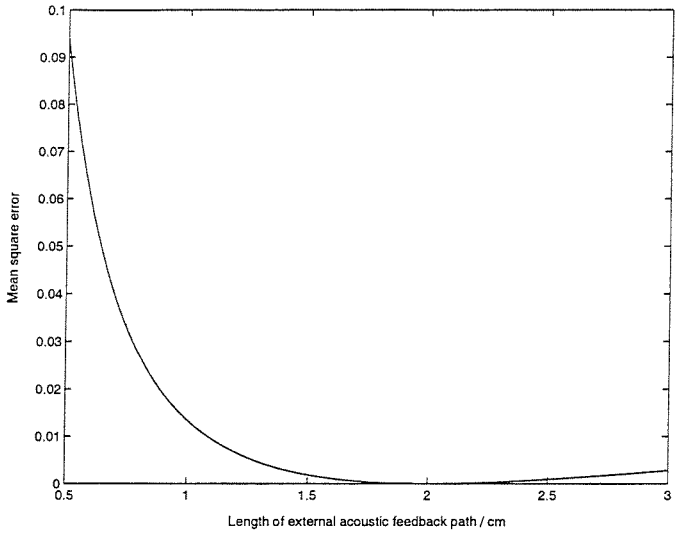

Figure 6.8: External acoustic feedback path length error surface: modelled actual feedback path, F(f)

Examining two-dimensional contour plots obtained by plotting the cost function against pairs of varying parameters, the irregularity of the error surface is obvious. A convex quadratic error surface would have parallel elliptical contours; these plots have irregular contours, spaced at non-constant intervals (Figures 6.9 – 6.12). Generally, the contours become more widely spaced around the minimum, indicating that the error surface is shallow around this point and the global minimum is poorly defined. The minimum is marked with a cross in each plot.

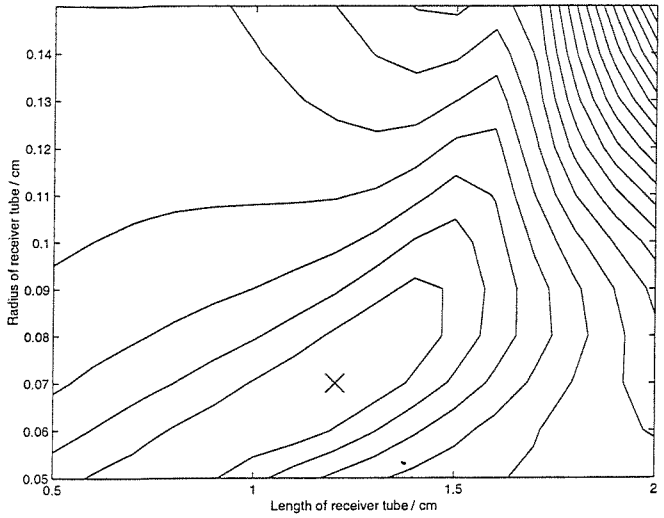

Figure 6.9: Contour plot of error surface, varying length and radius of receiver tube: modelled actual feedback path, F(f)

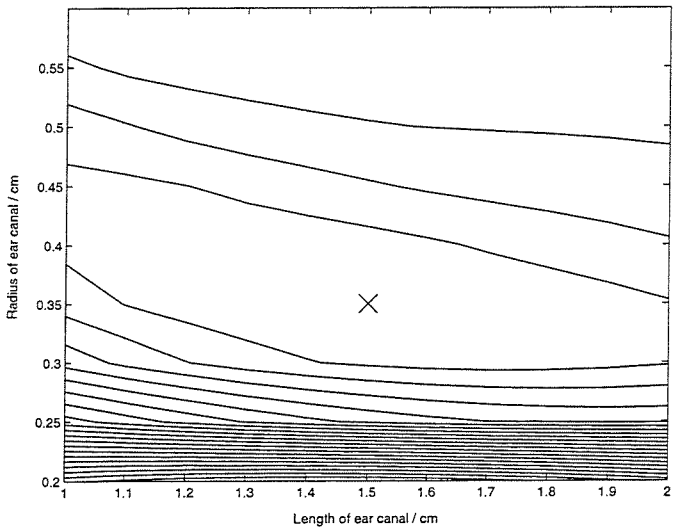

Figure 6.10: Contour plot of error surface, varying length and radius of ear canal tube: modelled actual feedback path, F(f)

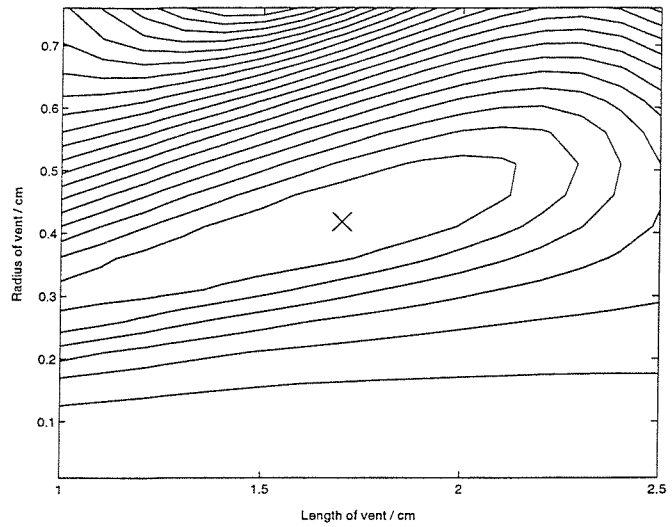

Figure 6.11: Contour plot of error surface, varying length and radius of vent: modelled actual feedback path, F(f)

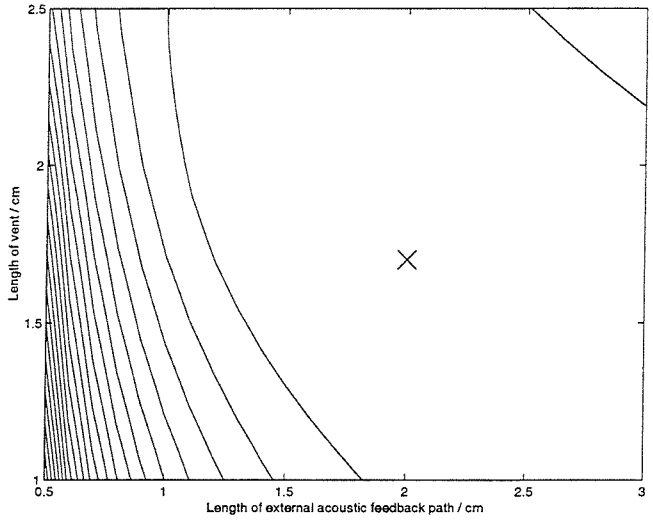

Figure 6.12: Contour plot of error surface, varying vent length and external acoustic feedback path length: modelled actual feedback path, F(f)

6.4 Error surface produced by fitting the analytic model to a measured feedback path

In this section, the actual feedback path, *F(f)*, was represented by measured data for the normal fit feedback path response for the right ear of subject BO (Rafaely *et al.*, 2000). The modelled feedback path, *M(f)*, varied the physical parameters to produce the error surface as before. The default parameter values are given in Table 6.4. The range of physical dimensions used in the model is given in Table 6.5. The constant parts of the model are given in Table 6.2 as before.

Parameter	*Symbol*	*Default value*
Receiver tube length	L_1	1.2 cm
Receiver tube radius	r_1	0.7 mm
Ear canal length	L_2	1.5 cm
Ear canal radius	r_2	3.5 mm
Vent length	L_3	1.7 cm
Vent radius	r_3	0.8 mm
External acoustic feedback path length	R	2.0 cm

Table 6.4: Default physical parameter values for the modelled feedback path, M(f)

Parameter	*Symbol*	*Range of values*	*Error surface shown in Figure:*
Receiver tube length	L_1	0.5 – 2.0 cm	6.13
Receiver tube radius	r_1	0.5 – 1.5 mm	6.14
Ear canal length	L_2	0.01 – 2.0 cm	6.15
Ear canal radius	r_2	1.0 – 4.0 mm	6.16
Vent length	L_3	0.5 – 3.0 cm	6.17
Vent radius	r_3	0.1 – 8.0 mm	6.18, 6.19
External acoustic feedback path length	R	0.05 – 4.0 cm	6.20

Table 6.5: Range of physical parameter values used in the model to produce the set of error surfaces shown in Figures 6.13 – 6.20

The set of error surfaces is shown in Figures 6.13 – 6.20. None were convex, but a global minimum occurred using the default values for the constant parameters in the model in all but the ear canal length, vent length and vent radius error surfaces (Figures 6.15, 6.17, 6.18 and 6.19 respectively). In the first and last of these cases, no well-defined minimum was observed over the range of interest, and in the second, local minima occurred. The surfaces were recalculated, changing the constant value of the ear canal radius r_2 from 3.5 mm to 2.0 mm. This changed the shape of the ear canal length error surface, making it almost convex with a global minimum near L_2 = 1.05 cm (Figure 6.15). However, even with this change in the value of a constant parameter, local minima remained in the vent length error surface (Figure 6.17). The constant value of the ear canal radius r_3 was changed from 0.8 mm to 1.2 mm as well as changing r_2 to 2.0 mm. This produced a non-convex surface with a global minimum (Figure 6.17). The vent radius error surface was not convex with the default constant parameter values and had no clear minimum (Figure 6.18). Changing the constant value of the

ear canal radius r_2 from 3.5 mm to 2.0 mm produced a clear global minimum near r_3 = 1 mm; this was seen more clearly over the range 0.1 mm to 2.5 mm (Figure 6.19).

This demonstrated that the choice of constant parameter values in the model had a significant effect on the shape of the error surface by affecting the amount of possible agreement between the modelled and measured responses.

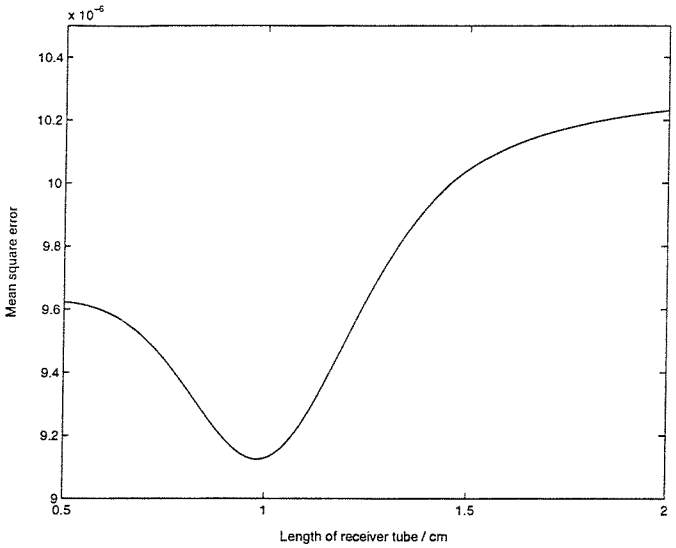

Figure 6.13: Receiver tube length error surface: measured actual feedback path, F(f)

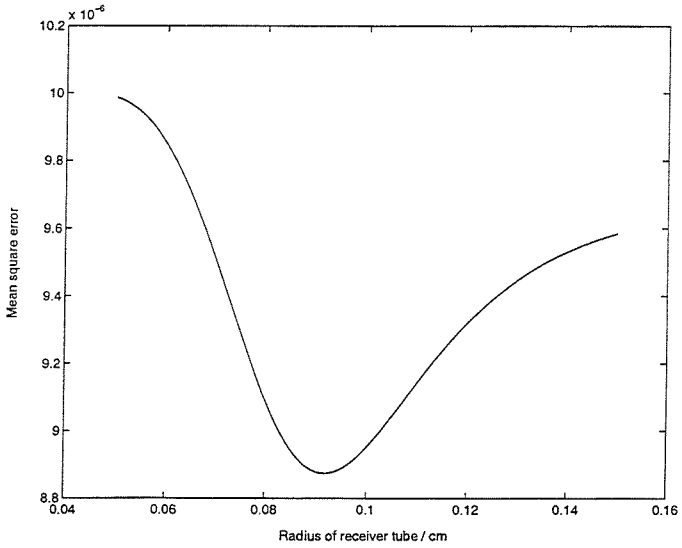

Figure 6.14: Receiver tube radius error surface: measured actual feedback path, F(f)

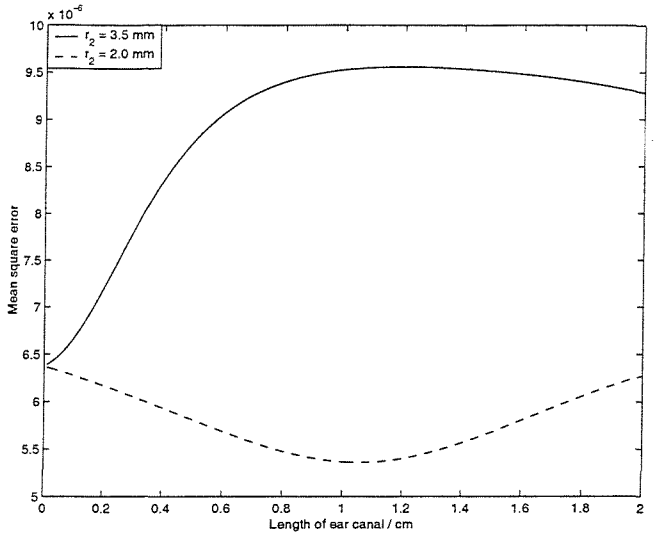

Figure 6.15: Ear canal length error surface, calculated with r_2 = 3.5 mm and r_2 = 2.0 mm: measured actual feedback path, F(f)

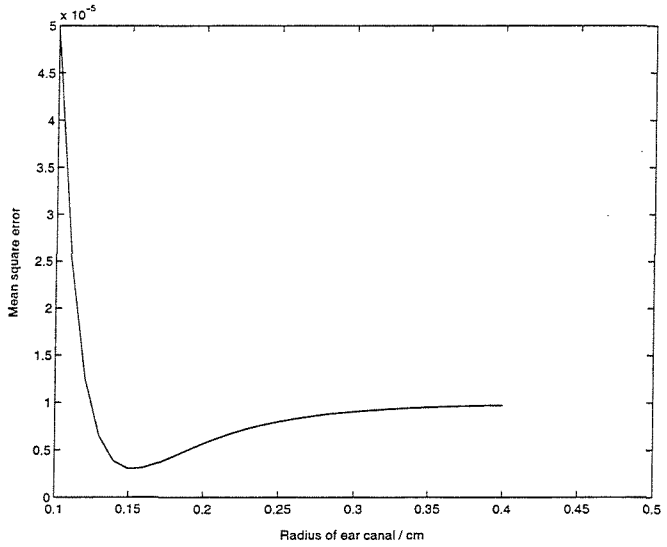

Figure 6.16: Ear canal radius error surface: measured actual feedback path, F(f)

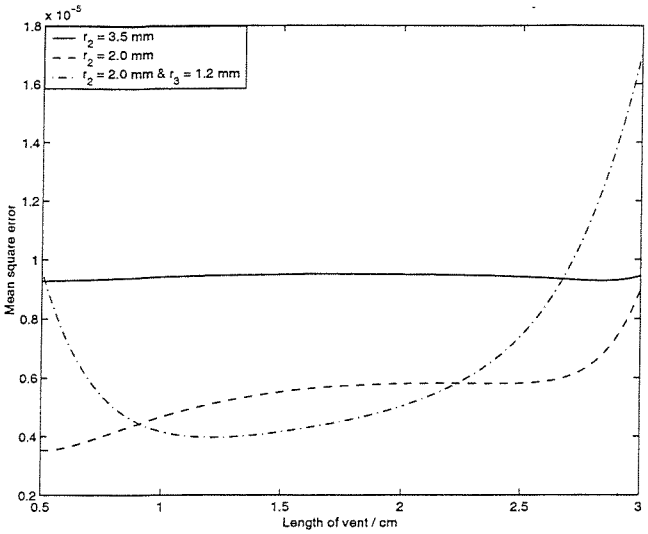

Figure 6.17: Vent length error surface, calculated with r_2 = 3.5 mm, r_2 = 2.0 mm, and r_2 = 2.0 mm and r_3 = 1.2 mm: measured actual feedback path, F(f)

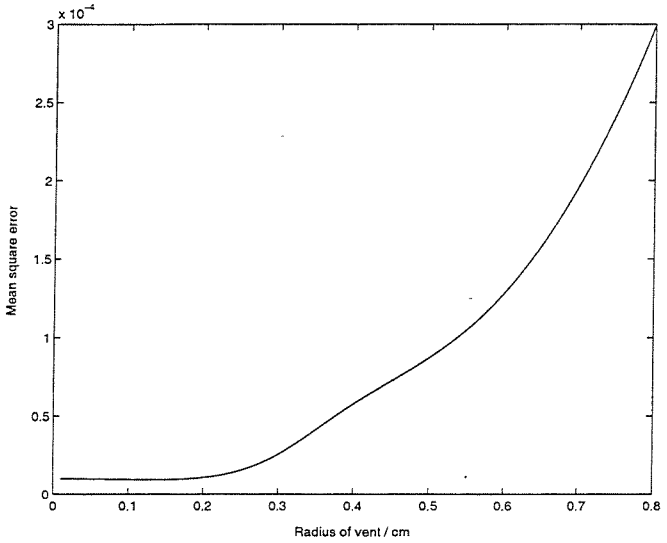

Figure 6.18: Vent radius error surface: measured actual feedback path, F(f)

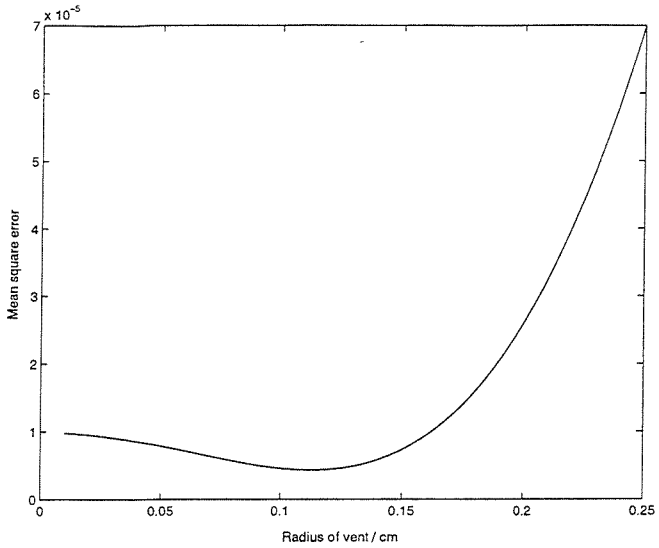

Figure 6.19: Vent radius error surface, calculated with r_2 = 2.0 mm: measured actual feedback path, F(f)

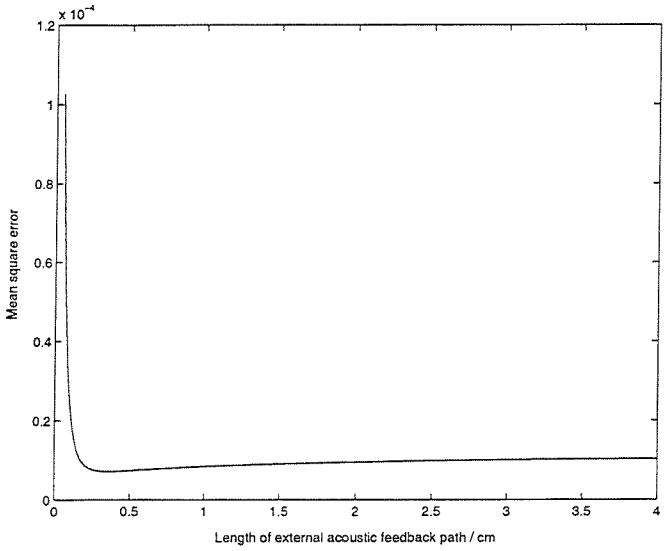

Figure 6.20: External acoustic feedback path length error surface: measured actual feedback path, F(f)

Therefore it has been shown that the choice of constant parameter values in the model affects the shape of the error surfaces calculated for measured feedback path response data. The error surfaces were ill-defined and not convex, indicating that a steepest descent-based algorithm may have difficulty finding the global minimum. Local minima may occur if the constant values in the model are poorly chosen.

As in the previous section, two-dimensional contour plots were obtained by plotting the cost function against pairs of varying parameters, using the default values given in Tables 6.2 and

6.4 for the constant physical parameters in the model unless stated otherwise. Again, these surfaces had irregular contours, spaced at non-constant intervals (Figures 6.21 – 6.24). The minimum of the error surface could not be shown as the parameter values required to obtain exact agreement with the actual feedback path response were unknown; however, the contour plots indicated that the global minimum could lie outside the range of interest for some parameters (e.g. Figure 6.21). This suggests that the parameter values required to fit the model in its current form to the measured response may not correspond with feasible physical dimensions, as observed in Chapter 5.

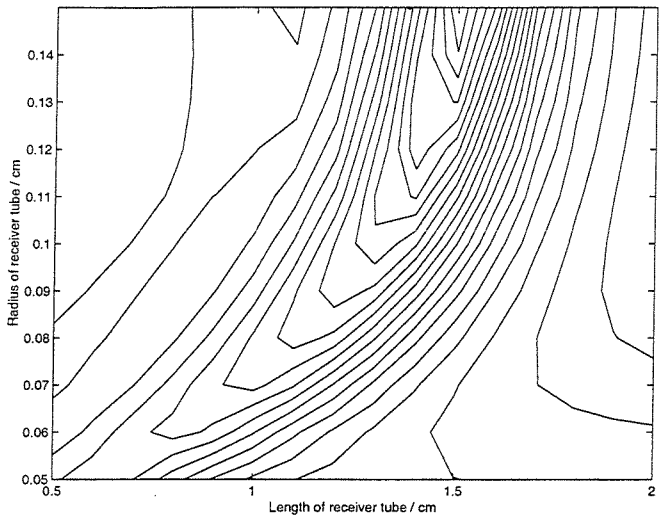

Figure 6.21: Contour plot of error surface, varying length and radius of receiver tube: measured actual feedback path, F(f)

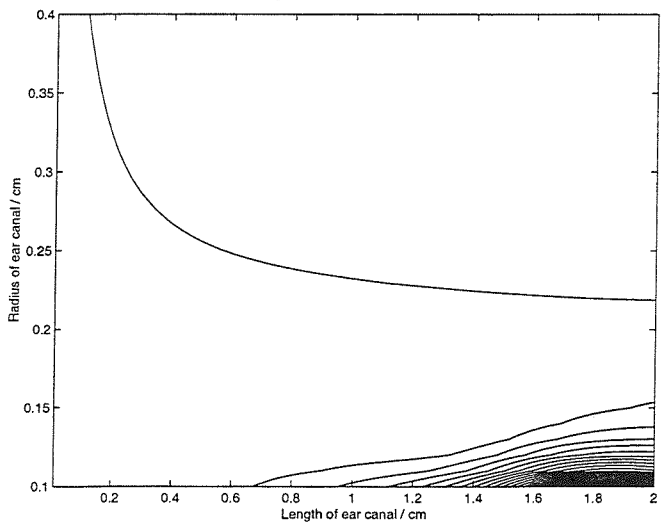

Figure 6.22: Contour plot of error surface, varying length and radius of ear canal: measured actual feedback path, F(f)

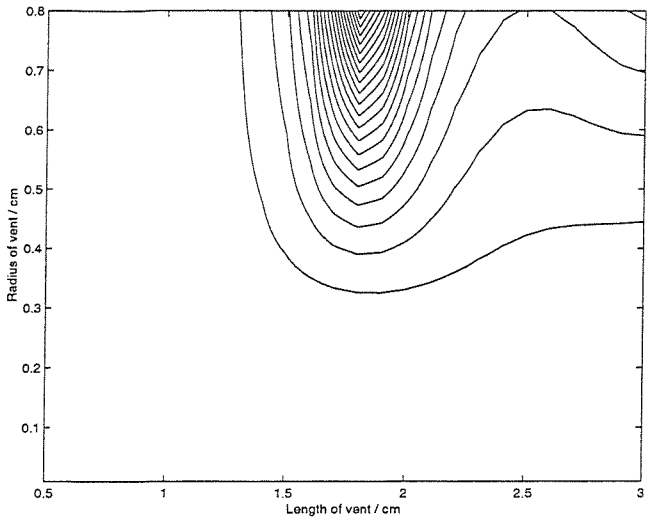

Figure 6.23: Contour plot of error surface, varying length and radius of vent: measured actual feedback path, F(f)

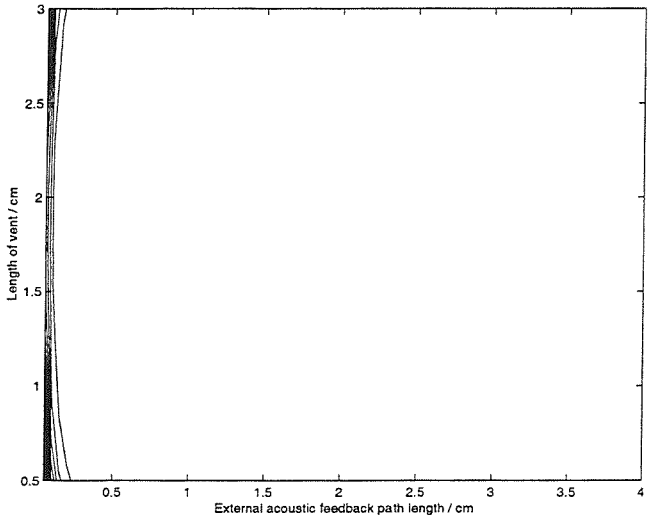

Figure 6.24: Contour plot of error surface, calculated using r_2 = 2.0 mm, varying vent length and external acoustic feedback path length: measured actual feedback path, F(f)

6.5 Conclusions

The error surfaces obtained with both modelled and measured actual feedback paths were non-convex and irregular and may present problems to a steepest descent-based algorithm. The choice of the constant parameter values in the model affects the amount of agreement that is possible between the modelled and actual responses and care must be taken that this does not result in local minima. This suggests that a more accurate model of the feedback path might be required with well-defined bounds on the parameter values in order to improve the behaviour of the error surface and thus improve the performance of steepest-descent based adaptation processes such as that proposed in Chapter 7.

7 Development of a parametric adaptive algorithm (PAA) for feedback cancellation

7.1 Introduction

This chapter presents a novel approach to the feedback cancellation problem, the parametric adaptive algorithm (PAA). This is intended to use knowledge of the components of the hearing aid system to produce a more accurate model of the feedback path, potentially leading to greater cancellation of the feedback signal and allowing stable use of higher gains. The algorithm uses the analytic model of the feedback path developed in previous chapters to form the estimate of the feedback path used to cancel the feedback signal. The estimated physical parameter values are adapted to track changes in the feedback path. The restricted number of parameters results in a low order algorithm that is intended to track changes in the feedback path quickly. The ability of the algorithm to remain robust to such changes is not investigated in this thesis and is a subject for future work. The PAA is derived from the method of steepest descent and compared with a steepest descent analysis of the LMS algorithm. A practical PAA is then presented which uses FIR filtering and is based on the structure of the LMS algorithm. The MATLAB implementation of the algorithm and its computational efficiency are discussed. The performance of the PAA is investigated in simulation studies in Chapters 8 and 9.

7.2 The feedback identification problem

Feedback occurs in hearing aids when amplified sound leaks back from the ear canal to the input of the microphone. The feedback signal is not known beforehand and must be identified in order for it to be cancelled successfully. Feedback cancellation aims to estimate the feedback signal and subtract it from the microphone input signal so that only the desired audio signal remains. Adaptive filters are commonly used in feedback cancellation to track changes in the feedback path. However, the estimated model produced by the filter is never perfect and the feedback signal is never cancelled entirely (Rafaely *et al.*, 2000). Instability can still occur, mainly at high gain levels. A block diagram of a hearing aid system with adaptive feedback cancellation is shown in Figure 7.1 overleaf.

F is the transfer function of the feedback path from the receiver input to the microphone output, shown in Figure 2.8 and modelled by Equation (4.22). K is the transfer function of the internal processing of the hearing aid, including amplification, shaping of the desired frequency response to suit the needs of the user, sub-band filtering, and compression (Kates, 1991, 1999; Greenberg *et al.*, 2000; Hellgren and Forsell, 2001; Hellgren, 2002). W is the transfer function of the adaptive feedback cancellation filter. Such a system operates in

closed-loop, so the identification of the time-varying feedback path F by the cancellation filter W is complicated by the action of the processing in K (Kates, 1999; Greenberg *et al.*, 2000).

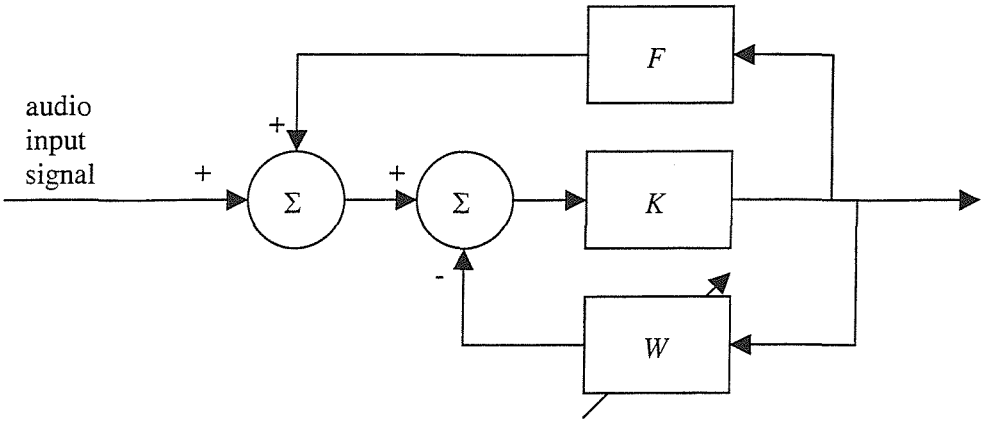

Figure 7.1: Block diagram of a hearing aid system with adaptive feedback cancellation

For the investigation of the proposed new algorithm in this thesis, the problem is simplified to open-loop operation, omitting the internal hearing aid processing, K. The study of the algorithm in closed-loop operation is a topic for future work.

A further simplification made in this work is the assumption that the input to the adaptive system, x, is a filtered white noise signal, as shown in the block diagram of the open-loop system in Figure 7.2. v is a white noise signal, T is a shaping filter, d is the desired signal, i.e. the feedback signal to be identified and cancelled, y is the estimated feedback signal produced by passing the input signal x through the adaptive filter W, and e is the error signal, the difference between the estimated and actual feedback signals, used to update the coefficients of W.

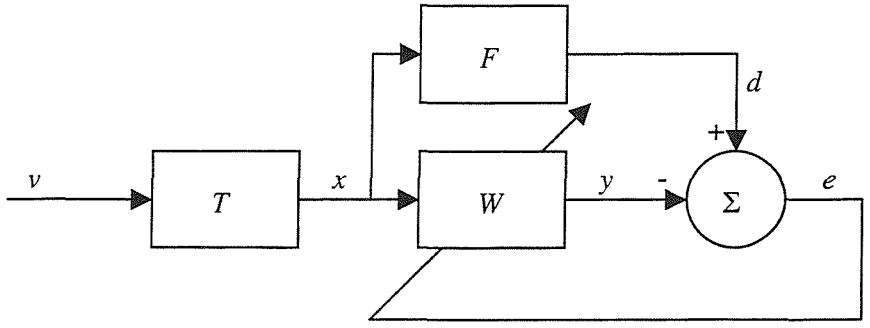

Figure 7.2: Block diagram of the open-loop feedback cancellation system

7.3 Adaptive identification using the NLMS algorithm

The Normalised Least Mean Square (NLMS) algorithm is a common approach to the feedback problem at the time of writing, for example in the direct method of feedback cancellation (Kates, 1999; Hellgren, 2002). It is widely used, being straightforward to implement and computationally efficient. The NLMS algorithm is used as a reference for the performance of the new parametric algorithm in Chapters 8 and 9.

The LMS algorithm is presented in Section 1.5. For the system shown in Figure 7.2, the set of filter coefficients $\mathbf{w}(n)$ are updated according to:

$$\mathbf{w}(n+1) = \mathbf{w}(n) + \alpha e(n)\mathbf{x}(n) \tag{7.1}$$

The NLMS algorithm has the form:

$$\mathbf{w}(n+1) = \mathbf{w}(n) + \frac{\alpha_0}{\mathbf{x}^T(n)\mathbf{x}(n) + \varepsilon} e(n)\mathbf{x}(n) \tag{7.2}$$

ε is a small constant used to avoid dividing by zero. The rate of convergence of the NLMS algorithm will be constant even when the input signal power fluctuates (see Section 1.5).

7.4 Steepest descent analysis of the LMS algorithm

Many adaptive feedback cancellation algorithms are based on the method of steepest descent (Widrow and Stearns, 1985). Initially, the parametric adaptive algorithm presented in this thesis is analysed using a non-stochastic algorithm based on the method of steepest descent (derived in Section 7.5), allowing investigation of the modes of convergence without the misadjustment caused by a stochastic estimated gradient. In this section, a steepest descent LMS algorithm is derived so that the performance of this form of the parametric adaptive algorithm can be compared directly to that of the LMS.

In the method of steepest descent, the filter coefficients are updated according to:

$$\mathbf{w}(n+1) = \mathbf{w}(n) - \alpha \frac{\partial J}{\partial \mathbf{w}(n)} \tag{7.3}$$

In the LMS algorithm, the cost function is the mean square error:

$$J = E\left[e^2(n)\right] = \mathbf{w}^T\mathbf{R}\mathbf{w} - 2\mathbf{w}^T\mathbf{p} + c \tag{7.4}$$

so

$$\frac{\partial J}{\partial \mathbf{w}} = 2\mathbf{R}\mathbf{w} - 2\mathbf{p} = \mathbf{R}\mathbf{w} - \mathbf{p} \tag{7.5}$$

R is the square matrix of autocorrelation functions of the input signal, **x**(n) (Widrow and Stearns, 1985). All the terms in every diagonal are the same; **R** is a Toeplitz matrix, i.e. all the elements on the main diagonal are equal and all the elements on any diagonal parallel to the main diagonal are also equal (Haykin, 1996).

$$\mathbf{R} = E[\mathbf{x}^T\mathbf{x}] = \begin{bmatrix} r_{xx}(0) & r_{xx}(1) & r_{xx}(2) & \cdots \\ r_{xx}(1) & r_{xx}(0) & r_{xx}(1) & \cdots \\ r_{xx}(2) & r_{xx}(1) & r_{xx}(0) & \cdots \\ \vdots & \vdots & \vdots & \ddots \end{bmatrix} \tag{7.6}$$

The autocorrelation function $r_{xx}(\tau)$ is given by the Inverse Fast Fourier Transform of the power spectral density $S_{xx}(f)$ (Haykin, 1996):

$$r_{xx}(\tau) = FFT^{-1}\{S_{xx}(f)\} \tag{7.7}$$

The cross-correlation function $\mathbf{p} = r_{xd}(\tau)$ is given by the Inverse Fast Fourier Transform of the cross-spectral density $S_{xd}(f)$ (Haykin, 1996):

$$\mathbf{p} = E[\mathbf{x}(n)d(n)] = [r_{xd}(0), r_{xd}(1), \ldots, r_{xd}(N-1)]^T \tag{7.8}$$

$$r_{xd}(\tau) = FFT^{-1}\{S_{xd}(f)\} \tag{7.9}$$

For the feedback cancellation system shown in Figure 7.2, the input signal x is produced by passing the white noise signal v through the filter T. The power spectral density of x, $S_{xx}(f)$, is given by (Widrow and Stearns, 1985);

$$S_{xx}(f) = |T(f)|^2 \, S_{vv}(f) \tag{7.10}$$

As v is white noise, $S_{vv}(f)$ is a constant, σ_v^2, therefore:

$$S_{xx}(f) = |T(f)|^2 \, \sigma_v^2 \tag{7.11}$$

and

$$r_{xx}(\tau) = FFT^{-1}\{\, |T(f)|^2 \, \sigma_v^2 \,\} \tag{7.12}$$

The cross-spectral density, $S_{xd}(f)$, is given by (Widrow and Stearns, 1985):

$$S_{xd}(f) = F(f)S_{xx}(f) = F(f)|T(f)|^2 \, \sigma_v^2 \tag{7.13}$$

so

$$\mathbf{p} = FFT^{-1}\{F(f)|T(f)|^2\ \sigma_v^2\} \tag{7.14}$$

Equations (7.6), (7.12) and (7.14) can be substituted into Equation (7.5) to find $\partial J / \partial \mathbf{w}$ and hence update the filter coefficients $\mathbf{w}$ according to Equation (7.3).

If $T = 1$, x becomes a white noise signal and $S_{xx}(f)$ is a constant, σ_x^2. Hence $r_{xx} = \delta(n)\sigma_x^2$ and $\mathbf{R} = \mathbf{I}\sigma_x^2$, where $\mathbf{I}$ is the identity matrix.

The cross-correlation function is now defined by:

$$S_{xd}(f) = F(f)\sigma_x^2 \tag{7.15}$$

so

$$\mathbf{p} = r_{xd} = FFT^{-1}\{\sigma_x^2 F(f)\} = \sigma_x^2 \mathbf{f}(n) \tag{7.16}$$

$\mathbf{f}(n)$ is the impulse response of the feedback path.

Thus

$$\frac{\partial J}{\partial \mathbf{w}} = \mathbf{R}\mathbf{w} - \mathbf{p} = \sigma_x^2 \mathbf{I}\mathbf{w} - \sigma_x^2 \mathbf{f}(n) \tag{7.17}$$

$$\Rightarrow \frac{\partial J}{\partial \mathbf{w}} = \sigma_x^2 (\mathbf{I}\mathbf{w} - \mathbf{f}(n)) \tag{7.18}$$

$$\Rightarrow \frac{\partial J}{\partial \mathbf{w}} = \sigma_x^2 (\mathbf{w}(n) - \mathbf{f}(n)) \tag{7.19}$$

Therefore, the update equation with a white noise input signal is:

$$\mathbf{w}(n+1) = \mathbf{w}(n) + \alpha\sigma_x^2 (\mathbf{w}(n) - \mathbf{f}(n)) \tag{7.20}$$

This update equation is independent of the input signal and so will not be affected by its stochastic nature. The impulse response of the feedback path is not known in a real hearing aid system, so this is not a practical algorithm.

7.5 Steepest descent analysis of the parametric adaptive algorithm (PAA)

In the previous chapter, the error surface formed by the 2-norm of the difference between the modelled and actual feedback path responses was examined. The method of steepest descent can be applied to find the global minimum of this surface. This method is used here to derive a new parametric adaptive algorithm for feedback cancellation.

Consider the general block diagram of the adaptive feedback cancellation system below (Figure 7.3):

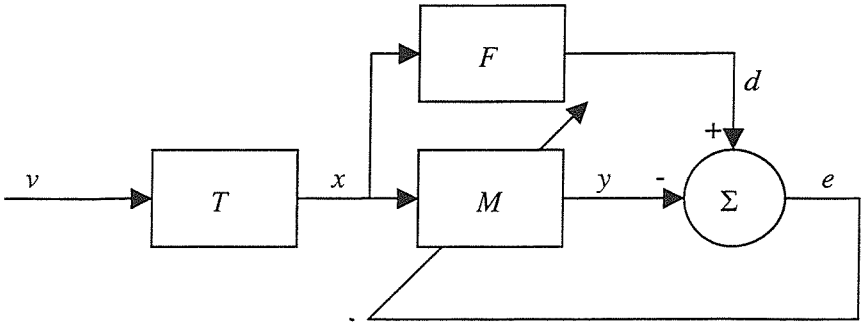

Figure 7.3: Block diagram of an adaptive feedback cancellation system using an adaptive modelled feedback path, M

T is the frequency response of the filter through which the white noise input signal, v, is passed. If $T = 1$, the input to the adaptive system, x, is white noise. If the input signal is speech-shaped noise, $|T|^2$ gives the averaged long term RMS speech spectrum. The aim of using a speech-shaped filter is to make the model of the system more realistic, and the effect is to increase the sound energy at some frequencies and decrease it at others. This will slow down the NLMS algorithm compared to its performance with white noise. (In white noise, all samples are uncorrelated so each filter coefficient adapts independently of the others. The LMS error surface is circular and all modes converge at the same speed. However, there is some correlation between samples in speech-shaped noise and the error surface has both fast and slow modes. These slow modes limit the overall speed of convergence (Widrow and Stearns, 1985).) The convergence speed of the parametric adaptive algorithm may be less affected by speech-shaped noise than the NLMS algorithm since it updates physical parameter values in the model rather than the filter coefficients, as will be shown in this section.

The cost function J is defined for the system in Figure 7.3 as the 2-norm of the difference between the actual and modelled feedback path responses:

$$J(\mathbf{p}) = \left\| T(f)\left(F(f) - M(f,\mathbf{p})\right)\right\|_2^2 \qquad (7.21)$$

The modelled feedback path M is a function of the set of varying parameters $\mathbf{p}$.

In conventional algorithms, such as the NLMS, the parameters are the filter coefficients. Here, the proposed algorithm updates estimates of the *physical* parameters used to generate

the modelled response $M(f, \mathbf{p})$. Each varying parameter p has its own convergence coefficient α_p and local gradient $\nabla_p = \left.\frac{\partial J}{\partial p}\right|_{\text{current value of } p.}$

To simplify the development of the algorithm, ∇_p is approximated by a fixed estimate $\Delta J / \Delta p$. Δp is a small constant fraction of p, chosen to allow sufficient resolution in the value of p. For each varying parameter p, we use two adjacent estimates to derive ΔJ:

$$p_+ = \left(p + \frac{\Delta p}{2} \right) \tag{7.22}$$

$$p_- = \left(p - \frac{\Delta p}{2} \right) \tag{7.23}$$

Firstly, the modelled response $M(f, p)$ is calculated for these estimated parameter values:

$$M_+ = M(f, p_+) \tag{7.24}$$

$$M_- = M(f, p_-) \tag{7.25}$$

The cost function is calculated for each of the estimated parameter values, p_+ and p_-:

$$J(p_+) = \left\| T(F - M_+) \right\|_2^2 \tag{7.26}$$

$$J(p_-) = \left\| T(F - M_-) \right\|_2^2 \tag{7.27}$$

Hence the local gradient of the error surface with respect to the parameter p is estimated by:

$$\nabla_p \approx \hat{\nabla}_p = \frac{\Delta J}{\Delta p} = \frac{J(p_+) - J(p_-)}{\Delta p} \tag{7.28}$$

The estimated parameter is then updated:

$$p(n+1) = p(n) - \alpha_p \hat{\nabla}_p \tag{7.29}$$

This is the principle behind the parametric adaptive algorithm (PAA).

For a white noise input signal, T=1 and

$$J(p_+) = \left\| F - M_+ \right\|_2^2 \tag{7.30}$$

$$J(p_-)=\|F-M_-\|_2^2 \qquad (7.31)$$

When studying the PAA using the steepest descent update equation (Equation (7.29)), it is assumed that $F(f)$ is known, either as a modelled or measured response, and since $M(f)$ can be calculated directly from the model of the hearing aid system, we can calculate $J(p_+)$ and $J(p_-)$ without performing any filtering. In this case, the estimate of the gradient of the error surface is independent of fluctuations in the input signal, so the convergence of the parametric algorithm is affected only by the shape of the error surface and is the same each time the simulation is performed.

In practice, $F(f)$ is unknown, so this steepest descent method can only be used in simulations where $F(f)$ is known and not in real-time feedback cancellation. However, the steepest descent PAA shows the modes of convergence more clearly and is useful for studying the effect of the error surface slope on convergence separately from the effect of misadjustment noise.

7.6 FIR filter-based implementation of the PAA

A practical implementation of the PAA which does not assume knowledge of the feedback path F has been developed. It uses FIR filtering and is based on the implementation of the LMS algorithm. The simplest case is that of a hearing aid system with a single varying parameter. Although several parameters may change simultaneously in reality, varying a single parameter allows the theory behind the algorithm to be presented clearly. The PAA with multiple parameters is presented in Section 7.7.

Consider the adaptive system in Figure 7.2, replacing the LMS FIR filter W with an FIR filter H representing the modelled feedback path M.

The coefficients of the FIR filter representing the actual feedback path F are obtained from the impulse response of the feedback path, i.e.

$$\mathbf{h}_{FB} = FFT^{-1}\{F(f)\} \qquad (7.32)$$

The desired signal $d(n)$ is given by

$$d(n)=\mathbf{h}_{FB}{}^{T}\mathbf{x}(n) \qquad (7.33)$$

The modelled feedback path, M, is dependent on both frequency f and the set of parameters $\mathbf{p}$, where $\mathbf{p} = (r_1, L_1, r_2, L_2, r_3, L_3, R, A_m, A_r, B_r, Z_T)$, and these parameters are defined in Chapter

2. $M(f, \mathbf{p})$ is given by the reciprocal of the simplified analytic expression for the feedback path response:

$$M(f,\mathbf{p}) = \frac{1}{A_{total}(f,\mathbf{p})} \tag{7.34}$$

where, at each frequency,

$$A_{total} = A_m \times (A_r Z_1 \sinh(\Gamma_1 L_1) + B_r \cosh(\Gamma_1 L_1)) \tag{7.35}$$
$$\times \left\{ \left(\frac{Z_3 \sinh(\Gamma_3 L_3)}{Z_T \cosh(\Gamma_2 L_2) + Z_2 \sinh(\Gamma_2 L_2)} \right) + \cosh(\Gamma_3 L_3) \right\} \times \left[\frac{2R\pi}{\rho_0 c k e^{j\left(\frac{\pi}{2} - kR\right)}} \right]$$

Γ_n and Z_n are defined by Equations (2.20) and (2.21) respectively.

For a single general varying parameter p, initially the estimated values are defined in the same way as for the method of steepest descent analysis:

$$p_+(n) = p + \frac{\Delta p}{2} \tag{7.36}$$

$$p_-(n) = p - \frac{\Delta p}{2} \tag{7.37}$$

The FIR filter coefficients are given by the Inverse Fast Fourier Transform of the modelled responses:

$$\mathbf{h}_+ = FFT^{-1}\{M(f, p_+)\} \tag{7.38}$$

$$\mathbf{h}_- = FFT^{-1}\{M(f, p_-)\} \tag{7.39}$$

The filter output signals are given by:

$$y_+(n) = \mathbf{h}_+^T \mathbf{x}(n) \tag{7.40}$$

$$y_-(n) = \mathbf{h}_-^T \mathbf{x}(n) \tag{7.41}$$

The error signals are calculated using:

$$e_+(n) = d(n) - y_+(n) \tag{7.42}$$

$$e_-(n) = d(n) - y_-(n) \tag{7.43}$$

The estimated gradient of the error surface with respect to p is given by the gradient of the instantaneous error surface:

$$\nabla_p = \frac{e_+^2(n) - e_-^2(n)}{\Delta p} \tag{7.44}$$

The estimated parameter values are then updated:

$$p_\pm(n+1) = p_\pm(n) - \alpha_p \nabla_p \tag{7.45}$$

The estimate of the gradient depends on $y_+(n)$ and $y_-(n)$, which in turn depend on the input signal $x(n)$. If $x(n)$ is stochastic, the estimated gradient will be stochastic as well.

A block diagram of the FIR filter implementation of the single parameter PAA is shown in Figure 7.4.

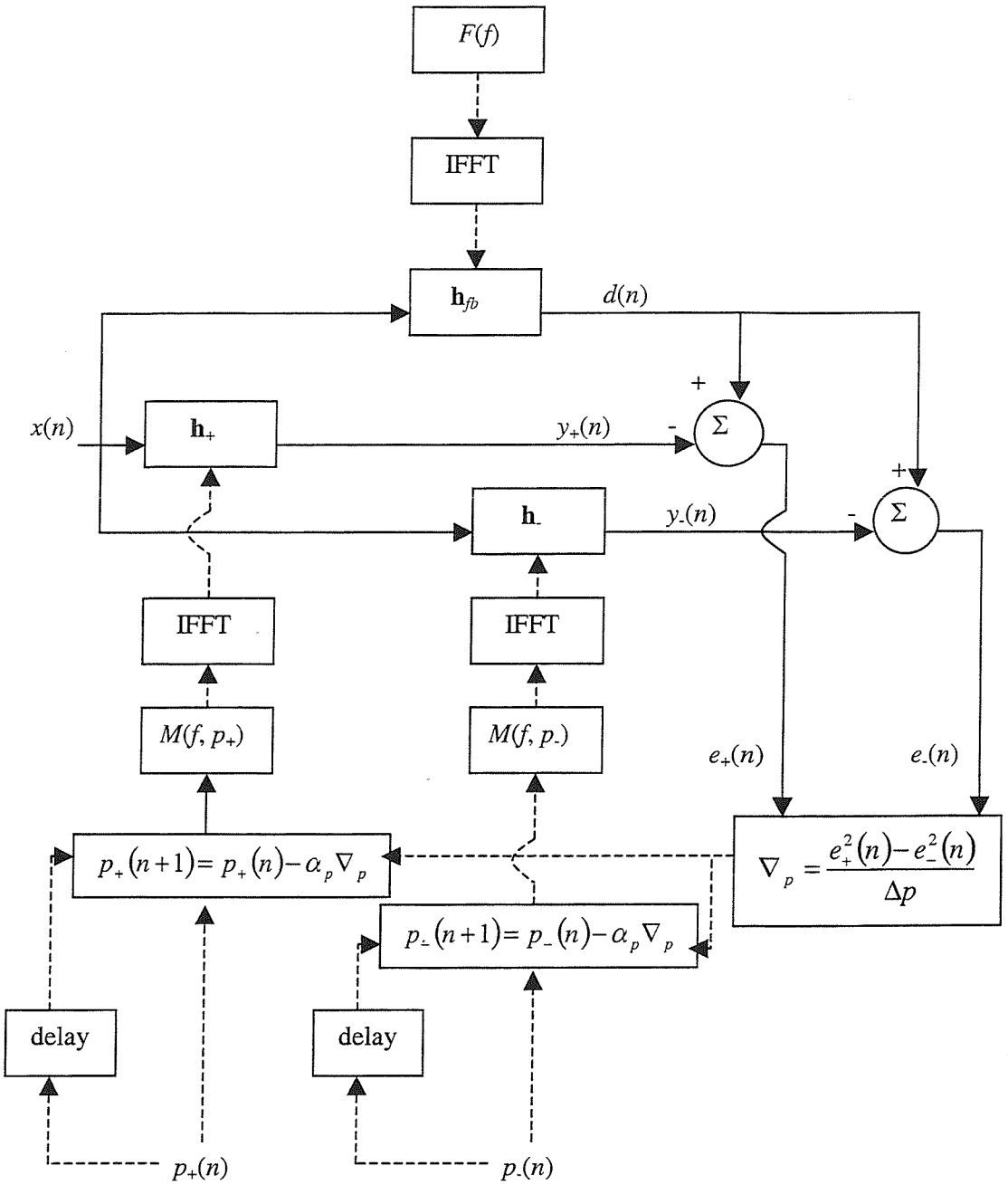

Figure 7.4: Block diagram of the FIR filter implementation of the single parameter PAA

7.7 Extending the PAA to multiple parameters

More than one varying parameter will be required to model a realistic feedback path, so this section presents the formulation of a multiparametric adaptive feedback cancellation algorithm. As stated in Section 2.7, some components of the feedback path vary over short time frames, such as changes in the external acoustic feedback path due to the presence of an obstruction or changes in the amount of slit leakage. Properties of other components such as the transducers change over a much longer time scale, so that they can be considered effectively constant for the purposes of the PAA. Table 7.1 presents likely time frames for variations in the parameters in the feedback path model (Oliveira, 1997; Hellgren *et al.*, 1999b). The structure of the model given by Equation (4.22) clearly shows that the equation can be separated into parts that will change over a short time frame and parts that are effectively constant (see Section 4.3).

Component	*Parameter symbols*	*Probable time frame for variation*
Microphone	A_m	Weeks – months
Receiver	A_r, B_r	Weeks – months
Receiver tube	L_1, r_1	Days – weeks
Ear canal	L_2, r_2	Milliseconds – minutes
Vent (incorporating slit leak)	L_3, r_3	Milliseconds – minutes
Middle ear impedance	Z_T	Days – weeks
External acoustic feedback path	R	Milliseconds – minutes

Table 7.1: Time frames for variation in components of the feedback path

Using the general approach described for the PAA with a single varying parameter, each additional parameter will require another pair of FIR filters, so the computational load will increase. As more parameters are added, the configuration of the algorithm becomes more complicated.

In a similar manner to the single parameter steepest descent analysis described in Section 7.5, each parameter has a pair of estimated filters calculated with the current estimated values of the parameter under consideration, p_{i+} and p_{i-}, and the values of the other parameters, p_{I-i}, where $p_i + p_{I-i} = \mathbf{p}$, the set of all I parameters.

$$p_{i+} = \left(p_i + \frac{\Delta p_i}{2} \right) \tag{7.46}$$

$$p_{i-} = \left(p - \frac{\Delta p_i}{2} \right) \tag{7.47}$$

The modelled response is calculated using these estimated values of the parameter under consideration and the set of all other parameters:

$$M_{i+} = M\left(f, p_{i+}, p_{I-i}\right) \tag{7.48}$$

$$M_{i-} = M\left(f, p_{i-}, p_{I-i}\right) \tag{7.49}$$

The cost function J is calculated for each estimated parameter:

$$J\left(p_{i+}\right) = \left\| T\left(F - M_{i+}\right) \right\|_2^2 \tag{7.50}$$

$$J\left(p_{i-}\right) = \left\| T\left(F - M_{i-}\right) \right\|_2^2 \tag{7.51}$$

Hence the local gradient of the error surface with respect to p_i is estimated by:

$$\nabla_i \approx \hat{\nabla}_i = \frac{J\left(p_{i+}\right) - J\left(p_{i-}\right)}{\Delta p_i} \tag{7.52}$$

The estimated parameters are then updated. Each parameter has its own convergence coefficient, α_i.

$$p_{i\pm}(n+1) = p_{i\pm}(n) - \alpha_i \hat{\nabla}_i \tag{7.53}$$

A practical implementation of the multiparametric algorithm can be made in a similar way to that shown in Section 7.6. For each parameter p_i, the coefficients of a pair of FIR filters are given by the impulse responses of the modelled responses M_{i+} and M_{i-}:

$$\mathbf{h}_{i+} = FFT^{-1}\left\{M\left(f, p_{i+}, p_{I-i}\right)\right\} \tag{7.54}$$

$$\mathbf{h}_{i-} = FFT^{-1}\left\{M\left(f, p_{i-}, p_{I-i}\right)\right\} \tag{7.55}$$

The filter output signals are given by:

$$y_{i+}(n) = \mathbf{h}_{i+}{}^T \mathbf{x}(n) \tag{7.56}$$

$$y_{i-}(n) = \mathbf{h}_{i-}{}^T \mathbf{x}(n) \tag{7.57}$$

The error signals are calculated using:

$$e_{i+}(n) = d(n) - y_{i+}(n) \tag{7.58}$$

$$e_{i-}(n) = d(n) - y_{i-}(n) \tag{7.59}$$

The estimated gradient is given by the gradient of the instantaneous error surface with respect to p_i:

$$\nabla_i = \frac{e_{i+}^2(n) - e_{i-}^2(n)}{\Delta p_i} \tag{7.60}$$

Each parameter has a particular convergence coefficient, α_i. The estimated parameter values are then updated for all **p** according to:

$$p_{i\pm}(n+1) = p_{i\pm}(n) - \alpha_i \nabla_i \tag{7.61}$$

A block diagram of the multiparametric algorithm is shown in Figures 7.5 and 7.6. Figure 7.6 shows the structure of the PAA for two varying parameters, p_1 and p_2, using the update procedure shown in detail in Figure 7.5 for each parameter, and indicates that the algorithm could be extended for additional parameters in the same way.

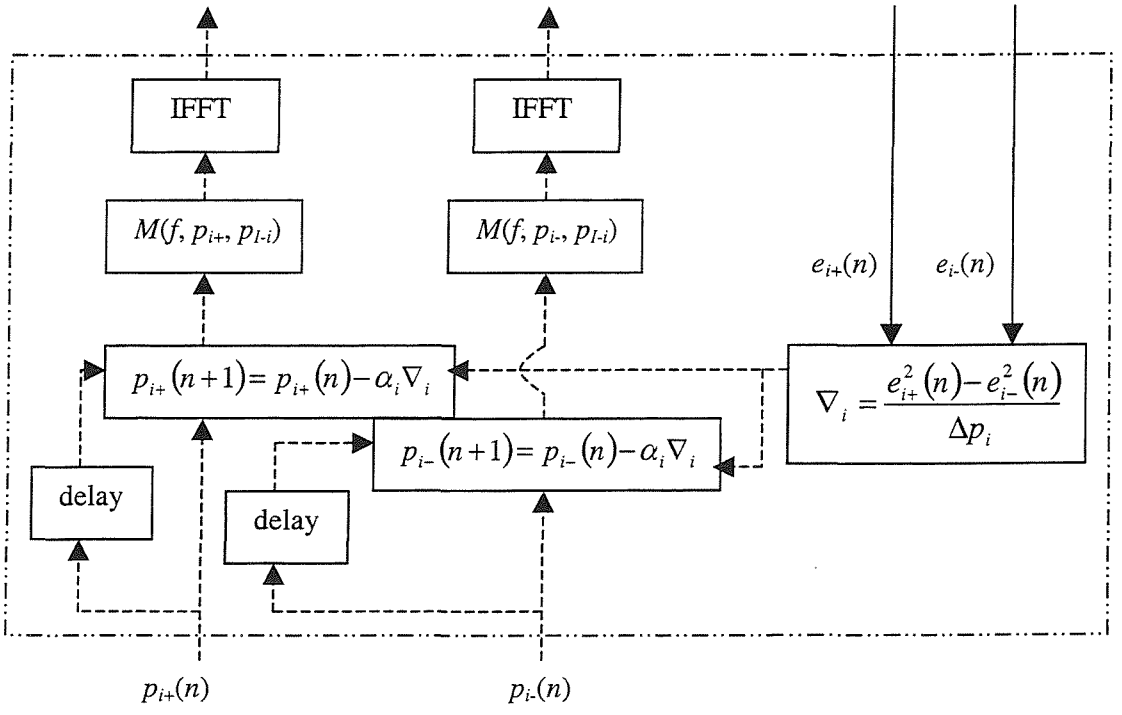

Figure 7.5: Block diagram of the update procedure for each varying parameter, p_i, used in the parametric adaptive algorithm shown in Figure 7.6

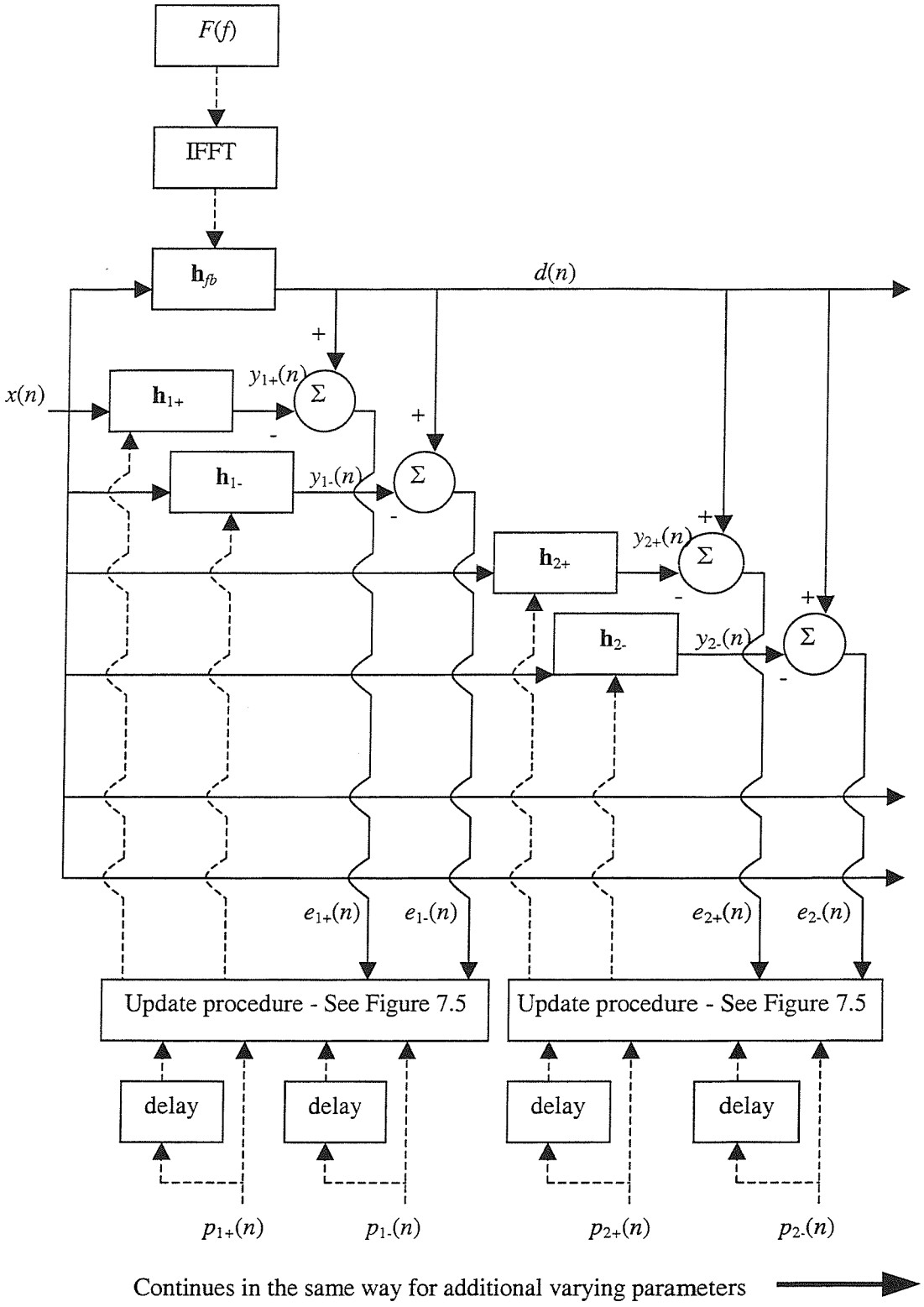

Figure 7.6: Block diagram of FIR filter implementation of the parametric adaptive algorithm with multiple parameters, using the update procedure for each parameter shown in Figure 7.5

7.8 Frequency domain PAA

Estimating the error surface gradient by FIR filtering as presented above is a crude method that requires more than one FIR filter for each varying parameter. For a multiparametric system, many filters will be required, resulting in a large computational load. It is preferable to obtain the gradient analytically. This is easier to do in the frequency domain. In Chapter 4, a set of expressions was derived for the analytic gradient with respect to each varying parameter. These expressions could be used when implementing the PAA in the frequency domain. The development of such an algorithm is outside the scope of this thesis, but a suggested approach is described here.

Consider the system in Figure 7.3. The cost function to be minimised, $J(\mathbf{f},\mathbf{p})$, depends on the range of frequencies, $\mathbf{f} = [f_0, f_1, f_2, \ldots]$, and on all the varying parameters in the model, $\mathbf{p} = [L_1, r_1, L_2, r_2, L_3, r_3, R, A_m, A_r, B_r, Z_T]$.

Each varying parameter p will require an update equation of the form:

$$p(n+1) = p(n) - \alpha_p \sum_f \frac{\partial J(f,p)}{\partial p} \qquad (7.62)$$

where $p(n+1)$ is the new estimate of the parameter, $p(n)$ is the old value of the parameter, α_p is the convergence coefficient for the parameter p and $\frac{\partial J(f,p)}{\partial p}$ is the gradient of the cost function with respect to p.

If the block mean square error, $\sum_n e^2(n)$, is chosen as the cost function J, and, using Parseval's relation (Oppenheim and Schafer, 1975):

$$\sum_{n=0}^{N-1} |e(n)|^2 = \frac{1}{N} \sum_{k=0}^{N-1} |E(k)|^2 = \frac{1}{N} \sum_{k=0}^{N-1} E(k) E^*(k) \qquad (7.63)$$

then, in the frequency domain for each frequency, f:

$$\frac{\partial J}{\partial p} = \frac{\partial E^* E}{\partial p} = E \frac{\partial E^*}{\partial p} + E^* \frac{\partial E}{\partial p} = 2\,\mathrm{Re}\left\{ E^* \frac{\partial E}{\partial p} \right\} \qquad (7.64)$$

The error signal $E(f)$ is given by:

$$E = D - Y = D - MX \qquad (7.65)$$

$D(f)$ is independent of the modelled feedback path and so is independent of all **p**. Therefore:

$$\frac{\partial E^* E}{\partial p} = 2\mathrm{Re}\left\{E^* \frac{\partial E}{\partial p}\right\} = -2\mathrm{Re}\left\{E^* \frac{\partial Y}{\partial p}\right\} = -2\mathrm{Re}\left\{E^* \frac{\partial (MX)}{\partial p}\right\} \tag{7.66}$$

Assuming that the input signal $X(f)$ is independent of all **p**, then at a single frequency,

$$\frac{\partial E^* E}{\partial p} = -2\mathrm{Re}\left\{E^* X \frac{\partial M}{\partial p}\right\} \tag{7.67}$$

Therefore, the update equation can be written as:

$$p(n+1) = p(n) + 2\alpha_p \sum_f \mathrm{Re}\left\{E^* X \frac{\partial M}{\partial p}\right\} \tag{7.68}$$

$X(f)$ and $E(f)$ are known. $\frac{\partial M}{\partial p}$ is given by the set of analytic expressions found by differentiating the expression for the feedback path, A_{total}, with respect to each parameter in **p**.

Recall that:

$$M(f,\mathbf{p}) = \frac{1}{A_{total}(f,\mathbf{p})} \tag{7.69}$$

Using the chain rule (James, 1996),

$$\frac{\partial M}{\partial p} = \frac{\partial M}{\partial A_{total}} \frac{\partial A_{total}}{\partial p} = -\frac{1}{A_{total}^2} \frac{\partial A_{total}}{\partial p} \tag{7.70}$$

$\frac{\partial A_{total}}{\partial p}$ is given by the set of analytic expressions for the gradient derived in Section 4.4.

The amount of filtering required for the frequency domain PAA would be of the order of N log$N$ for a filter of length N, the same as for the frequency domain LMS algorithm.

A practical implementation of this frequency domain algorithm is a topic for future work.

7.9 Misadjustment and block adaptation

Both the NLMS and parametric adaptive algorithms use an instantaneous estimate of the true gradient of the error surface. The filter weights for the NLMS algorithm, and the estimated parameter values for the PAA, will converge towards the optimum values over time. However, even when the algorithm is close to the optimum values, the error will not be zero,

so that the filter weights or parameter values have a random variation causing an excess mean square error. The magnitude of this excess m.s.e., J_{excess}, is used to define the misadjustment ζ (Haykin. 1996):

$$\zeta = \frac{J_{excess}}{J_{\min}} \tag{7.71}$$

J_{min} is the minimum m.s.e. produced by the optimum values of the filter coefficients or physical parameter values.

The misadjustment ζ is a measure of how close the algorithm gets to the optimum solution. The smaller the value of ζ, the more accurate the algorithm. The misadjustment can be reduced by using a smaller convergence coefficient, α, at the expense of slowing down the rate of convergence.

Another method for reducing misadjustment is block adaptation. The basic LMS algorithm updates the filter coefficients after every iteration. Consider the update equation below:

$$\mathbf{w}(n+L) = \mathbf{w}(n) + \alpha(\mathbf{x}(n)e(n) + \ldots + \mathbf{x}(n+L-1)e(n+L-1)) \tag{7.72}$$

$$\mathbf{w}(n+L) = \mathbf{w}(n) + \alpha\sum_{l=0}^{L-1}\mathbf{x}(n+l)e(n+l) \tag{7.73}$$

Changing the sample index n to an index of a block of L samples, m, where $n = mL$, the update equation can now be written as:

$$\mathbf{w}(m+1) = \mathbf{w}(m) + \alpha L\left[\frac{1}{L}\sum_{l=0}^{L-1}\mathbf{x}(mL+l)e(mL+l)\right] \tag{7.74}$$

The instantaneous estimates of the gradient are collected over L iterations, summed and averaged before being added to the previous estimate of the filter coefficients. This gives smoother convergence than the basic LMS algorithm and reduces the misadjustment. For a block of size L, the convergence coefficient becomes αL.

Block adaptation can be implemented in a similar way for the PAA:

$$p(m+1) = p(m) + \alpha_p L\left[\frac{1}{L}\sum_{l=0}^{L-1}\frac{e_+^2(mL+l) - e_-^2(mL+l)}{\Delta p}\right] \tag{7.75}$$

Although convergence is smoother with block adaptation, this is at the expense of the speed of convergence, since several iterations must elapse before a new estimate of the gradient is

produced. Nevertheless, block adaptation is used in the stochastic gradient simulation examples in Chapters 8 and 9 to overcome problems with misadjustment and noisy gradient estimates.

7.10 Choosing a suitable convergence coefficient

The value of the convergence coefficient, α, must be chosen with care if fast convergence is to be achieved without overshooting the minimum of the error surface. Currently, a method has yet to be developed for selecting the parametric convergence coefficients, α_p, analytically. The values of α_p used in the simulations presented in Chapters 8 and 9 were chosen empirically and adjusted after inspection of the estimated gradient for a preliminary simulation. The maximum step size $|\alpha_p \nabla_p|$ was limited to 1 mm for all parameters to limit the amount of misadjustment, although it may have been preferable to use a smaller limit for parameters with smaller values such as the vent radius; this could be applied in future versions of the algorithm. As a rule of thumb, the values of α_p were chosen to give $|\alpha_p \nabla_p| \approx 1$ mm for the largest value of ∇_p. The gradient was usually large at the beginning of the adaptation, reducing as the algorithm adapted towards the minimum of the error surface.

7.11 Computational complexity

The number of operations performed by the LMS algorithm is of the order of $2N$, where N is the filter length. The small computational load is one of the reasons for the widespread use of the algorithm. The PAA, in contrast, has a large computational load, since it must calculate the modelled feedback path response twice for each varying parameter ($p \pm \Delta p/2$) at each iteration, as well as performing filtering and updating the estimates of the parameters. In its current form, the real-time efficiency of the PAA is less important than demonstrating its potential as a robust method of feedback cancellation capable of converging to a good estimate of the actual feedback path in relatively few iterations.

All simulations in this thesis were performed using MATLAB version 6.1.0.450 with the specifications given in Section 4.5. The MATLAB implementation of the PAA has not been optimised for efficiency. This project investigates the feasibility of the algorithm and does not yet cover a practical implementation that could be compared with the real time operation of the NLMS algorithm. This is a topic for future work.

7.12 Effect of parameter variability on the modelled response

It is possible that changing a particular parameter may have a similar effect on the feedback path to changing a different parameter so that the PAA may be unable to determine the cause

of the change in the feedback path and may try to compensate with inappropriate changes in the parameter values used in the model. Figures 7.7 to 7.13 show the effect of varying each parameter in turn over the range considered in the model of the hearing aid system. It can be seen that some parameters have a greater effect on the frequencies of the resonance peaks and some have a greater effect on the overall amplitude of the response. As expected, some parameters have similar effects on the feedback path to other parameters within certain frequency ranges. Compare Figures 7.12 and 7.13 around the receiver resonance peaks between 2 – 8 kHz, for example. Altering both the vent radius and external acoustic feedback path length affects the amplitude of the frequency response in this range.

The estimated gradient between the two responses in each figure can be calculated using steepest descent analysis. Recall that in the PAA with a white noise input signal, the cost function is given by:

$$J = \|F - M\|_2^2 \qquad (7.76)$$

If it is assumed that both F and M are modelled responses at two estimates of the same parameter, p and p', i.e. $F = M(p)$ and $M = M(p')$, then

$$J = \|M(p) - M(p')\|_2^2 \qquad (7.77)$$

The instantaneous gradient of the error surface between p and p' is then given by:

$$\hat{\nabla} = \frac{\|M(p) - M(p')\|_2^2}{|p - p'|} \qquad (7.78)$$

The gradients of the error surface with respect to each varying parameter are shown in Table 7.2. It is clear that changing the vent radius, r_3, has the greatest effect on the feedback path response (compared to the other changes in these examples) since the gradient is at least two orders of magnitude greater than that due to other parameters.

Varying parameter	*Symbol*	*Estimated gradient*	*Response shown in Figure:*
Receiver tube length	L_1	9.9175×10^{-7} cm^{-1}	7.7
Receiver tube radius	r_1	1.1921×10^{-6} cm^{-1}	7.8
Ear canal length	L_2	4.7906×10^{-7} cm^{-1}	7.9
Ear canal radius	r_2	5.6812×10^{-6} cm^{-1}	7.10
Vent length	L_3	3.5661×10^{-7} cm^{-1}	7.11
Vent radius	r_3	1.3658×10^{-4} cm^{-1}	7.12
External acoustic feedback path length	R	2.5821×10^{-6} cm^{-1}	7.13

Table 7.2: Estimated gradient of the error surface with respect to each varying parameter

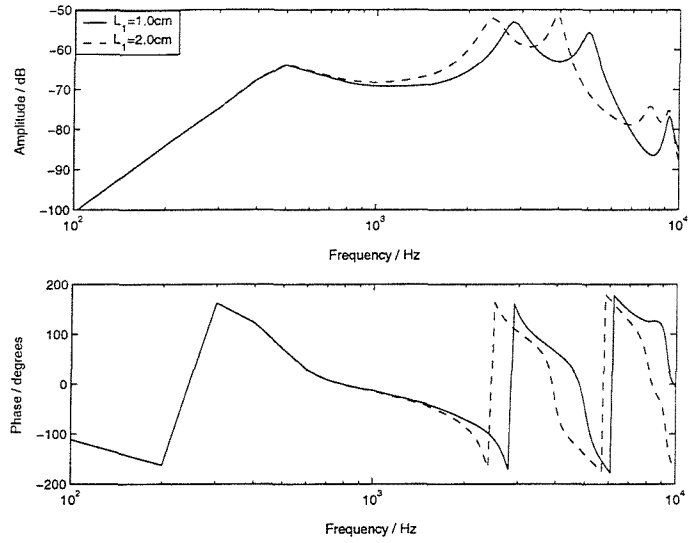

Figure 7.7: Effect on the feedback path response of varying only the receiver tube length, L_1

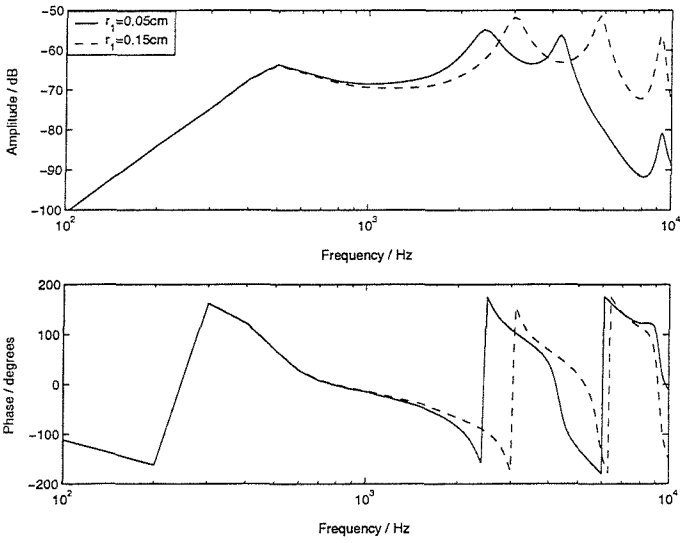

Figure 7.8: Effect on the feedback path response of varying only the receiver tube radius, r_1

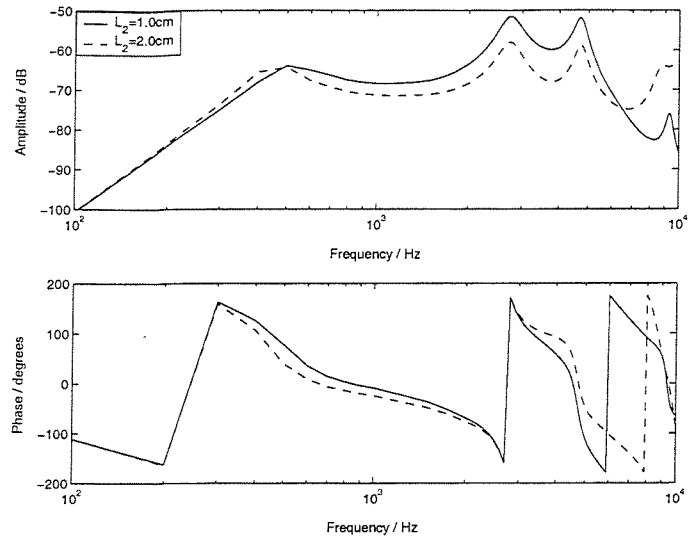

Figure 7.9: Effect on the feedback path response of varying only the ear canal length, L_2

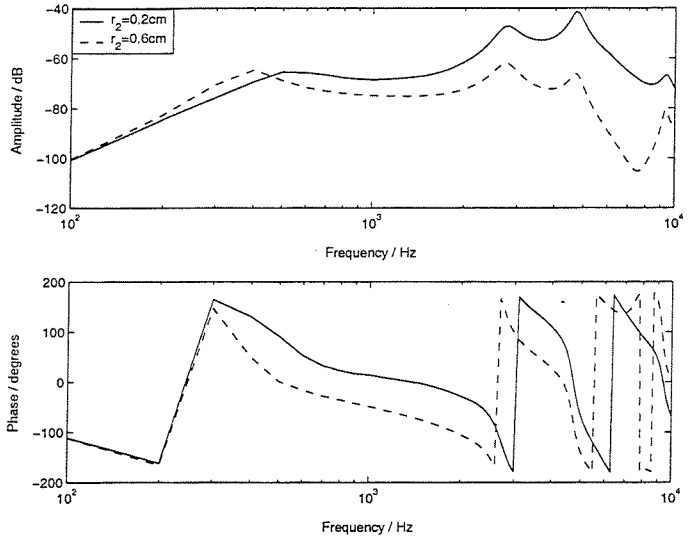

Figure 7.10: Effect on the feedback path response of varying only the ear canal radius, r_2

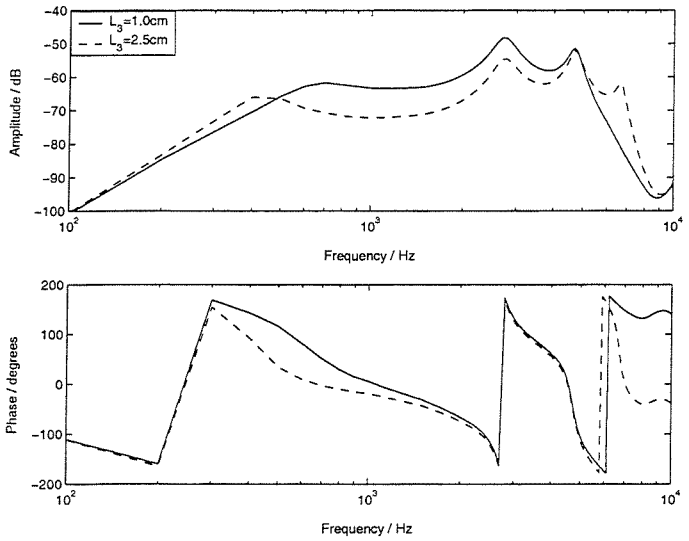

Figure 7.11: Effect on the feedback path response of varying only the vent length, L_3

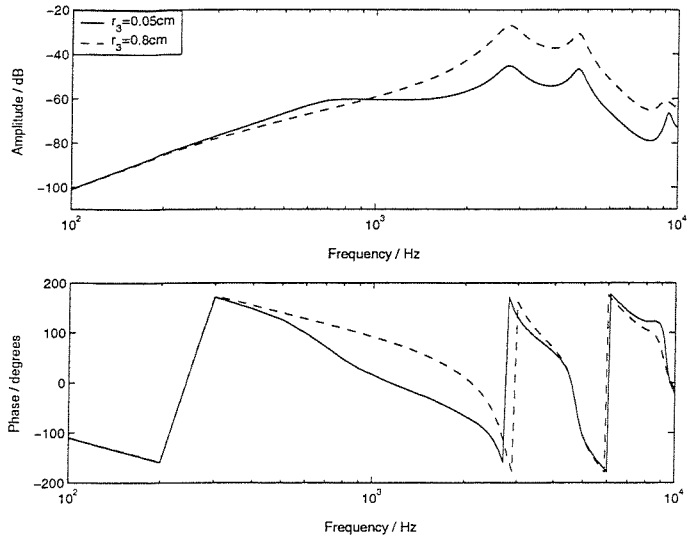

Figure 7.12: Effect on the feedback path response of varying only the vent radius, r_3

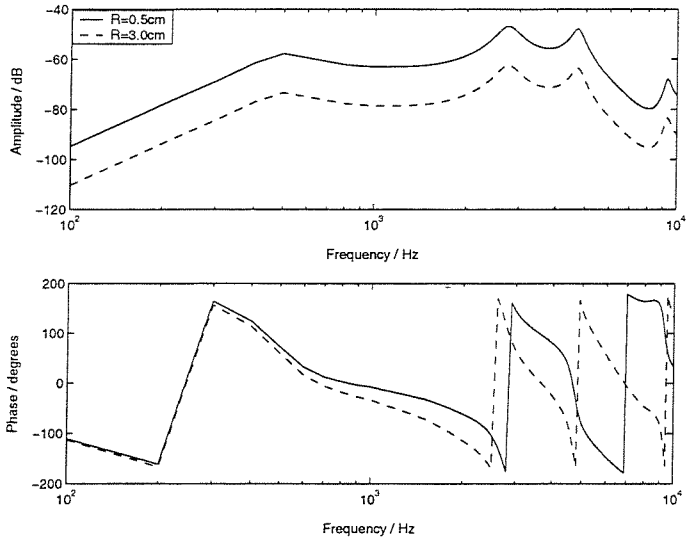

Figure 7.13: Effect on the feedback path response of varying only the external acoustic feedback path length, R

7.13 Conclusions

A novel approach to the feedback cancellation problem, the parametric adaptive algorithm (PAA), has been presented through steepest descent analysis and in the form of an FIR filter-based algorithm developed from the LMS algorithm. The performance of the PAA will be compared with that of the NLMS algorithm in simulations using both steepest descent analysis and FIR filter implementation in subsequent chapters. A frequency domain implementation of the PAA has been suggested as a topic for future work.

The effect on the modelled feedback path response of changing a specific parameter has been investigated. It was found that the effect of a particular parameter on the feedback path

response might be similar to that of another so that the PAA may adapt unsuitable parameters to compensate for changes in the feedback path. This must be taken into consideration in the simulation studies.

8 Simulation studies of the PAA using modelled feedback path data

8.1 Introduction

This chapter presents simulation results for the parametric and NLMS algorithms using a modelled response to represent the actual hearing aid feedback path. The use of a known model gives control of the varying parameters and hence of changes in the feedback path. This allows assessment of the performance of the algorithms under fully controlled conditions. Simulation studies with measured feedback path data are presented in Chapter 9. In this chapter, the convergence behaviour of the parametric and LMS algorithms is investigated. The first simulation example examines the steepest descent forms of both algorithms using a feedback path with two varying parameters and a white noise input signal. This investigates the basic operation of the PAA and compares it to that of the LMS algorithm. The second simulation example investigates the effect on convergence of using a speech-shaped noise input signal. The effect of increasing the number of varying parameters is then investigated in a simulation with four varying parameters and a speech-shaped noise input signal. The steepest descent forms of the algorithms can only be used in theoretical simulations where the feedback path response is known. The use of the stochastic gradient algorithms is a more realistic approach and this is investigated in a simulation with four varying parameters and a speech-shaped noise input signal.

8.2 Implementation of the parametric and LMS algorithms for the simulation studies

In this and the following chapter the performance of the PAA described in Chapter 7 is compared with that of the LMS algorithm in simulation studies performed in MATLAB. (The specifications for MATLAB are given in Section 4.5.) Both the actual and estimated feedback path responses are produced in this chapter using the model shown in Figure 2.8 and described by Equation (4.22). The default parameter values are given in Table 8.1 overleaf.

Each simulation has the same form. Initially, the actual feedback path $F(f, \mathbf{p})$ is defined by the set of parameters $\mathbf{p}$, consisting of the constant parameters, $\mathbf{p}_{con}$, and the initial values of the varying parameters, $\mathbf{p}_{fb1}$: $F_{fb1} = F(f, \mathbf{p}_{con}, \mathbf{p}_{fb1})$. After a number of iterations, the actual feedback path undergoes a step change so that the varying parameters now have the values $\mathbf{p}_{fb2}$, giving $F_{fb2} = F(f, \mathbf{p}_{con}, \mathbf{p}_{fb2})$. A single step change is the simplest case to model: a series of step changes could be used to approximate continuous changes in the feedback path. The step change from initial to final values was made after 100 iterations in every simulation. This delay was used in the steepest descent simulations to be consistent with the stochastic gradient simulations (see Sections 8.6 and 9.3) in which the delay was necessary to allow transient effects of the FIR filters to die away.

Component	*Symbols*	*Fixed or varying*	*Value*
Filter length	N	Fixed	128
Frequency	f	Varying	1 Hz – 10 kHz
Sampling frequency	f_s	Fixed	20 kHz
Receiver tube length	L_1	Fixed	1.2 cm
Receiver tube radius	r_1	Fixed	0.7 mm
Ear canal length	L_2	Varying	1.5 cm or defined in Sections 8.5 – 8.6
Ear canal radius	r_2	Fixed	3.3 mm
Vent length	L_3	Varying	Defined in Sections 8.3 – 8.6
Vent radius	r_3	Varying	Defined in Sections 8.3 – 8.6
External acoustic feedback path length	R	Varying	1.0 cm or defined in Sections 8.5 – 8.6
Microphone two-port network parameters	A_m	Fixed	Modelled using Knowles EM-3046 microphone analogue
Receiver two-port network parameters	A_r, B_r	Fixed	Modelled using Knowles ED-1913 receiver analogue
Middle ear impedance	Z_T	Fixed	Modelled by mean measured data (Shaw, 1974)

Table 8.1: Definition of parameter values used throughout Chapter 8

In the LMS algorithm, the initial set of filter coefficients, $\mathbf{w}$, is equal to the impulse response of the initial actual feedback path, $\mathbf{f}_{fb1} = \text{FFT}^{-1}[F(f, \mathbf{p}_{con}, \mathbf{p}_{fb1})]$. After the change in the feedback path, the coefficients are updated according to the steepest descent LMS (LMS_{sd}) algorithm presented in Section 7.4 (see Sections 8.3 – 8.5) or according to the NLMS algorithm presented in Section 1.5 (see Section 8.6).

For the PAA, initially, the modelled feedback path M is in agreement with the actual path F. For a general varying parameter p_i, the initial estimated values are given by:

$$p_{i+} = \left(p_{fb1} + \frac{\Delta p_i}{2} \right) \tag{8.1}$$

$$p_{i-} = \left(p_{fb1} - \frac{\Delta p_i}{2} \right) \tag{8.2}$$

where p_{fb1} is the actual initial value of p_i and Δp_i is a small, constant fraction of p_i as defined in Section 7.5. After the change in the feedback path, the estimated parameter values are updated according to the steepest descent algorithm presented in Section 7.5 or the stochastic gradient algorithm presented in Section 7.7. Block adaptation is used in the stochastic PAA to reduce the amount of fluctuation caused by stochastic signals (see Sections 8.6 and 9.3). A block size of 7 was chosen empirically to give a good balance between speed and smoothness of convergence.

The simulation in Section 8.3 assumes a white noise input signal to the system. This is the simplest example, in which the energy of the signal is distributed equally across all frequencies. The simulations in Sections 8.4 – 8.6 and in Chapter 9 present a more realistic situation, using speech-shaped noise, i.e. white noise filtered by an averaged long term RMS speech spectrum. The coefficients of the speech-shaping IIR filter were obtained by interpolating from averaged combined spectra for male and female subjects (Byrne and Dillon, 1986; Shusina, 2003). The sampling frequency and filter length are given in Table 8.1. The filter length N was chosen as the shortest length that avoided significant truncation of the impulse response of the measured feedback path used in Chapter 9. The impulse response of the speech-shaping filter is shown in Figure 8.1 and the frequency response in Figure 8.2.

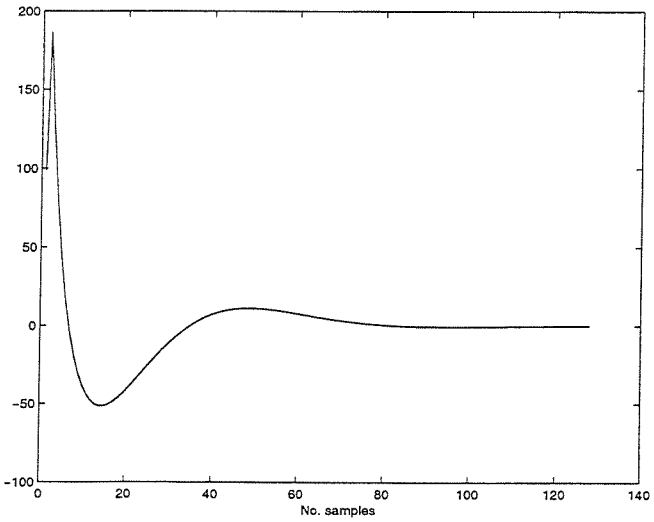

Figure 8.1: Impulse response of the speech-shaping filter used in Sections 8.4 – 8.6 and Chapter 9

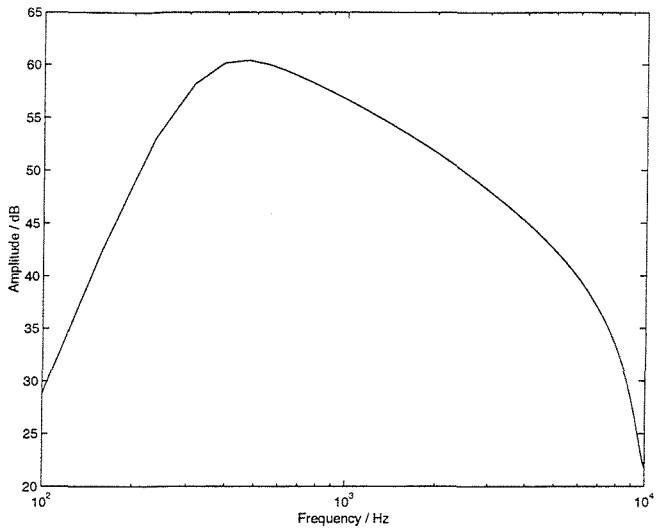

Figure 8.2: Frequency response of the speech-shaping filter used in Sections 8.4 – 8.6 and Chapter 9

8.3 Performance of the steepest descent algorithms with two varying parameters and a white noise input signal

The first simulation presented in this chapter is the simple case of two varying parameters and a white noise input signal. A single parameter simulation has been omitted since this would be too straightforward. A white noise input signal was used, requiring the form of the steepsest descent LMS (LMS_{sd}) algorithm given by Equation (7.20) and of the steepest descent parametric adaptive algorithm (PAA_{sd}) given by Equations (7.22) – (7.31) with $T = 1$ (see Figures 7.2 and 7.3).

The actual feedback path F was modelled using the constant parameter values given in Table 8.1. The varying parameters in this simulation were the vent radius r_3 and the vent length L_3. The initial and final values of these parameters are given in Table 8.2.

Parameter	*Symbol*	*Initial value*	*Final value*
Vent radius	r_3	1.204 mm	4.176 mm
Vent length	L_3	1.2 cm	1.7 cm

Table 8.2: Initial and final values of the varying vent radius and vent length used in the actual feedback path, F

The LMS_{sd} algorithm was simulated for a total of 400 iterations using the arbitrary convergence coefficient $\alpha = 0.5$. For the first 100 iterations, the response of the algorithm was in agreement with that of the initial actual feedback path. The actual feedback path then

underwent a step change, as described in Section 8.2. After the final iteration, the LMS_{sd} response was in very good agreement with that of the final actual feedback path (Figure 8.3).

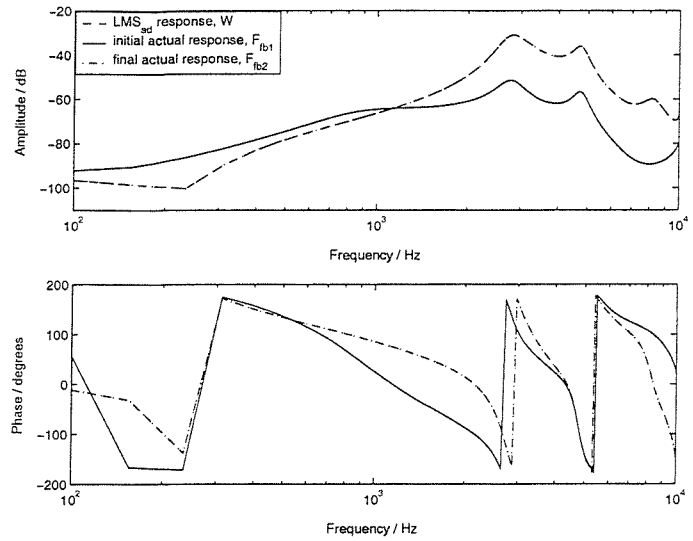

Figure 8.3: Comparison of the LMS_{sd} response with the initial and final actual feedback path responses

Examining the mean square error (Figure 8.4), it can be seen that the LMS_{sd} algorithm has converged rapidly to the correct solution after the change in the feedback path, taking about 5 iterations to reach zero m.s.e.. With $\alpha = 1$, the algorithm converged in 2 iterations.

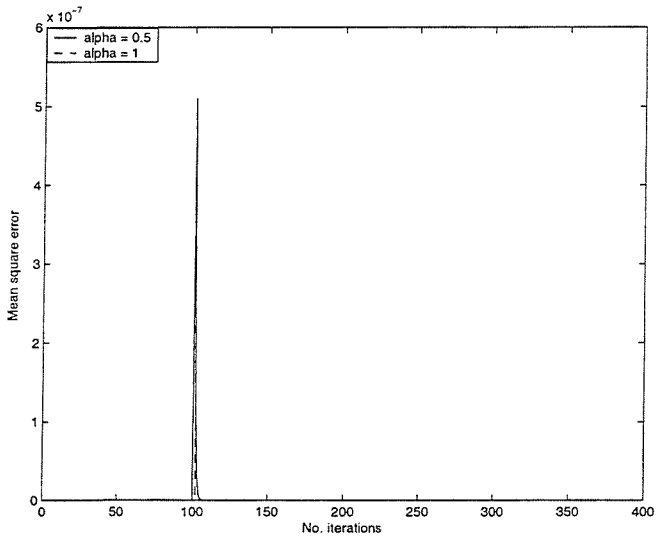

Figure 8.4: Convergence behaviour of the LMS_{sd} mean square error

The estimated gradient, $(\mathbf{w}(n) - \mathbf{f}(n))$, is an N x 1 vector (N is defined in Table 8.1) and cannot be plotted. The normalised mean square error, $\|(\mathbf{w} - \mathbf{f}) / \mathbf{f}\|_2^2$, after the change in the feedback path is shown in Figure 8.5. It can be seen that the LMS_{sd} algorithm reached an extremely

small m.s.e. about 55 iterations after the change in the feedback path. With α = 1, the normalised m.s.e. was zero after 2 iterations; this cannot be plotted on a dB scale.

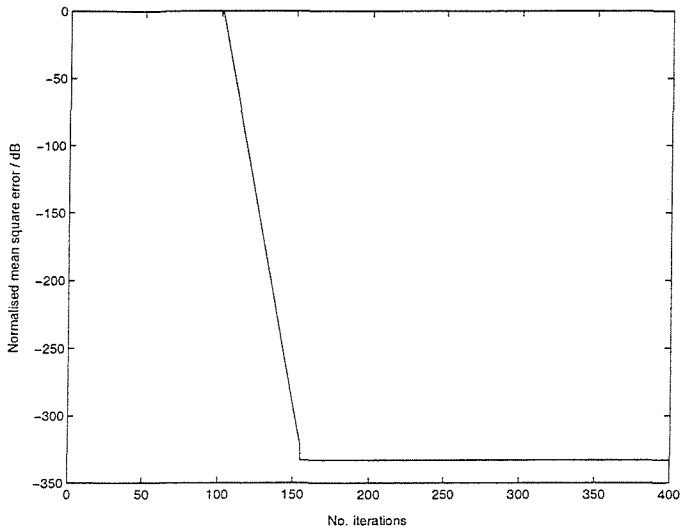

Figure 8.5: Normalised mean square error for the LMS_{sd} algorithm

In the presence of a white noise input signal, the method of steepest descent behaves like Newton's method (Widrow and Stearns, 1985), taking steps directly towards the minimum of the error surface. This gives the LMS_{sd} algorithm an advantage over the steepest descent parametric adaptive algorithm, which adapts in the direction of the negative gradient of the error surface. This is only in the direction of the minimum when the origin of the surface lies on one of its principle axes (Widrow and Stearns, 1985), so the PAA_{sd} is likely to require more iterations for convergence than the LMS_{sd} under these conditions. Although the LMS_{sd} convergence is very fast, it should be noted that this simulation is theoretical. A practical algorithm would not have the prior knowledge of the actual feedback path necessary to estimate the gradient of the error surface in this way and so would need to perform filtering of the input signal in order to estimate the feedback path.

The steepest descent PAA (PAA_{sd}) was simulated for the same change in the feedback path with a white noise input signal. The initial and final values of the varying parameters and their respective convergence coefficients are shown in Table 8.3. The values of the coefficients were chosen empirically to give fast convergence. As observed for the LMS_{sd} algorithm, the estimated response produced by the PAA_{sd} was in very good agreement with that of the final actual feedback path after 400 iterations (Figure 8.6).

Parameter	*Symbol*	*Convergence coefficient*	*Initial value*	*Estimated final value*	*Actual final value*
Vent radius	r_3	$\alpha_{r3} = 100$	1.204 mm	4.189 mm	4.176 mm
Vent length	L_3	$\alpha_{L3} = 2250$	1.2 cm	1.7055 cm	1.7 cm

Table 8.3: Convergence coefficients and values for the varying vent radius and vent length in the steepest descent PAA with a white noise input signal

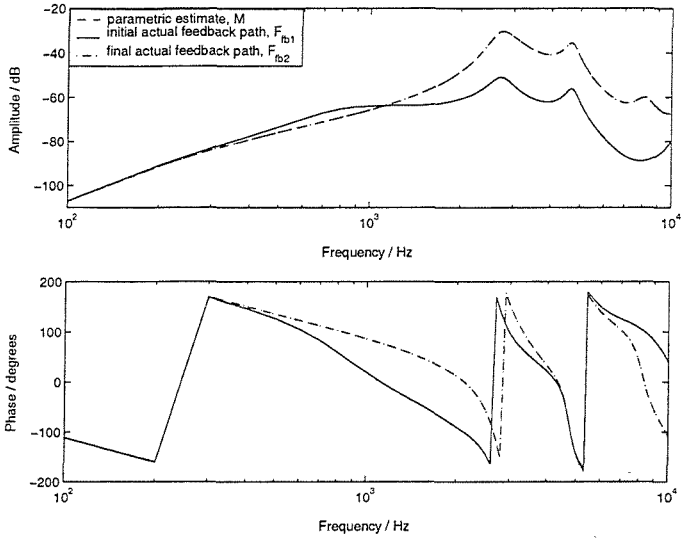

Figure 8.6: Comparison of the parametric response with the initial and final actual feedback path responses

The radius mean square errors, J_{r3+} and J_{r3-}, are shown in Figure 8.7. The errors decreased rapidly after the change in the actual feedback path before reaching a constant level. The length error signals behaved in the same way. The overall m.s.e., defined by Equations (8.3) – (8.5), is shown in Figure 8.8, allowing direct comparison with the steepest descent LMS algorithm. It fell to zero about 60 iterations after the change in the actual feedback path.

$$J = \left\| F - M\left(\mathbf{p}_{est}\right) \right\|_2^2 = \left\| F - M\left(r_{3est}, L_{3est}\right) \right\|_2^2 \tag{8.3}$$

where

$$r_{3est} = \frac{r_{3+} + r_{3-}}{2} \tag{8.4}$$

and

$$L_{3est} = \frac{L_{3+} + L_{3-}}{2} \tag{8.5}$$

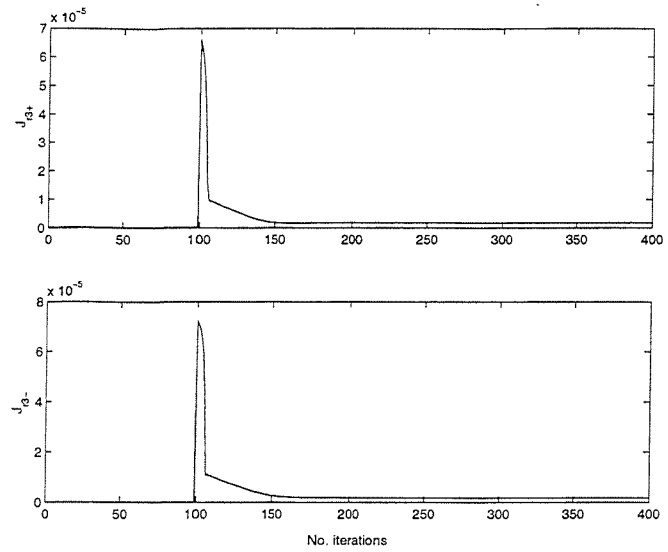

Figure 8.7: Convergence behaviour of the radius mean square errors, J_{r3+} and J_{r3-}.

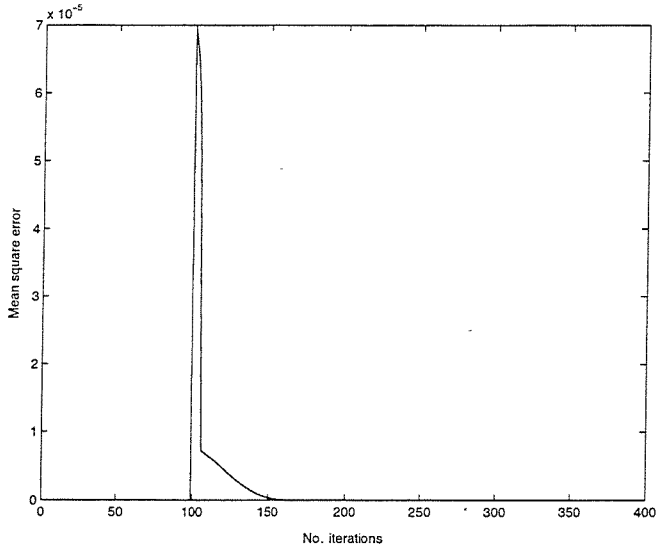

Figure 8.8: Convergence behaviour of the parametric mean square error, J

The estimated vent radius, r_{3est}, is shown in Figure 8.9. It can be seen that the estimated radius adapted quickly and smoothly to the correct solution in about 80 iterations after the change in the actual feedback path. The final estimated value of r_{3est} was 4.189 mm, which compared well with the actual value, $r_{fb2} = 4.176$ mm.

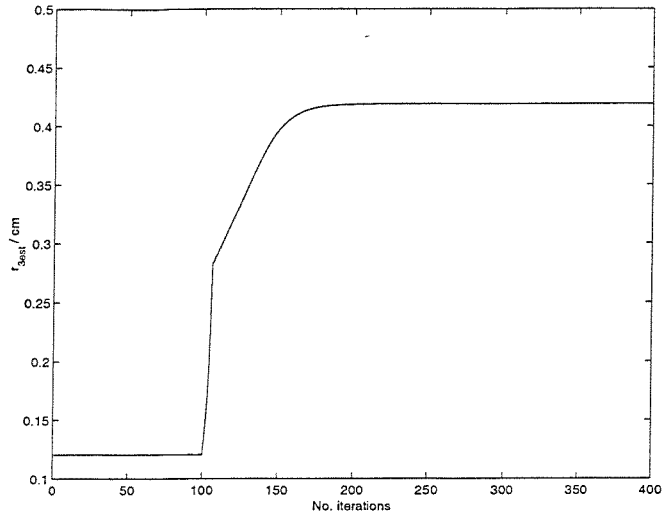

Figure 8.9: Convergence behaviour of the estimated vent radius, r_{3est}

The estimated vent length, L_{3est}, is shown in Figure 8.10. Initially, the length adapted in the wrong direction, i.e. towards a shorter length, before recovering to converge to the correct solution about 100 iterations after the change in the actual feedback path. The final estimated value of L_{3est} was 1.7055 cm, which compared well with the actual value, L_{fb2} = 1.7 cm. The initial adaptation in the wrong direction was a consequence of the irregular shape of the error surface. This is explained by examining the gradient of the error surface with respect to both parameters and by examining the progress of the algorithm over the error surface.

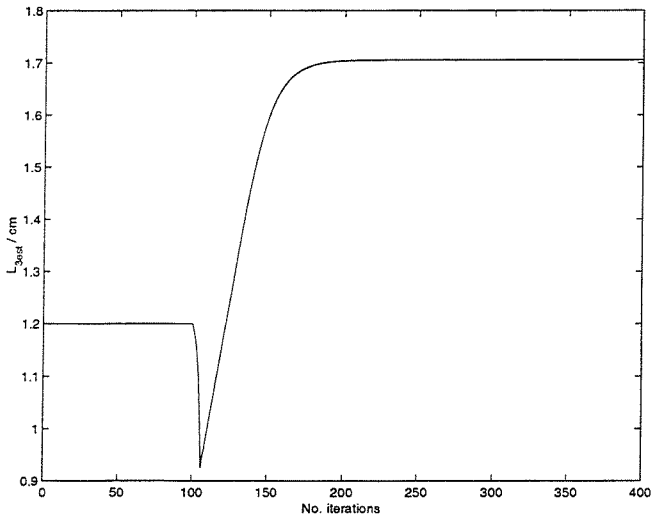

Figure 8.10: Convergence behaviour of the estimated vent length, L_{3est}

The estimated gradient of the error surface with respect to the vent radius exhibited a large step to a negative value, then returned rapidly towards zero, indicating that the steepest descent PAA took a large step towards the minimum of the error surface, then ceased to adapt once the minimum had been reached (Figure 8.11).

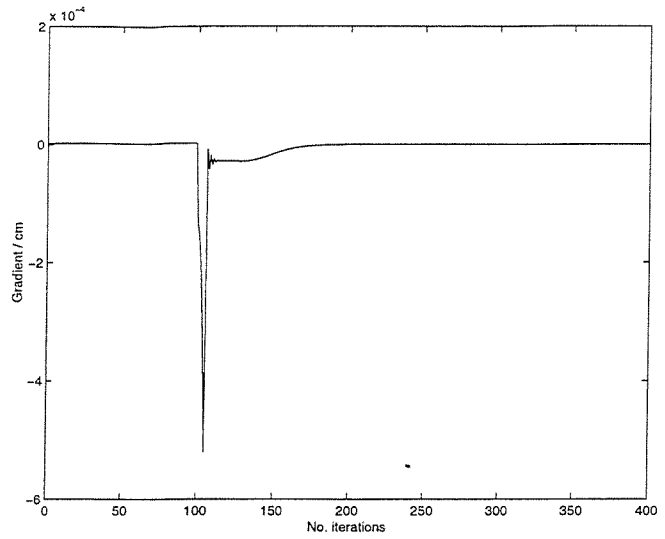

Figure 8.11: Convergence behaviour of the gradient of the error surface with respect to the vent radius, r_{3est}

The estimated gradient with respect to the vent length exhibited a large step to a positive value, initially, causing the estimated vent length to move away from the correct solution. This was followed by a large step back to negative gradient and subsequent return towards zero gradient as the algorithm converged (Figure 8.12).

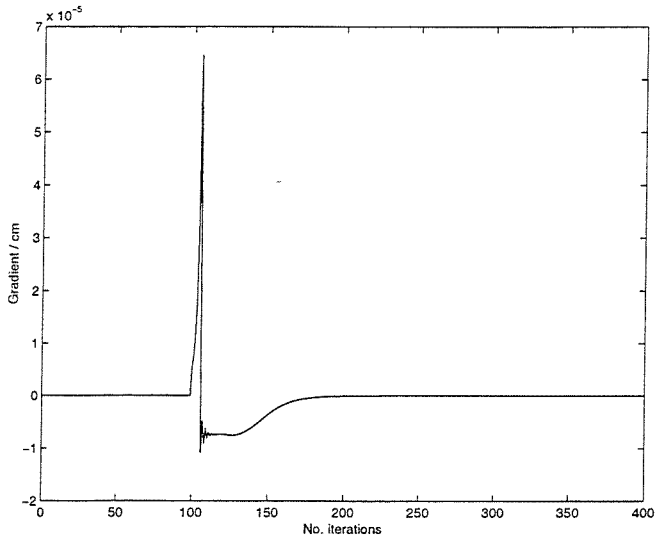

Figure 8.12: Convergence behaviour of the gradient of the error surface with respect to the vent length, L_{3est}

The contour plot in Figure 8.13 shows the adaptation of the steepest descent PAA over the error surface shown in Figure 6.11. The parametric m.s.e., given by Equation (8.3), is plotted as the thick line on the contour plot. The dot marks the starting point of the adaptation, r_{fb1} = 1.204 mm and L_{fb1} = 1.2 cm. The cross marks the end point of the adaptation, r_{fb2} = 4.176 mm

and L_{fb2} = 1.7 cm. It can be seen that the algorithm adapted quickly in the direction of increasing radius, at the same time moving towards shorter length, i.e. adapting the radius in the right direction pulled the length estimate *away* from the minimum temporarily. This is contrary to the behaviour of the LMS algorithm, which would adapt towards the minimum of the error surface directly by the shortest route. Once the parametric algorithm had taken fast steps towards the correct value of r_{fb2}, it adapted more slowly in the direction of the actual length, L_{fb2}.

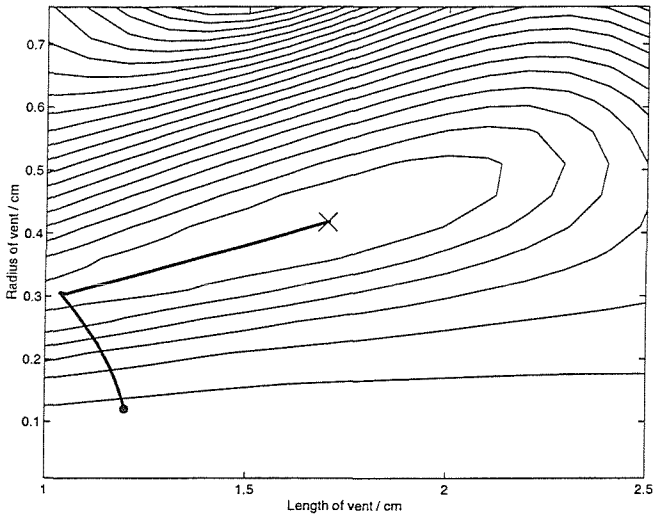

Figure 8.13: Contour plot showing adaptation of the parametric adaptive algorithm towards the minimum of the error surface

The normalised m.s.e., defined by Equation (8.6), where $\mathbf{p}_{est} = (r_{3est}, L_{3est})$ in this example, decreased rapidly after the change in the actual feedback path to reach a constant value (Figure 8.14), although the level was not as low as that reached by the LMS_{sd} algorithm. However, a level of –50 dB is sufficiently small for the algorithm to be regarded as converged. A slight dip in the m.s.e. occurred just before the constant estimated radius was reached and was due to the gradients with respect to each parameter being small but non-zero at this point, i.e. the gradients were only estimated and caused the algorithm to overshoot the true minimum slightly. The error surface was shallow around the minimum, so the algorithm did not return to the minimum after overshooting. The values of r_{3est} and L_{3est} were not in exact agreement with the true values r_{fb2} and L_{fb2}, so the final m.s.e. was slightly above its minimum level. This effect is due to the irregular, non-convex shape of the error surface.

$$J_{norm} = \left\| \frac{(F(f) - M(f, \mathbf{p}_{est}))}{F(f)} \right\|_2^2 \qquad (8.6)$$

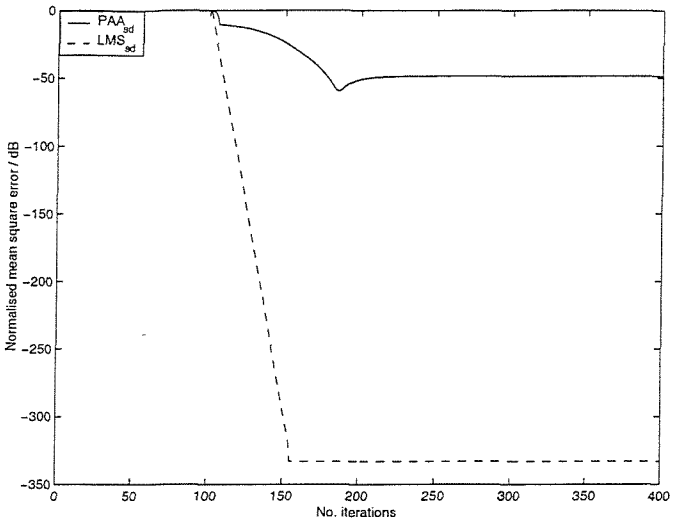

Figure 8.14: Convergence behaviour of the normalised mean square error with white noise, comparing the steepest descent LMS and parametric adaptive algorithms

The convergence of the steepest descent PAA was slower than that of the LMS_{sd} algorithm in this example, but this is because the LMS_{sd} algorithm behaves as Newton's method when a white noise input signal is used and so has an advantage over the PAA_{sd}.

8.4 Performance of the steepest descent algorithms with two varying parameters and a speech-shaped noise input signal

The simulations presented in this section use the same initial and final actual feedback path responses as in the previous section, defined by Tables 8.1 and 8.2. The input signal was produced by filtering white noise with the speech-shaped filter described in Section 8.2.

The LMS_{sd} algorithm was simulated for a total of 400 iterations as before. The increased amplitude of the m.s.e. caused by the speech-shaping filter required the LMS_{sd} convergence coefficient to be changed to 1×10^{-6}. After the final iteration, the LMS_{sd} response was not in agreement with the final actual feedback path response at frequencies below about 250 Hz and above 6 kHz. Agreement was still not close at frequencies above 8 kHz after a total of 1000 iterations (Figure 8.15).

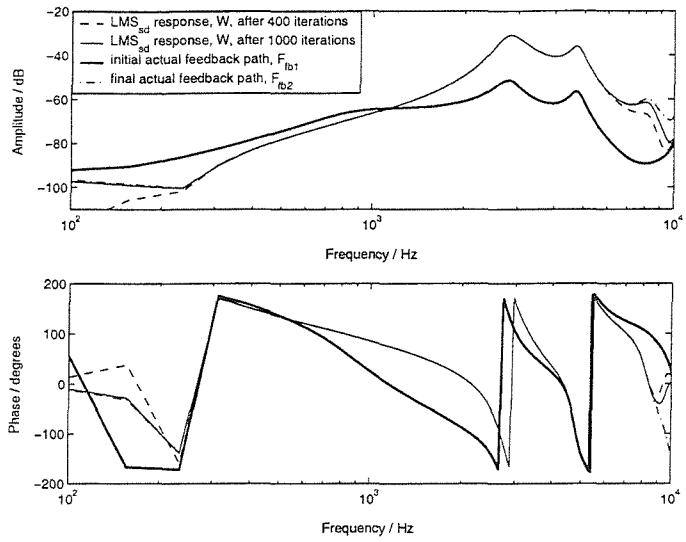

Figure 8.15: Comparison of the LMS_{sd} response after 400 and 1000 iterations with the initial and final actual feedback path responses

The m.s.e. converged close to zero about 150 iterations after the change in the feedback path (Figure 8.16); this is 30 times slower than the example with white noise and $\alpha = 0.5$.

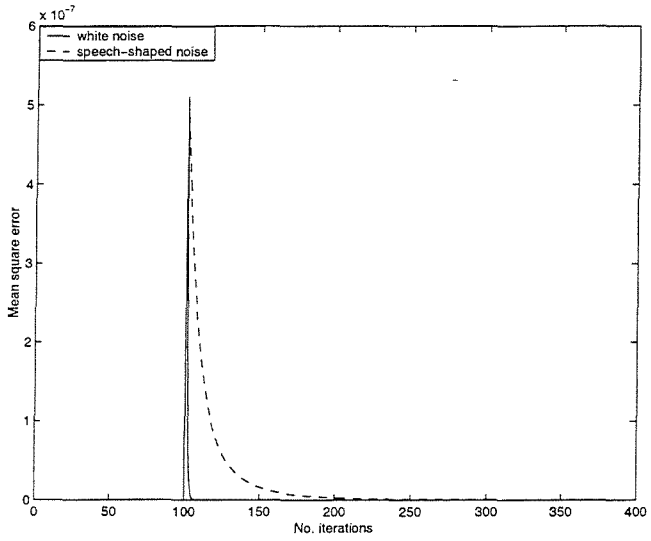

Figure 8.16: Convergence behaviour of the LMS_{sd} mean square error with white noise and speech-shaped noise

The normalised m.s.e. fell at a slower rate than with white noise, and did not reach as low a level as before (Figure 8.17).

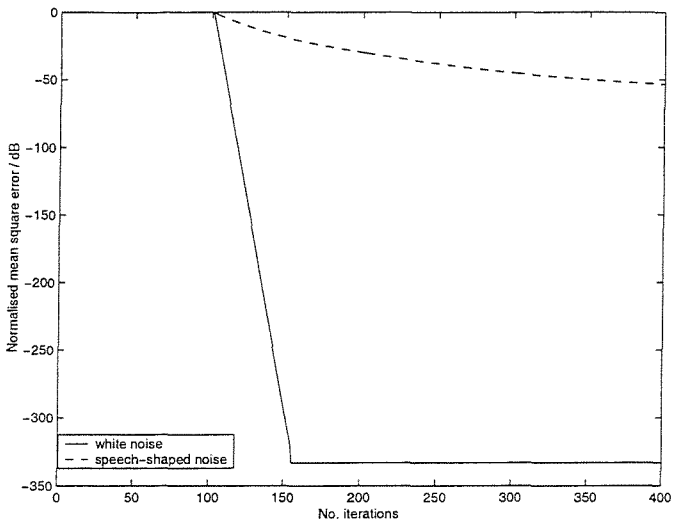

Figure 8.17: Normalised mean square error for the LMS_{sd} algorithm with white noise and speech-shaped noise

Therefore it is clear that the convergence of the LMS_{sd} algorithm is slowed down significantly in the presence of speech-shaped noise compared to its performance in the presence of white noise. This is because, for the LMS algorithm, the error surface is circular for white noise and the LMS_{sd} algorithm adapts quickly to the minimum in the same way as Newton's method (Widrow and Stearns, 1985). With speech-shaped noise, the error surface is non-circular. This introduces slow modes of convergence and reduces the overall rate of convergence of the LMS_{sd} algorithm.

The steepest descent PAA was simulated for the speech-shaped noise condition using the initial parameter values and convergence coefficients given in Table 8.4. The values of the convergence coefficients were changed to compensate for the increase in the amplitude of the error and hence in the estimated gradient due to the increased amplitude of the speech-shaped noise signal compared to the white noise signal. These values were found empirically.

Parameter	*Symbol*	*Convergence coefficient*	*Initial value*	*Estimated final value*	*Actual final value*
Vent radius	r_3	$\alpha_{r3} = 0.001$	1.204 mm	4.189 mm	4.176 mm
Vent length	L_3	$\alpha_{L3} = 0.02$	1.2 cm	1.7055 cm	1.7 cm

Table 8.4: Convergence coefficients and values for the varying vent radius and vent length in the steepest descent PAA with a speech-shaped noise input signal

The estimated feedback path response was in very good agreement with the final actual feedback path after a total of 400 iterations, i.e. 300 iterations after the change in the feedback

path (Figure 8.18), and the final estimated parameters were the same as those obtained in Section 8.3. This shows that the performance of the algorithm is the same as that observed with white noise.

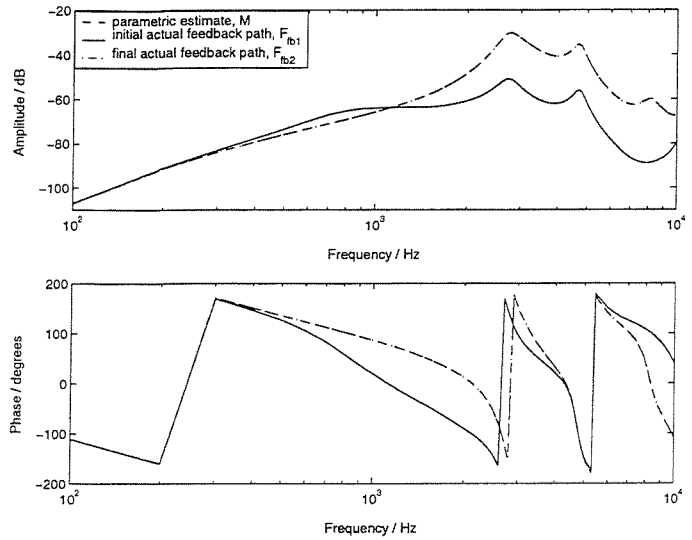

Figure 8.18: Comparison of the parametric response with the initial and final actual feedback path responses

The estimated vent radius, r_{3est}, is shown in Figure 8.19. It can be seen that the convergence behaviour is identical to that in the previous example, i.e. the nature of the input signal has no effect on the rate of convergence of the parametric adaptive algorithm. The same is observed for the estimated vent length, L_{3est} (Figure 8.20).

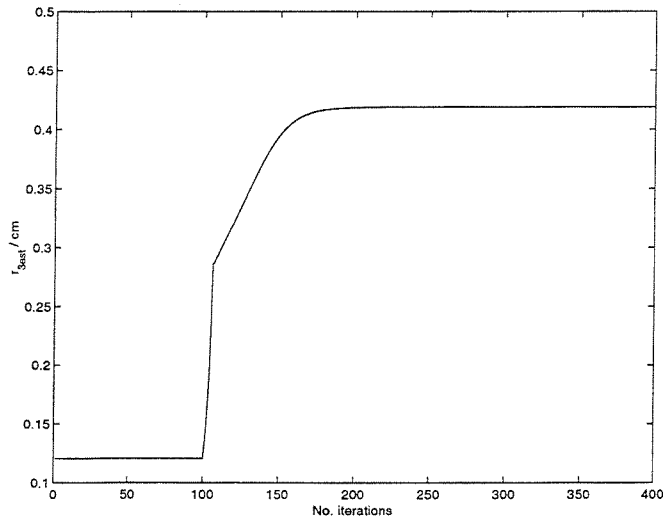

Figure 8.19: Convergence behaviour of the estimated vent radius, r_{3est}

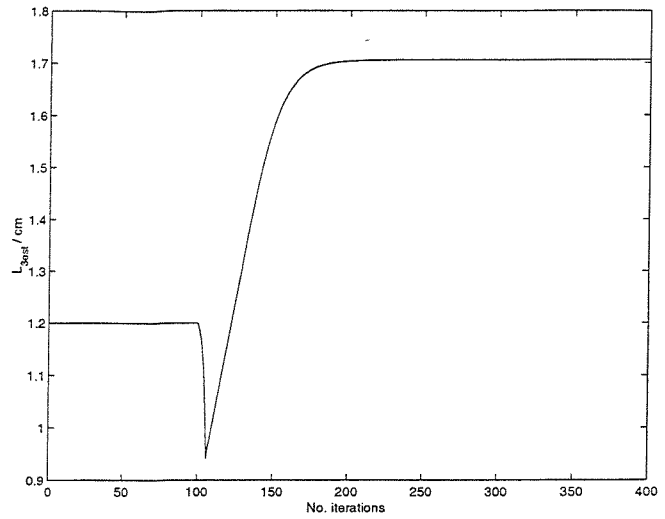

Figure 8.20: Convergence behaviour of the estimated vent length, L_{3est}

The estimated gradient of the error surface with respect to the vent radius (Figure 8.21) behaved in the same way as in the previous example (Figure 8.11), but the numerical value of the gradient differed due to the change in the amplitude of the error signal caused by the speech-shaping filter.

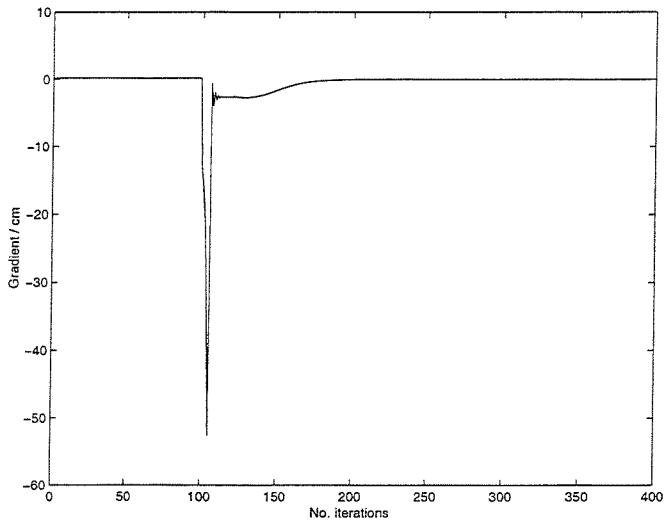

Figure 8.21: Convergence behaviour of the gradient of the error surface with respect to the vent radius, r_3

The normalised m.s.e. obtained with speech-shaped noise behaved in the same way as with white noise, though the dip before the constant level was reached was deeper (Figure 8.22). The PAA_{sd} m.s.e. decreased more quickly initially that that of the LMS_{sd} algorithm before reaching the constant level.

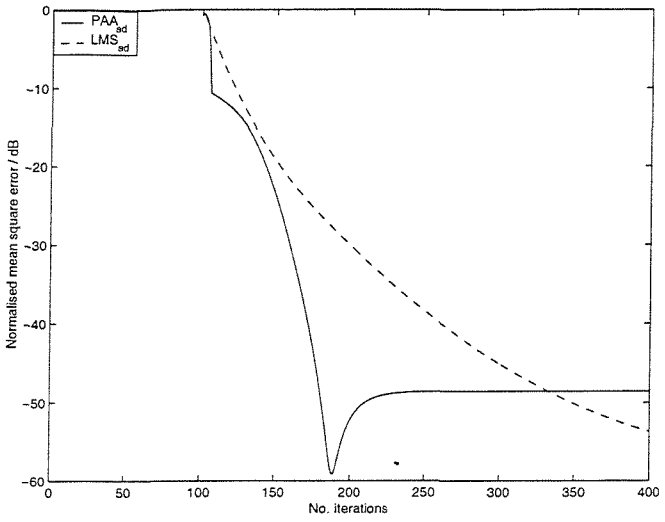

Figure 8.22: Convergence behaviour of the normalised mean square error with speech-shaped noise, comparing the steepest descent LMS and parametric adaptive algorithms

Therefore the convergence of the steepest descent PAA is independent of the nature of the input signal, whereas the LMS_{sd} algorithm is slowed down significantly by speech-shaped noise compared to its performance with white noise.

8.5 Performance of the steepest descent algorithms with four varying parameters and a speech-shaped noise input signal

It is unlikely that only two parameters will vary in a real hearing aid system. A more realistic model had four parameters varying simultaneously: the ear canal length, the vent radius and length and the length of the external acoustic feedback path. This was a simplified representation of the hearing aid moving in the ear canal, causing an increase in sound leakage.

The initial and final values of the varying parameters in the actual feedback path are given in Table 8.5. The constant parameter values are given in Table 8.1 as before.

Parameter	*Symbol*	*Initial value*	*Final value*
Ear canal length	L_2	1.2 cm	1.5 cm
Vent radius	r_3	1.204 mm	4.176 mm
Vent length	L_3	1.2 cm	1.7 cm
External acoustic feedback path length	R	1.0 cm	2.0 cm

Table 8.5: Initial and final values of the varying ear canal length, vent radius, vent length and external acoustic feedback path length used in the actual feedback path, F

The LMS_{sd} algorithm was simulated for a total of 1000 iterations as before with α_{LMS} = 1 x 10^{-6}. The estimated feedback path response was not in very close agreement with the actual final response below about 250 Hz and above 6 kHz after a total of 400 iterations, i.e. 300 iterations after the change in the feedback path, and above about 8 kHz after a total of 1000 iterations (Figure 8.23). This behaviour was the same as that obtained using an actual feedback path with two varying parameters.

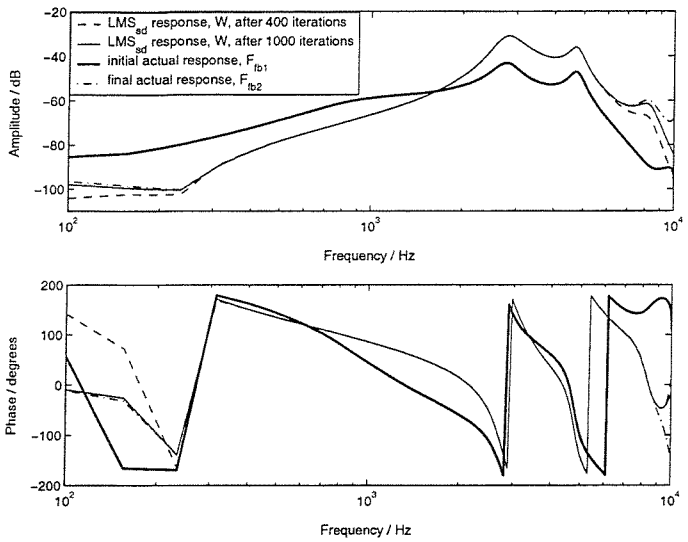

Figure 8.23: Comparison of the LMS_{sd} response after 400 and 1000 iterations with the initial and final actual feedback path responses

The m.s.e. converged at the same rate as with two varying parameters, although the amplitude differed due to the change in amplitude of the feedback path caused by the change in the physical parameter values (Figure 8.24).

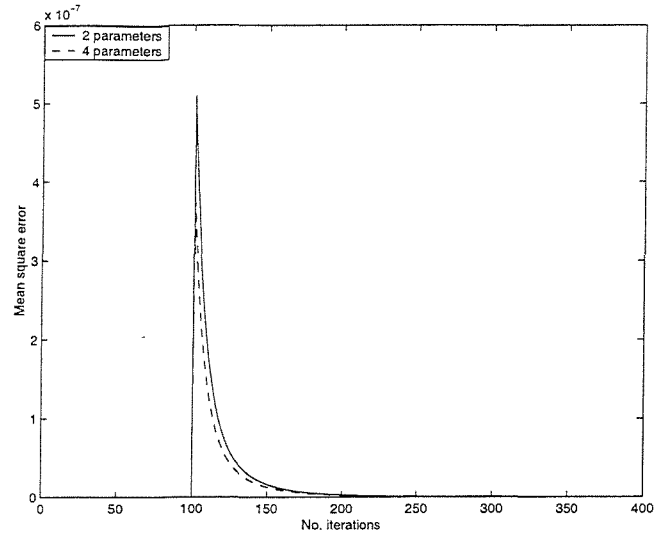

Figure 8.24: Convergence behaviour of the LMS_{sd} mean square error with two and four varying parameters

The normalised m.s.e. decreased in a similar way to that in the two-parameter simulation (Figure 8.25).

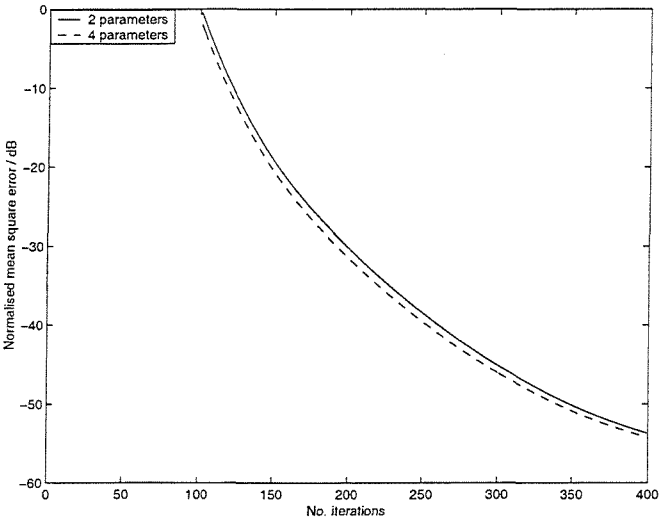

Figure 8.25: Normalised mean square error for the LMS_{sd} algorithm, with two and four varying parameters

Therefore the convergence behaviour of the steepest descent LMS algorithm is unaffected by the number of varied physical parameters. This is to be expected, since the LMS algorithm is independent of the parameters within the hearing aid system and depends only on the response of the actual feedback path.

The steepest descent PAA (PAA_{sd}) was simulated with four varying parameters. The initial values and convergence coefficients are given in Table 8.6. Again, these coefficients were chosen empirically to give the best balance between convergence speed and misadjustment. After a total of 1200 iterations, i.e. 1100 iterations after the change in the actual feedback path, the estimated feedback path response was in very close agreement with the final actual feedback path (Figure 8.26). The estimated parameter values after 1200 iterations are given in Table 8.6. The increase in the number of iterations required for convergence was due to the dependence of the algorithm on the physical parameters in the hearing aid system. The number of modes of convergence increased as more parameters were varied, slowing down the adaptation.

Parameter	*Symbol*	*Convergence coefficient*	*Initial value*	*Estimated final value*	*Actual final value*
Ear canal length	L_2	$\alpha_{L2} = 0.02$	1.2 cm	1.5393 cm	1.5 cm
Vent radius	r_3	$\alpha_{r3} = 0.001$	1.204 mm	4.334 mm	4.176 mm
Vent length	L_3	$\alpha_{L3} = 0.005$	1.2 cm	1.7247 cm	1.7 cm
External acoustic feedback path length	R	$\alpha_R = 0.01$	1.0 cm	2.0329 cm	2.0 cm

Table 8.6: Convergence coefficients and values for the varying ear canal length, vent radius, vent length and external acoustic feedback path length in the steepest descent PAA with a speech-shaped noise input signal

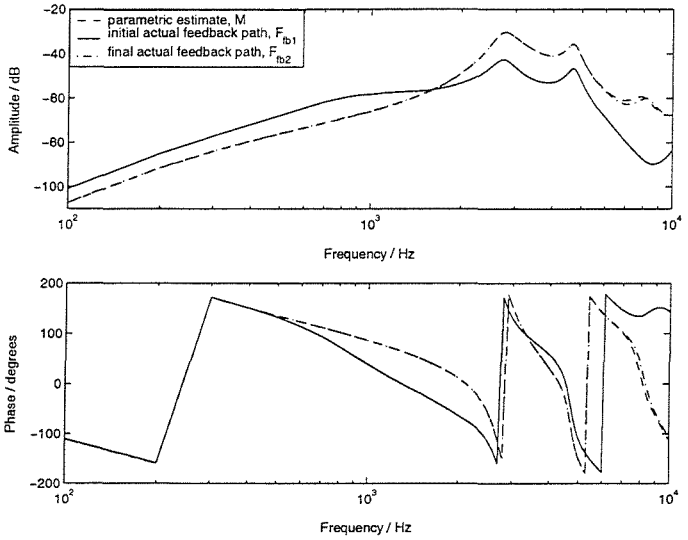

Figure 8.26: Comparison of the parametric response with the initial and final actual feedback path responses

The mean square error, J, between the modelled and actual feedback path responses is defined by Equation (8.3), with $\mathbf{p}_{est} = (L_{2est}, r_{3est}, L_{3est}, R_{est})$, and is shown in Figure 8.27. The m.s.e. decreased close to zero about 300 iterations after the change in the actual feedback path. Initially, the m.s.e. was noisy as the algorithm suffered from fluctuation through estimating four parameters simultaneously; it was shown in Chapter 7 that the effects of changing a particular parameter may be similar to those produced by changing another parameter and this may affect the ability of the PAA to track such changes. The irregular nature of the error surface means that a step towards the minimum for one parameter may cause the other parameters to move away from the minimum temporarily as shown in Section 8.3. In consequence, the algorithm requires more iterations to recover from this action. It should be noted that an alternative method updating one parameter at a time in blocks of 50 – 200 iterations prevented the PAA reaching good agreement with the actual feedback path response and returned estimated parameter values that were not close to the true values. It is not known why this method was unsuccessful. It may be that adapting only a single parameter at a time prevented the algorithm compensating for the bias caused as the estimate moves away from the minimum of the error surface in the direction of negative gradient for one parameter, which may not be in the direction of negative gradient with respect to the other parameters.

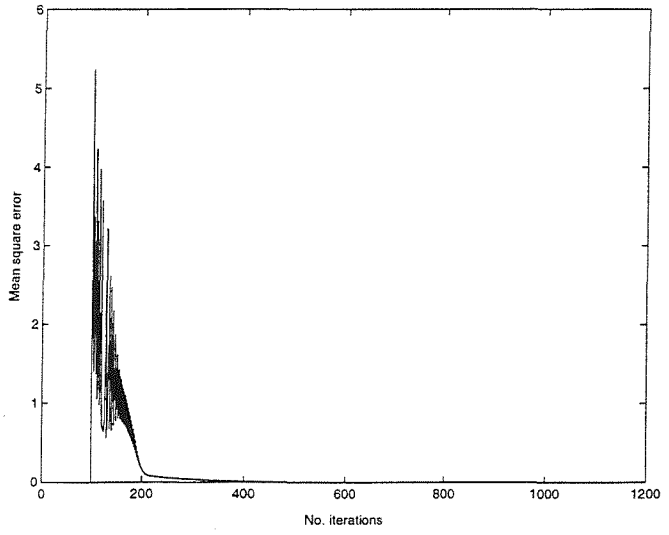

Figure 8.27: Convergence behaviour of the parametric mean square error, J

The estimated ear canal length, L_{2est}, is shown in Figure 8.28. It can be seen that initially the algorithm adapted in the wrong direction and L_{2est} suffered from fluctuation for the first 125 iterations after the change in the actual feedback path. Subsequently, the length adapted towards the correct values, with the convergence slowing down as the algorithm approached the minimum.

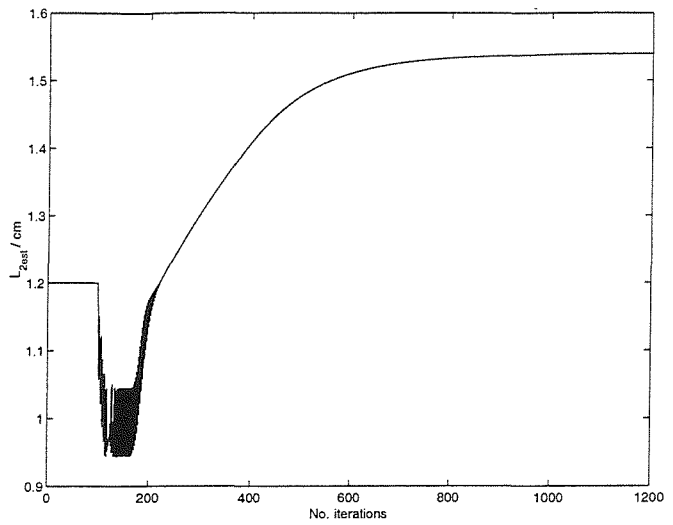

Figure 8.28: Convergence behaviour of the estimated ear canal length, L_{2est}

The estimated vent radius r_{3est} adapted in a similar way, with slight fluctuation for the first 125 iterations after the change in the actual feedback path, followed by smooth convergence which slowed down as the correct value was approached (Figure 8.29). This behaviour was also observed for the vent length L_{3est} (Figure 8.30) and the external acoustic feedback path length R_{est} (Figure 8.31). The amount of fluctuation differed for each parameter, since the contribution of each parameter to changes in the feedback path was not equal (see Section 7.12) and changing a particular parameter may cause more severe fluctuation in some parameters than others as the algorithm moves over the error surface.

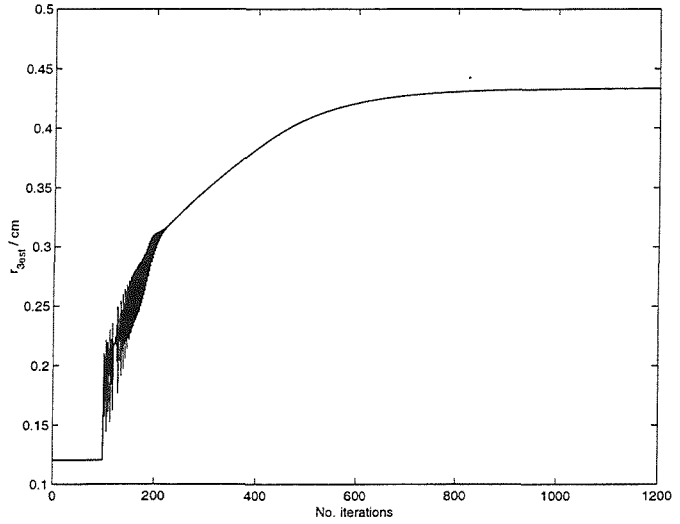

Figure 8.29: Convergence behaviour of the estimated vent radius, r_{3est}

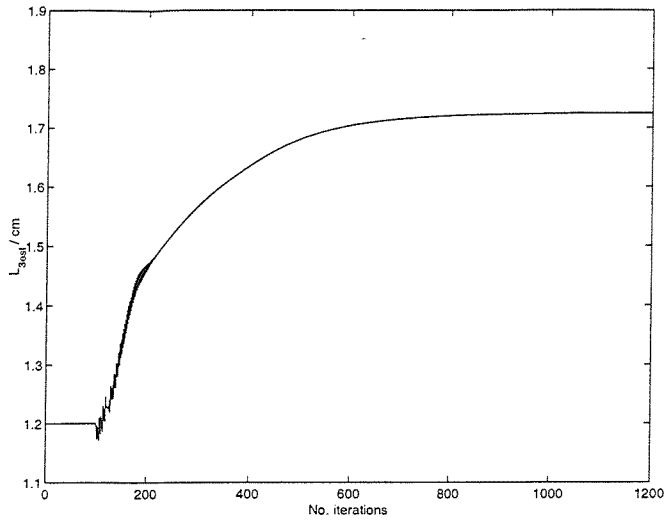

Figure 8.30: Convergence behaviour of the estimated vent length, L_{3est}

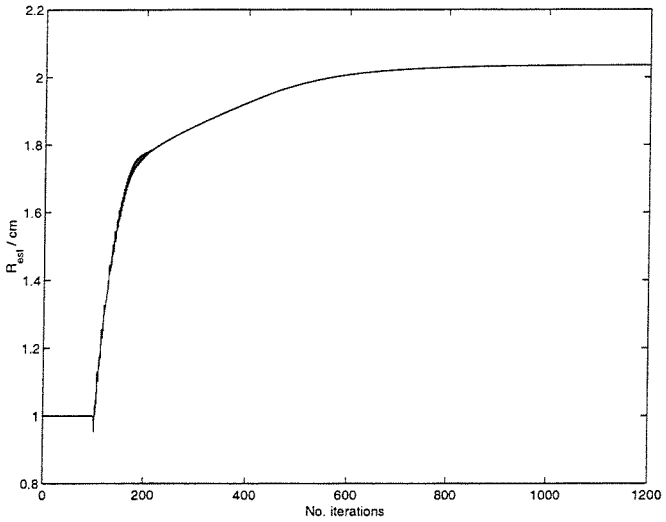

Figure 8.31: Convergence behaviour of the estimated external acoustic feedback path length, R_{est}

The estimated gradient behaved in the same way for each estimated parameter: large amplitude with severe fluctuation for the first 125 iterations after the change in the actual feedback path, followed by a great reduction in amplitude. This is illustrated by the estimated gradient with respect to the ear canal length (Figure 8.32). The convergence coefficients for each parameter were chosen to give smooth convergence after the period of fluctuation. The step size $|\alpha\nabla|$ was limited to 1 mm for each parameter to prevent the fluctuation causing extreme changes in the estimated parameters (see Section 7.10).

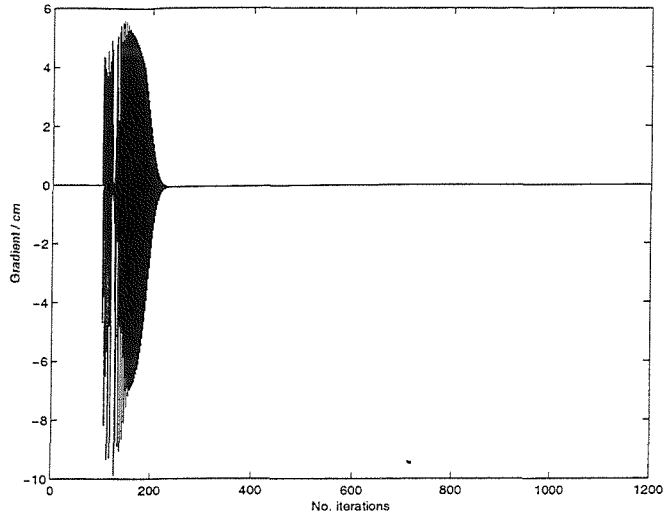

Figure 8.32: Convergence behaviour of the gradient of the error surface with respect to the ear canal length, L_2

The normalised m.s.e. exhibited fluctuation effects for the first 125 iterations after the change in the feedback path, as expected. The m.s.e. decreased smoothly, without the dip observed in the simulation with two varying parameters (Figure 8.33). This indicated that the convergence coefficients had been well chosen to give steady progress over the error surface with minimal fluctuation. The normalised m.s.e. fell to an approximately constant level of – 58 dB about 900 iterations after the change in the feedback path.

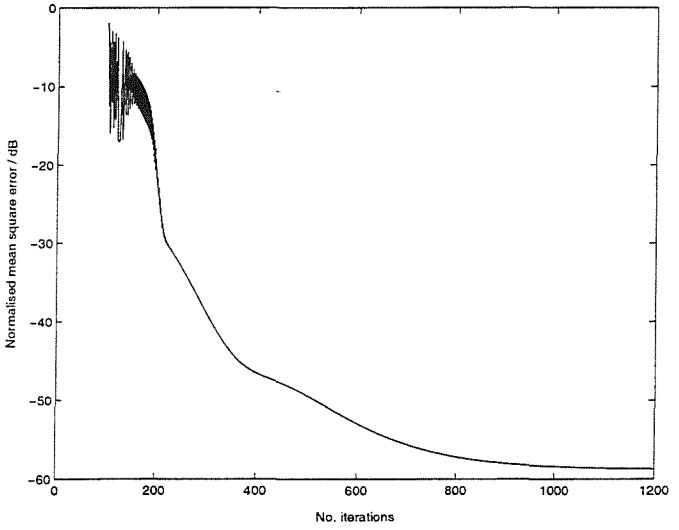

Figure 8.33: Convergence behaviour of the normalised mean square error with speech-shaped noise for the steepest descent parametric adaptive algorithm

Comparing the normalised m.s.e. of the PAA_{sd} with that of the LMS_{sd} algorithm over the first 400 iterations (Figure 8.34), it can be seen that initially the parametric m.s.e decreases faster

than that of the LMS_{sd}, but fluctuates severely for 100 iterations after the change in the feedback path. After this point, the normalised m.s.e. decreases at a similar rate for both algorithms.

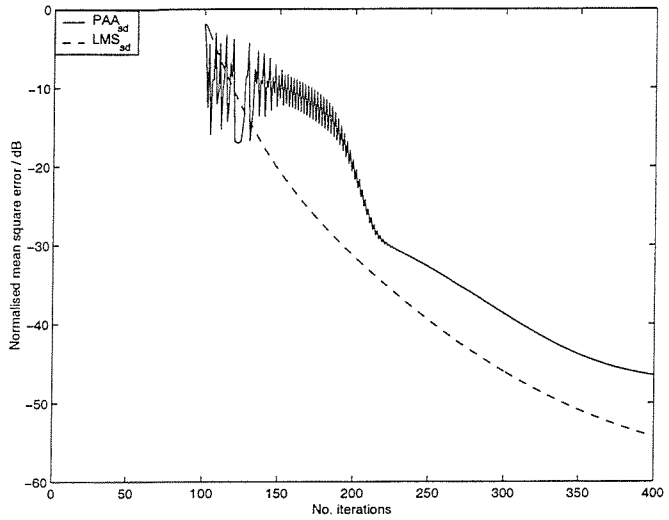

Figure 8.34: Convergence behaviour the normalised mean square error for both algorithms over the first 400 iterations

Therefore the convergence of the steepest descent parametric adaptive algorithm is slowed down significantly as the number of simultaneously varied parameters increases. The mean square error decreased close to zero about 300 iterations after the change in the actual feedback path compared with 150 iterations for the steepest descent LMS algorithm. It is likely that the number of iterations required for convergence will increase further as the number of varying parameters increases. Care must be taken to obtain convergence coefficients that give the optimum speed of convergence without increasing the fluctuation to a level that degrades the estimates of the parameter values.

These results indicate that the convergence speed of both algorithms is of the same order when the PAA_{sd} has four varying parameters.

8.6 Performance of the stochastic gradient algorithms with four varying parameters and a speech-shaped noise input signal

A practical feedback cancellation system has no prior knowledge of the feedback path, so the steepest descent methods cannot be used. In this section, the stochastic gradient algorithms used FIR filters to represent the modelled and actual feedback path responses, M and F. The filter length and sampling frequency are given in Table 8.1 along with the constant parameter

values in the model. The initial and final parameter values in the actual feedback path are given in Table 8.5 in the previous section.

The use of stochastic signals will greatly increase the number of iterations required for convergence for both algorithms due to the random nature of the estimated gradient, and the irregularity of the error surface will also slow down the PAA as described previously. The parametric adaptive and NLMS algorithms were simulated for a total of 16 000 iterations. The NLMS algorithm was implemented as given in Section 1.5, Equations (1.14) – (1.17), with α_0 = 0.5. The convergence coefficients and initial and estimated final parameter values for the PAA are given in Table 8.7. The responses obtained after 16 000 iterations are shown in Figure 8.35. The NLMS response was in good agreement with the actual response between 200 Hz and 7 kHz, while the parametric estimate was in good agreement between 300 Hz and about 5.5 kHz.

Parameter	*Symbol*	*Convergence coefficient*	*Initial value*	*Estimated final value*	*Actual final value*
Ear canal length	L_2	$\alpha_{L2} = 0.02$	1.2 cm	1.6605 cm	1.5 cm
Vent radius	r_3	$\alpha_{r3} = 0.001$	1.204 mm	4.831 mm	4.176 mm
Vent length	L_3	$\alpha_{L3} = 0.005$	1.2 cm	1.8037 cm	1.7 cm
External acoustic feedback path length	R	$\alpha_R = 0.01$	1.0 cm	2.1160 cm	2.0 cm

Table 8.7: Convergence coefficients and values for the varying ear canal length, vent radius, vent length and external acoustic feedback path length in the stochastic gradient PAA with a speech-shaped noise input signal

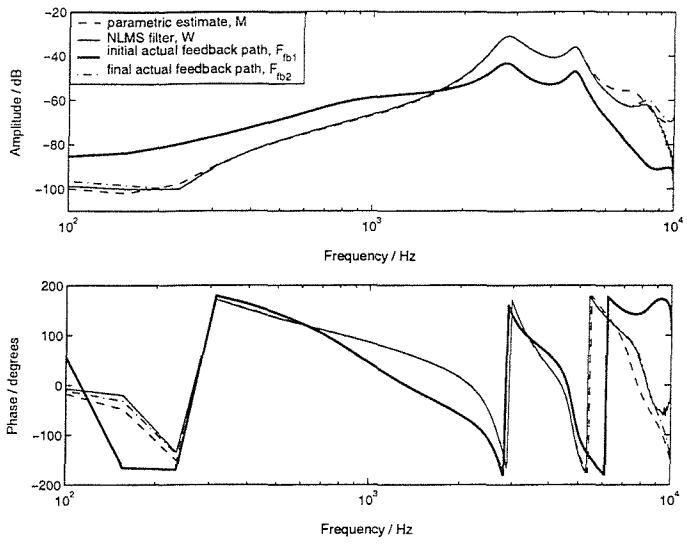

Figure 8.35: Comparison of the parametric and NLMS responses with those of the initial and final actual feedback paths

The error signal, $e = d - y$, converged for both algorithms, but the parametric error e_{est} exhibited greater bursting, probably due to a combination of the stochastic nature of the input signal and the misadjustment caused by varying four physical parameters simultaneously (Figure 8.36). It could be seen that the parametric error reached a minimum amplitude about 6000 iterations after the change in the actual feedback path before increasing. This indicated that the misadjustment was large enough to cause the algorithm to move away significantly from the minimum of the error surface. The NLMS error e_{NLMS} remained small after convergence, indicating that the algorithm had reached the minimum of the error surface successfully.

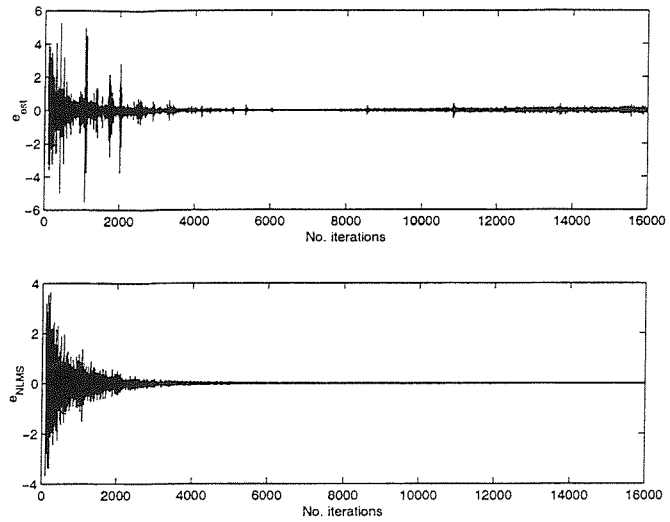

Figure 8.36: Convergence behaviour of the parametric and NLMS error signals, e_{est} and e_{NLMS}

Examining the convergence behaviour of the estimated physical parameters in the PAA, it can be seen that the overall behaviour was similar to that observed for the steepest descent PAA: greater misadjustment initially, followed by a stage of fast convergence, then slower convergence with less misadjustment (Figures 8.37 – 8.40). The effects of the stochastic input signal combined with the irregular shape of the error surface caused an increase in misadjustment which greatly reduced the ability of the parametric algorithm to converge rapidly to the correct solution. The estimated parameter values after 16 000 iterations (Table 8.7) show that the PAA overshot the actual values slightly.

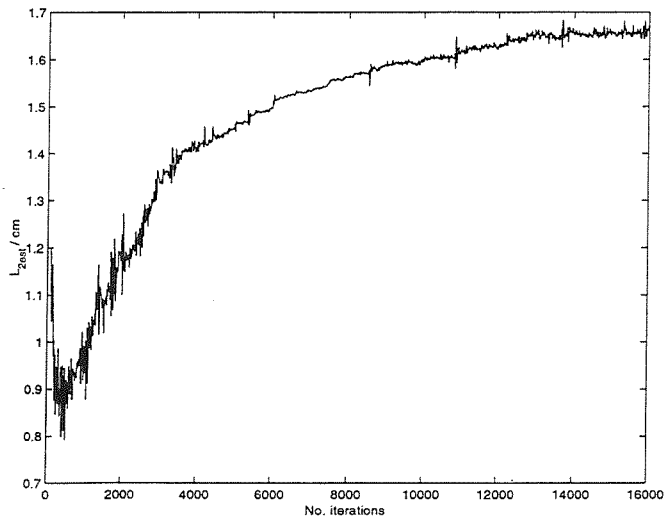

Figure 8.37: Convergence behaviour of the estimated ear canal length, L_{2est}

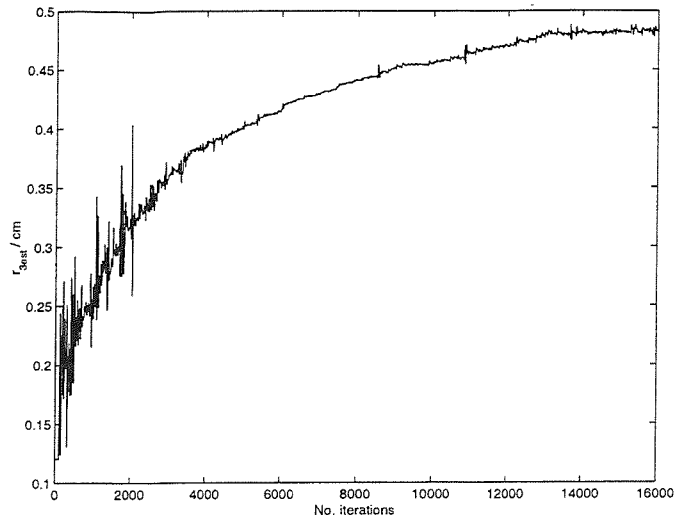

Figure 8.38: Convergence behaviour of the estimated vent radius, r_{3est}

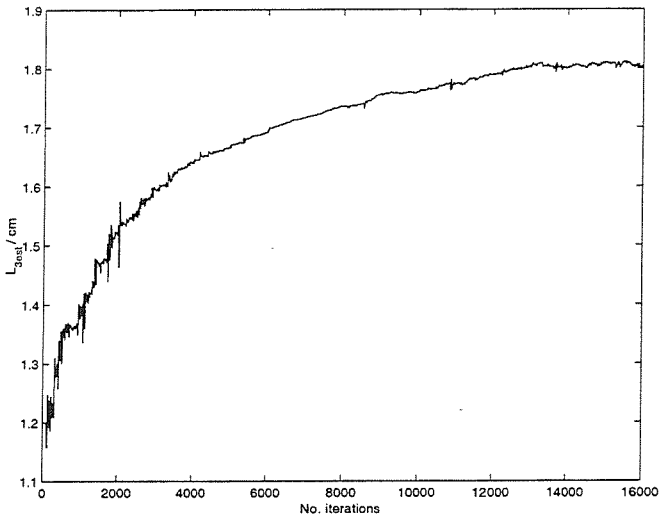

Figure 8.39: Convergence behaviour of the estimated vent length, L_{3est}

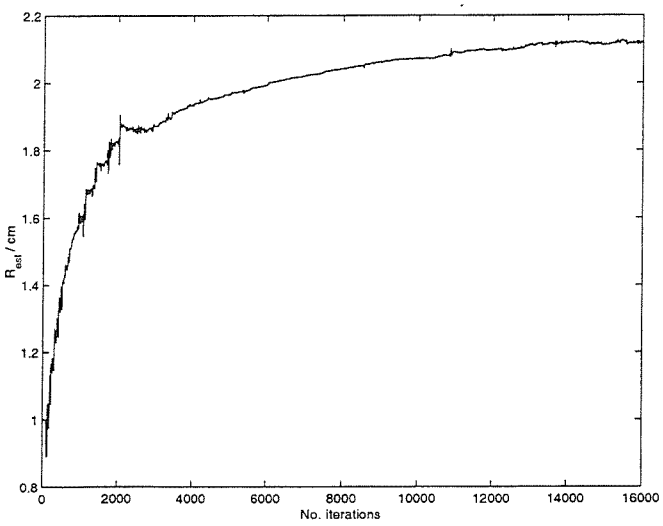

Figure 8.40: Convergence behaviour of the estimated external acoustic feedback path length, R_{est}

The large amount of fluctuation in the estimated gradient with respect to each parameter is illustrated by the gradient with respect to the ear canal length (Figure 8.41). It is clear that such a gradient will cause the algorithm to move over the error surface erratically. As before, the step size $|\alpha_p \nabla_p|$ was limited to 1 mm for each parameter p to limit the amount of misadjustment transmitted to the estimated parameters (see Section 7.10).

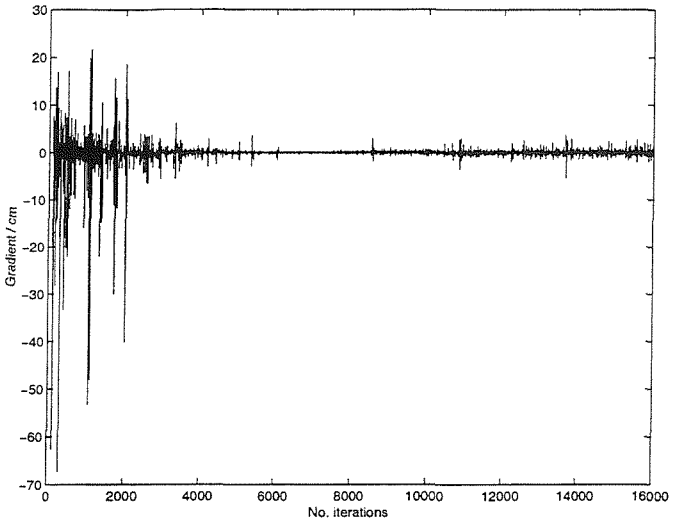

Figure 8.41: Convergence behaviour of the gradient of the error surface with respect to the ear canal length, L_2

The normalised m.s.e., defined by Equation (8.6) for the PAA and by $\|(F - W) / F\|_2^2$ for the NLMS algorithm, decreased smoothly for the NLMS algorithm, but exhibited severe misadjustment effects for the PAA (Figure 8.42).

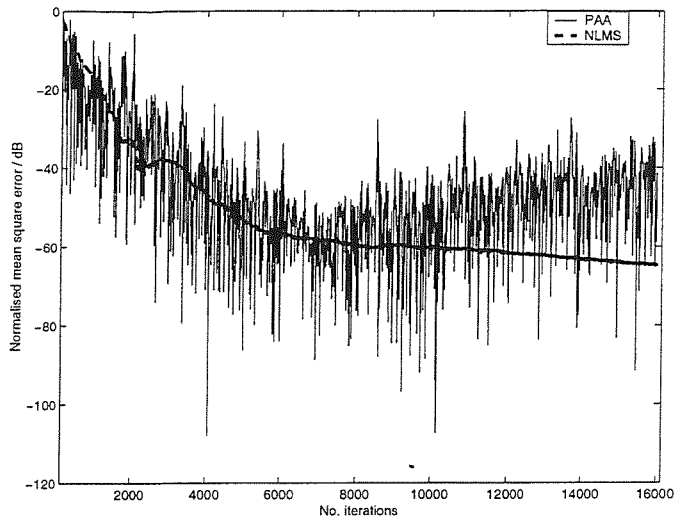

Figure 8.42: Convergence behaviour of the normalised mean square error for the NLMS and parametric algorithms

Examining the normalised m.s.e. over the first 2000 iterations (Figure 8.43), it can be seen that the normalised m.s.e. of the PAA decreased by 20 dB faster than that of the NLMS algorithm, taking about 300 iterations (averaging the fluctuations approximately) while the NLMS algorithm required about 1000 iterations to reach this level. The normalised m.s.e. of the PAA fluctuated considerably throughout the simulation.

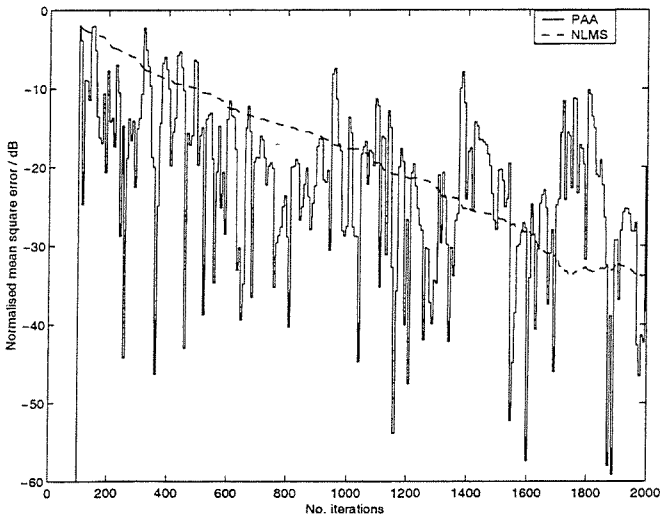

Figure 8.43: Convergence behaviour of the normalised mean square error for the NLMS and parametric algorithms over the first 2000 iterations

However, examining the modelled responses generated by the PAA after 2000, 6000 and 12 000 iterations, it can be seen that although the estimated parameter values continued to adapt, the modelled response remained approximately constant between 300 Hz and 6 kHz (Figure

8.44). The closest agreement with the actual feedback path occurred around the 6000th iteration, as indicated by the parametric error signal (Figure 8.36).

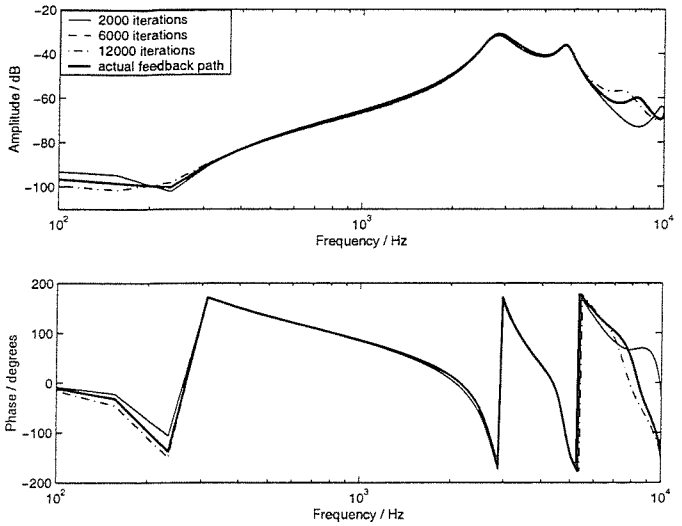

Figure 8.44: Variation over time of the feedback path response estimated by the PAA

Comparing the parametric estimate of the actual feedback path response with that given by the NLMS algorithm after 2000 iterations, it can be seen that the PAA was in closer agreement with the actual response than the NLMS algorithm (Figure 8.45), and so it can be concluded that, with a modelled actual feedback path, the PAA is capable of reaching good agreement with the actual feedback path faster than the NLMS algorithm.

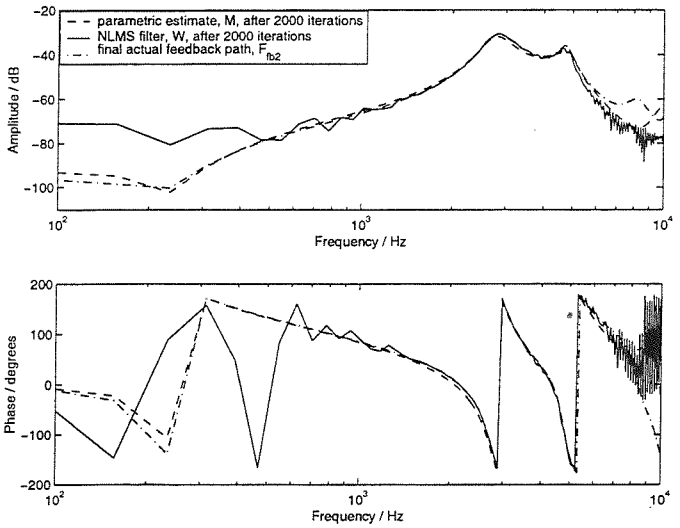

Figure 8.45: Comparison of the parametric and NLMS responses after 2000 iterations with the actual final feedback path

Summarising, the convergence of both algorithms is slowed down considerably when FIR filtering is performed compared to the theoretical steepest descent analysis, as expected. The parametric adaptive algorithm suffers from severe fluctuation as a result of varying several parameters simultaneously. However, the PAA is able to produce a good estimated response in comparatively few iterations that remains approximately constant over much of the frequency range of interest. It is especially important that the estimated response remains very close to the actual response around the high amplitude receiver resonance peaks (near 3 kHz and 5 kHz in this example); instability is most likely to occur at these frequencies and an effective feedback cancellation algorithm must be able to model these peaks accurately in order to cancel them and maintain stability.

8.7 Conclusions

Steepest descent analysis of the LMS and parametric adaptive algorithms found that, although the convergence of the LMS algorithm was unaffected by the number of parameters varied in the modelled actual feedback path, it was slowed down considerably by the presence of a speech-shaped noise signal compared to its performance in the presence of white noise. The performance of the parametric adaptive algorithm was unaffected by the nature of the input signal, but as the number of varying parameters increased, the corresponding increase in fluctuation slowed down convergence significantly. A simulation study using the more realistic stochastic gradient implementation of the algorithms demonstrated that misadjustment became a severe problem for the PAA as the stochastic gradient caused the algorithm to move erratically over the irregular error surface. However, the PAA was capable of reaching its best fit to the actual feedback path response rapidly and was able to maintain this estimated response in the frequency range in which instability was most likely to occur, despite continuing changes in the values of the estimated parameters. With a modelled actual feedback path, the PAA converged to a close estimate of the actual feedback path more quickly than the NLMS algorithm.

9 Simulation studies of the PAA using measured feedback path data

9.1 Introduction

This chapter presents simulation results for the parametric and LMS algorithms, starting from a modelled actual feedback path and changing to a measured feedback path response. Both the steepest descent and stochastic gradient methods are used. It has been shown in Chapter 5 that the analytic model cannot fit measured responses exactly due to limitations in the current form of the model arising from lack of knowledge of the transducers and middle ear impedance and approximations used for the dimensions of the ear canal and the external acoustic feedback path. It is likely that more than four physical parameters must be varied for the parametric adaptive algorithm to track changes in measured feedback paths. Extending the PAA to include more parameters is a topic for future work. The simulation studies presented in this chapter are intended to show whether the present form of the PAA is capable of converging to a solution that approximates the actual measured feedback path response. Both algorithms are initially in agreement with a modelled feedback path response rather than a measured response so that the PAA does not have the disadvantage of not being in exact agreement with the initial actual feedback path.

9.2 Performance of the steepest descent algorithms with a speech-shaped noise input signal

The simulations in this chapter were implemented as described in Section 8.2. Initially, the responses of the steepest descent and LMS algorithms matched that of a modelled feedback path, F_{fb1}, generated with the parameter values in Table 9.1. After 100 iterations, the actual feedback path underwent a step change to the measured feedback path for the right ear of subject BO with the earmould fitted normally, F_{fb2} (Rafaely *et al.*, 2000). The measured response used a Knowles ED-1975 receiver, which was represented in the model with the electrical analogue for the ED-1913 receiver (see Section 3.5). The speech-shaped noise signal was produced as described in Section 8.2.

Component	*Symbols*	*Fixed or varying*	*Value*
Filter length	N	Fixed	128
Frequency	f	Varying	1 Hz – 10 kHz
Sampling frequency	f_s	Fixed	20 kHz
Receiver tube length	L_1	Fixed	1.0050 cm
Receiver tube radius	r_1	Fixed	0.7 mm
Ear canal length	L_2	Varying	1.5029 cm or defined in Sections 9.2 – 9.3
Ear canal radius	r_2	Fixed	1.968 mm
Vent length	L_3	Varying	1.9740 cm or defined in Sections 9.2 – 9.3
Vent radius	r_3	Varying	0.8 mm or defined in Sections 9.2 – 9.3
External acoustic feedback path length	R	Varying	2.3618 cm or defined in Sections 9.2 – 9.3
Microphone two-port network parameters	A_m	Fixed	Modelled using Knowles EM-3046 microphone analogue
Receiver two-port network parameters	A_r, B_r	Fixed	Modelled using Knowles ED-1913 receiver analogue
Middle ear impedance	Z_T	Fixed	Modelled by mean measured data (Shaw, 1974)

Table 9.1: Definition of parameter values used in modelled responses F_{fb1} and M throughout Chapter 9

The steepest descent LMS (LMS_{sd}) algorithm was simulated for a total of 1000 iterations with $\alpha_{LMS} = 1 \times 10^{-6}$. The estimated feedback path response was not in close agreement with the actual final response below about 150 Hz and above 7 kHz after a total of 400 iterations, i.e. 300 iterations after the change in the feedback path, and above about 8 kHz after a total of 1000 iterations (Figure 9.1). This behaviour was similar to that obtained using a modelled actual feedback path with two and four varying parameters (Sections 8.4 – 8.6).

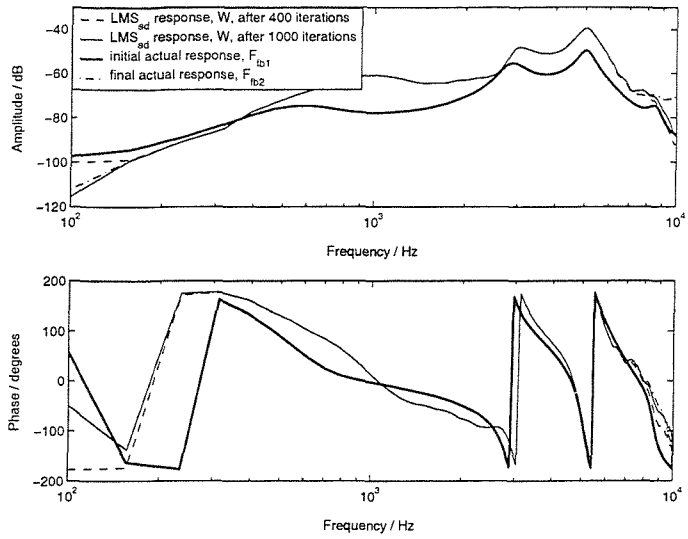

Figure 9.1: Comparison of the LMS_{sd} response after 400 and 1000 iterations with the initial and final actual feedback path responses

The mean square error, $\|\mathbf{w} - \mathbf{f}\|_2^2$, converged slightly more slowly than with the modelled final actual feedback path, taking about 300 iterations after the change in the feedback path (Figure 9.2). Since the performance of the LMS_{sd} algorithm was independent of the way in which the feedback path responses were produced, it is likely that this difference was due to using different initial and final feedback path responses in this simulation to those used in the previous chapter.

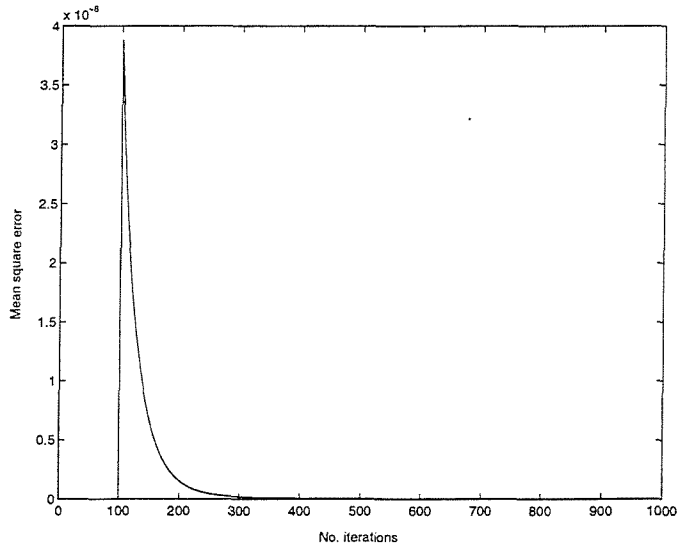

Figure 9.2: Convergence behaviour of the LMS_{sd} mean square error

The normalised m.s.e. of the LMS_{sd} algorithm, calculated as $\|(\mathbf{w} - \mathbf{f}) / \mathbf{f}\|_2^2$, is shown in Figure 9.3. It decreased more slowly than with the modelled actual feedback path, as for the mean square error.

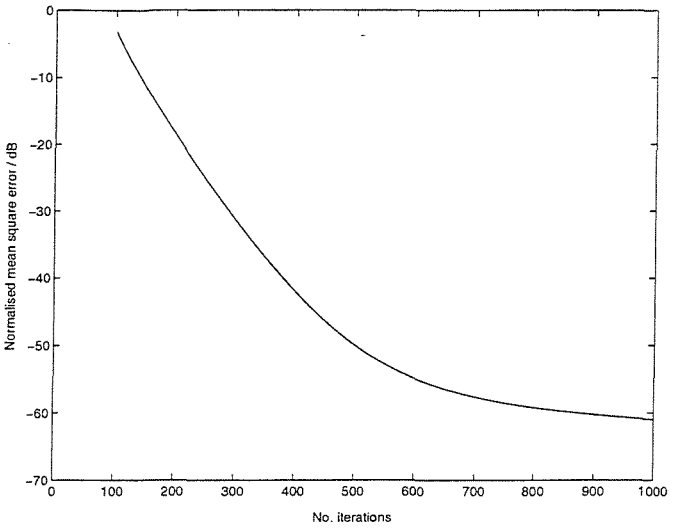

Figure 9.3: Normalised mean square error for the LMS_{sd} algorithm

Therefore the convergence of the steepest descent LMS algorithm with a measured final actual feedback path was slightly slower than that with a modelled feedback path.

The steepest descent PAA was simulated for the same change in the actual feedback path with a speech-shaped noise signal. The initial and final values of the varying parameters and the corresponding convergence coefficients are given in Table 9.2. The constant values are given in Table 9.1.

Parameter	*Symbol*	*Convergence coefficient*	*Initial value*	*Estimated final value*
Ear canal length	L_2	$\alpha_{L2} = 0.02$	1.5029 cm	1.3045 cm
Vent radius	r_3	$\alpha_{r3} = 0.001$	0.8 mm	1.177 mm
Vent length	L_3	$\alpha_{L3} = 0.005$	1.9740 cm	2.2122 cm
External acoustic feedback path length	R	$\alpha_R = 0.01$	2.3618 cm	1.8945 cm

Table 9.2: Convergence coefficients and values for the varying ear canal length, vent radius, vent length and external acoustic feedback path length in the steepest descent PAA with a speech-shaped noise input signal

After a total of 1200 iterations, i.e. 1100 iterations after the change in the actual feedback path, the estimated feedback path response was in close agreement with the final actual feedback path (Figure 9.4). The estimated parameter values after 1200 iterations (Table 9.2) were not expected to relate to the true physical dimensions. (Recall that numerical

optimisation fitting the model to measured data resulted in unrealistic parameter values due to the limitations introduced by varying only a few parameters; see Chapter 5.) The parametric response was in close agreement to the actual final response around the receiver resonance peaks between 3 kHz and 6 kHz. The amplitude of the response was greatest in this region: the PAA had been most successful at adapting to match the actual response in the frequency range at which most energy was present and therefore at which the hearing aid system was most at risk of becoming unstable.

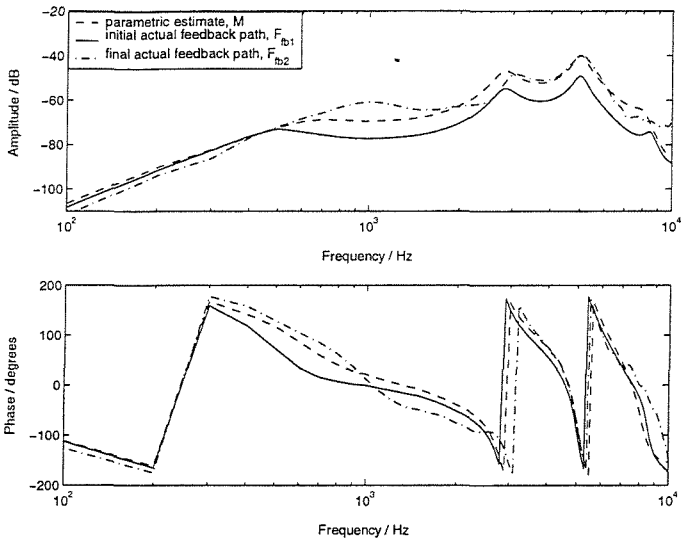

Figure 9.4: Comparison of the parametric response with the initial and final actual feedback path responses

The mean square error, J, between the modelled and actual feedback path responses, defined by Equation (8.3), is shown in Figure 9.5. Although it did not fall to zero, the m.s.e. fell sharply from a high level immediately after the change in the feedback path to a lower level in about 100 iterations. The m.s.e. continued to decrease at a much slower rate from then on. The m.s.e. exhibited no fluctuations.

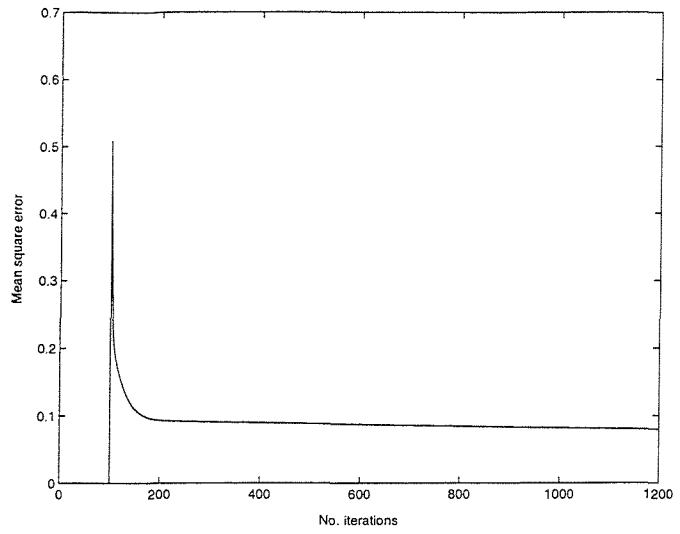

Figure 9.5: Convergence behaviour of the parametric mean square error, J

The estimated ear canal length, L_{2est}, is shown in Figure 9.6. The length decreased rapidly over the first 100 iterations after the change in the actual feedback path before increasing again at a slower rate. This indicates that the estimated ear canal length overshot the minimum of the error surface initially. This behaviour was observed for the two-parameter algorithm in the previous chapter and was due to the misadjustment caused by updating several physical parameters simultaneously.

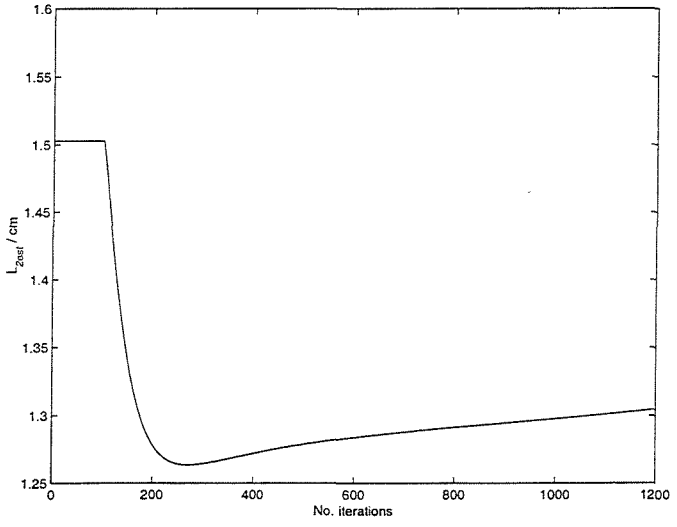

Figure 9.6: Convergence behaviour of the estimated ear canal length, L_{2est}

The vent radius r_{3est} increased rapidly to a larger value as the feedback path changed before decreasing more slowly for the duration of the simulation (Figure 9.7). It is likely that this large change in r_{3est}, (relative to the scale of r_3) caused the tubing length parameters to adapt in the wrong direction temporarily. The estimated vent length L_{3est} decreased by a small

amount for the first 100 iterations after the change in the actual feedback path before increasing (Figure 9.8). The external acoustic feedback path length R_{est} decreased rapidly over the first 100 iterations after the change in the feedback path before continuing to decrease more slowly (Figure 9.9). Both the external acoustic feedback path length and vent radius affect the amplitude of the feedback path (see Section 7.12), so changes in one of these parameters will affect the estimate of the other.

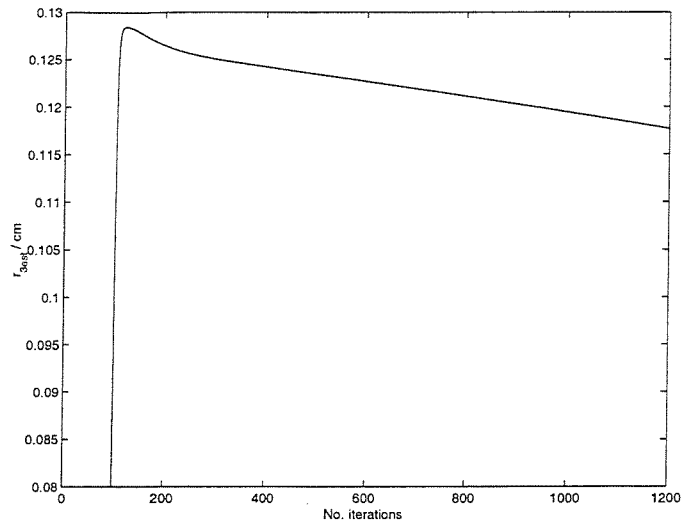

Figure 9.7: Convergence behaviour of the estimated vent radius, r_{3est}

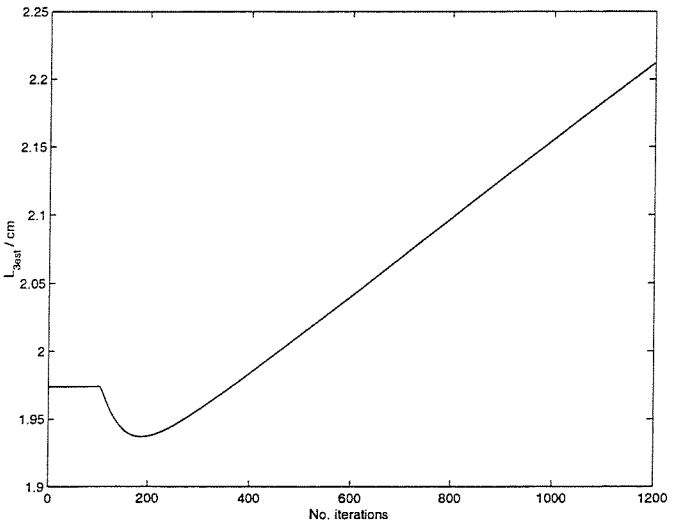

Figure 9.8: Convergence behaviour of the estimated vent length, L_{3est}

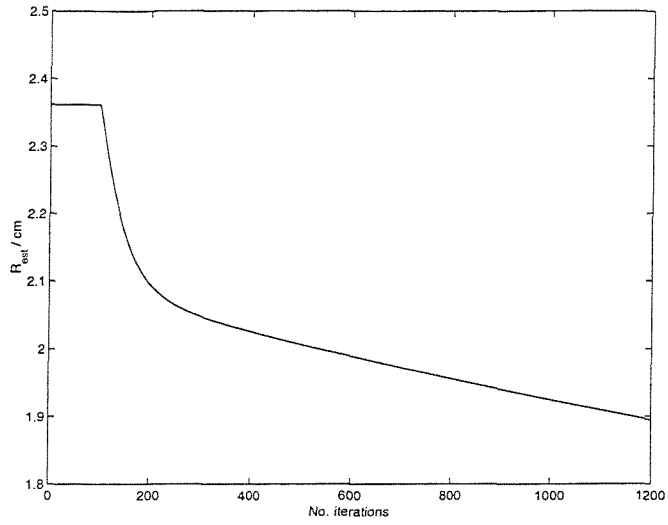

Figure 9.9: Convergence behaviour of the estimated external acoustic feedback path length, R_{est}

The estimated gradient behaved in the same way for each estimated parameter: large amplitude immediately after the change in the actual feedback path, followed by a decrease in amplitude that was fast initially before reaching a constant level near zero. This is illustrated by the estimated gradient with respect to the ear canal length, L_2 (Figure 9.10), which decreased over about 200 iterations, and with respect to the ear canal radius, r_3 (Figure 9.11), which decreased over about 20 iterations. As before, the step size $|\alpha_p \nabla_p|$ was limited to 1 mm for each parameter to prevent misadjustment causing extreme changes in the estimated parameters.

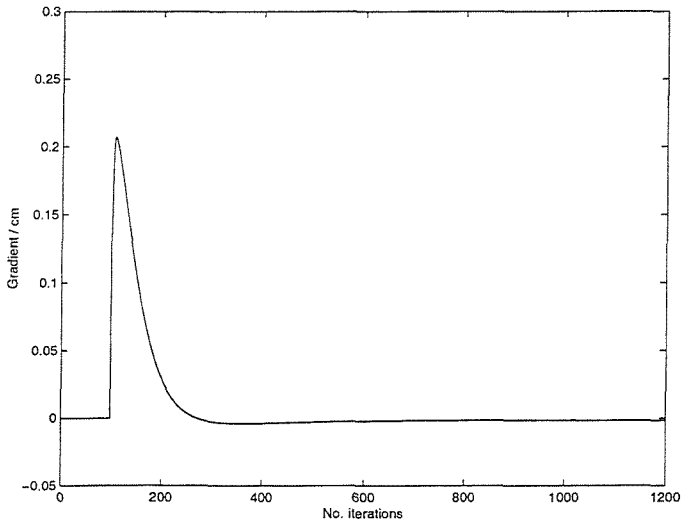

Figure 9.10: Convergence behaviour of the gradient of the error surface with respect to the ear canal length, L_2

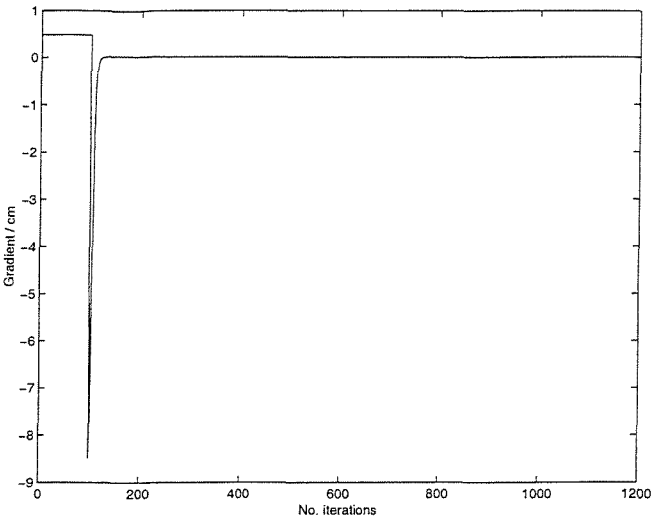

Figure 9.11: Convergence behaviour of the gradient of the error surface with respect to the vent radius, r_3

The normalised m.s.e., given by Equation (8.6), exhibited no fluctuation and decreased rapidly for the first 100 iterations after the change in the feedback path before decreasing more slowly (Figure 9.12). The level reached by the normalised m.s.e. (-20 dB after 1100 iterations) indicated that agreement between the parametric estimate and the actual feedback path response was not as close as with a modelled actual feedback path.

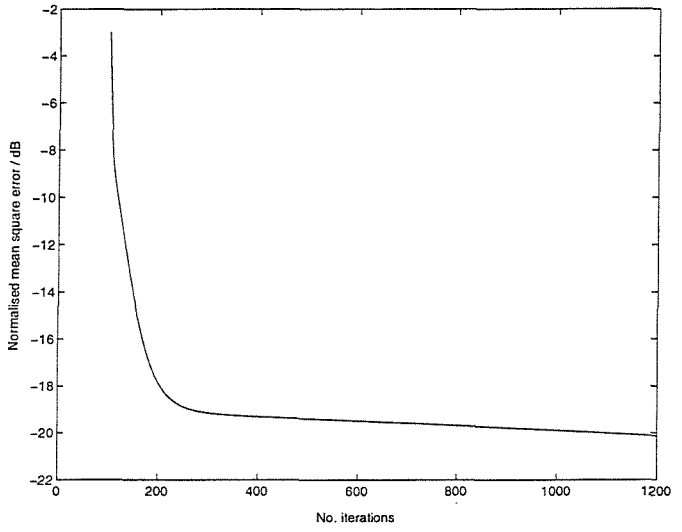

Figure 9.12: Convergence behaviour of the normalised mean square error, J_{norm}

Comparing the normalised m.s.e. for both algorithms over the first 400 iterations, it can be seen that, initially, for about 100 iterations after the change in the actual feedback path, the PAA_{sd} converged faster than the LMS_{sd} but did not reach as low a level overall (Figure 9.13).

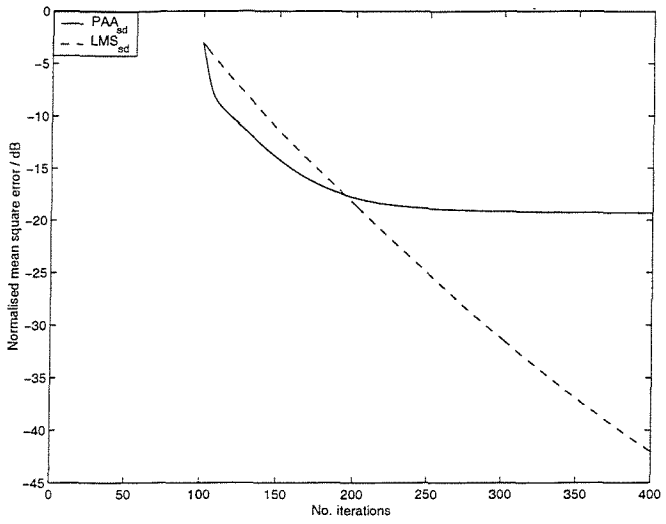

Figure 9.13: Convergence behaviour of the normalised mean square error for both algorithms over the first 400 iterations

Although the m.s.e. did not fall to zero (Figure 9.5), it did reach an approximately constant level soon after the change in the actual feedback path response. Examining the modelled response after 200 iterations, 500 iterations and 1200 iterations, i.e. 100, 400 and 1100 iterations after the change in the actual feedback path, it can be seen that there is very little change in the estimated response, with no more than 5 dB difference in amplitude above 6 kHz and very close agreement between the estimated responses below 6 kHz (Figure 9.14).

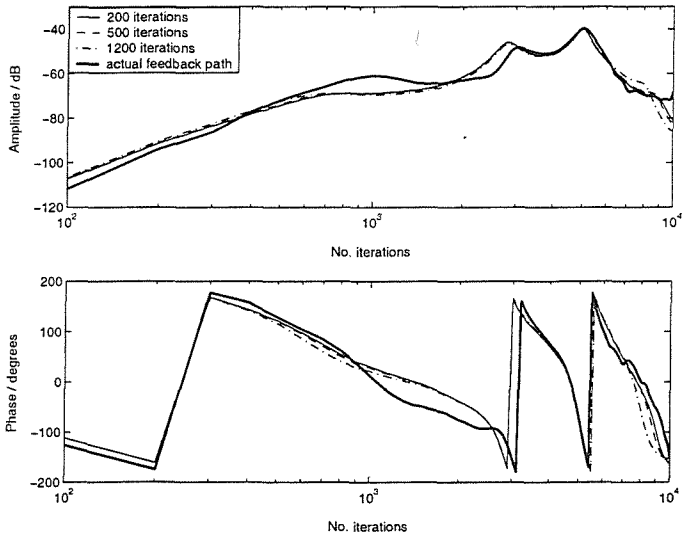

Figure 9.14: Variation over time of the feedback path response estimated by the PAA

Therefore although the PAA was not able to achieve an exact match with the measured feedback path response, it reached its closest possible match 100 iterations after the change in the feedback path and maintained this response even though the estimated parameter values

continued to adjust. If the analytic model could fit measured data exactly, it should be possible to develop the PAA further to achieve very close agreement with the actual feedback path. This could make the performance of the steepest descent PAA comparable with that of the steepest descent LMS algorithm in the presence of speech-shaped noise.

9.3 Performance of the stochastic gradient algorithms with a speech-shaped noise input signal

As before, a more realistic test of the algorithms used the stochastic gradient approach, described in Section 1.5 for the NLMS algorithm and Section 7.7 for the PAA, with the filter length N and sampling frequency f_s given in Table 9.1. The initial and final actual feedback paths were defined in the previous section.

The responses obtained after 16 000 iterations are shown in Figure 9.15. The NLMS response was in good agreement with the actual response between 200 Hz and 8 kHz. The parametric estimate was in close agreement around the high amplitude receiver resonance peaks, as observed in the steepest descent simulation. Again, the final parameter values reached by the PAA (Table 9.3) were not expected to be realistic since the model is not able to reach very close agreement with measured responses when varying only four parameters.

Parameter	*Symbol*	*Convergence coefficient*	*Initial value*	*Estimated final value*
Ear canal length	L_2	$\alpha_{L2} = 0.02$	1.5029 cm	1.3878 cm
Vent radius	r_3	$\alpha_{r3} = 0.001$	0.8 mm	1.163 mm
Vent length	L_3	$\alpha_{L3} = 0.005$	1.9740 cm	2.1581 cm
External acoustic feedback path length	R	$\alpha_R = 0.01$	2.3618 cm	1.9713 cm

Table 9.3: Convergence coefficients and values for the varying ear canal length, vent radius, vent length and external acoustic feedback path length in the stochastic gradient PAA with a speech-shaped noise input signal

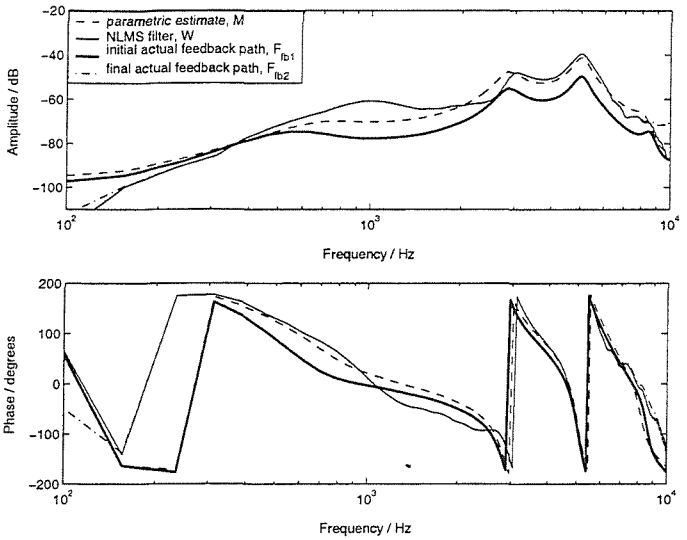

Figure 9.15: Comparison of the parametric and NLMS responses with those of the initial and final actual feedback paths

The behaviour of the NLMS error signal, $e_{NLMS} = d - y_{NLMS}$, was similar to that with the modelled actual feedback path, converging to a small value after about 8000 iterations. However, the parametric error signal, $e_{est} = d - y_{est}$, showed no sign of convergence over the entire simulation (Figure 9.16). This was due to the inability of the model to represent the measured feedback path response exactly combined with the problems observed previously with the stochastic input signal and the misadjustment caused by varying four physical parameters simultaneously. The parametric error signal suggested that the PAA was unable to reach a solution.

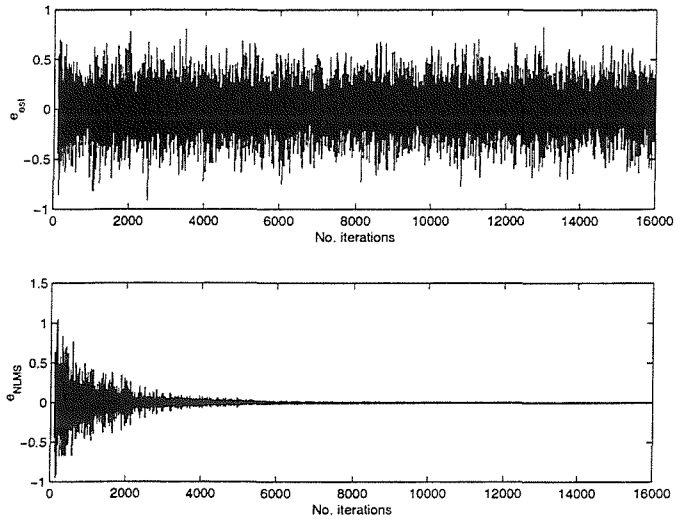

Figure 9.16: Convergence behaviour of the parametric and NLMS error signals, e_{est} and e_{NLMS}

The overall convergence behaviour of the estimated physical parameters in the PAA was similar to that observed for the steepest descent PAA, but, as with the modelled actual feedback path simulations, considerably slower (Figures 9.17 – 9.20).

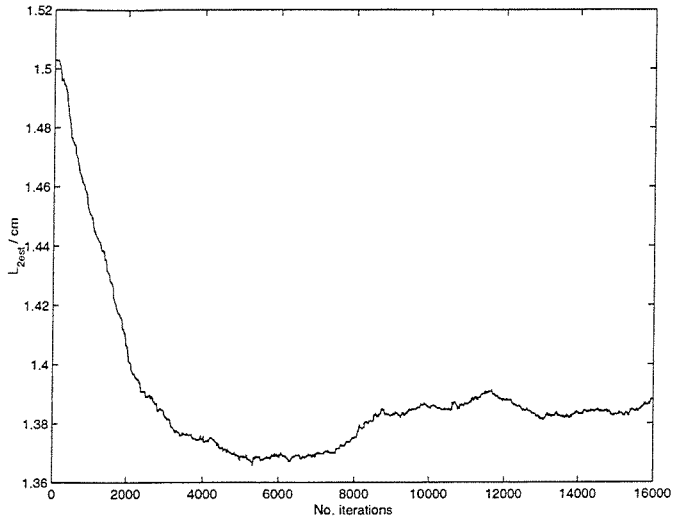

Figure 9.17: Convergence behaviour of the estimated ear canal length, L_{2est}

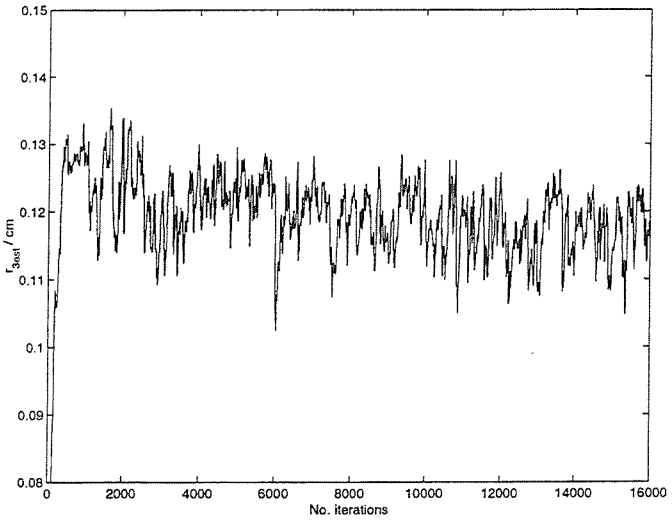

Figure 9.18: Convergence behaviour of the estimated vent radius, r_{3est}

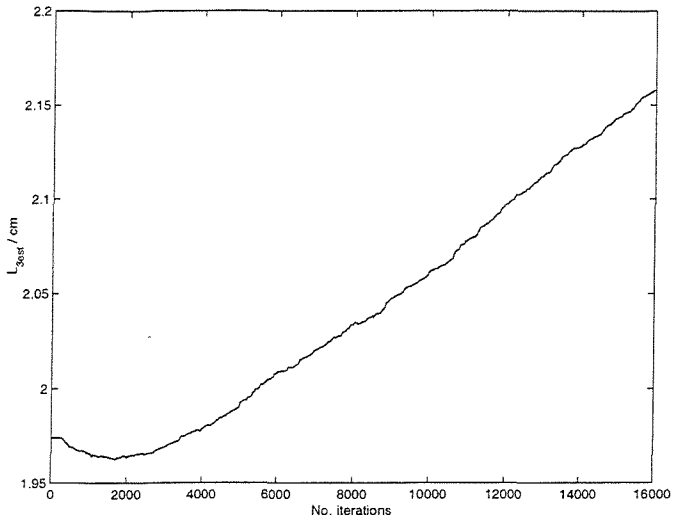

Figure 9.19: Convergence behaviour of the estimated vent length, L_{3est}

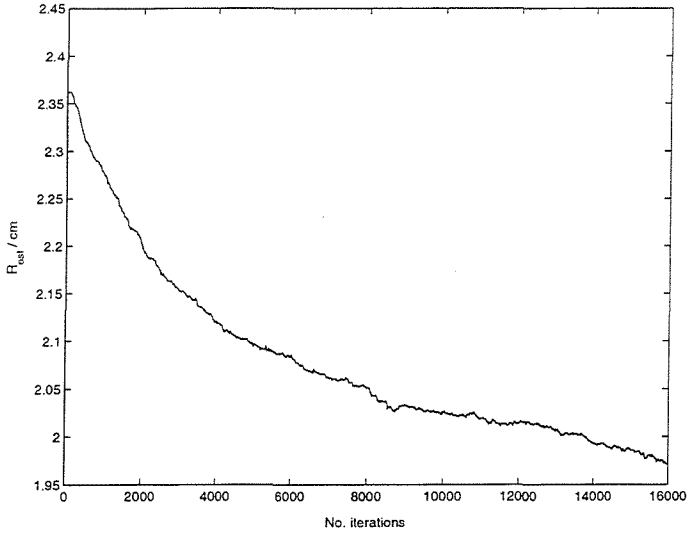

Figure 9.20: Convergence behaviour of the estimated external acoustic feedback path length, R_{est}

The severe fluctuation of the estimated gradient with respect to each parameter is illustrated by the gradient with respect to the ear canal length, L_2 (Figure 9.21). The full effect of this fluctuation was not transmitted to the estimated parameters themselves because of the 1 mm limit placed on the maximum possible step size $|\alpha_p \nabla_p|$ (see Section 7.10). The algorithm managed to overcome this fluctuation and adapt towards the minimum, albeit at a much slower rate than the steepest descent algorithm.

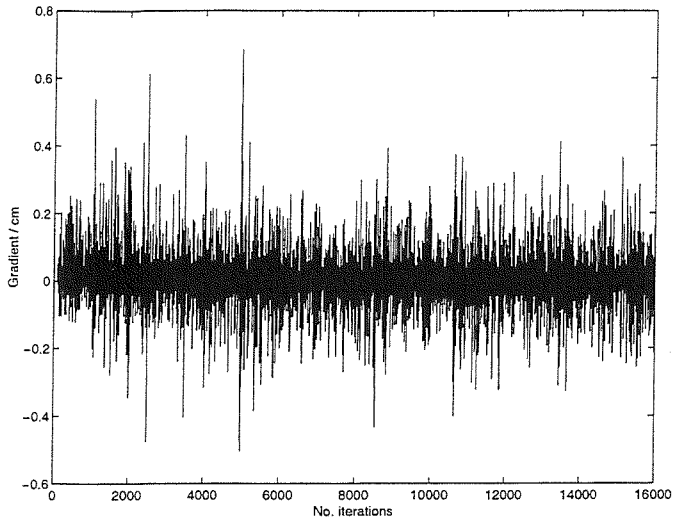

Figure 9.21: Convergence behaviour of the gradient of the error surface with respect to the ear canal length, L_2

The normalised m.s.e. decreased smoothly for the NLMS algorithm (Figure 9.22), as observed for the modelled actual feedback path simulation. The normalised m.s.e. of the PAA (given by Equation (8.6)) exhibited severe misadjustment effects and was unable to decrease to a low level compared with the reduction of the NLMS m.s.e.; the parametric m.s.e. was about 45 dB above the level reached by the NLMS algorithm after 16 000 iterations.

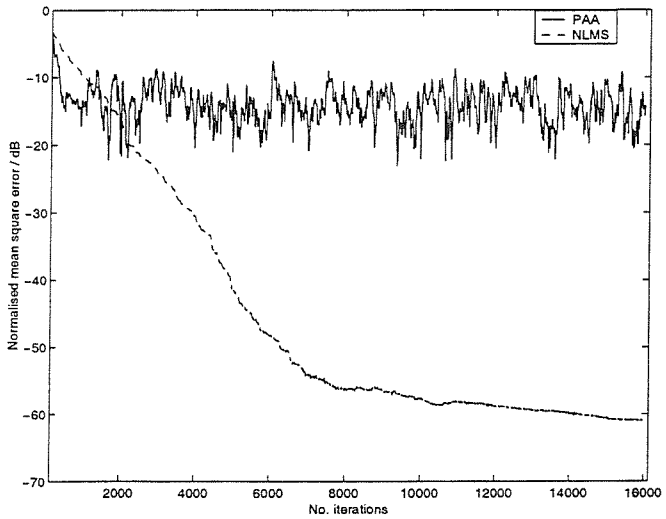

Figure 9.22: Convergence behaviour of the normalised mean square error for the NLMS and parametric algorithms

However, examining the normalised m.s.e. for both algorithms over the first 2000 iterations (Figure 9.23), it can be seen that the parametric m.s.e. decreased more rapidly than that of the NLMS algorithm, reaching an average level of approximately – 15 dB after about 500

iterations. The m.s.e. of the PAA continued to fluctuate about this level. This indicated that the convergence of the PAA was initially faster than that of the NLMS algorithm, although exact agreement with the measured response could not be reached.

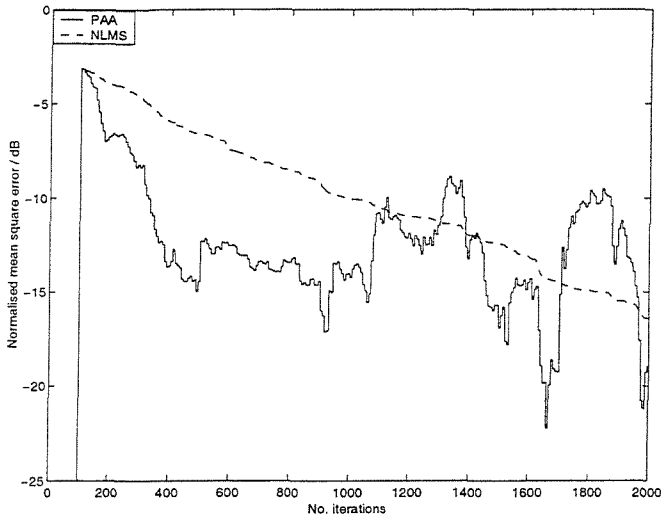

Figure 9.23: Convergence behaviour of the normalised mean square error for the NLMS and parametric algorithms over the first 2000 iterations

Examining the modelled responses generated by the PAA after 500, 1000 and 12 000 iterations, it can be seen that despite the severe misadjustment and the continued adaptation of the estimated parameter values, the modelled response remained approximately constant over the entire frequency range (Figure 9.24).

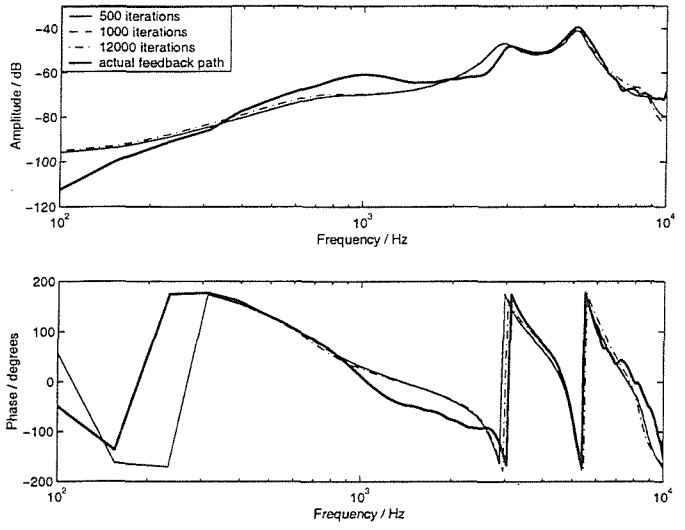

Figure 9.24: Variation over time of the feedback path response estimated by the PAA

Comparing the parametric estimate of the actual feedback path response with that given by NLMS algorithm after 500 iterations, the PAA had reached its best estimate of the actual

response while the NLMS algorithm had yet to converge (Figure 9.25), and so it can be concluded that, with a measured actual feedback path, the PAA is capable of reaching its best estimate of the actual feedback path faster than the NLMS algorithm.

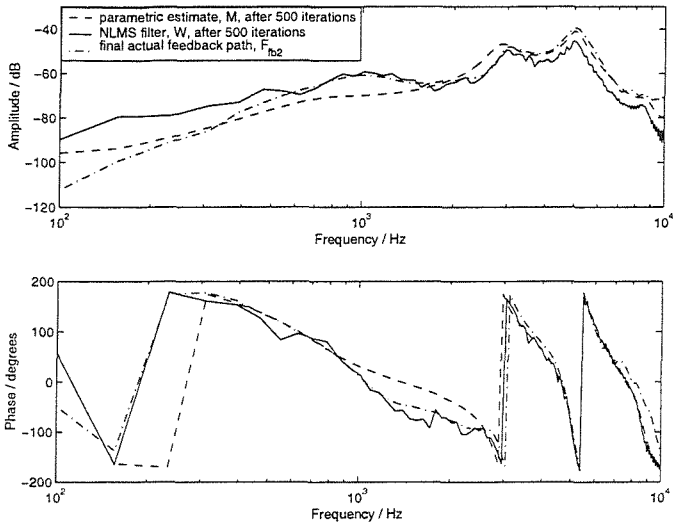

Figure 9.25: Comparison of the parametric and NLMS responses after 500 iterations with the actual final feedback path

The overall performance of both algorithms with a final actual feedback path represented by measured data is similar to that with a modelled final actual feedback path. The convergence is considerably slower when FIR filtering is performed compared to the theoretical steepest descent analysis and the parametric adaptive algorithm appears to compare poorly with the NLMS algorithm in this respect. However, the PAA is able to produce its closest approximation of the measured response rapidly (400 iterations after the change in the actual feedback path) and the response remains approximately constant although the estimated parameter values continue to vary. The closest agreement between the parametric model and the actual response is around the receiver resonance peaks where instability is most likely to occur. This indicates that the PAA would be able to approximately cancel the measured feedback path sufficiently to prevent oscillation occurring in this frequency range and allow the use of higher stable gain. The fit of the parametric model to the measured response could be improved by further development of the parametric adaptive algorithm to allow variation of more physical parameters, although this would increase the misadjustment and slow down the rate of convergence.

9.4 Conclusions

The performance of the NLMS and parametric adaptive algorithms has been evaluated in simulation studies with measured feedback path data. The performance of the NLMS

algorithm was unaffected by the nature of the actual feedback path, but the limited agreement attainable between the analytic model and the measured feedback path response increased the level of misadjustment for the parametric algorithm. However, it was found that the parametric algorithm was able to reach its closest possible estimate of the actual response in relatively few iterations and maintain this response although the estimated parameter values continued to adapt. The stochastic gradient PAA reached its best approximation 400 iterations after the change in the feedback path, compared with the several thousand iterations required for the NLMS algorithm to reach close agreement with the actual response. If the parametric model could be improved to achieve an exact fit to measured data, it may be possible to develop the PAA further to vary more parameters simultaneously and take advantage of this rapid attainment of the best possible fit to give fast cancellation of measured feedback signals.

10 Conclusions and discussion of the future development of the PAA

10.1 Introduction

The work presented in this thesis describes the development of an entirely new approach to feedback cancellation, using adaptation of physical parameter values in a model of the feedback path to cancel the feedback signal. This chapter presents the conclusions of the feasibility study of this parametric adaptive algorithm (PAA), followed by a discussion of proposed future work on the development and extension of the algorithm and its practical implementation in real hearing aids.

10.2 Conclusions

The conclusions drawn from this work are presented below:

1. The two-port network model of an *in situ* hearing aid system can be implemented using a combination of the MATLAB and PSpice software packages.
2. The two-port network model could be simplified to give an analytic expression for the feedback path from the receiver input to the microphone output.
3. The analytic model was verified experimentally and numerical optimisation was used to demonstrate that it could be fitted to a range of measured feedback path responses for different human subjects and feedback conditions.
4. Good agreement with measured data was achieved but closer agreement is required for the model to be used in a practical feedback cancellation algorithm. Further development of the model is necessary, especially an accurate representation of the effects of an obstruction in the external acoustic feedback path.
5. The error surfaces obtained with both modelled and measured actual feedback paths were highly irregular and non-convex. Local minima could occur if the values of the constant parameters in the model were chosen poorly. The irregular nature of the surface, combined with the stochastic properties of some input signals, may result in severe fluctuation and poor convergence of a steepest descent-based feedback cancellation algorithm.
6. The verified simplified analytic model of the feedback path was used to develop the parametric adaptive algorithm (PAA). Its modes of convergence were investigated through steepest descent analysis and compared with a steepest descent implementation of the Least Mean Square algorithm. The performance of the PAA was found to be independent of the nature of the input signal, unlike the LMS algorithm, which was slowed down considerably in the presence of speech-shaped noise compared to its performance with white noise.

7. The performance of the LMS algorithm was unaffected by the number of varying parameters in the actual feedback path or by the nature of the actual path (modelled or measured).
8. The PAA required more iterations to converge as the number of varying parameters increased and was unable to reach close agreement with measured responses over the entire frequency range of interest due to limitations in the analytic model.
9. A more realistic simulation study used stochastic gradient estimates, increasing the number of iterations required for convergence for both the parametric and normalised LMS algorithms. The random nature of the signal, combined with the irregularity of the error surface, produced severe misadjustment in the PAA.
10. Although the PAA could not model measured responses exactly, it achieved its closest possible fit more rapidly than the NLMS algorithm.
11. The fit was closest around the receiver resonance peaks where instability was most likely to occur.
12. If a better fit over all frequencies can be achieved with more varying parameters, the PAA has the potential to be a fast method of adaptive feedback cancellation.

10.3 Future development of the PAA

A model capable of a very close fit to the measured feedback path might require detailed knowledge of a specific hearing aid system for a wide range of conditions (slit leakage, obstructions near the ear, etc.). Measurements must be made of all parts of the physical system (transducers, tubes, middle ear impedance, the external acoustic feedback path and the effects of the pinnae and maybe also of the upper body) and accurate analytic expressions must be obtained for the various components. To date, an accurate model of the effects of an obstruction in the external acoustic feedback path has not been developed. This will be required for the study of a specific system and is also needed in a more general form since this is one of the important causes of oscillation. The present form of the model has simplified the system to a series of narrow cylindrical tubes and acoustic loads. A comprehensive model must be more rigorous. This in depth study of a single system should give greater knowledge of changes in the feedback path and their causes, and the conclusions drawn from such a study will be true for all similar systems.

The current form of the parametric adaptive algorithm estimates the gradient of the error surface with respect to each varying parameter. Section 4.4 presents a set of expressions for the analytic gradient with respect to each parameter. It may be that the expressions increase the computational load without producing a significant improvement in accurate tracking of changes in the feedback path, in which case the estimated gradient method would be

preferable. A frequency domain implementation of the PAA using these analytic gradient expressions has been proposed (Section 7.8) and should be investigated.

The simulations presented in this thesis featured a single step change in the actual feedback path. A more realistic test of the parametric adaptive algorithm would change the actual feedback response several times during the simulation and evaluate the ability of the algorithm to follow these changes. Many step changes over a suitable time frame would represent a continuous change in the actual feedback path.

In this study, the PAA operated in open-loop. The algorithm should be extended to closed-loop operation, since this is a more desirable approach to feedback cancellation. Preferably, the algorithm should operate without probe noise (Kates, 1999) and should be computationally efficient so that the modelled path is recalculated rapidly. Ideally, the algorithm should be capable of fast, stable convergence, simultaneously updating the model and tracking changes in the feedback path in real time without introducing a delay or artefacts or compromising the desired audio signal in any way. The effect of the PAA on sound quality must be investigated. To be considered preferable to conventional methods of feedback cancellation, such as those based on the LMS algorithm, the PAA needs to converge to the correct solution significantly faster or more accurately or to be more robust to changes in the feedback path, or a combination of these, while being cost effective in terms of both processing and the hardware and software required for operation.

The algorithm needs to be implemented on a DSP chip small enough to fit into the limited space available in an ITE or ITC aid, and cannot have a high power consumption. The small size of hearing aid batteries limits their lifetime and the available voltage (Agnew, 1994) and hence the drain on the power source due to the feedback cancellation processing must be small for the method to be useful. An effective algorithm would be inappropriate if it caused the battery to become exhausted rapidly. Before developing a DSP chip, the algorithm can be tested in real time using a PC connected to an *in situ* hearing aid on a human subject to measure changes in the feedback path in a controlled acoustic environment, e.g. an audiometric booth.

In its current form, the parametric algorithm is unsuitable for real time implementation, but further development may lead to a greater understanding of the hearing aid system and this in turn may lead to a fast, robust alternative method of feedback cancellation.

11 References

1. Agnew, J., "Application of a notch filter to reduce acoustic feedback", Hear. J., Vol. 46, No. 3, 1993, pp. 37-43, cited by Maxwell and Zurek (1995).
2. Agnew, J., "Acoustic advantages of deep canal hearing aid fittings", Hear. Instrum., Vol. 45, No. 8, 1994, pp. 22, 24-25.
3. Alvord, L.S., Farmer, B.L., "Anatomy and orientation of the human external ear", J. Am. Acad. Audiol., Vol. 8, No. 6, December 1997, pp. 383-390.
4. Attia, J.O., "Two-Port Networks", in: Attia, J.O. (ed.), *Electronics and Circuit Analysis Using MATLAB*, Boca Raton: CRC Press LLC, 1999.
5. Austin, D.F., "Anatomy of the ear", in: Ballenger, J.J. (ed.), *Diseases of the Nose, Throat, Ear, Head and Neck*, 14th. ed., Philadelphia: Lea and Febiger, 1991, pp. 922-947, cited by Alvord and Farmer (1997).
6. Bade, P.F., Engebretson, A.M., Heidbreder, A.F., Niemoller, A.F., "Use of a personal computer to model the electroacoustics of hearing aids", J. Acoust. Soc. Am., Vol. 75, No. 2, February 1984, pp. 617-620.
7. Bisgaard, N., "Digital feedback suppression: Clinical experiences with profoundly hearing impaired", in: Beilin, J., Jensen, G.R. (eds.), *Recent Developments in Hearing Instrument Technology: 15th. Danavox Symposium*, Kolding, Denmark, 1993, pp. 370-384, cited by Kates (1999).
8. Burkhard, M.D., Sachs, R.M., "Anthropometric mannikin for acoustic research", J. Acoust. Soc. Am., Vol. 58, 1975, pp. 214-222.
9. Bustamante, D.K., Worrell, T.L., Williamson, M.J., "Measurement of adaptive suppression of acoustic feedback in hearing aids", Proc. 1989 Int. Conf. Acoust. Speech and Sig. Proc., Glasgow, 1989, pp. 2017-2020.
10. Byrne, D., Dillon, H., "The National Acoustic Laboratories' (NAL) New Procedure for Selecting the Gain and Frequency Response of a Hearing Aid", Ear Hear., Vol. 7, No. 4, 1986, pp. 257-265.
11. Cox, R.M., "Combined Effects of Earmould Vents and Suboscillatory Feedback on Hearing Aid Frequency Response", Ear Hear., Vol. 3, No. 1, 1982, pp. 12-17.
12. de Jonge, R., "Real-ear Measures: Individual Variation and Measurement Error", in: Valente, M., (ed.), *Hearing Aids: Standards, Options and Limitations*, Thieme, 1996, pp. 72-125.
13. Dillon, H., "Allowing for real ear venting effects when selecting the coupler gain of hearing aids", Ear Hear., Vol. 12, No. 6, December 1991, pp. 406-416.

14. Dyrlund. O., Bisgaard, N., "Acoustic feedback margin improvements in hearing instruments using a prototype DFS (digital feedback suppression) system", Scand. Audiol., Vol. 23, 1991, pp. 49-53.

15. Egolf, D.P., "A Mathematical Scheme for Predicting the Electro-Acoustic Frequency Response of Hearing Aid Receiver-Earmold-Ear Systems", PhD. thesis, Purdue University, West Lafayette, IN, August 1976.

16. Egolf, D.P., "Mathematical modeling of a probe tube microphone", J. Acoust. Soc. Am., Vol. 61, No. 1, January 1977, pp. 200-205.

17. Egolf, D.P., "Review of the Acoustic Feedback Literature from a Control Systems Point of View", in: Studebaker, G.A., Bess, F.H. (eds.), *The Vanderbilt Hearing-Aid Report: State of the Art - Research Needs*, Monographs in Contemporary Audiology, 1982, pp. 94-103.

18. Egolf, D.P., Leonard, R.G., "Experimental scheme for analyzing the dynamic behavior of electroacoustic transducers", J. Acoust. Soc. Am., Vol. 62, No. 7, October 1977, pp. 1013-1023.

19. Egolf, D.P., Howell, H.C, Weaver, K.A., Barker, D.S., "The hearing aid feedback path: Mathematical simulations and experimental verification", J. Acoust. Soc. Am., Vol. 78, No. 5, November 1985, pp. 1578-1587.

20. Egolf, D.P., Haley, B.T., Bauer, K.M., Howell, H.C. Larson, V.D., "Experimental determination of cascade parameters of a hearing-aid microphone via the two-load method", J. Acoust. Soc. Am., Vol. 83, No. 6, June 1988a, pp. 2439-2446.

21. Egolf, D.P., Haley, B.T., Howell, H.C., Larson, V.D., "A technique for simulating the amplifier-to-eardrum transfer function of an *in situ* hearing aid", J. Acoust. Soc. Am., Vol. 84, No. 1, July 1988b, pp. 1-10.

22. Egolf, D.P., Haley, B.T., Howell, H.C., Legowski, S., Larson, V.D., "Simulating the open-loop transfer function as a means for understanding acoustic feedback in hearing aids", J. Acoust. Soc. Am., Vol. 85, No. 1, January 1989, pp. 454-467.

23. Engebretson, A.M., O'Connell, M.P., Gong, F., "An adaptive feedback equalization algorithm for the CID digital hearing aid", Proc. 12th. Annual Int. Conf. of the IEEE Eng. in Medicine and Biology Soc., Part 5, Philadelphia, PA, 1990, pp. 2286-2287, cited by Kates (1999).

24. French-St. George, M., Wood, D.J., Engebretson, A.M., "Behavioral assessment of adaptive feedback cancellation in a digital hearing aid", J. Rehabil. Res. Dev., Vol. 30, 1993, pp. 17-25.

25. Gatehouse, S., "Limitations on insertion gains with vented earmoulds imposed by oscillatory feedback", Br. J. Audiol., Vol. 23, 1989, pp. 133-136.

26. Gelfand, S.A., *Hearing: An Introduction to Psychological and Physiological Acoustics*, Marcel Dekker Inc., 1998.

27. Gilman, S., Dirks, D.D., Stern, R., "The Effect of Occluded Ear Impedances on the Eardrum SPL Produced by Hearing-Aids", J. Acoust. Soc. Am., Vol. 70, No. 2, 1981, pp. 370-386.

28. Greenberg, J.E., Zurek, P.M., Brantley, M., "Evaluation of feedback-reduction algorithms for hearing aids", J. Acoust. Soc. Am., Vol. 108, No. 5, Pt. 1, November 2000, pp. 2366-2376.

29. Haykin, S., *Adaptive Filter Theory*, Prentice Hall, 3rd. ed., 1996.

30. Hellgren, J., "Analysis of Feedback Cancellation in Hearing Aids With Filtered-X LMS and the Direct Method of Closed Loop Identification", IEEE Trans. Speech Audio Process., Vol. 10, No. 2, February 2002, pp. 119-131.

31. Hellgren, J., Forsell, U., "Bias of feedback cancellation algorithms in hearing aids based on direct closed loop identification", IEEE Trans. Speech Audio Process., Vol. 9, No. 8., November 2001, pp. 906-913.

32. Hellgren, J., Lunner, T., Arlinger, S., "System Identification of Feedback in Hearing Aids", J. Acoust. Soc. Am., Vol. 105, No. 6, June 1999a, pp. 3481-3496.

33. Hellgren, J., Lunner, T., Arlinger, S., "Variations in the feedback of hearing aids", J. Acoust. Soc. Am., Vol. 106, No. 5, November 1999b, pp. 2821-2833.

34. Iberall, A.S., "Attenuation of oscillatory pressures in instrument lines", J. Res. Nat. Bur. Stand., Vol. 45, 1950, pp. 85-108, cited by Egolf (1977).

35. Isaacs, A. (ed.), *A Concise Dictionary of Physics*, Oxford University Press, 1990.

36. James, G., *Modern Engineering Mathematics*, Addison-Wesley, 2nd. ed., 1996.

37. Johansen, P.A., "An evaluation of the acoustic feedback damping for behind the ear hearing aids", report, Research Laboratory for Technical Audiology, State Hearing Centres, Odense, Denmark, 1975.

38. Joson, H.A.L., Asano, F., Suzuki, Y., Tone, T., "Adaptive feedback cancellation with frequency compression for hearing aids", J. Acoust. Soc. Am., Vol. 94, No. 6, December 1993, pp. 3248-3254.

39. Kates, J.M., "Acoustic Effects in In-The-Ear Hearing Aid Response: Results from a Computer Simulation", Ear Hear., Vol. 9, No. 3, 1988a, pp. 119-132.

40. Kates, J.M., "A computer simulation of hearing aid response and the effects of ear canal size", J. Acoust. Soc. Am., Vol. 83, No. 5, May 1988b, pp. 1952-1963.

41. Kates, J.M., "A time-domain digital simulation of hearing aid response", J. Rehabil. Res. Dev., Vol. 27, No. 3, 1990, pp. 279-294.

42.Kates, J.M., "Feedback Cancellation in Hearing Aids: Results of a Computer Simulation", IEEE Trans. Sig. Process., Vol. 39, No. 3, March 1991, pp. 553-562.

43.Kates, J.M., "Constrained adaptation for feedback cancellation in hearing aids", J. Acoust. Soc. Am., Vol. 106, No. 2, August 1999, pp. 1010-1019.

44.Killion, M.C., Wilber, L.A., Gudmundsen, G.I., "Zwislocki was right...", Hear. Instrum., Vol. 39, No. 1, 1988, pp. 14-18.

45.Kinsler, L.E., Frey, A.R., Coppens, A.B., Sanders, J.V., *Fundamentals of Acoustics*, John Wiley & Sons, 1982.

46.Knowles Electronics Inc., ED Series receiver data sheet, Issue 01 - 0999, 1997.

47.Leavitt, R., "Earmolds: Acoustic and structural considerations", in: Hodgson, W.R., *Hearing Aid Assessment and Use in Audiologic Habilitation*, 3rd. ed., Baltimore: Williams and Wilkins, 1986, pp. 71-108.

48.LoPresti, J.L., Carlson, E.V., "Electrical Analogs For Knowles Electronics, Inc. Transducers", Report No. 10531-3, Release 6, Knowles Electronics, Inc., 1151 Maplewood Drive, Itasca, IL 60143, 1999.

49.Lutman, M.E., Martin, A.M., "Development of an electroacoustic analogue model of the middle ear and acoustic reflex", J. Sound Vibr., Vol. 64, 1979, pp. 133-157.

50.Lybarger, S.F., "Controlling hearing aid performance by earmold design", in: Larson, V.D., Egolf, D.P., Kirlin, R.L., Stile, S.W. (eds.), *Auditory and Hearing Prosthetics Research*, New York: Grune and Stratton, 1979, pp. 101-132.

51.Lybarger, S.F., "Earmould venting as an acoustic control factor", in: Studebaker, G.A., Hochberg, I. (eds.), *Acoustical Factors Affecting Hearing Aid Performance*, Baltimore: University Park Press, 1980, pp. 197-217.

52.MacKenzie, K., Browning, G.G., McClymont, L.G., "Relationship between earmould venting, comfort and feedback", Br. J. Audiol., Vol. 23, 1989, pp. 335-337.

53.Macrae, J., "Earmould venting and the earcanal occlusion effect", Informal Report No. 74, National Acoustic Laboratories, Commonwealth Department of Health, Australia, November 1980.

54.Macrae, J.H., "A comparison of the effects of different methods of impression build-up on earmoulds", Br. J. Audiol., Vol. 25, No. 3, June 1991, pp. 183-199.

55.Madell, J.R., Gendel, J.M., "Earmolds for Patients with Severe and Profound Hearing Loss", Ear Hear., Vol. 5, No. 6, 1984, pp. 349-351.

56.Maxwell, J.A., Zurek, P.M., "Reducing Acoustic Feedback in Hearing Aids", IEEE Trans. Speech Audio Process., Vol. 3, No. 4, July 1995, pp. 304-313.

57.Northern, J.L., Kepler, L.J., Gabbard, S.A., "Deep canal fittings and real ear measurements", Hear. Instrum., Vol. 42, No. 9, 1991, pp. 34-35, 53.

58. Nyquist, H., "Regeneration Theory", The Bell System Technical Journal, Vol. XI, No. 1, 1932, pp. 126-147.

59. Oliveira, R.J., "The Active Earcanal", J. Am. Acad. Audiol., Vol. 8, No. 6, December 1997, pp. 401-410.

60. Oppenheim, A.V., Schafer, R.W., *Digital Signal Processing*, Prentice-Hall International, Inc., 1975, p. 125.

61. Pierce, A.D., *Acoustics: An Introduction to its Physical Principles and Applications*, McGraw-Hill, 1981.

62. Pipes, L.A., *Applied Mathematics For Engineers And Physicists*, McGraw-Hill, 2nd ed., 1958, p. 349.

63. Press, W.H., Flannery, B.P., Teukolsky, S.A., Vetterling, W.T., *Numerical Recipes in C*, Cambridge University Press, 1988.

64. Rafaely, B., Roccasalva-Firenze, M., Payne, E., "Control of Feedback in Hearing Aids", ISVR Technical Memorandum No. 836, Institute of Sound and Vibration Research, University of Southampton, March 1999.

65. Rafaely, B., Roccasalva-Firenze, M., "Control of feedback in hearing aids - a robust filter design approach", IEEE Trans. Speech Audio Process., Vol. 8, 2000, pp. 754-756.

66. Rafaely, B., Roccasalva-Firenze, M., Payne, E., "Feedback path variability modeling for robust hearing aids", J. Acoust. Soc. Am., Vol. 107, No. 5, 2000, pp. 2665-2673.

67. Revit, L.J., "Two techniques for dealing with the occlusion effect", Hear. Instrum., Vol. 43, No. 12, 1992, pp. 16-18.

68. Roesel, G.W., "CIC + WDRC = A logical combination", Hear. Instrum., Vol. 45, No. 8, 1994, pp. 26-27.

69. Rschevkin, S.N., *A Course of Lectures on the Theory of Sound*, Pergamon Press, 1963

70. Schweitzer, C., Smith, D.A., "Solving the "occlusion effect" electronically", Hear. Instrum. Vol. 43, No. 6, 1992, pp. 30, 32-33.

71. Shaw, E.A.G., "The external ear", in: Keidel, W.D., Neff, W.D. (eds.), *Handbook of Sensory Physiology, Vol. V/1, Auditory System: Anatomy, Physiology (Ear)*, Springer-Verlag, 1974, pp. 455-490.

72. Shusina, N.A, "Unbiased adaptive feedback cancellation in hearing aids", PhD. thesis, Institute of Sound and Vibration Research, University of Southampton, 2003.

73. Staab, W.J., Finlay, B, "A fitting rationale for deep fitting canal hearing instruments", Hear. Instrum., Vol. 42, No. 1, 1991, pp. 6, 8-10, 48.

74. Staab, W.J., Lybarger, S.F., "Characteristics and use of hearing aids", in: Katz, J. (ed.), *Handbook of Clinical Audiology*, 4th. ed., Baltimore: Williams and Wilkins, 1994, pp. 657-722.

75. Stremler, F.G., *Introduction To Communication Systems*, 3rd. ed., Addison-Wesley, 1990.

76. Stroud, K.A., *Engineering Mathematics*, 4th. ed., Macmillan Press Ltd., 1995, pp. 264-267.

77. Stuart, A., Allen, R., Downs, C.R., Carpenter, M., "The Effects of Venting on In-the-Ear, In-the-Canal, and Completely-in-the-Canal Hearing Aid Shell Frequency Responses: Real-Ear Measures", J. Speech Lang. Hear. Res., Vol. 42, No. 4, August 1999, pp. 804-813.

78. Tecca, J.E., "Real ear vent effects in ITE hearing instrument fittings", Hear. Instrum., Vol. 42, No. 12, 1991, pp. 10-12.

79. Tecca, J.E., "Further investigation of ITE vent effects", Hear. Instrum., Vol. 43, No. 12, 1992, pp. 8-10.

80. Valente, M., Valente, M., Potts, L.G., Lybarger, E.H., "Options: Earhooks, Tubing and Earmolds", in: Valente, M. (ed.), *Hearing Aids: Standards, Options and Limitations*, Thieme, 1996, pp. 252-326.

81. Westermann, S., "The occlusion effect", Hear. Instrum., Vol. 38, No. 6, 1987, p.43.

82. Widrow, B., Stearns, S.D., *Adaptive Signal Processing*, Prentice-Hall Inc., Englewood Cliff, N.J., 1985.

83. Wimmer, V.H., "The occlusion effect from earmoulds", Hear. Instrum., Vol. 37, No. 12, 1986, pp. 19, 57-58.

84. Zwislocki, J., "Acoustic attenuation between the ears", J. Acoust. Soc. Am., Vol. 25, No. 4, July 1953, pp. 752-759.

85. Zwislocki, J., "Analysis of the Middle-Ear Function. Part I: Input Impedance", J. Acoust. Soc. Am., Vol. 34, No. 8, Part 2, September 1962, pp. 1514-1523.